

University of Strathclyde  
Department of Biomedical Engineering

**Design and Fabrication of Micro-scale  
High Frequency Ultrasonic Diagnostic  
Devices for *in-vivo* Pathology**

**Robert Tamale Ssekitoleko**

A thesis submitted in fulfilment of the requirements for the  
Doctor of Engineering degree (EngD) in Medical Devices

**2014**

# Preface

---

This thesis is the result of the author's original research. It has been composed by the author and has not been previously submitted for examination which has led to the award of a degree.

The copyright of this thesis belongs to the author under the terms of the United Kingdom Copyright Acts as qualified by the University of Strathclyde Regulation 3.50. Due acknowledgement must always be made of the use of any material contained in, or derived from, this thesis.

Signed:

Date:

# Acknowledgments

---

Firstly, I would like to thank my primary supervisors, Dr. Christine Démoré and Prof Sandy Cochran, for their unfading support, guidance and enthusiasm throughout the duration of my research at the University of Dundee. I have learnt a tremendous amount from them during this period. I would also like to thank my Third supervisor Prof Geo Corner for his always being there for encouragement and helping me with a placement in Medical Physics department at Ninewells Hospital. I am also very grateful to my Strathclyde support team including Prof Terry Gourlay, Prof Trish Connolly and Ms Carol McInness for ensuring that I always got the support I needed.

I would also like to thank my colleagues at the Bioengineering department at the University of Strathclyde and at IMSAT, University of Dundee, for their support and motivation. I want to particularly thank the MSc students I supervised, Jian Jiao, Shuo Guo and Jullien Fortineau for helping me with various aspects of my research. I want to also thank Srikanta Sharma for helping with developing the scanning tank that I used for testing my transducers.

Special mention must also go to the team at Heriot Watt University for their input towards the flexi-circuit design and fabrication through the ISPUD project. I should mention Jack Ng, Prof Marc Desmulliez and Dr David Flynn who were particularly helpful.

I also want to thank the industrial partners to the project including Dr Jim McAneny (now at Crystapol International), Keith Maine (now at Noutronix), John Sweet (now at JHS Consulting) and Gerry Harvey for their tremendous input.

I also want to thank my relatives and friends for their undue support and especially my grandmother, Mrs Hetty Sabayinda and Jjaaja Peter Kefero for having seen the good in me.

Finally, I dedicate this thesis to my parents (Ms Edith Ndagire and Mr Francis Tamale) as well as my grandfather Dr Micheal Sabayinda who all sadly passed away.

# Abstract

---

Transducer arrays operating above 15 MHz enable real time high resolution imaging of tissue, capable of resolving features below 200 $\mu\text{m}$ . Clinical applications such as oncology and gastroenterology could significantly benefit from the improved resolution for high frequency ultrasound (HFUS) characterization of tissues. However, this is presently challenging due to the limited penetration depth of HFUS and limited access.

Since the device dimensions scale with imaging wavelength, it becomes feasible to integrate HFUS arrays with interventional tools such as biopsy needles. Although there are many design and fabrication challenges associated with incorporating transducers with interventional tools such as biopsy needles, it creates opportunities for timely and accurate characterisation of tissue, leading to *in-vivo* pathology.

This study reports progress in the development of fabrication processes for miniature linear arrays suitable for integration with biopsy needles. While patterning high frequency transducer arrays based on piezocomposites has been shown to be feasible, there remain many challenges to miniaturize the interconnect and cabling of an ultrasound probe suitable for *in vivo* pathology. Novel packaging techniques for integrating an ultrasound array into a needle were developed. Wafer scale fabrication was adopted to reduce the overall cost of fabrication.

Microfabrication and precision micromachining processes were developed to overcome the technical challenges in fabricating miniature arrays operating up to 25 MHz. Array elements are defined by precision dicing and the necessary external flex circuit cabling was fed through the needle. A flexible printed circuit is connected to back surface electrodes using low-temperature bonding methods.

A flex circuit connected to the 1-3 piezocomposite was patterned with 60  $\mu\text{m}$  pitch to define array elements suitable for a 25 MHz linear array. The polyimide flexible printed circuit, with fine pitch traces, was twisted into a helical structure so that it can fit within the core of the biopsy needle and permit large numbers of elements and electrode traces.

The spiral-helical flexi-circuit design was developed as a way to fit multiple conductive tracks into a needle. The definition of fine-pitch conductive tracks on polyimide polymer was achieved using dry-film photoresist and the application of a megasonic transducer to provide agitation and small bubbles for copper etching.

Investigation and evaluation of low temperature bonding methods was undertaken. This overcomes the problem of using high temperature methods on the temperature sensitive single crystal materials. Bonding techniques such as ultrasonic bonding and magnetically aligned anisotropic UV curable epoxy were investigated.

A Resolution integral was applied to simulated beam plots as a way of evaluating transducers at a design stage. This considers the ultrasound beams and a measure of the beam at -6 dB is taken as the lateral resolution. This is measured over the depth of field. A transducer with a higher resolution integral would have a narrow beam over a long distance

The process was validated with a single element transducers made from fine-scale single crystal composites involving PMN-PT and Manganese doped Lead Indium Niobate-Lead Magnesium NiobateLead Titanate (Mn-PIN-PMN-PT). These were fabricated using the conventional dice and fill method, and incorporated into needles and tested. These composites had pitches as small as 50  $\mu\text{m}$  with kerf of 18  $\mu\text{m}$ . Images were generated using these transducers.

Arrays operating at 5 MHz and 15 MHz were fabricated. The fabrication process development and testing demonstrated the feasibility of a linear array integrated into a biopsy needle. The extension of the fabrication processes to higher frequency arrays.

# Table of Contents

Preface .....	i
Acknowledgments.....	ii
Abstract.....	iii
Table of Contents.....	v
List of symbols and abbreviations .....	xi
List of Symbols.....	xi
List of Abbreviations .....	xiii
List of Figures.....	xv
List of Tables .....	xx
CHAPTER 1 .....	1
Introduction.....	1
Chapter profile .....	1
1.1 Medical Ultrasound Imaging .....	1
1.1.1 History of ultrasound .....	1
1.1.2 Current ultrasound usage .....	2
1.1.3 High resolution ultrasound.....	3
1.2 Needle biopsies .....	4
1.3 Rationale, Aims and objectives.....	5
1.3.1 Aims.....	8
1.3.2 Objectives.....	8
1.3.3 The ISPUD partnership .....	9
1.4 Thesis structure .....	9
1.5 References.....	11
CHAPTER 2 .....	14
Background Theory and Literature Review.....	14
Chapter Profile .....	14
2.1 Overview of Medical Imaging Modalities .....	14
2.1.1 Radiography.....	15
2.1.2 Positron Emission Tomography (PET) .....	16

2.1.3	<i>Magnetic Resonance Imaging (MRI)</i> .....	17
2.1.4	<i>Optical Coherence Tomography (OCT)</i> .....	17
2.1.5	<i>Ultrasound Imaging</i> .....	18
2.2	Transducers Stacks and Ultrasound Generation .....	21
2.2.1	<i>Passive Materials</i> .....	22
2.3	Piezoelectricity and Piezoelectric Materials .....	24
2.3.1	<i>Types of Piezoelectric Materials</i> .....	25
2.3.2	<i>Electrical Impedance and matching</i> .....	29
2.3.3	<i>Electromechanical coupling coefficient</i> .....	31
2.4	Transducer Design and Performance .....	31
2.4.1	<i>Axial Resolution</i> .....	32
2.4.2	<i>Beam profile and lateral resolution</i> .....	32
2.4.3	<i>Sensitivity and image contrast (or dynamic range)</i> .....	34
2.5	Ultrasound Arrays, Beam Forming and Focusing.....	35
2.5.1	<i>Imaging with Arrays</i> .....	35
2.5.2	<i>Array Imaging System</i> .....	39
2.6	Current Array Fabrication and State of The Art Methods .....	41
2.6.1	<i>Lapping and Polishing</i> .....	41
2.6.2	<i>Kerfless Arrays</i> .....	42
2.6.3	<i>Diced Arrays</i> .....	42
2.6.4	<i>Piezocomposite fabrication</i> .....	44
2.6.5	<i>Fabrication of 1-3 Single Crystals Composites</i> .....	45
2.7	Electrical Interconnects.....	45
2.8	Other Transducer fabrication methods.....	46
2.9	Ultrasound Transducers Integrated in Small Packages .....	47
2.9.1	<i>Fabrication of Needle Based Transducers</i> .....	48
2.10	Chapter discussion .....	50
2.11	References.....	50
CHAPTER 3 .....		57
Design Considerations and Evaluation Methods .....		57
Chapter Profile .....		57
3.1	Introduction to Design Considerations .....	57
3.2	The Needle Sizes.....	59

3.3	Transducer Operational Frequency .....	59
3.4	Packaging in Instrumentation.....	60
3.4.1	<i>Array Orientations</i> .....	61
3.4.2	<i>Flexi Circuit Orientations</i> .....	63
3.5	Clinical Performance.....	66
3.6	Fabrication techniques .....	66
3.7	Performance Characterisation .....	67
3.7.1	<i>Electrical Characterisation</i> .....	67
3.7.2	<i>Passive Material Characterisation</i> .....	67
3.8	Basic Functional Testing of Prototypes .....	69
3.8.1	<i>The scanning system</i> .....	72
3.8.2	<i>Phantom Imaging</i> .....	73
3.9	Chapter Discussion and Conclusions .....	75
3.10	References.....	75
CHAPTER 4 .....		78
Array Modelling and Beam Simulation .....		78
Chapter Profile .....		78
4.1	Introduction.....	79
4.2	Transducer Materials.....	79
4.2.1	<i>Passive Materials</i> .....	80
4.2.2	<i>Active materials</i> .....	80
4.3	Array Modelling and Simulation Methods .....	81
4.4	One-Dimensional Modelling (ODM).....	81
4.4.1	<i>Transducer Stack Model</i> .....	82
4.4.2	<i>Transducer stack results</i> .....	83
4.5	Virtual Prototyping of Devices .....	85
4.5.1	<i>Ceramic plate</i> .....	86
4.5.2	<i>Single crystal plate</i> .....	87
4.5.3	<i>Single crystal composite</i> .....	90
4.5.4	<i>15 MHz array element stack</i> .....	91
4.6	FIED II Simulation .....	92
4.6.1	<i>The beam pattern</i> .....	93
4.6.2	<i>Transducer Simulation Evaluation</i> .....	97

4.7	Chapter discussion and conclusions.....	99
4.8	References.....	100
CHAPTER 5 .....		104
Fabrication Process Development.....		104
Chapter Profile.....		104
5.1	Process Development.....	105
5.2	Transducer Fabrication Process .....	110
5.2.1	<i>The Transducer Stack</i> .....	110
5.2.2	<i>Electrode Definition</i> .....	116
5.3	Single Element Transducer Fabrication.....	117
5.3.1	<i>The Transducer Stack</i> .....	117
5.4	Piezoelectric Composite Fabrication .....	118
5.5	Material Thinning .....	120
5.4.1	<i>Surface Profile</i> .....	121
5.6	Flexi-Circuit Design and Fabrication.....	122
5.6.1	<i>Dicing to Pattern the Flexi-Circuit</i> .....	124
5.6.2	<i>Chemical copper etching of the flexi- circuit</i> .....	125
5.7	Novel Conductive Bonding and Interconnect Methods .....	128
5.7.1	<i>UV Curable Anisotropic Conductive Adhesive</i> .....	129
5.7.2	<i>Ultrasonic Bonding</i> .....	133
5.8	Chapter Discussion and Conclusions.....	134
5.9	References.....	135
CHAPTER 6 .....		137
Single Element Transducers Results: Fabrication and Performance .....		137
Chapter Profile.....		137
6.1	Introduction.....	137
6.2	High Frequency Piezocomposite Fabrication .....	139
6.3	Device Fabrication .....	142
6.3.1	<i>CTS 3203HD Composite Transducer</i> .....	142
6.3.2	<i>Binary composite Transducer</i> .....	143
6.3.3	<i>Ternary Composite Transducer</i> .....	143

6.4	The Imaging Transducer .....	144
6.5	Electrical Characterisation .....	145
6.5.1	<i>Electrical Impedance Matching</i> .....	146
6.5.2	<i>CTS 3203HD Composite Transducer</i> .....	147
6.5.3	<i>Binary Single Crystal Composite Transducer</i> .....	149
6.5.4	<i>Ternary Composite Transducer</i> .....	150
6.6	Acoustic Characterisation .....	151
6.6.1	<i>CTS 3203HD Composite Transducer</i> .....	151
6.6.2	<i>Binary Single Crystal Composite Transducer</i> .....	153
6.6.3	<i>Ternary Composite Transducer</i> .....	156
6.7	Chapter discussion and conclusions.....	159
6.8	References.....	162
CHAPTER 7 .....		164
Array Transducers Results: Fabrication and Performance.....		164
Chapter Profile .....		164
7.1	Array fabrication.....	164
7.2	The 5 MHz Arrays .....	166
7.2.1	<i>Array Fabrication</i> .....	166
7.2.2	<i>Electrical Impedance testing</i> .....	169
7.2.3	<i>Pulse-echo testing</i> .....	171
7.3	The 15 MHz Arrays .....	172
7.3.1	<i>Array Fabrication</i> .....	172
7.3.2	<i>Electrical Impedance testing</i> .....	174
7.3.3	<i>Pulse-echo testing</i> .....	175
7.4	Chapter discussion and conclusions.....	176
CHAPTER 8 .....		177
Discussion, Conclusions and Future Work.....		177
Chapter profile .....		177
8.1	Summary of results .....	177
8.1.1	<i>Fabrication process development</i> .....	177
8.1.2	<i>Simulation and modelling</i> .....	178

8.1.3	<i>Fabricated transducers</i> .....	178
8.2	Suggestions for future work .....	181
8.2.1	<i>Composite fabrication</i> .....	181
8.2.2	<i>Array element definition</i> .....	182
8.2.3	<i>Silicon integration</i> .....	183
8.2.4	<i>Stencil printing of layers</i> .....	183
8.3	Further Grants Awarded .....	184
8.4	References .....	185
APPENDIX A .....		186
APPENDIX B .....		206
APPENDIX C .....		215
	Publications .....	215

# List of symbols and abbreviations

---

Below is a list of symbols and abbreviations used in this Thesis. Other expressions are defined in the text as appropriate.

## List of Symbols

$\mu\text{m}$	Micrometer
Au	Gold
c	Acoustic Velocity
c / V	Speed / velocity
$c^D$	Elastic stiffness at constant displacement
$c^E$	Elastic stiffness at constant electric field
Cr	Chromium
D	Electric displacement
d	Sample thickness
$d_{33}$	Transmission coefficient
dB	Decibels
E	Electric field
f	Operating frequency of the transducer
f #	f-number
$f_a$	Anti-resonance frequencies
$f_e$	Electrical resonance frequency
$f_m$	Mechanical resonance frequency
$f_r$	Resonance frequency
$g_{33}$	Reception coefficient
$k_{33}$	Longitudinal coupling coefficient
kHz	Kilohertz
$k_t$	Electromechanical coupling coefficient
LNO	Lithium niobate
MHz	Megahertz
MRayl	MegaRayleigh
N	Length of the near field

$p$	Pitch
$r$	Focal length
$S$	Strain
$s^D$	Specific elastic compliances at constant displacement
$s^E$	Specific elastic compliances at constant electric field
$T$	Stress
$t$	Time
$T_c$	Curie Temperature
$t_p$	Time duration for the pulse amplitude to decay to -6 dB of its maximum amplitude
$V_l$	Longitudinal velocity
$v_t$	Sound velocity in tissue
$V_w$	Sound velocity in water
$X$	Distance between the two transducers
$Z$	Acoustic impedance
$Z_e$	Electrical impedance
$\alpha$	Attenuation coefficient
$\Delta t$	Time of flight
$E$	Dielectric constant
$\epsilon_{33}$	Clamped dielectric permittivity
$\epsilon_{33}^S/\epsilon^0$	Relative permittivity at constant strain
$\epsilon_{33}^T/\epsilon^0$	Relative permittivity at constant stress
$\epsilon^S$	Permittivity at constant strain
$\epsilon^T$	Permittivity at constant stress
$\lambda$	Wavelength
$\rho$	Density
$\Omega$	Ohms

## List of Abbreviations

2D	two-dimensional
3D	three-dimensional
4D	four-dimensional
ACA	Anisotropic conductive adhesive
ACF	Anisotropic conductive film
CMUT	Capacitive micromachined ultrasound transducer
CT	Computed tomography
EPSRC	Engineering and Physical Science Research Council
FEA	Finite element analysis
Fr size	French size
HFUS	High frequency ultrasound
ICA	Isotropic conductive adhesive
ID	Inner diameter
IMSaT	Institute for Medical Science and Technology
ISO	International Organization for Standardization
ISPUD	Integrated Silicon Piezoelectric Ultrasound Devices project.
IVUS	Intravascular Ultrasound
MISEC	Micro Systems Engineering Centre
Mn-PIN- PMN-PT	Manganese doped Lead Indium Niobate-Lead Magnesium NiobateLead Titanate
MRI	Magnetic resonance imaging
OCT	Optical Coherence Tomography
OD	Outer diameters
ODM	One dimensional modelling
PBS	Phosphate buffered saline

PET	Positron emission tomography
PMN-PT	Lead magnesium niobate-lead titanate
PRAP	Piezoelectric Resonance Analysis Program
PVDF	Poly(vinylidene fluoride)
PZT	Lead Zirconate titanate
PZT	Lead zirconate titanate
R <sub>A</sub>	Axial resolution
RF	Radio frequency
R <sub>L</sub>	Lateral resolution
SNR	Signal to noise ratio
SWG	Standard Wire Gauge
TSV	Through silicon via
UBM	Ultrasound biomicroscopes
UV	Ultraviolet
VF	Volume fraction

# List of Figures

---

FIGURE 1.1: ILLUSTRATION OF LIMITATION OF CONVENTIONAL AND EXTERNAL HIGH FREQUENCY ULTRASOUND TRANSDUCERS. THE CONVENTIONAL PROBE SHOWN IN (A) HAS A LIMITATION OF LOW RESOLUTION BUT PENETRATES DEEP IN THE TISSUE.....	6
FIGURE 2. 1: PULSE-ECHO IMAGING SHOWING A-MODE SCAN OF STRUCTURES AT DIFFERENT TIMES $T_1, T_2$ AND $T_3$ . THE SIGNAL IS RECEIVED AS A VOLTAGE WITH A SPECIFIC AMPLITUDE (COURTESY S. COCHRAN, UNIVERSITY OF DUNDEE). .....	18
FIGURE 2. 2: COMPARISON OF IMAGING MODALITIES IN TERMS OF RESOLUTION AND IMAGING DEPTH .....	21
FIGURE 2. 3: THE STRUCTURE OF AN ULTRASOUND TRANSDUCER WITH DETAILS OF DIFFERENT LAYERS. IT SHOW THE ACTIVE LAYER WHICH IS THE PIEZOELECTRIC MATERIAL, THE MATCHING, BACKING AND OTHER COMPONENTS .....	22
FIGURE 2. 4: A SKETCH OF AN A SCAN SHOWING HOW THE RESOLUTION IMPROVES WITH MATCHING AND BACKING LAYERS. THE BACKING AND MATCHING LAYERS LOWERS MECHANICAL Q WHICH IMPROVES THE RESOLUTION.....	23
FIGURE 2. 5: A SCHEMATIC REPRESENTATION OF A 1-3 COMPOSITE. THE PIEZOELECTRIC MATERIAL PILLARS ARE SURROUNDED BY A POLYMER MATERIAL. ....	28
FIGURE 2.6: ELECTRICAL IMPEDANCE PLOTS SHOWING A TYPICAL MAGNITUDE AND PHASE FOR A PIEZOELECTRIC CERAMIC PLATE RESONATING IN THICKNESS-MODE: (A) A PLATE WITHOUT MATCHING AND BACKING LAYER; (B) THE SAME PLATE WITH MATCHING AND BACKING LAYER.....	30
FIGURE 2. 7: A DIAGRAM ILLUSTRATING THE PULSE-ECHO RESPONSE OF A TRANSDUCER AND THE PULSE LENGTH $T_p$ WHICH IS USED TO DETERMINE THE AXIAL RESOLUTION (DEMORE 2006) .....	32
FIGURE 2. 8: BEAM PROFILE OF A SINGLE ELEMENT CIRCULAR TRANSDUCER (BUSHBERG ET AL. 2011) .....	34
FIGURE 2. 9: TYPES OF ARRAYS; (A) PHASED ARRAY, (B) LINEAR ARRAY, (C) ANNULAR ARRAY .....	36
FIGURE 2. 10: THE PARAMETERS OF LINEAR ARRAY WITH SPATIAL COORDINATES SYSTEM: W IS THE WIDTH OF THE ELEMENT; L IS THE LENGTH, P IS THE PITCH AND D IS THE APERTURE.....	38
FIGURE 2. 11: FOCUSING AND STEERING USING ARRAYS; (A) LINEAR ARRAY, (B) PHASED ARRAY, (C) BEAM STEERING WITH PHASED ARRAY .....	38
FIGURE 2.12: A SIMPLIFIED BLOCK DIAGRAM OF AN ARRAY BASED IMAGING SYSTEM .....	40
FIGURE 2.13: AN EXAMPLE OF A COMPOSITE MADE THROUGH THE DICE AND FILL METHOD. THE PIEZOELECTRIC PILLARS ARE THE LIGHT SQUARES WITH THE EPOXY IN THE DARK SHADE.....	44
FIGURE 2.14: AN EXAMPLE OF A FORWARD-LOOKING NEEDLE TRANSDUCER USED AS AN ULTRASOUND BIO-MICROSCOPE (ZHOU ET AL. 2007).THE ACTIVE APERTURE HAS A DIAMETER 0.44 MM. ....	49
FIGURE 3. 1: THE MAIN AREAS CONSIDERED DURING THE DEVICE DESIGN SHOWING THE DIFFERENT ASPECTS THAT AFFECT THE DEVICE PERFORMANCE.....	58
FIGURE 3. 2: POSSIBLE ORIENTATIONS OF AN ULTRASOUND TRANSDUCER ON A NEEDLE, WITH DIRECTION OF THE BEAM INDICATED; (A) AXIAL CROSS SECTION, (B) FORWARD VIEWING, (C) SIDE VIEWING.....	62
FIGURE 3. 3: AN ILLUSTRATION OF THE TRANSDUCER STACK CAN BE FITTED INTO THE NEEDLE: (A) 3D NEEDLE WITH ARRAY ELEMENTS POSITION INDICTED, (B) CROSS SECTION VIEW, (C) SIDE VIEW .....	63
FIGURE 3. 4: EXAMPLE OF A MULTIPLEXER IN ARRAYS EDITED FROM (EBERLE AND FINSTERWALD 2003) .....	64
FIGURE 3. 5: MULTILAYER THROUGH FOLDING A FLEXIBLE CIRCUIT .....	65
FIGURE 3. 6: AN EXAMPLE OF A HELIX ROLLED FLEXI CIRCUIT .....	65
FIGURE 3. 7: SET UP FOR THE THROUGH TRANSMISSION MEASUREMENT. THE TRANSMITTING TRANSDUCER EMITS A SIGNAL AND THE RECEIVING TRANSDUCER RECEIVES THE SIGNAL. ....	68
FIGURE 3. 8: SET UP FOR THE PULSE-ECHO MEASUREMENT. THE SAME TRANSDUCER IS USED FOR BOTH EMITTING AND RECEIVING THE SIGNAL.....	69
FIGURE 3. 9: APPARATUS SETUP OF THE PULE –ECHO TECHNIQUE THAT WAS USED IN SCANNING. THE SET-UP ALSO WAS USED TO GET SIGNAL AT ONE POSITION OF A STAINLESS STEEL BLOCK .....	71
FIGURE 3. 10: A BLOCK DIAGRAM OF THE IN-HOUSE BUILT SCANNING SYSTEM .....	72

FIGURE 3. 11: STAINLESS STEEL BLOCK WITH WIRES ATTACHED WITH DOUBLE SIDED TAPE. THE WIRES WERE 130 $\mu\text{M}$ , 420 $\mu\text{M}$ AND 1.16 MM THICK; THEY WERE SPREAD ARBITRARY DISTANCES APART. ....	74
FIGURE 3. 12: WIRE PHANTOM: (A) BLOCK SIDE VIEW CONFIGURATION, (B) CROSS-SECTION VIEW WITH WIRE POSITIONS. THE TRANSDUCER AT THE TOP IS SCANNED IN A DIRECTION LATERAL TO THE BLOCK. THE ULTRASOUND IMAGE PRODUCED IS SIMILAR TO (B).....	74
FIGURE 4. 1: THE TRANSDUCER STACK USED FOR ONE DIMENSIONAL MODELLING, INCORPORATING A MATCHING LAYER, A PIEZOELECTRIC MATERIAL AS THE ACTIVE LAYER AND BACKING LAYER. ACTIVE LAYER THICKNESS IS 80 $\mu\text{M}$ , MATCHING LAYER THICKNESS IS 50 $\mu\text{M}$ AND BACKING THICKNESS IS 800 $\mu\text{M}$ .....	82
FIGURE 4. 2: ELECTRICAL IMPEDANCE MAGNITUDE AND PHASE OF A 0.082 MM THICK ELEMENT CALCULATED WITH ODM. THE PMN-PT/EPOXY COMPOSITE ELEMENT WITH 0.36 VOLUME FRACTION; (A) IMPEDANCE MAGNITUDE, (B) IMPEDANCE PHASE .....	84
FIGURE 4. 3: CONFIGURATIONS USED IN INCREMENTAL MODEL OF LINEAR ARRAY. (A) BULK PIEZOELECTRIC PLATE, (B) 1-3 PIEZOCOMPOSITE, (C) MATCHED COMPOSITE TRANSDUCER, AND (D) MATCHED AND BACKED COMPOSITE TRANSDUCER. THIS IMAGE GIVES ILLUSTRATIONS OF STEPS TAKEN DURING SIMULATION. ....	86
FIGURE 4.4: ELECTRICAL IMPEDANCE MAGNITUDE RESPONSE FOR 10 MM SQUARE PLATE WITH A THICKNESS OF 1 MM MADE OF CTS 3203HD MATERIAL COMPARING THE SIMULATION TO THE EXPERIMENTAL RESULTS. ....	87
FIGURE 4. 5: ELECTRICAL IMPEDANCE MAGNITUDE RESPONSE FOR A PMN-PT SINGLE CRYSTAL PLATE. (A) COMPARING EXPERIMENTAL MEASUREMENTS OF 1 MM PLATE FROM TRS TO SIMULATION RESULTS WITH MODIFIED PIEZOELECTRIC CONSTANTS. (B) VARIATION BETWEEN EXPERIMENTAL RESULTS FOR PLATES FROM TRS COMPARED TO MODEL WITH MODIFIED MATERIAL PROPERTIES. (C) VARIATION BETWEEN EXPERIMENTAL RESULTS FOR 0.5 MM THICK PLATES FROM SINOCERAMICS COMPARED TO A MODEL WITH MODIFIED MATERIAL PROPERTIES. ....	89
FIGURE 4.6: ELECTRICAL IMPEDANCE MAGNITUDE FOR A PMN-PT SINGLE CRYSTAL/EPOXY COMPOSITE, BEFORE AND AFTER RE-POLING AND COMPARED WITH SIMULATION USING MODIFIED MATERIAL PROPERTIES. ....	91
FIGURE 4. 7: ELECTRICAL IMPEDANCE MAGNITUDE RESPONSE FOR A MODELLED HIGH FREQUENCY ARRAY ELEMENT WITH 1-3 PIEZOCOMPOSITE OF PMN-PT. THE THICKNESS OF THE MATCHING LAYER FOR THE STACK WITH BACKING IS 50 $\mu\text{M}$ . ....	92
FIGURE 4. 8: PLOTS SHOWING THE RESOLUTION INTEGRAL. '(A) A GRAPH SHOWING L AGAINST A FOR A COLLIMATED BEAM WITH LOW CONTRAST PENETRATION $L_0$ AND BEAM WIDTH $D_0$ . A IS THE RECIPROCAL OF BEAM WIDTH, AND $L(A')$ CORRESPONDS TO THE DEPTH RANGE IN THE IMAGE OVER WHICH THE BEAM WIDTH IS LESS THAN $1/A'$ . (B) A PLOT OF L AGAINST A FOR A WEAKLY FOCUSED ULTRASOUND BEAM WITH LOW CONTRAST PENETRATION $L_0$ AND MINIMUM BEAM WIDTH $D_0$ . IN (A) AND (B) THE RESOLUTION INTEGRAL R IS EQUAL TO THE AREA UNDER THE CURVE'' (MACGILLIVRAY ET AL. 2010). ....	94
FIGURE 4. 9: TWO-WAY BEAM PLOTS FOR LINEAR ARRAYS SIMULATED USING FIELD II, WITH (A) 8 ELEMENTS, (B) 16 ELEMENTS (C) 32 ELEMENTS IN THE ACTIVE APERTURE. AMPLITUDES ARE NORMALISED THE PEAK VALUE. THE ELEMENT PITCH IS $\lambda$ .....	96
FIGURE 4. 10: TWO-WAY BEAM PLOTS FOR PHASED ARRAYS SIMULATED USING FIELD II, WITH (A) 32 ELEMENTS, (B) 48 ELEMENTS (C) 64 ELEMENTS IN THE ACTIVE APERTURE. AMPLITUDES ARE NORMALISED THE PEAK VALUE. THE ELEMENT PITCH IS $\lambda/2$ .....	96
FIGURE 4. 11: LINEAR ARRAYS PLOTS FOR OBTAINING THE RESOLUTION INTEGRAL (A) 8 ELEMENTS, (B) 32 ELEMENTS ..	97
FIGURE 4. 12: PHASED ARRAYS PLOTS FOR OBTAINING THE RESOLUTION (A) 32 ELEMENTS, (B) 64 ELEMENTS .....	97
FIGURE 5. 1: THE PROCESS FLOW DIAGRAM FOR FABRICATING AN ULTRASOUND ARRAY THAT CAN BE INTEGRATED INTO A BIOPSY NEEDLE .....	109
FIGURE 5. 2: DICED PIEZOELECTRIC MATERIAL BEFORE FILLING WITH EPOXY .....	110
FIGURE 5. 3: PIEZOCOMPOSITE PILLARS FILLED WITH EPOXY BEFORE LAPPING.....	111
FIGURE 5. 4: LAPPED COMPOSITES SHOWING THE PILLARS AND EPOXY .....	111
FIGURE 5. 5: ILLUSTRATION OF A CONDUCTIVE ELECTRODE ON TOP A PIEZOELECTRIC COMPOSITE .....	112
FIGURE 5. 6: PRINTED CONDUCTIVE STRIPS ON TOP OF THE CONDUCTIVE LAYER.....	112

FIGURE 5. 7: ILLUSTRATION OF MATCHING LAYER ON TOP OF THE PIEZOELECTRIC MATERIAL WITH AN ELECTRODE IN THE MIDDLE.....	113
FIGURE 5. 8: STACK AFTER LAPPING THE BACK FACE TO APPLY THE BACK ELECTRODE .....	113
FIGURE 5. 9: BACK FACE ELECTRODE ON TOP OF THE OTHER LAYERS .....	114
FIGURE 5. 10: FLEXI CIRCUIT BONDED ON TO THE BACK ELECTRODE.....	114
FIGURE 5. 11: BACKING LAYER CAST ON TOP OF THE OTHER LAYERS .....	115
FIGURE 5. 12: (A) E-BEAM EVAPORATION CHAMBER AND (B) SAMPLE WITH EVAPORATED THIN FILM ELECTRODE. TWO REGIONS OF PIEZOELECTRIC MATERIAL FROM WHICH ARRAYS CAN BE MADE ARE SHOWN SURROUNDED BY EPOXY. ....	117
FIGURE 5. 13: AN ILLUSTRATION OF THE MICROACE DICING SAW INTERIOR AND THE ARRAY WITH THE FLEXI-CIRCUIT DURING DICING.....	118
FIGURE 5. 14: SINGLE CRYSTAL MATERIAL AFTER DICING BUT BEFORE FILLING TO MAKE A COMPOSITE; (A) SHOWS GOOD PILLARS, (B) SHOWS PILLARS WHICH HAVE BEEN BROKEN DURING DICING. ....	119
FIGURE 5. 15: AN ILLUSTRATION OF A LAPPING AND POLISHING MACHINE USED FOR THINNING DOWN ACTIVE AND PASSIVE LAYERS .....	121
FIGURE 5. 16: AN EXAMPLE OF A SURFACE PROFILE OF A LAPPED AND POLISHED COMPOSITE WITH ZYGO WHITE LIGHT INTERFEROMETRY: (A) IS THE SURFACE VIEW OF THE COMPOSITE WITH THE RED COLOUR HIGHLIGHT AREAS WITH RAISED SURFACES, (B) IS THE SURFACE PROFILE ACROSS THE LINE IN (A). ....	122
FIGURE 5. 17: A SCHEMATIC ILLUSTRATION OF A SPIRALLY ROLLED FLEXI-CIRCUIT ATTACHED TO THE SIDE OF AN ULTRASOUND ARRAY. A COMMERCIAL NEEDLE IS ALSO SHOWN; IT HAS A LENGTH OF 10 CM AND AN INNER DIAMETER OF 1.5 MM (NG ET AL. 2011). ....	122
FIGURE 5. 18: THE FLEXI-CIRCUIT DESIGNED TO MEET THE CHALLENGES OF FITTING INTO A NEEDLE. THE TIP IS STRAIGHT TO ALLOW FOR DICING AND THE ANGLE ALLOWS FOR ROLLING. ....	123
FIGURE 5. 19: THE DESIGNED FLEXI-CIRCUIT WITH ALL THE DIMENSIONS. THE DARK PART IS WHERE THE PITCH IS TOO SMALL TO BE SHOWN. ....	124
FIGURE 5. 20: THE SECOND DESIGN OF FLEXI-CIRCUIT THAT WAS USED TO GET MORE PROTOTYPES.....	124
FIGURE 5. 21: DICED FLEXI-CIRCUIT WITH AN ETCHED FAN-OUT. A PHOTOLITHOGRAPHY PATTERNED END WAS ATTACHED TO A DICED FLEXI-CIRCUIT. ....	125
FIGURE 5. 22: THE SET UP FOR THE WATER TANK USED FOR ACOUSTIC STREAMING FOR ENHANCING ETCHING EFFICIENCY FOR FLEXIBLE SUBSTRATES (NG ET AL., 2011) .....	127
FIGURE 5. 23: MICROSCOPE IMAGE OF COPPER MICRO-TRACKS ON POLYIMIDE. THE COPPER TRACKS AT THE TIP ARE 18.49 $\mu\text{m}$ WITH A GAP OF 43.62 $\mu\text{m}$ GIVING A PITCH OF 62.11 $\mu\text{m}$ . THE GRAY-SCALE IMAGE SHOWS THAT THE TRACKS WIDEN AS WELL AS THE GAP WHEN THEY ARE AWAY FROM THE TIP-END OF THE FLEXI-CIRCUIT.....	128
FIGURE 5. 24: (A) A SCHEMATIC OF THE OF ROOM-TEMPERATURE ACA BONDING USING PARAMAGNETIC CONDUCTIVE PARTICLES AND UV CURABLE EPOXY, (B) EXPERIMENTAL SET-UP.....	130
FIGURE 5. 25: (A) ALL THE BUMPS OF THE EPOXY CURED UNDER UV LIGHT, (B) THICK LINES ABOVE 267 $\mu\text{m}$ DID NOT CURE UNDER UV LIGHT.....	131
FIGURE 5. 26: A FLEXI-CIRCUIT WITH A LASER CUT-THROUGH TO ALLOW UV LIGHT TO REACH THE EPOXY FOR CURING	131
FIGURE 5. 27: SCRATCH DICED PMN-PT SINGLE CRYSTAL PLATE FOR KERFLESS ARRAYS .....	132
FIGURE 5.28: (A) SCRATCH DICED ARRAY OF PMN-PT SINGLE CRYSTAL MATERIAL ATTACHED TO A FLEXI-CIRCUIT BY UV ACA, (B) ELECTRICAL IMPEDANCE MAGNITUDE PLOTS OF THE WORKING ELEMENTS ON THE ARRAY. ....	132
FIGURE 5.29: ZYGO WHITE LIGHT INTERFEROMETRY IMAGES OF LAPPED SAMPLES: (A) LAPPED WITH A 9 $\mu\text{m}$ ALUMINA ABRASIVE, (B) LAPPED WITH 3 $\mu\text{m}$ ALUMINA ABRASIVE .....	134
FIGURE 6. 1: EXAMPLES OF 1-3 PIEZOCOMPOSITE : (A) AFTER DICING BOTH DIRECTIONS BEFORE FILLING WITH EPOXY; (B) AFTER FILLING WITH EPOXY AND LAPPING; (C) AN EXAMPLE OF STRIPS OF PIEZOELECTRIC MATERIAL REMOVED BY DICING IN THE FIRST DIRECTION; (D) AN EXAMPLE OF AIR BUBBLE AFTER FILLING WITH EPOXY .....	140
FIGURE 6. 2: A DIAGRAM COMPARING THE DIMENSIONS OF THE THREE TRANSDUCER ACTIVE ELEMENTS FABRICATED ..	141

FIGURE 6. 3: AN ILLUSTRATION OF A SINGLE ELEMENT TRANSDUCER IN A METAL TUBE ATTACHED TO A ROD FOR EASY TESTING. THE ACTIVE AREA IS MAGNIFIED TO SHOW THE LAYERS OF MATCHING WITH ALUMINA FILLED EPOXY, COMPOSITE AND THE BACKING WITH TUNGSTEN FILLED EPOXY .....	145
FIGURE 6. 4: A TRANSDUCER SHOWING MATCHING LAYER, BACKING LAYER, ACTIVE COMPOSITE, CONDUCTIVE EPOXY FOR ELECTRICAL CONNECTION TO THE CABLING. THIS FIGURE IS FOR THE SAME ELEMENT AS THAT SHOWN IN FIGURE 6.2. ....	145
FIGURE 6. 5: IMPEDANCE MAGNITUDE AND PHASE PLOT OF A 1 M COAXIAL CABLE. THE IMPEDANCE MAGNITUDE AT 15 MHZ IS ABOUT 221 $\Omega$ , AT 22 MHZ IS ABOUT 143 $\Omega$ AND AT 17 MHZ IS ABOUT 189 $\Omega$ .....	147
FIGURE 6. 6: IMPEDANCE MAGNITUDE AND PHASE OF CTS 3203HD/EPOFIX COMPOSITE TRANSDUCER WITH ACOUSTIC MATCHING AND BACKING AT 15 MHZ; (A) BEFORE ELECTRICAL IMPEDANCE MATCHING, (B) AFTER ELECTRICAL IMPEDANCE MATCHING WITH COAXIAL CABLE .....	148
FIGURE 6. 7: IMPEDANCE MAGNITUDE AND PHASE OF PMN-PT COMPOSITE TRANSDUCER AT 21.83 MHZ; (A) BEFORE ELECTRICAL IMPEDANCE MATCHING WHICH WAS MEASURED AT THE END OF THE FLEX CIRCUIT, (B) AFTER IMPEDANCE MATCHING WITH COAXIAL CABLE .....	149
FIGURE 6. 8: IMPEDANCE MAGNITUDE AND PHASE OF Mn-PIN-PMN-PT COMPOSITE TRANSDUCER AT 17 MHZ; (A) BEFORE ELECTRICAL IMPEDANCE MATCHING, (B) AFTER IMPEDANCE MATCHING WITH COAXIAL CABLE FOR ALL THESE ELEMENTS, IS THE ELECTRICAL IMPEDANCE AS EXPECTED FOR THE DIMENSIONS AND VF OF THE COMPOSITE .....	150
FIGURE 6. 9: THE MEASURED PULSE-ECHO WAVEFORM REFLECTED FROM A STEEL BLOCK SHOWING THE PULE LENGTH AND THE FREQUENCY SPECTRUM OF THE CTS 3203HD/EPOFIX COMPOSITE TRANSDUCER .....	152
FIGURE 6. 10: IMAGE OF THE THREE WIRES ON A STAINLESS STEEL BLOCK OBTAINED WITH THE CTS 3203HD/EPOFIX COMPOSITE TRANSDUCER .....	152
FIGURE 6. 11: THE MEASURED PULSE-ECHO WAVEFORM REFLECTED FROM A STEEL BLOCK SHOWING THE PULE LENGTH AND THE FREQUENCY SPECTRUM OF THE PMN-PT/EPOFIX COMPOSITE TRANSDUCER .....	153
FIGURE 6. 12: IMAGES WITH THE PMN-PT COMPOSITE TRANSDUCER: (A) STEEL BLOCK WITH THREE WIRES ON DOUBLE SIDED TAPE PRODUCED GOOD RESULTS; (B) WIRE PHANTOM WITH NINE 20 $\mu$ M TUNGSTEN WIRES; (C) LATERAL ENVELOP OF ECHO SIGNALS FROM THE WIRES LOCATED AT 5.5 MM FROM THE PMN-PT/EPOFIX COMPOSITE TRANSDUCER .....	155
FIGURE 6. 13: IMAGE OF EX-VIVO BOWEL TISSUE RESECTED FROM TWO MICE WITH ULTRASOUND IMAGE REPRESENTED IN (A) FALSE COLOUR AND (B) GREYSCALE.....	156
FIGURE 6. 14: THE MEASURED PULSE-ECHO WAVEFORM REFLECTED FROM A STEEL BLOCK SHOWING THE PULE LENGTH AND THE FREQUENCY SPECTRUM OF THE Mn:PIN-PMN-PT/EPOFIX COMPOSITE TRANSDUCER .....	156
FIGURE 6. 15: IMAGES WITH THE Mn-PIN-PMN-PT COMPOSITE TRANSDUCER: (A) STEEL BLOCK WITH THREE WIRES ON A DOUBLE SIDED TAPE PRODUCED GOOD RESULTS; (B) WIRE PHANTOM WITH NINE 20 $\mu$ M TUNGSTEN WIRES; (C) LATERAL ENVELOP OF ECHO SIGNALS FROM THE WIRES LOCATED AT 5.5 MM FROM THE Mn:PIN-PMN-PT/EPOFIX COMPOSITE TRANSDUCER.....	158
FIGURE 6. 16: IMAGE OF EX-VIVO BOWEL TISSUE RESECTED FROM TWO MICE WITH ULTRASOUND IMAGE REPRESENTED IN (A) FALSE COLOUR AND (B) GREYSCALE.....	159
FIGURE 7. 1: SOME OF THE STAGES OF ARRAY FABRICATION: (A) TWO FLEXI-CIRCUITS ARE CONNECTED TO A PIEZOELECTRIC STACK TO GET DIFFERENT SETS OF ARRAYS AT THE SAME FREQUENCY; (B) AN 8-ELEMENT 5 MHZ ARRAY WITH THE FLEXI-CIRCUIT FAN-OUT FOR CABLE CONNECTION; (C) THE INITIAL ROLLING OF THE FLEXI-CIRCUIT FOR THE ARRAY TO FIT INTO A TUBE.....	166
FIGURE 7. 2: AN EXAMPLE OF A DICED 5 MHZ ARRAY. THE INTER-ELEMENTAL PITCH IS 300 $\mu$ M AND THE ELEVATION LENGTH IS 1.8 MM.....	167
FIGURE 7. 3: CLOSE-UP IMAGES OF AN 18-ELEMENT 5 MHZ ARRAY AFTER DICING: (A) TOP VIEW; (B) PERSPECTIVE VIEW. THE INTER-ELEMENTAL PITCH IS 300 $\mu$ M AND THE ELEVATION LENGTH IS 1.2 MM .....	167
FIGURE 7. 4: A FINISHED 5 MHZ PROTOTYPE BEFORE IT IS INSERTED INTO A METAL TUBE. THE INTER-ELEMENTAL PITCH IS 300 $\mu$ M AND THE ELEVATION LENGTH IS 1.8 MM .....	168

FIGURE 7. 5: ARRAYS INSERTED INTO TUBES OF APPROXIMATELY 3 MM INNER DIAMETER FOR PULSE-ECHO TESTING: (A) ROLLED FLEXI-CIRCUIT BEFORE INSERTION INTO TUBE; (B) ROLLED FLEXI-CIRCUIT AFTER INSERTION INTO TUBE; (C) FLEXI-CIRCUIT IN A TUBE WITH OPENING FOR THE ARRAY; (D) MICRO-COAXIAL CABLES ATTACHED TO A FLEXI-CIRCUIT FAN-OUT.....	169
FIGURE 7.6: IMPEDANCE MAGNITUDE (A) AND PHASE (B) PLOTS OF A 5 MHZ TRANSDUCER ARRAY SHOWING ELEMENTS WITH A MEASURABLE IMPEDANCE RESPONSE. TWELVE ELEMENTS (#2-13) HAVE A MAGNITUDE RESPONSE AND THIRTEEN ELEMENTS (#2-14) HAVE A PHASE RESPONSE, OUT OF 18 ELEMENTS IN THE ARRAY.....	170
FIGURE 7. 7: PULSE ECHO RESPONSES OF ALL THE 18 ELEMENTS OF THE 5 MHZ ARRAY TRANSDUCER ARRAY.....	171
FIGURE 7. 8: DICED ELEMENTS FOR THE 15 MHZ ARRAYS: A) CLEAR INDICATION OF THE CAST LAYERS AND DICING THROUGH THE BACKING; B) SEPARATION OF ELEMENTS AND SOME BREAKAGE. THE INTER-ELEMENTAL PITCH IS 100 $\mu\text{M}$ WITH THE ACTIVE LAYER THICKNESS OF 120 $\mu\text{M}$ AND MATCHING LAYER THICKNESS OF 51 $\mu\text{M}$ . ....	172
FIGURE 7.9: EXAMPLE OF DICED 15 MHZ ARRAY ELEMENTS WITH FLEXI-CIRCUIT: (A) IS A FLEXI-CIRCUIT WITH A 64 ELEMENT ARRAY CONNECTED AT THE TIP; (B) THE 64 ELEMENT ARRAY NEXT TO A COMMERCIAL NEUROSURGERY BIOPSY NEEDLE; (C) IS ANOTHER 32 ELEMENT ARRAY SET WITH A DIFFERENT TYPE OF FLEXI-CIRCUIT; .....	173
FIGURE 7. 10: IMPEDANCE MAGNITUDE (A) AND PHASE OF ELEMENTS IN A 15 MHZ ARRAY .....	174
FIGURE 7. 11: EXAMPLE PULSE-ECHO RESPONSES OF TWO ELEMENTS OF THE 15 MHZ ARRAY .....	175
FIGURE 8. 1: AN EXAMPLE OF RANDOM MICROMOULDED COMPOSITES. (A) OPTICAL IMAGES OF A TYPICAL RANDOM COMPOSITE (JIANG ET AL. 2012); (B) KERFLESS ARRAY SECTIONS WITH MICRO-MOULDED PIEZOCOMPOSITE (DÉMORÉ ET AL. 2009).....	182
FIGURE 8. 2: A PHOTOLITHOGRAPHY ELECTRODE PATTERN ON TOP OF A DICED AND FILLED COMPOSITE (BERNASSAU ET AL. 2009).....	182
FIGURE B. 1: FABRICATION PROCESS PLAN INCORPORATING A CONDUCTIVE MATCHING LAYER .....	207
FIGURE B. 2: FABRICATION PROCESS PLAN INCORPORATING A CONDUCTIVE LAYER .....	209
FIGURE B. 3: FABRICATION PROCESS PLAN INCORPORATING SILICON MICRO-VIAS.....	211
FIGURE B. 4: EXAMPLE OF FLEXI-CIRCUIT BOND PADS TO BE BONDED AT THE BACK END OF THE SILICON HOLDING THE TRANSDUCER STACK .....	212
FIGURE B. 5: FABRICATION PROCESS PLAN INCORPORATING WAFER SCALE .....	213
FIGURE B. 6: FABRICATION PROCESS PLAN INCORPORATING FLEXI-CIRCUIT MATCHING .....	214

# List of Tables

---

TABLE 2. 1: COMPARISON OF MEDICAL IMAGING MODALITIES (SZABO 2004) ( <a href="http://usedophthalmology.com">HTTP://USEDOPHTHALMOLOGY.COM</a> ) ..	15
TABLE 2. 2: TYPICAL HUMAN TISSUE ACOUSTIC PROPERTIES (AZHARI 2010).....	19
TABLE 2. 3: COMPARISON BETWEEN PZT, PVDF AND SINGLE CRYSTAL PROPERTIES .....	26
TABLE 2. 4: COMPARISON OF 64 ELEMENT LINEAR ARRAY PARAMETERS WITH DIFFERENT FREQUENCIES .....	37
TABLE 4. 1: PROPERTIES OF SOME OF THE PASSIVE MATERIALS USED IN THE TRANSDUCER PROTOTYPES .....	80
TABLE 4. 2: COMPARISON OF THE ODM MODELLED PMN-PT AND PMN-PT/EPOXY COMPOSITE.....	85
TABLE 4. 3: MATERIAL PROPERTIES OF PMN-PT SINGLE CRYSTAL .....	88
TABLE 4. 4: INPUT PARAMETERS FOR SIMULATION OF THE 15 MHZ ARRAYS .....	95
TABLE 4. 5: IMAGE QUALITY PARAMETERS DETERMINED FROM BEAM SIMULATION OF LINEAR AND PHASED ARRAYS .....	97
TABLE 5. 1: SUMMARY OF THE DIFFERENT FABRICATION PROCESSES CONSIDERED .....	106
TABLE 6.1: COMPARISON OF PROPERTIES OF FABRICATED PIEZOELECTRIC COMPOSITES AND A BULK SINGLE CRYSTAL MATERIAL .....	141
TABLE 6. 2: A TABLE COMPARING THE DIMENSIONS OF THE COMPOSITES MADE INTO TRANSDUCERS.....	142
TABLE 6. 3: SUMMARY OF THE PROPERTIES OF THE SINGLE ELEMENT TRANSDUCERS DEVELOPED .....	160
TABLE 7. 1: DESIGN PARAMETERS FOR MINIATURE ARRAY ON NEEDLE.....	165
TABLE B. 1: SUMMARY OF THE DIFFERENT FABRICATION PROCESSES CONSIDERED .....	206

# CHAPTER 1

---

## Introduction

---

### Chapter profile

This chapter gives a general overview of medical ultrasound imaging, explaining where it started and the current trends as well as predicting the future developments. It also presents the rationale of the thesis, detailing the main aims of the research. The thesis structure, the statement of original work and are also outlined in this chapter.

### 1.1 Medical Ultrasound Imaging

Ultrasound is defined as sound waves operating at frequencies above the human hearing frequency limit of 20 kHz (Lutz and Buscarini 2011). Conventional medical diagnostic ultrasound transducers have an operational frequency of between 1 MHz and 15 MHz (Szabo 2004), with the current commercially available systems using arrays of piezoelectric transducers to produce two-dimensional (2D) or three-dimensional (3D) images of the region of interest. The transducer is excited by a pulsed voltage and in response it emits ultrasound pulses, which travel through the tissues and organs. The reflected echoes from the tissues and organs are detected by the same transducer and converted into a voltage. These electrical signals are used to reconstruct the image of the tissues in the path of the sound waves.

#### *1.1.1 History of ultrasound*

The application of ultrasound as a medical diagnostic tool is credited to the second half of the twentieth century. The physics and principles of operations have however existed as early as 1842 when Christian Doppler published his work on what is now known as the Doppler shift (Doppler 1842; Censor 1984; Hagen-Ansert 2006; McNay and Fleming 1999). In 1877 Lord Rayleigh published the theory of sound, with the

piezoelectric effect being described in 1880 by the brothers; Jacques and Pierre Curie (Strutt 1877; Curie and Curie 1880b; Curie and Curie 1880a; Mason 1981; Ballato 1996). These and many other findings contributed substantially to what is now used as medical ultrasound. The 1950s saw great steps towards what is the present-day ultrasound imaging system when Professor Ian Donald along with Mr Tom Brown carried out experiments to produce A-scan images of human tissue. These images were able to provide convincing evidence of differences in the signals obtained from solid and simple cystic tissues (Donald et al. 1958; Hagen-Ansert 2006; McNay and Fleming 1999). Donald and Brown also developed practical early B-scan technology and investigated obstetric applications for ultrasound. Another notable name in the use of ultrasound in medicine is Karl Theodore Dussick in Austria who published his preliminary findings in 1942 (Dussik 1942), suggesting that he was able to use ultrasound for detecting intracranial tumours by 1947 (Dussik 1947; Shampo and Kyle 1995).

Most early work using ultrasound in medicine was undertaken on obstetrics and gynaecology patients but ultrasound has since expanded in its applications now including, but not limited to tumour growth, blood flow measurements and blood vessel blockage detection. The discovery and integration of microchips into ultrasound systems in the 1970s facilitated exponential growth in processing power, leading to the introduction of faster and more powerful systems with digital beam-forming, signal processing, and new ways of developing and displaying data (Lyons 2004). These developments triggered a movement from mechanical scanning with single element transducers to the use of electronically controlled arrays for obtaining images.

### ***1.1.2 Current ultrasound usage***

The newest ultrasound imaging systems have advanced functions such as elastography and harmonic imaging which give more information about the tissue of interest. Three-dimensional imaging is also among the recent advances to be introduced in clinical ultrasound systems. Increased interest in the use of ultrasound has led to identification of numerous areas of application and led to improvements in the overall performance the systems. The future of ultrasound imaging is predicted to produce 3D tomography,

picking up small details that are missed by the current 4D systems. The 4D technology permits taking a 3-dimensional image in real time (Nelson 2006). The 4<sup>th</sup> dimension is time.

The medical application of ultrasound is rapidly growing and now closely follows X-rays as the most commonly used imaging modality around the world (Shung 2011; www.researchandmarkets.com 2012). The current global market for medical ultrasound is approximately US\$5.6 billion with a projected increase to US\$8.1 billion by 2017 which gives a compound annual growth rate of 6.2% (Foster et al. 2000). Trolley-based systems are the most common but there is a developing trend of device miniaturisation. This miniaturisation trend is seen in the transducers themselves and the imaging systems as a whole, as the trolleys become laptop-type portable systems. The miniaturisation of devices correlates closely with developing systems that use high frequency ultrasound for obtaining high resolution images.

### **1.1.3 High resolution ultrasound**

When technological advances in ultrasound imaging are used in combination with high frequency transducers, more avenues for clinical applications are opened. The main advantage of using high frequency ultrasound is improved resolution, which is related to the transducer wavelength (Lockwood et al. 1996). The resolution is improved from approximately 1 mm of the conventional transducers to better than 100  $\mu\text{m}$  with transducers operating above 25 MHz. The improved resolution has the potential to help in identifying small features such as tumours on the order a few cells thick. The limitation of the high frequency transducers however, is that the penetration into the tissue is reduced.

There is an unmet clinical need for imaging fine-scale features such as small tumours deep in the tissue or body. High resolution images from such regions would enable easy collection of biopsies or a potential for *in-vivo* pathological investigation if the probe can be made small enough and positioned close to the tissue region of interest. The size of an ultrasound transducer scales with the imaging wavelength, which is inversely proportional to the operational frequency. Therefore, increasing the frequency leads to smaller transducer dimensions. This has over the years presented

great challenges in achieving high frequency transducers, particularly arrays operating above 20 MHz. With recent advances in piezoelectric materials and microfabrication techniques, it has now become possible to explore the development of entire devices with millimetre scale dimensions for imaging well beyond sub-millimetre resolution.

## 1.2 Needle biopsies

Existing imaging modalities such as MRI, CT and X-rays are limited in their application. In instances such as prostate cancer, the most used modality is ultrasound imaging (Chopra et al. 2008). This however, is limited to the lower (~1 mm) resolution of the current commercially available transducers and the probe design does not allow easy access to the region of interest.

Biopsies of tissue are commonly collected where further examination of tissue or staging of disease using optical microscopy is required. Biopsy needles are positioned by a clinician in the region of interest, often using guidance from an imaging modality. Breast imaging is routinely done using low-dose X-rays but these present low resolution images. Magnetic resonance imaging (MRI) provides high resolution images of breast scans but the problem of breathing moves tissue out of position, making it difficult to accurately pin-point micro-features in the region of interest. Spinal epidural procedures are performed based on touch and feel techniques and they would benefit from imaging guidance. MRI is used to guide biopsy needles for collecting tissue samples in specific regions (Chen et al. 2004).

With all the existing imaging technologies, there is still a need to take a large number of biopsy samples from locations other than the disease focal points. This means that multi-location samples are taken and in many cases patients need to return to hospitals for second or third biopsies due to regions being missed in earlier samples. Biopsy needles come in different shapes and sizes based on their applications. The largest biopsy needle is a 14 gauge and this translates to 2 mm outside diameter (Helbich et al. 1998). A larger needle would collect more tissue but is also likely to cause more collateral damage to normal tissue. In very sensitive areas such as lymph nodes, smaller needles are used to collect biopsies.

The main impetus for the current research is the limitations of existing modalities for accurately pin-pointing regions for biopsy. This research aims to integrate an imaging device on the tip of a needle which would enable practitioners to visualise tissue at very close proximity to where the tissue samples are taken. Ultrasound presents a viable option for this technology since high frequency transducers are small enough to fit on needles and other interventional tools. The end application of the work in this thesis is to obtain a high resolution image of the whole structure, potentially giving more information than the biopsy on its own.

### 1.3 Rationale, Aims and objectives

The work presented in this thesis focuses on solving the limitation of low frequency ultrasound. Figure 1.1 shows how high frequency ultrasound can have a practical application, overcoming its own limitations. Conventional arrays similar to that in Figure 1.1(a) are limited in two ways:

- First, at lower frequencies, they have a poor spatial resolution particularly with features in the tissue structures of interest at the sub-millimetre scale. Generally, the spatial resolution is related to the wavelength, with shorter wavelengths corresponding to higher frequencies and providing better resolution (Lutz and Buscarini 2011). Thus, imaging can be improved by increasing the frequency (Figure 1.1(b)), assuming other system factors also change correspondingly.
- Second, the penetration depth is reduced when the frequency is increased, due to increased ultrasound energy absorption in tissue (Cannata et al. 2003; Foster et al. 2000). This can only be overcome fundamentally by placing the array closer to the target as illustrated in Figure 1.1(c). An example is to place the array on a needle to be inserted into the patient.

The approach of incorporating ultrasound arrays on the tip of an interventional tool (Figure 1.1(c)) such as biopsy needle is the main focus of this thesis, which sets out to provide a solution to both of the two limitations detailed above. By inserting the array at the tip of a biopsy needle, application-specific, high frequency, high resolution transducers can be used, and the limitation of sound energy attenuation by tissue at high frequencies can be overcome. This also changes the nature of the

diagnosis from non-invasive to invasive; however, clinicians often claim that such invasion would be worthwhile (Larsen 2002). The ultimate use would be to replace biopsy collection where possible with high resolution *in vivo* diagnosis using newer tissue characterisation techniques such as elastography that can be used to distinguish cancerous tissue. The potential applications of devices overcoming these challenges are numerous in oncology and their development is therefore worthwhile.

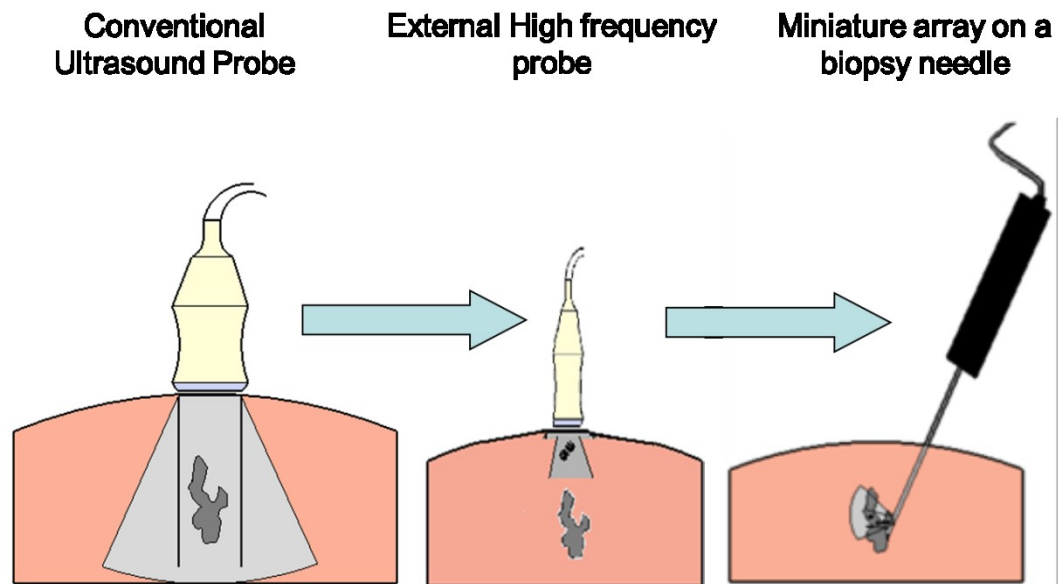


**Figure 1.1: Illustration of limitation of conventional and external high frequency ultrasound transducers. The conventional probe shown in (a) has a limitation of low resolution but penetrates deep in the tissue. The external high frequency probe (b) has the benefit of high resolution but limited tissue penetration. The miniature array on a needle (c) overcomes both the problem of resolution and tissue penetration.**

There are three main challenges to overcome:

- first, the need for a small package;
- second, the need for a high performance, high frequency array to achieve high resolution images;
- and third, the need for economical means of manufacturing.

According to the first challenge, the complete array must be packaged to fit within the dimensions of a needle. This thesis aims to contribute to the development of a package which fits within a 14 Standard Wire Gauge SWG) (2.032 mm diameter) needle. It is important to note that this is presently taken as the maximum size, with smaller diameters being better for patient comfort.

High frequency transducers have a wide use in catheters for high resolution imaging. Many commercially available catheter transducers use single element transducer which are mechanically rotated to obtain a radial image of the region of interest (van der Steen et al. 2006). Arrays with relevant dimensions have been produced previously for intravascular ultrasound (IVUS), but their configurations are generally different and, more importantly, their dimensions are bigger. For example, the AcuNav (Proulx et al. 2005) sideways-looking phased array (Siemens Healthcare, Mountain View, CA, USA) is available in 8French (F) (2.7 mm diameter) and 10F (3.3 mm diameter) versions. On the other hand, a catheter requires a significant insertion length; 110 cm for the AcuNav, which requires long cabling. The typical solution is to have some electrical switching or signal processing on a chip integrated within the probe. These custom electronic chips are very expensive but there are then minimal signal cables running the length of the catheter. However needle *in vivo* pathology allows a much shorter length between the array and the end of the needle, potentially down to just a few centimetres. Because of this, the work in this thesis assumed a positive, simplifying effect on the design by assuming hard-wiring from the flexi-circuit attached to the array head to external instrumentation.

According to the second challenge, a high frequency array is needed. A transducer with an operational frequency of 15 MHz would theoretically yield a lateral resolution of 200 - 600  $\mu\text{m}$  (Baun 2010). Although there are other factors contributing to the image resolution, the operational frequency plays the biggest part. Other factors include: element dimensions, properties of matching and backing layers, as well as focusing with a lens. Transducers with even higher frequencies, towards 100 MHz, will resolve features close to a few cells thick. The main challenge with increasing the frequency is the reduction in the dimensions of the transducer. The layers that make a transducer are all determined by the operational frequency. These micro-scale features present many challenges during the fabrication. In the work reported in this thesis, the target is to fabricate a 15 MHz ultrasound array in a needle. Another study was undertaken prior to this project to demonstrate the feasibility of fabrication of array prototype transducers operating up to 100 MHz (Demore et al. 2009), but this did not consider packaging into small probes and the overall dimensions were large. Various means to achieve such high frequencies are being explored. A key part of this thesis

describes devices made with ultrahigh performance, lead magnesium niobate-lead titanate (PMN-PT) piezocrystal composite material for high frequency applications.

According to the third challenge, the devices must be made economically. To this end, techniques were explored which lend themselves to small wafer-scale manufacturing and to efficient mass manufacturing of other components. For example, spirally-wound flexible circuits for the external connections were investigated along with initial considerations of using kerfless arrays in the future. Automated and mask-based design techniques were also under active investigation.

### **1.3.1 Aims**

The main aim of the work presented in this thesis is to investigate the feasibility of integrating ultrasound imaging arrays within needles for *in-vivo* pathological investigation.

The second aim is to develop a process for fabricating high frequency arrays incorporated into interventional tools.

### **1.3.2 Objectives**

The objectives of this research are:

- 1 Development of novel packaging techniques for integrating an ultrasound array into a needle. Wafer scale fabrication is adopted to reduce the overall cost of fabrication.
- 2 Designing a flexi-circuit to connect multiple tracks through a small diameter needle.
- 3 Define fine-pitch conductive tracks on polyimide polymer. This is to permit fabrication of high frequency transducer.
- 4 Fabrication of fine-scale single crystal composites involving PMN-PT and Manganese doped Lead Indium Niobate-Lead Magnesium NiobateLead Titanate (Mn-PIN-PMN-PT) using the conventional dice and fill method, and incorporated into transducers. These composites with pitches as small as 50  $\mu\text{m}$  with kerf of 18  $\mu\text{m}$  would allow for an operational frequency of above 15 MHz.

- 5 Investigation and evaluation of low temperature bonding methods. This overcomes the problem of using high temperature methods on the temperature sensitive single crystal materials. Bonding techniques such as ultrasonic bonding and magnetically aligned anisotropic UV curable epoxy were investigated.
- 6 Investigating the resolution integral as applied to simulated beam plots as a way of evaluating transducers at a design stage. This considers the ultrasound beams and a measure of the beam at -6 dB is taken as the lateral resolution. This is measured over the depth of field. A transducer with a higher resolution integral would have a narrow beam over a long distance

### ***1.3.3 The ISPUD partnership***

The work in this thesis was done under the Integration of Silicon and Piezoelectric Ultrasound Devices (ISPUD) project. This project involved experts from different fields from three universities and three companies. The main work was done at IMSaT, University of Dundee, by the author of this thesis, who undertook the main fabrication and packaging of the ultrasound transducer in a needle. The author's formal affiliation is to the University of Strathclyde.

The flexi-circuit fabrication and investigation of bonding techniques used in the prototypes was led by MISEC, Heriot-Watt University. Different expertise input was contributed from transducer building to dicing and lapping. The author of this thesis was fully involved in all aspects of the work done in this thesis such as the design and fabrication of the flexi-circuit and experimenting with the different bonding techniques.

## **1.4 Thesis structure**

Chapter 2 compiles a review of literature, explaining the working principles of medical ultrasound transducers, drawing on the physics and engineering mechanisms. A comprehensive review of ultrasound transducers is detailed, focusing on the trend towards high frequency transducers: applications of these transducers are highlighted.

Chapter 3 explains the different design approaches used for this research. Trade-offs are explained to enable the feasibility of the transducer. Techniques for characterising the active and passive materials as well as the finished prototypes are described

Chapter 4 discusses, with in-depth results, the different stages of fabrication with results such as impedance of plates and composites as well as the passive material velocities and attenuation. Characterisation of materials, active and passive, leading to one dimensional modelling (ODM) and virtual prototyping for the ideal transducer are presented in this chapter. The effects of limiting the transducer dimensions to fit in the needle are examined through simulation with beam patterns for the single element, linear and phased arrays explained

Chapter 5 explains in detail the process development for integrating a high frequency ultrasound transducer incorporated into a biopsy needle. The micro-fabrication methods employed are explained. The process for making high frequency piezocomposites from PMN-PT single crystals using low temperature processes, to maintain the high performance of the material, is explained. The design and fabrication of the flexi-circuit is also presented. Results investigating different bonding methods are also presented in this chapter.

Chapter 6 illustrates the fabrication of single element transducers focusing on small pitch single crystal composites. Low temperature techniques are presented as the basis for fabricating with single crystal materials. Dicing parameters for fine-scale single crystal composites are presented. Electrical matching with a micro-coaxial cable is explained and demonstrated. Results of characterising the transducers including impedance, pulse-echo and tissue imaging are illustrated.

Chapter 7 presents results from arrays at 5 MHz and 15 MHz. Results are shown demonstrating the steps of wafer scale fabrication, highlighting some of the challenges and how they are overcome. Flexi-circuit design and fabrication are also presented. The 5 MHz array is fitted into a needle and tested. Results from images of simple wire targets and tissues are shown.

Chapter 8 draws together the conclusions from the thesis, highlighting the successful steps and those requiring further improvements are discussed as future work.

## 1.5 References

Ballato, A. 1996. Piezoelectricity: history and new thrusts. In: *1996 IEEE Ultrasonics Symposium. Proceedings*. IEEE, pp. 575–583.

Baun, J. 2010. Beam Geometry. In: *Vascular Ultrasound Physics, Instrumentation, & Hemodynamics*. San Francisco, California: ProSono Publishing, pp. 101–112.

Cannata, J.M., Ritter, T. a, Chen, W.-H., Silverman, R.H. and Shung, K.K. 2003. Design of efficient, broadband single-element (20-80 MHz) ultrasonic transducers for medical imaging applications. *IEEE transactions on ultrasonics, ferroelectrics, and frequency control* 50(11), pp. 1548–57.

Censor, D. 1984. Theory of the Doppler effect: Fact, fiction and approximation. *Radio Science* 19(4), pp. 1027–1040.

Chen, X., Lehman, C.D. and Dee, K.E. 2004. MRI-Guided Breast Biopsy : *Breast* (April), pp. 1075–1080.

Chopra, R., Baker, N., Choy, V., Boyes, A., Tang, K., Bradwell, D. and Bronskill, M.J. 2008. MRI-compatible transurethral ultrasound system for the treatment of localized prostate cancer using rotational control. *Medical Physics* 35(4), p. 1346.

Curie, J. and Curie, P. 1880a. Contractions et dilatations produites par des tensions dans les cristaux hémiedres à faces inclinées. *C R Acad Sci Gen* 93, pp. 1137–40.

Curie, J. and Curie, P. 1880b. Sur l'électricité polaire dans les cristaux hémiedres à faces inclinées. *C R Acad Sci Gen* 91, pp. 383–6.

Demore, C.E.M., Bernassau, A.L., Hutson, D., Cochran, S., Garcia-Gancedo, L Dauchy, F., Meggs, C., Button, T.W., Bush, N. and Bamber, J.C. 2009. Functional characterisation of high frequency arrays based on micro-moulded 1–3 piezocomposites. In: *IEEE International Ultrasonics Symposium*. pp. 1134–1137.

Donald, I., MacVicar, J. and Brown, T.. 1958. Investigation of abdominal masses by pulsed ultrasound. *Lancet* 1(7032), pp. 1188–95.

Doppler, C. 1842. Über das farbige Licht der Doppelsterne und einiger anderer Gestirne des Himmels (About the coloured light of the binary stars and some other stars of the heavens). In: *Proceedings of the Royal Bohemian Society of Sciences*. p. Part V 465–482.

Dussik, K.. 1942. On the possibility of using ultrasound waves as a diagnostic aid. *Neurol. Psychiat.* 174, pp. 153–168.

Dussik, K.. 1947. Verfahren zur Untersuchung von Korpem mittels Ultraschall Osterreichisches.

Foster, F.S., Pavlin, C.J., Harasiewicz, K.A., Christopher, D.A. and Turnbull, D.H. 2000. Advances in ultrasound biomicroscopy. *Ultrasound in Medicine & Biology* 26(1), pp. 1–27.

Hagen-Ansert, S.L. 2006. Society of Diagnostic Medical Sonographers: A Timeline of Historical Events in Sonography and the Development of the SDMS: In the Beginning... *Journal of Diagnostic Medical Sonography* 22(4), pp. 272–278.

Helbich, T.H., Rudas, M., Haitel, A., Kohlberger, P.D., Thurnher, M., Gnant, M., Wunderbaldinger, P., Wolf, G. and Mostbeck, G.H. 1998. Evaluation of needle size for breast biopsy: comparison of 14-, 16-, and 18-gauge biopsy needles. *AJR. American journal of roentgenology* 171(1), pp. 59–63.

Larsen, S.S. 2002. Endoscopic ultrasound guided biopsy of mediastinal lesions has a major impact on patient management. *Thorax* 57(2), pp. 98–103.

Lockwood, G.R., Turnbull, D.H., Christopher, D.. and Foster, F.S. 1996. Beyond 30 MHz, Application of High-Frequency Ultrasound Imaging. *IEEE Engineering in Medicine and Biology*, pp. 60–71.

Lutz, H. and Buscarini, E. 2011. *WHO manual of diagnostic ultrasound*. Malta: WHO publications.

Lyons, E.A. 2004. Zone sonography: The next major advance in medical ultrasound.

Mason, W.P. 1981. Piezoelectricity, its history and applications. *The Journal of the Acoustical Society of America* 70(6), p. 1561.

McNay, M.B. and Fleming, E.E. 1999. Forty years of obstetric ultrasound 1957-1997: From A-scope to three dimensions. *Ultrasound in Medicine & Biology* 25(1), pp. 3–56.

Nelson, T.R. 2006. Three-dimensional Ultrasound Imaging. In: *UIA Annual Meeting*. pp. 1–5.

Proulx, T.L., Tasker, D. and Bartlett-Roberto, J. 2005. Advances in catheter-based ultrasound imaging Intracardiac Echocardiography and the ACUSON AcuNavTM Ultrasound Catheter. In: *IEEE Ultrasonics Symposium, 2005*. IEEE, pp. 669–678.

Shampo, M.A. and Kyle, R.A. 1995. For personal use . Mass reproduce only with permission from Mayo Clinic Proceedings . In: *Mayo Clinic Proceedings*. p. 1136.

Shung, K.K. 2011. Diagnostic Ultrasound : Past , Present , and Future. *Journal of Medical and Biological Engineering* 31(6), pp. 371–374.

Van der Steen, A.F.W., Baldewsing, R. a, Levent Degertekin, F., Emelianov, S., Frijlink, M.E., Furukawa, Y., Goertz, D., Karaman, M., Khuri-Yakub, P.T., Kim, K., Mastik, F., Moriya, T., Oralkan, O., Saijo, Y., Schaar, J. a, Serruys, P.W., Sethuraman, S., Tanaka, A., Vos, H.J., Witte, R. and O'Donnell, M. 2006. IVUS beyond the horizon. *EuroIntervention : journal of EuroPCR in collaboration with the Working Group on Interventional Cardiology of the European Society of Cardiology* 2(1), pp. 132–42.

Strutt, J.W. 1877. *The Theory of Sound*. London: Macmillan and Co.

Szabo, T.L. 2004. Diagnostic Ultrasound Imaging: Inside Out. In: Elsevier Academic Press, pp. 23–26, 269.

www.researchandmarkets.com 2012. Medical Diagnostic & Therapeutic Ultrasound Devices Market (2012 - 2017) - Global Trends & Competitive Analysis [Online].

# CHAPTER 2

---

## Background Theory and Literature Review

---

### Chapter Profile

The development and use of medical ultrasound transducers has continued for over 50 years, with ultrasound closely following X-rays as the most commonly used imaging modality. High resolution ultrasound imaging is one of the areas that have received much attention in recent years with researchers now focusing on translational research, investigating how the devices can be applied clinically. Such devices use high frequency transducers to obtain high resolution images.

This chapter begins with an overview of common imaging modalities, and illustrates the benefits of ultrasound. The working principles of medical ultrasound transducers are explained, drawing on physics and engineering mechanisms. An overview of the advances in ultrasound transducer development is given, focusing on the trend of high frequency transducers. Applications of these transducers are highlighted.

### 2.1 Overview of Medical Imaging Modalities

Medical imaging has provided a platform for examining the anatomy without the need for invasive surgical techniques. Since its discovery, medical imaging has changed the ways through which medicine is practised (Leiserson 2010). Techniques involving radiography, magnetic resonance imaging (MRI), positron emission tomography (PET) and ultrasound have been used over the years to assist in accurately diagnosing a wide range of diseases, abnormalities or structural defects in the body. One of the most frequent uses of imaging is in oncology, where tumours are routinely diagnosed. In some cases, such as use of X-rays to diagnose a fracture, one imaging modality provides sufficient information to obtain good medical conclusions. However, due to limitations of each imaging modality, it is becoming more common to use two or more

modalities with still a further investigation at a central biochemistry laboratory needed (Curiel et al. 2007). It is therefore useful to review the most common imaging modalities with their associated strengths and weaknesses.

A good medical imaging modality must accurately depict anatomical structures at a useful resolution, with high contrast and without any adverse side effects. Different structures are investigated using different modalities due to inherent capabilities and limitations of each modality. It is important to know what needs to be diagnosed and choose the appropriate imaging modality. The widely available modalities are radiography (X-rays and computed tomography (CT)), positron emission tomography (PET), magnetic resonance imaging (MRI), ultrasound, and optical coherence tomography (OCT). Most of these imaging systems produce a 2D representation of 3D structures but there is a trend towards obtaining volumetric images (Sakas 2002). A comparison of the different imaging modalities is summarised in Table 2.1.

**Table 2. 1: Comparison of medical imaging modalities (Szabo 2004) (<http://usedophthalmology.com>)**

<b>Modality</b>	<b>MRI</b>	<b>CT</b>	<b>OCT</b>	<b>X-ray</b>	<b>Ultrasound</b>
<b>What is imaged</b>	Biochemistry	Mean tissue absorption (density)	Optical scattering	Tissue absorption (density)	Mechanical properties
<b>Access</b>	Circumferential Around body	Circumferential Around body	Surface or external tissues	2 sides needed	Small window
<b>Spatial resolution</b>	~ 1mm	~ 1mm	0.02mm	~ 1mm	Frequency and depth dependent (0.05-3mm)
<b>Penetration</b>	Excellent	Excellent	Poor	Excellent	Frequency dependent (3-25 cm)
<b>Safety</b>	Very good	Ionising radiation	Very good	Ionising radiation	Very good
<b>Maximum Speed</b>	10 frames/sec	½ minute to minutes	27,000 A-scans per sec	minutes	100 frames/sec
<b>Cost</b>	\$\$\$\$\$\$\$\$	\$\$\$\$	\$\$	\$	\$
<b>Portability</b>	Poor	Poor	Good	Good	Excellent

### 2.1.1 Radiography

Radiography employs electromagnetic radiation from the x-ray region of the spectrum to generate an image based on how it is absorbed by the tissue. X-rays are absorbed more by tissues with higher density, so the images effectively show the relative density of tissues. The application of X-rays originates from their discovery by the physicist

Wilhelm Roentgen in 1895 (Roentgen 1895; Rontgen 1972). It was quickly adopted for medical imaging. The current systems used have an image resolution of approximately 1 mm (Szabo 2004), and this depends on the beam width and the detectors or films used to acquire the image. The current systems are moving from film to fully digital imaging X-rays and do not have sufficient contrast for differentiating between soft tissues, however they provide excellent contrast between soft tissue and dense tissue such as bone. They are commonly used for detecting bone fracture (Szabo 2004). Employing radioactive contrast agents permits the imaging of blood vessel through this modality. The main drawback of X-rays is that they are ionising radiation. The dose can be cumulative and therefore effective precautions are taken to avoid unnecessary exposure. X-rays are cheap and relatively straight forward to use which has made them the mostly commonly used modality.

The first successful implementation of CT scanners in medicine was in 1972 by G N Hounsfield (Hounsfield 1973; Kalender 2006). Computed Tomography (CT) imaging also involves the use of X-rays with the application of mathematical reconstruction to produce slices of tomographic views. In effect, CT produces images with better contrast for soft tissues than those obtained by conventional X-rays. CT scanners are most commonly used in the diagnosis of neurological disorders including tumours or haemorrhage. The resolution depends on the slice thickness, number of pixels, algorithms, data sampling as well as computer hardware. Conventional scanners have resolution of over  $0.44 \text{ mm}^3$  (Mollet et al. 2005). There are also scanners in the micro-CT category and these can produce resolutions as good as  $1 \text{ }\mu\text{m}$  with the capability of imaging both soft tissues and bones (Zagorchev et al. 2010). However these are limited to only *ex-vivo* examination of tissue with a total volume of  $1 \text{ cm}^3$ . The main drawbacks of CT scanners are that a much higher dose of radiation must be used to obtain the high resolution images, and it is expensive and not portable.

### **2.1.2 Positron Emission Tomography (PET)**

Developed in the 1970s, PET uses scintillation detectors surrounding a patient to detect positrons to produce an image. A radionuclide is either swallowed or injected into the body causing positrons to be emitted when there is interaction with positron emitting radioisotopes found in the body, for instance,  $^{11}\text{C}$ ,  $^{13}\text{N}$  and  $^{15}\text{O}$ . Due to poor spatial

resolution and signal to noise ratio (SNR), PET is mainly used for metabolic function studies, which cannot be effectively done using the other modalities (Acharya et al. 1995).

### **2.1.3 Magnetic Resonance Imaging (MRI)**

This modality, also known as nuclear magnetic resonance, was discovered in 1946 and was thereafter adopted as a medical diagnostic tool (Acharya et al. 1995; Geva 2006). The spatial resolution is dependent on the number of pixels in a given area, which in turn depends on the signal sensitivity of the scanner. When the resolution of an MRI image is increased, the signal to noise ratio is greatly reduced. It is the strength of the magnet that gives the signal strength which leads to a good resolution. It is argued that MRI currently provides the bench mark for medical imaging; it is non-ionising, minimally invasive with the capability to distinguish between soft and hard structures in the body; it provides spatial resolution of approximately 1 mm (Szabo 2004) but at research stages, strong magnets are used to yield a much better resolution. The drawbacks to using MRI are not many but very significant: it is very expensive requiring above £700,000 (Price et al. 2008) for installation along with high running and maintenance costs; it is not portable; artefacts are produced due to movement of the patient in the machine and therefore it is not real-time; people with metallic implants cannot be imaged with MRI; it is known to cause dizziness, with increased strength of magnetic fields. MRI in the form of functional MRI (fMRI) can be used to monitor haemodynamic activities in the brain but it is not real time.

### **2.1.4 Optical Coherence Tomography (OCT)**

In this technique, low-coherence interferometry is used to generate images of the optical scattering of the microstructures in tissue. It scans in the same way an ultrasound pulse-echo device works. It is credited for its outstanding spatial resolution of below 2  $\mu\text{m}$ , with commercial devices being utilised in ophthalmology (Gabriele et al. 2011; Fujimoto et al. 2000). The drawback of OCT is the limited depth of penetration with the maximum being around 2 mm in high scattering tissues such as skin and small blood vessels (Schmitt 1999). In optically translucent tissues similar to the eye and frog embryos, it has been reported to have a penetration of about 2 cm

(Schmitt 1999). However, the tissues of interest for *in vivo* pathology are not optically translucent and therefore the penetration depth is limited to 1 – 2 mm (Schmitt 1999).

### 2.1.5 Ultrasound Imaging

Medical ultrasound imaging is an imaging modality for soft tissue which uses the pulse-echo technique to form images of the structures. The pulses of ultrasound are emitted into the object of interest as shown in Figure 2.1. The sound energy propagates through the object until there is discontinuity in the acoustic impedance of the material. The energy is reflected back at the interface and the time taken for the echoes from the object to return to the transducer is used to determine its position. The amplitude of the received signal determines how reflective the structure is to the ultrasound energy.

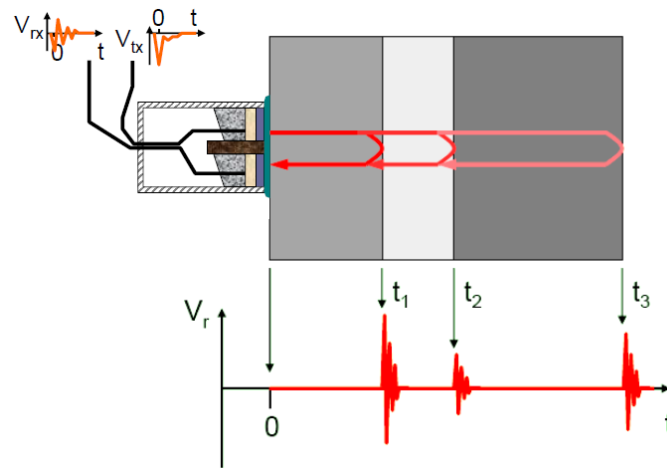


**Figure 2. 1: Pulse-echo imaging showing A-mode scan of structures at different times  $t_1, t_2$  and  $t_3$ . The signal is received as a voltage with a specific amplitude (courtesy S. Cochran, University of Dundee).**

The information obtained by the ultrasound probe can be displayed in form of A-mode or B-mode. A-mode: A-mode is also called the amplitude mode and is where the information is represented by amplitude according to the strength of the signal. In B-mode, the strength of the signal is represented by brightness. This is the most common mode and is more commonly referred to as 2D mode.

Conventionally, diagnostic ultrasound has an operational frequency below 15 MHz (Szabo 2004; Smith and Fry 2004) corresponding to a minimum imaging wavelength of 100  $\mu\text{m}$  in tissue, with equivalent best resolution. As a non-invasive diagnostic tool, ultrasound uses real-time B-mode for application in various fields of clinical medicine

(Schmid-Wendtner and Dill-Müller 2008). These include, among many others, internal medicine, gynaecology, and ear, nose and throat conditions. The ultrasound scans can also be used to monitor the effectiveness of a given therapy such as chemotherapy or radiotherapy by monitoring the size of tumours. It should be noted however that currently it is difficult to identify malignant tumours with ultrasound scans, and tissue specimens are typically needed to definitively diagnose cancer type or staging by pathologists. The tissue property that ultrasound imaging detects is the change of acoustic impedance. The acoustic impedance is the opposition to the flow of sound waves through a surface. Typical acoustic properties of tissue are shown in Table 2.2. Although human soft tissues have similar acoustic impedances, the high sensitivity and corresponding high image contrast detect scattering due to differences in the tissues.

**Table 2. 2: Typical human tissue acoustic properties (Azhari 2010)**

Tissue or Material	Density (g/cm <sup>3</sup> )	Speed of Sound (m/sec)	Acoustic Impedance [kg/(sec·m <sup>2</sup> )] × 10 <sup>6</sup>
Water	1	1480	1.48
Blood	1.055	1575	1.66
Fat	0.95	1450	1.38
Liver	1.06	1590	1.69
Kidney	1.05	1570	1.65
Brain	1.03	1550	1.60
Heart	1.045	1570	1.64
Muscle (along the fibers)	1.065	1575	1.68
Muscle (across the fibers)	1.065	1590	1.69
Skin	1.15	1730	1.99
Eye (lens)	1.04	1650	1.72
Eye (vitreous humor)	1.01	1525	1.54
Bone axial (longitudinal waves)	1.9	4080	7.75
Bone axial (shear waves)	1.9	2800	5.32
Teeth (dentine)	2.2	3600	7.92
Teeth (enamel)	2.9	5500	15.95

The particular imaging application normally dictates the size and configuration of the transducers. Most common types have a large footprint and obtain images transcutaneously from outside the body. With increased research in material science and micro-fabrication techniques, new classes of transducers have been developed. These are small transducers that can access small areas via endoscopes and are also used in minimally invasive surgery (Zhou et al. 2011). As a result of the size of these

transducers, their operational frequencies (10-50 MHz) are in some cases considerably higher than the conventional transducers. These high frequency ultrasound transducers (HFUS) have applications in areas where high resolution images are required. Such applications include ophthalmology, dermatology and intravascular (IVUS) imaging (Lockwood et al. 1996) where they are used as single element mechanically scanned devices. The mechanical scanning happens when the transducer is either rotated by a motor or moved in translational way to collect information for forming an image.

Dermatology and Ophthalmology can use fairly big probes, but need the high frequency. In these instances these applications have adopted HFUS earlier. It has been easier to fabricate such probes, usually using single element transducers and mechanical scanning rather than arrays.

Figure 2.2 illustrates a summary of the common imaging modalities comparing the resolution and the depth of penetration through the tissue. The resolution of ultrasound varies with operational centre frequency and also depends on the size of the active aperture of the transducer, the transducer bandwidth, the focal depth and pulse length (Szabo 2004). The resolution of HFUS can be comparable to OCT but penetrates deeper into the tissue although one of the drawbacks of these HFUS devices is the increased attenuation, with increased frequency, which leads to reduced level of penetration into the tissue. The attenuation comes mainly from increased scattering at the high frequency due to a short wavelength. Transducers operating at about 50 MHz can image up to a depth of 20 mm as opposed to the conventional ones operating at about 3.5 MHz that can be beyond 150 mm.

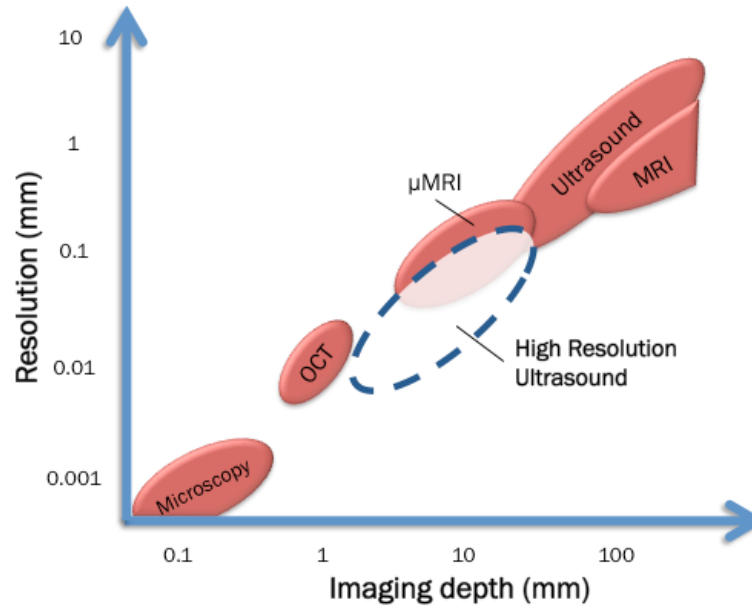


**Figure 2. 2: Comparison of imaging modalities in terms of resolution and imaging depth**

The advantage of using high frequency ultrasound imaging over other modalities can be summarised as follows:

- It is non-destructive, non-ionising
- Probes can be integrated into clinical tools
- Images show differences in mechanical properties
- It is relatively cheap and mobile
- It provides images in real-time imaging
- It also has the possibility to build up a 3D image by moving or rotating a 2D probe.

These properties mean that HFUS would be the most suitable for integration into a biopsy needle, which is the focus of this thesis.

## 2.2 Transducers Stacks and Ultrasound Generation

A medical imaging transducer is composed of a piezoelectric material, a backing medium, matching layers and cables to transmit power and information. The piezoelectric material is excited with a short voltage pulse and as a result, it expands and contracts to emit an ultrasound wave. The thickness of the piezoelectric material is a half of the wavelength,  $\lambda$ , in the piezoelectric material at the operating frequency

of the transducer,  $f$ . The wavelength and frequency are related by the speed of sound in a particular material,  $c$ , by the equation:

$$f = \frac{c}{\lambda} \quad 2.1$$

Medical diagnostic ultrasound uses a pulse-echo technique, which uses the same transducer for transmitting and receiving signals (Hunt et al. 1983; Hendree and Ritenour 2002).

Ultrasound transducers can either be single element or array based with many independent elements in one probe. A single element transducer with its important components is shown in Figure 2.3. There are many design rules to consider when developing a new transducer. The primary design considerations are discussed below and in the following sections.

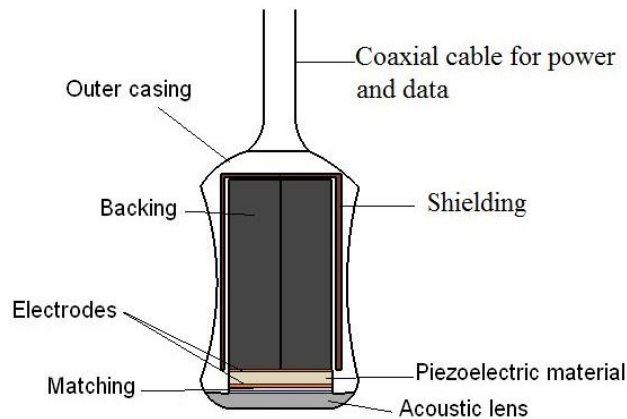


**Figure 2. 3: The structure of an ultrasound transducer with details of different layers. It show the active layer which is the piezoelectric material, the matching, backing and other components**

The ultrasound waves generated by the piezoelectric material are transmitted to the tissue through matching layers, which allow efficient transfer of ultrasound energy. They are designed with an acoustic impedance which lies between that of the piezoelectric material and the tissue to be imaged. In order to have a broadband transducer, a backing material is used and this improves the resolution. Radiofrequency (RF) interference is limited by shielding with a conductive medium.

### 2.2.1 *Passive Materials*

The acoustic impedance of the transducer must be effectively coupled with human tissue for smooth energy transfer. The design of passive matching and backing layers is useful in improving the resolution of the system through increasing the transducer

bandwidth (Gururaja and Panda 1998). Passive materials are usually polymers often filled with particles to achieve the desired acoustic properties.

Backing layers are dense, acoustically lossy materials (Wang et al. 2001). They provide structural support to the transducer and also are most importantly used to improve the bandwidth of a transducer. Using a backing layer with similar acoustic impedance as the active substrate will damp down the vibration and therefore reduce the mechanical Q of the transducer as illustrated in Figure 2.4. The lower Q results in an improved image resolution since it signifies reduction of reflections within the transducer that otherwise would generate longer signals and consequently a longer pulse-echo response for the image. It also damps ringing and gives wider bandwidth. It however reduces the sensitivity by absorbing much of the energy. A trade-off is therefore needed between resolution and sensitivity. Typical backing layers are polymers filled with heavy metal particles such as tungsten.

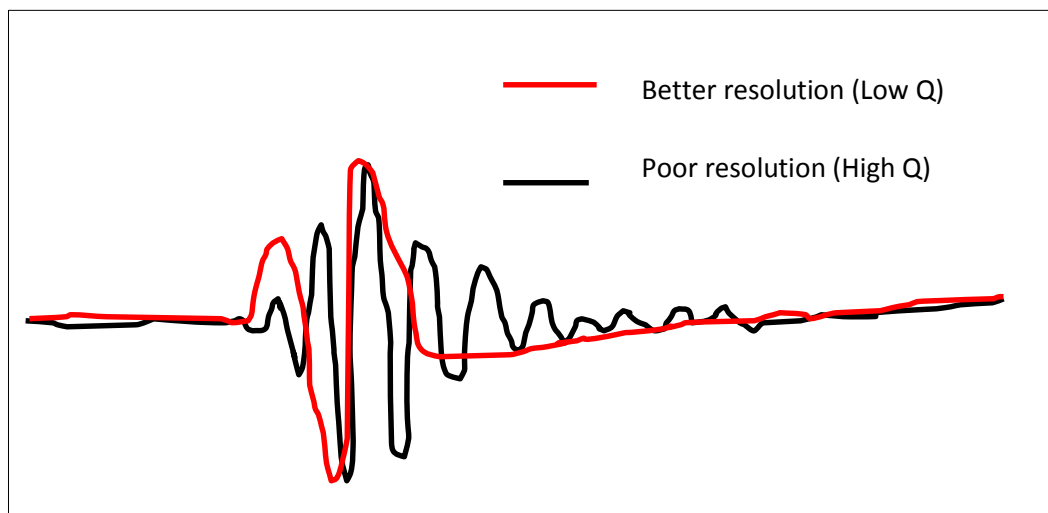


**Figure 2. 4: A sketch of an A scan showing how the resolution improves with matching and backing layers. The backing and matching layers lowers mechanical Q which improves the resolution.**

Matching layers are commonly polymers filled with alumina particles (Draheim and Cao 1996; Zhou et al. 2009). There can be as many as four of these layers sitting between the active piezoelectric substrate and tissue. They are designed to be a quarter of a wavelength thick and at the operating frequency are used to improve the transmission of energy between the low acoustic impedance of tissue, which is approximately 1.5 MRayl, to match that of the piezoelectric material, which is usually

greater than 15 MRayl. An ideal matching layer design and selection is to achieve maximum sensitivity with the shortest ring down. The details of how the matching layers were designed for the devices in this thesis are given in Chapter 4.

The lens is use for focusing the beam so that the resolution is improved.

### 2.3 Piezoelectricity and Piezoelectric Materials

Medical imaging ultrasound transducers use the inverse piezoelectric effect to generate ultrasound waves, and the piezoelectric effect to receive mechanical echoes which are transformed into an image. Piezoelectricity, identified by the Curie brothers in 1880, is a phenomenon where certain materials produce an electric potential difference upon application of pressure. Piezoelectricity is closely linked to crystal asymmetry and polarity, and is not present in completely isotropic materials. The charge created on the surface of the material is approximately proportional to the mechanical stress applied. These materials are known as piezoelectric materials. They also exhibit the inverse piezoelectric effect, where applying a voltage to these materials creates a deformation (Madou 1997).

The material either expands or contracts based on the polarity of the applied electrical field. By applying an alternating current, the material will continuously resonate generating a mechanical wave. The resonance will be at a frequency which is based on the mechanical properties of the material. This resonance frequency can be detected by measuring the electrical response of a device with a network analyser or impedance analyser.

The behaviour of piezoelectric materials is characterised by electromechanical properties. These properties are anisotropic and the piezoelectric constitutive equations take into account the varying mechanical, electrical and the different piezoelectric properties in directions of action (Cobbold 2007). The mechanical variables (stress  $T$  and strain  $S$ ), which are second rank tensors, are related to the electrical variables (electric displacement  $D$  and the electric field  $E$ ), which are vectors, through the four equivalent forms of the constitutive equations (Smits 1976) below:

$$\begin{pmatrix} S \\ D \end{pmatrix} = \begin{pmatrix} s^E & d' \\ d & \epsilon^T \end{pmatrix} \begin{pmatrix} T \\ E \end{pmatrix} \quad 2.2$$

$$\begin{pmatrix} S \\ E \end{pmatrix} = \begin{pmatrix} s^D & g' \\ -g & \beta^T \end{pmatrix} \begin{pmatrix} T \\ D \end{pmatrix} \quad 2.3$$

$$\begin{pmatrix} T \\ D \end{pmatrix} = \begin{pmatrix} c^E & -e' \\ e & \epsilon^S \end{pmatrix} \begin{pmatrix} S \\ E \end{pmatrix} \quad 2.4$$

$$\begin{pmatrix} T \\ E \end{pmatrix} = \begin{pmatrix} c^D & -h' \\ -h & \beta^S \end{pmatrix} \begin{pmatrix} S \\ D \end{pmatrix} \quad 2.5$$

where,  $s^E$  and  $s^D$  are the specific elastic compliances at constant electric field and displacement respectively;  $c^E$  and  $c^D$  are the elastic stiffness at constant electric field and displacement respectively;  $\epsilon^T$  and  $\epsilon^S$  are the permittivity at constant stress (unclamped) and constant strain (clamped) respectively; and  $\beta^T$  and  $\beta^S$  are the inverse permittivity at constant stress and strain respectively; and the suffix, ', symbolises the transpose of the tensor. The variables  $e$  and  $h$  are piezoelectric stress constants and  $d$  and  $g$  are piezoelectric strain constants.

The displacement of the piezoelectric material depend on the applied electric field, the piezoelectric material used and the length.

### 2.3.1 Types of Piezoelectric Materials

There are a few classes of piezoelectric materials each with different properties. Among these are polymers, ceramics, single crystals and composites (Smith 1986). All these classes have been studied for medical imaging, each having some advantages and drawbacks. Among the desired material characteristics for imaging transducer materials are: acoustic impedance close to that of tissue to enable efficient energy transfer into the tissue; high electromechanical coupling coefficient ( $k$ ) for efficient conversion between electrical and mechanical energy; high clamped (constant strain) dielectric permittivity ( $\epsilon_{33}$ ) for easy electrical matching to power cables and low or moderate mechanical  $Q$  for improved axial resolution. The clamped dielectric

permittivity is used to determine the electrical operating impedance of the transducer. Table 2.3 compares one type of single crystal material, PMN-PT and a common piezoelectric polymer, poly(vinylidene fluoride) (PVDF) to a common type of piezoelectric ceramic material, PZT-5H, that is very widely used in medical imaging transducers.

**Table 2. 3: Comparison between PZT, PVDF and single crystal properties**

Property	Symbol (Units)	PZT-5H (Ming Lu and Proulx 2005)	PMN-29PT (Single crystal) (Qiu et al. 2011)	PVDF (Foster et al. 2000; Dargaville et al. 2005)
Relative permittivity at constant strain	$\epsilon_{33}^S/\epsilon_0$	1300	3026	6.0
Relative permittivity at constant stress	$\epsilon_{33}^T/\epsilon_0$	3800	8266	10
Transmission coefficient	$d_{33}$ (C/N) $\times 10^{-12}$	593	1380	25
Reception coefficient	$g_{33}$ (VmN <sup>-1</sup> )	28.2	30.33	230
Thickness mode coupling coefficient	$k_t$	0.50	0.57	0.15
Longitudinal coupling coefficient	$k_{33}$	0.70	0.89	0.20
Density	$\rho$ (kg/m <sup>3</sup> )	7450	8050	1780
Acoustic Velocity	$c$ (m/s)	3970	4660	2200
Acoustic impedance	$Z$ (MRayl)	30	37.9	3.9
Curie Temperature	$T_c$ (°C)	190	150	195 °C

PVDF is a piezoelectric polymer material that is more commonly used for imaging applications above 15 MHz ( Foster et al. 2000). Among the desirable characteristics are: it can easily be made into thin films; has low acoustic impedance close to human tissue; and can be easily focused without the need of lenses. However, it has very low electromechanical coupling coefficient which compromises efficiency. Crucially, the very low permittivity means they would not be suitable for making arrays, which are the main focus of this thesis.

The most commonly used piezoelectric materials for imaging transducers are lead zirconate titanate (PZT) ceramics. These are polycrystalline ceramic materials with crystalline grains of 1-10  $\mu\text{m}$  randomly fitted together. The random arrangement means that the overall piezoelectric effect is cancelled out in the material and it is reintroduced upon application of a large electric field, usually near the Curie temperature, in a process known as poling. This aligns material domains in the direction of the applied field. Removing the electric field will leave the ceramic

material with a remnant polarisation, making it piezoelectric. The material is anisotropic, with the poling axis showing different properties to the other axes. PZT materials have an acoustic impedance of around 30 MRayl and have a permitted device fabrication temperature of slightly above 100°C (Ming Lu and Proulx 2005). This temperature is  $\frac{3}{4}$  of the Curie temperature  $T_c$  which is the temperature at which a piezoelectric material de-poles. The PZT materials are made with different dopants to tailor the performance for specific applications. PZT-5H (Navy Type VI) ceramic, which is one of the PZT materials, is suitable for small elements of the transducer array areas due to its large dielectric permittivity (Shung et al. 2007). This makes it easier to match to the resistance of the driving electronics and hence more efficient at transferring signals. This property makes it suitable for medical imaging applications.

Single crystals piezoelectric materials on the other hand have no grain boundaries. For imaging applications, they exhibit considerably higher performance than other piezoelectric materials. The materials have a high electromechanical coupling coefficient ( $k_t$ ), permittivity and transmission coefficient. The main drawback is that the current single crystal materials need lower temperatures, below 60°C, during fabrication processes because of the lower Curie temperatures and a crystal symmetry phase transition at about 80°C (Qiu et al. 2011). They are also significantly more expensive than the other materials. They are brittle and easy to break due to lack of grain boundaries. Recently, much research is pointing towards using single crystals. They have superior properties than the other materials but their limitation lies in them being very difficult to work with. To this end, an extensive review on fabrication of transducers with single crystals is given in Section 2.6.5.

Lead magnesium niobate-lead titanate (PMN-PT) is a binary material and it is a relatively new generation of single crystal piezoelectric material with the desired improved properties. It has gained much interest, with many researchers and companies using it in new transducers. It can only withstand a working temperature of 60°C (Qiu et al. 2011) and it is very brittle. An even newer type of this material (Neumann et al. 2011), manganese doped lead indium niobate-lead magnesium niobate lead titanate (Mn:PIN-PMN-PT) is a doped ternary material and has improved Curie temperature and also a higher phase transition temperature. This means it can be

worked upon at over 80°C. It is, however, more expensive and have not yet achieved wide use. Because of their improved properties, these two types of single crystal materials were chosen to evaluate the fabrication of prototype arrays in this thesis. The fabrication process developed is based on the fabrication temperature limitations of binary PMN-PT single crystal since it is more common and cheaper than the doped ternary material.

Piezoelectric composites used in ultrasound transducers incorporate a union of passive polymers and a piezoelectric material (Figure 2.5) (Smith 1986; Smith 1990). The optimal structure is the 1-3 connectivity where piezoelectric pillars are surrounded by a passive polymer matrix. The addition of a polymer lowers the acoustic impedance, from about 36 MRayl to below 17 MRayl, depending on the volume fraction. This is a benefit of composites. Another primary benefit is that the coupling coefficient is close to the pillar longitudinal coupling coefficient ( $k_{33}$ ), which is always higher than the thickness mode coupling coefficient ( $k_t$ ).

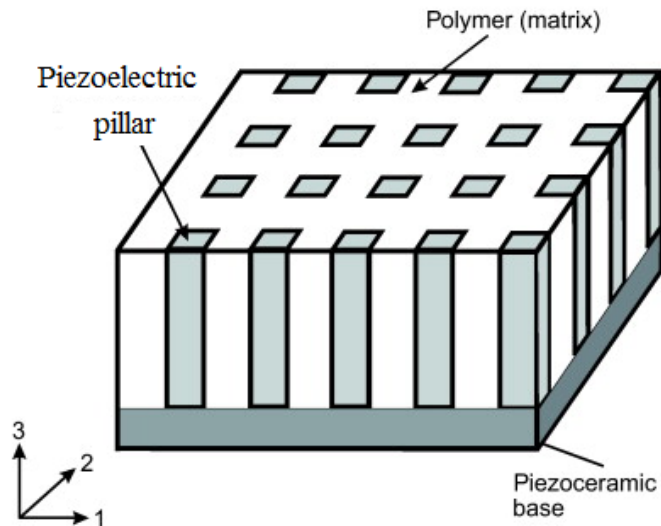


**Figure 2. 5: A schematic representation of a 1-3 composite. The piezoelectric material pillars are surrounded by a polymer material.**

For any of the materials, composites can take advantage of the desired properties while minimising the poor qualities. They provide the best compromise among all the properties of the materials including acoustical impedance, bandwidth, dielectric properties, electromechanical efficiency and signal-to-noise ratio for single-element and array transducers (Foster et al. 2000).

Due to the advantages of piezoelectric composites, they will be used in the devices developed and discussed in this thesis.

### ***2.3.2 Electrical Impedance and matching***

The electrical impedance is a factor in ultrasound transducer design and fabrication. It is one of the ways to characterise the performance of a transducer starting from the piezoelectric material itself and the effect of adding other layers and cables. Introducing a matching or backing layer will damp the resonance, which will give a wide and broader profile. This is an indication of increased bandwidth. A typical electrical impedance spectrum is shown in Figure 2.6. It shows the resonance modes of a transducer obtained from a simulation of a PZT plate to show the main modes of resonance. When a voltage is applied across the piezoelectric material, it vibrates at a given frequency. The resonance (electrical) frequency is the frequency at which the material vibrates at its natural frequency. At this frequency, the piezoelectric material vibrates with the minimum impedance (maximum admittance). The maximum impedance (minimum admittance) frequency is the anti-resonance (mechanical) frequency. The electrical impedance is a measure of the opposition to current upon application of a voltage. Impedance has both phase and magnitude and it applies to AC circuits. Admittance is the inverse of impedance.

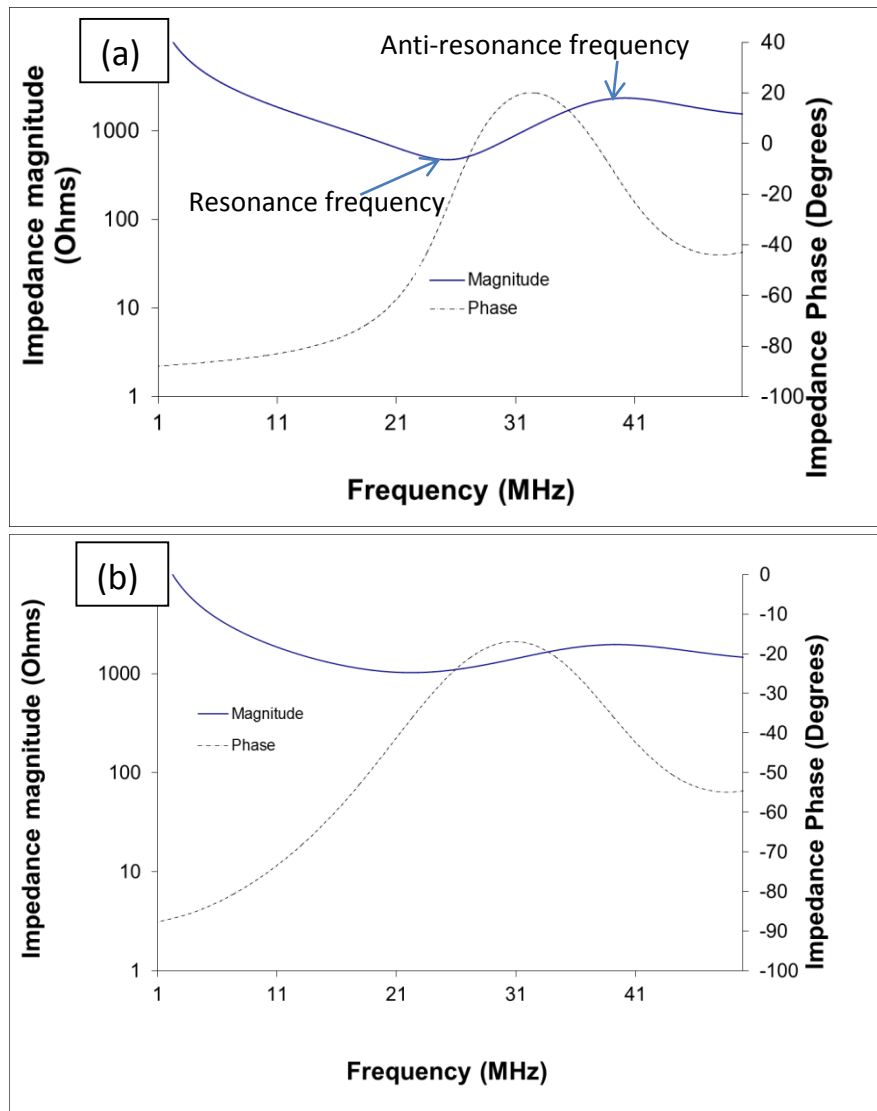


**Figure 2.6: Electrical impedance plots showing a typical magnitude and phase for a piezoelectric ceramic plate resonating in thickness-mode: (a) A plate without matching and backing layer; (b) the same plate with matching and backing layer.**

When the piezoelectric plate thickness dimensions are close to the width or the length of the piezoceramic, a second, unwanted, resonance corresponding with the lateral dimension is seen close to the frequency range of interest (Demore 2006). This leads to a reduction in the sensitivity of the thickness-mode resonance and gives a poor pulse. It is therefore necessary to have a width-to thickness (or length-to-thickness) aspect ratio of less than 0.6 for a thin, tall pillar in a composite (Liu et al. 2001), or more than 3 for a wide, flat plate in order to allow only thickness mode resonance.

The plot gives an indication of how the electrical impedance magnitude matches to the transmit and receive circuit electronics. A well electrically matched transducer leads

to efficient transfer of signals through the transmission cables. In order to eliminate reflections in the signal cable, the electrical impedance of the transducer should ideally be matched to  $50 \Omega$ , which is the characteristic electrical impedance of the transmission cables. Arrays with small elements can have large electrical impedance since the electrical impedance magnitude has an inverse proportional relationship with the transducer area. A small transducer element would need a material with a large dielectric constant,  $\epsilon$ , since the electrical impedance is also inversely proportional to the dielectric constant of the transducer substrate.

### 2.3.3 Electromechanical coupling coefficient

The coupling coefficient is a commonly used property of the piezoelectric material. It measures the efficiency of conversion of the electrical energy to mechanical energy and vice-versa. Higher coupling coefficient signifies a more efficient material or transducer. For a thickness mode material, the coupling coefficient,  $k_t$ , is given by (Liu et al. 2001):

$$k_t = \sqrt{\frac{\pi f_r}{2 f_a} \tan \frac{\pi f_a - f_r}{2 f_a}} \quad 2.6$$

Where  $f_r$  and  $f_a$  are the resonance and anti-resonance frequencies respectively as illustrated in Figure 2.6.

When matching and backing layers are used to increase the damping the distance between the resonance and the anti-resonance frequencies increases (as illustrated in Figure 2.6, and there increasing the  $k_t$  of a transducer.

## 2.4 Transducer Design and Performance

Apart from choosing the right materials for the transducers, there are many other factors to be considered in order to produce a good image. The driving factor is to get a good contrast resolution with the anatomic features easily distinguishable (Cobbold 2007). The image quality depends on three main performance criteria: axial resolution; lateral resolution; and dynamic range in the image. These in turn depend on three main design criteria: the design of the transducer layers; the geometry; and the image processing system.

### 2.4.1 Axial Resolution

Axial resolution of a transducer is the ability to distinguish between closely placed reflectors along the wave propagation direction. This is determined by the duration of the pulse-echo response of the transducer. The axial resolution  $R_A$  is given by the equation:

$$R_A = \frac{1}{2} v_t t_p \quad 2.7$$

where  $v_t$  is the sound velocity in tissue and  $t_p$  is the time duration for the pulse amplitude to decay to -6 dB of its maximum amplitude shown in in Figure 2.7. This is improved by effective design of the matching and backing layers since it is affected by the resonance frequency and damping of the resonance. A heavily damped transducer will have a very short pulse length and therefore improved resolution and bandwidth of the transducer (Qiu et al. 2011). However the heavy damping also reduces the sensitivity of the transducer.

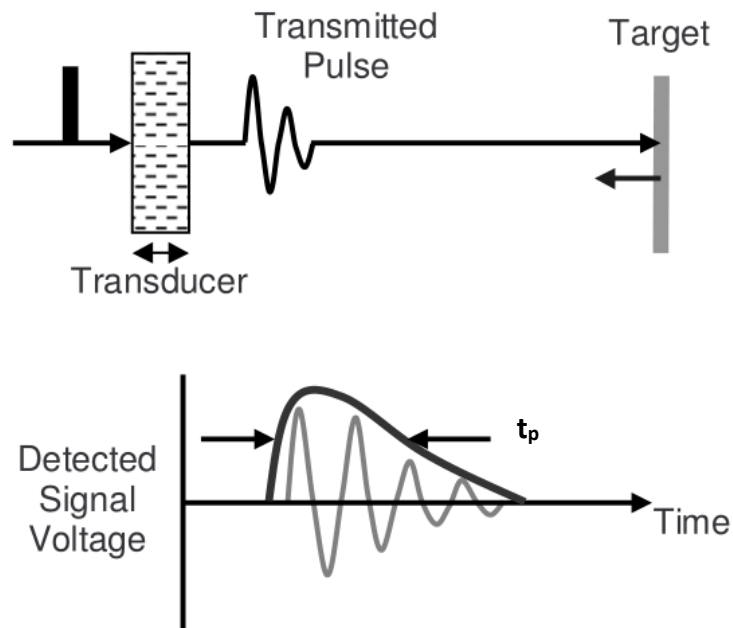


Figure 2. 7: A diagram illustrating the pulse-echo response of a transducer and the pulse length  $t_p$  which is used to determine the axial resolution (Demore 2006)

### 2.4.2 Beam profile and lateral resolution

The shape of a beam from a circular transducer is illustrated in Figure 2.8. The ultrasound beam depends on the aperture size. The aperture of the single element is

the element size whereas that of an array means all the elements activated simultaneously. A larger aperture produces a narrow beam which improves the resolution at a given frequency. For this, the aperture needs to be much larger than wavelength at the transducer operating frequency. A beam from a small element aperture will diverge more compared to that with a larger aperture and there will be larger side lobes. Side lobes are unwanted parts of the ultrasound beam emitted off axis that produce image artefacts due to error in positioning the returning echo (Paul et al. 1997). They are multiple beams of low-amplitude ultrasound energy that project from the main beam axis.

The lateral resolution is the ability to separately detect closely placed reflectors in a line perpendicular to the transducer. The size of the transmit and receive aperture greatly affects the performance of the transducer. Large aperture size leads to improved lateral spatial resolution in a focused transducer. Single element transducers can be fabricated with a geometric curve to enable focusing at a given depth along the axis of the beam. The width of the beam determines the spatial resolution and therefore, at the focused region, the resolution of the transducer will be maximised. Some single element transducers and arrays use lenses for focusing. In this respect the lens must be acoustically matched to the tissue. The focusing power of a transducer is determined by the f-number (f #) which is given by:

$$f\# = \frac{r}{D} \quad 2.8$$

where r is the focal length and D is the aperture diameter; this is in turn used to determine the lateral resolution  $R_L$ , by:

$$R_L = \lambda \frac{r}{D} = \lambda f\# \quad 2.9$$

where r is the focal distance, which is the distance from the transducer to the focal point; D is the diameter of the transducer; and  $\lambda$  is the wavelength. For planar transducers, the beam generated by an ultrasound transducer has two separate regions: the near field (Fresnel), which is the region between the transducer and the focal point; and the far field (Fraunhofer) which is after the focal zone. The width dimension of

the focal zone, also termed the depth of field, defines a region over which the pulse-echo signal is within -6 dB of the maximum at the focal point. This is the region that can be used for imaging with a focused single element transducer. The better the resolution, the smaller the depth of field in single element transducers.

The length of the near field  $N$ , can be approximated by:

$$N = \frac{D^2}{4\lambda} \quad 2.10$$

This approximation fits best to continuous mode application but can also be used for pulsed systems.

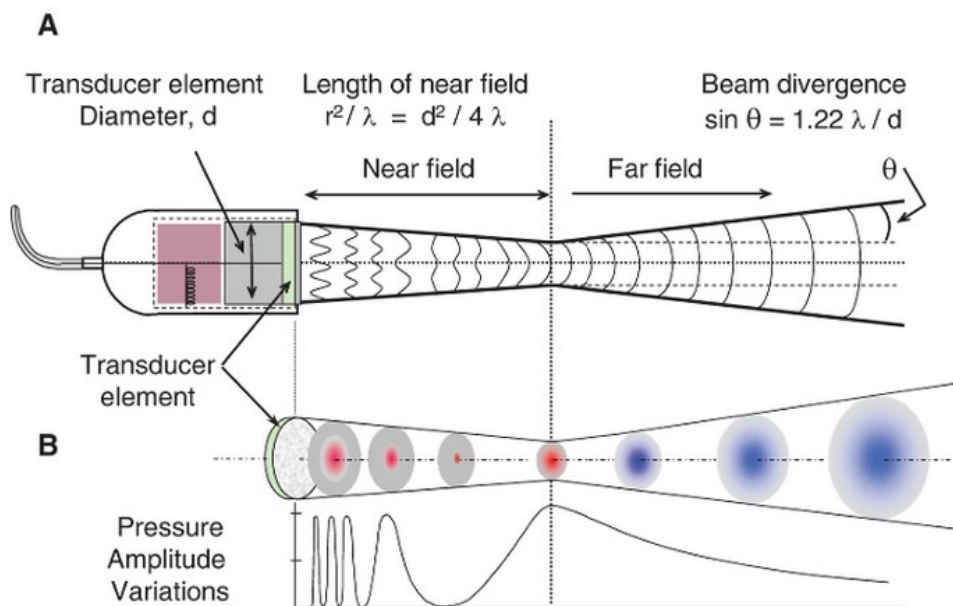


Figure 2. 8: Beam profile of a single element circular transducer (Bushberg et al. 2011)

### 2.4.3 Sensitivity and image contrast (or dynamic range)

Sensitivity is the ability of a transducer to detect reflectors in the imaging medium. A transducer with high sensitivity will have increased penetration and higher signal to noise ratio (SNR). High SNR will lead to increased dynamic range. As well as the matching and backing design, sensitivity is affected by the  $k_t$  of the piezoelectric components used. When designing a good transducer, a trade-off has to be made between sensitivity and resolution.

The Dynamic range of the image is the ratio of the maximum to the minimum signal to noise strength in an image. It determines how many shades of gray are visible in an image

## **2.5 Ultrasound Arrays, Beam Forming and Focusing**

Ultrasound arrays have received much attention over the recent years due to their advantages compared to single element transducers. In comparison to single element transducers, arrays provide quicker imaging with more flexibility over the beam pattern and direction. This is because beam focusing with arrays is done by electronics rather than mechanical scanning needed for single element transducers. This enables focusing throughout the depth of the beam, which is not possible with single element transducers.

### **2.5.1 *Imaging with Arrays***

Ultrasound arrays can have linear or annular configurations as shown in Figure 2.9. The design requirements differ dependent on the type of array. Linear and linear phased arrays have the same advantages over annular arrays as over single element transducers. They require no moving parts due to electronic scanning and therefore can generally achieve higher frame rate. This permits real time and blood flow imaging.

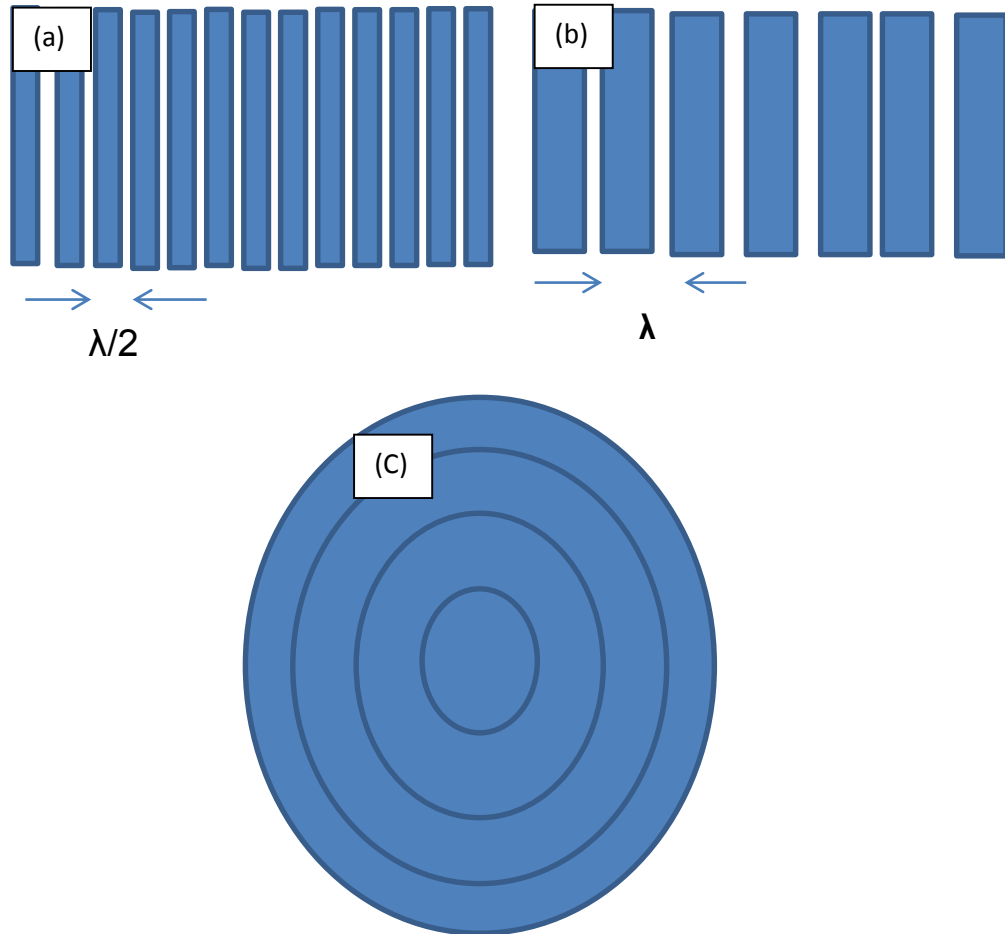


**Figure 2.9: Types of arrays; (a) Phased array, (b) Linear array, (c) Annular array**

A linear array is subdivided into elements in the azimuthal direction as illustrated in Figures 2.9 and 2.10. The transmitted acoustic energy travels in the axial plane. The dimensions of each element and the spacing between them are important in producing the desired beam pattern. The spacing between the elements, the kerf, is usually cut into the matching and backing layers to reduce acoustic crosstalk improving the image. The pitch,  $p$ , is the distance between the centres of two neighbouring elements.

The main difference between a linear and a phased array is the inter-element pitch. Linear arrays have a pitch of around one wavelength ( $\lambda$ ) and phased arrays have a pitch of  $\lambda/2$  in the material the wave will be transmitted in, which is, in the case of this project, human tissue. The inter-element pitch is determined by the way an image is acquired. A linear array forms an image through sequential activation of sub-apertures (small groups of elements). For this reason, linear arrays can have as many as 256

elements, which give the approximate width of the image related to the aperture. A linear array will preferably have at least 64 active elements. Table 2.4 below compares three arrays with different design parameters, pitch and length, operating at different frequencies. A phased array produces a steered sector scan and this requires the ability to steer the beam at big angles from the axis. For this, narrow elements with broad directivity are required. Phased arrays can be steered due to the small pitch and therefore the size of the image can be bigger than the aperture. The steering depends on whether the steering angle does not introduce interference lobes in the main image. Time delays to the array elements are defined by a beamformer which performs focusing and ultrasound beam steering.

**Table 2. 4: Comparison of 64 element linear array parameters with different frequencies**

Frequency (MHz)	Pitch ( $\mu\text{m}$ )	Total array length (mm)	Image resolution ( $\mu\text{m}$ )	Image depth (mm)
5	300	19	600 – 1500	200
15	100	6.4	200-600	60
50	30	1.9	60 -150	10

Focusing and steering with linear arrays is limited to one plane (azimuth plane) shown in Figure 2.10. Focusing in the elevation plane is usually achieved by using a lens. The beam width in the elevation plane determines the slice thickness of the imaging plane. Since the lateral resolution is dependent on the lateral beam width, focusing is also important in getting a good resolution. In arrays, focusing is done by the electronics, which is an advantage they have over single element transducers. Linear arrays can focus and steer the ultrasound beam electronically by having pitch which is  $\frac{1}{2}$  of the wavelength of sound in tissue (Silva and Fatemi 2002). These phased arrays can direct the beam radiation pattern well enough that spurious artefacts are not introduced into the image from grating lobes (Clay et al. 1999).

A linear phased array is similar to a linear array but it can both focus and steer the ultrasound beam (Figure 2.11) by introducing time delays to the element exciting and reception signals (Shung and Zipparo 1996).

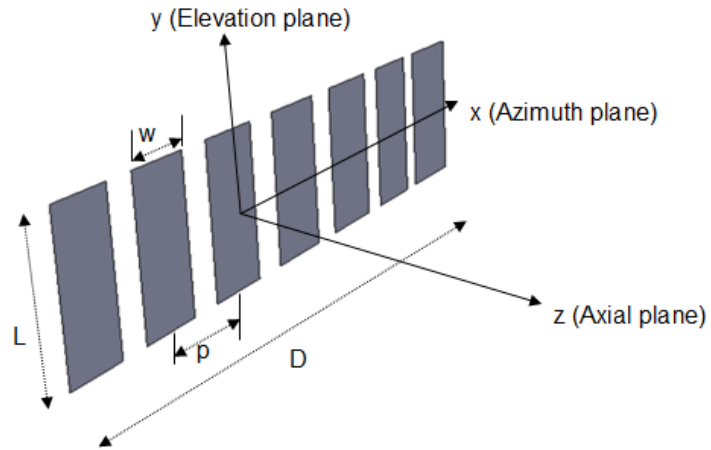


Figure 2. 10: The parameters of linear array with spatial coordinates system:  $w$  is the width of the element;  $L$  is the length,  $p$  is the pitch and  $D$  is the aperture.

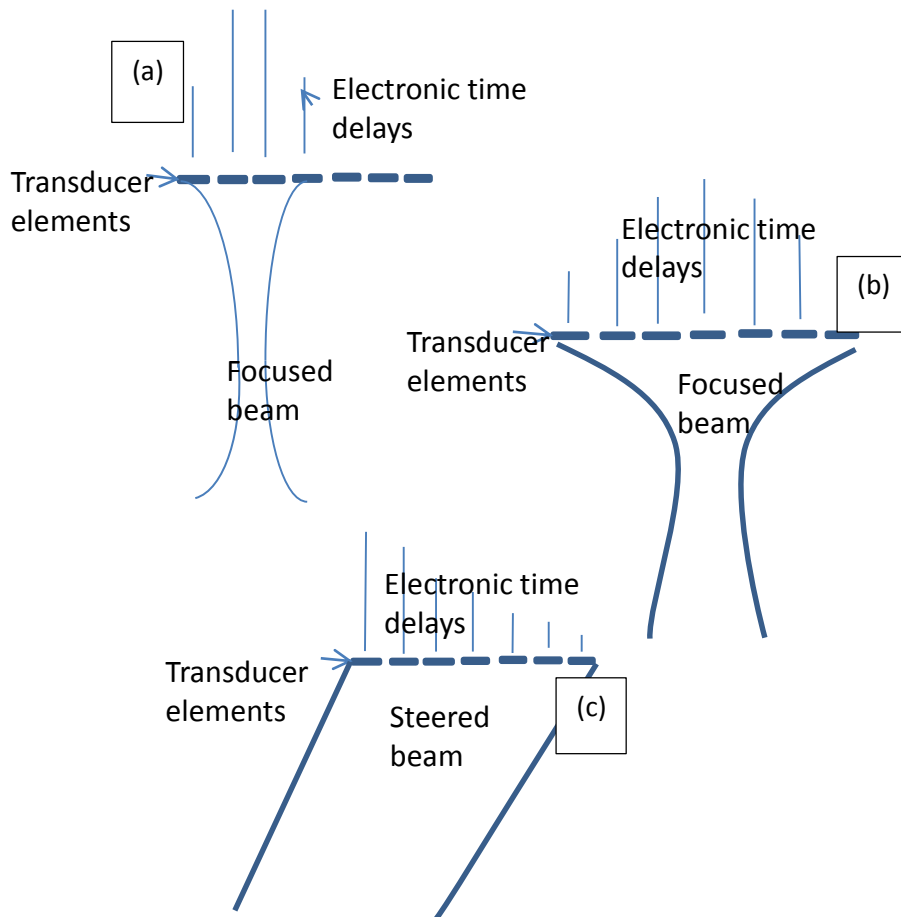


Figure 2. 11: Focusing and steering using arrays; (a) linear array, (b) phased array, (c) beam steering with phased array

The pitch of an array determines how the image is obtained. A phased array has a pitch of  $\lambda/2$  whereas a linear array has a pitch of  $\lambda$  as shown in Figure 2.11.

The parameters of the array can be optimised during the design stage using simulation, which is explained in Chapter 4. A carefully designed array is important to get good performance from a transducer small enough to fit into a biopsy needle.

### 2.5.2 *Array Imaging System*

Producing a good ultrasound image involves a sophisticated combination of hardware and software. It requires an inter-disciplinary approach involving the sciences of acoustics and vibration, electronics, and software engineering among others. Designing a good transducer is essential but the supporting system makes it useable. In Figure 2.12, the relationships between the different parts on the system are illustrated. A transmit beamformer sends out signals to the transducer array elements. This beamformer works with the computer controller and the de-multiplexer to select the transmitting elements, which determine the transmit active aperture and shape of the ultrasound field. Time delays to the array elements are also defined by the beamformer which causes focusing and ultrasound beam steering. Apodization is also done through the transmit beamformer. This is where the different array elements receive excitation signals with different amplitudes. This is so that the focal depth is increased, the side lobes levels are decreased, and the shape of the transmitted beam improved. The receive beamformer also provides time delays for steering and focusing, applying apodization and selecting the receive active elements. It should be noted that steering is dependent on the type of array used. The receive beam former also sums the received signal into a single RF line.

The signal leaves the receive beamformer to go into the signal processing unit. This is slightly different for various imaging system but it generally includes time-gain compensation, which provides amplification of signals with time of flight. Time-gain compensation compensates for the lost signal due to attenuation as the signal travels through the region of interest. Logarithmic compression is used to reduce the dynamic range of the signal so that the signals of low and high intensity echoes are shown within a range of 60 dB. The demodulated signal is filtered before it is sent to a scan converter which adapts the processed image for display. The process described above produces

one scan line, and a typical image would involve between 48 and 196 scan lines, with real-time displays employing a frame rate close to 30 frames per second.

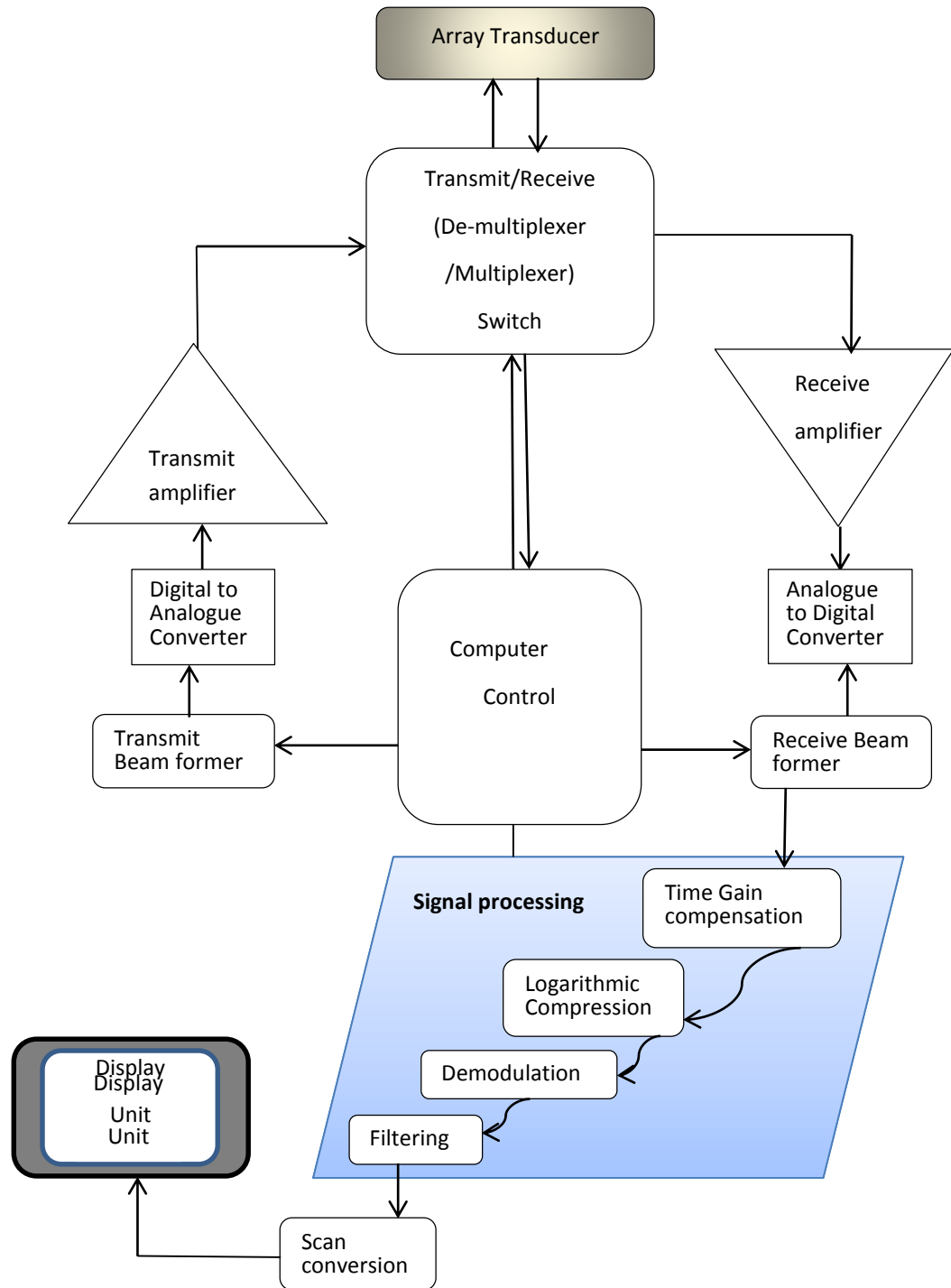


Figure 2.12: A simplified block diagram of an array based imaging system

## 2.6 Current Array Fabrication and State of The Art Methods

The fabrication of ultrasound arrays has some variations, however the process can be summarised in the steps below;

- The piezoelectric material is thinned down to get the desired operation frequency
- Electrodes are applied to either side of the piezoelectric plate
- Ground electrical connections are added
- Matching layers are then applied and thinned down
- Active electrical connections are added
- Backing layers are applied
- Dicing into individual elements is then done
- Lenses and electrical insulation are added before encasing.

The challenge with array fabrication is to be able to sandwich the piezoelectric layer between matching and backing layers, in a way that allows electrical connections to access the electrode on the active element for electrical excitation.

High frequency ultrasound arrays present particular challenges in fabrication due to their small sizes. Researchers around the world have taken different routes to simplify the fabrication of these transducers. The details of the fabrication steps are important to the success of a well fabricated high frequency array. The most common types of arrays involve mechanically diced elements with kerfs separating one element from another. This ensures that elements can be excited individually, enabling beam steering and focusing. Kerfless arrays also provide an alternative with simpler fabrication steps.

### 2.6.1 *Lapping and Polishing*

For all transducers, the piezoelectric layer must be thinned to the correct dimension, usually using a lapping process. In this method, a mechanical abrasive is used to remove material from a bulk substrate to thin it down to a desired thickness which in effect determines the resonance frequency. Chemical-mechanical polishing process makes a smooth and flat surface of the piezoelectric substrate for further fabrication steps such as photolithography. Previous work has demonstrated the feasibility of thinning composites and making them into very flat surfaces suitable for photolithography (Bernassau et al. 2007). The earlier techniques, such as using sand

paper and grinding, for thinning the piezoelectric material would not yield accurate results.

### 2.6.2 *Kerfless Arrays*

Kerfless arrays with bulk ceramic material have been researched as an alternative to the diced ones due to reduced fabrication steps. Kerfless arrays as a technique have been investigated to produce a cheap and simple alternative to diced arrays (Demore 2006). This is more useful for high frequency transducers where the small dimensions make fabrication more challenging. The kerfless array design, however, has practical limitations. It can only be used for linear arrays where there is no steering of the acoustic beam. This is due to the decreased directivity which is a result of increased electromechanical cross-talk between elements. Cannata et al (Cannata et al. 2005) developed a 30 MHz kerfless linear array which was compared with a conventional array of the same frequency. The fabrication took the form of 33.3  $\mu\text{m}$  pitch 2-2 composite plate (3 sub-elements per array element) and a monolithic plate, which were lapped down to thickness. After electroplating, a conductive backing was applied. The backing was cut into desired sizes and bonded to a premade frame with epoxy. Sputtering of 4500  $\text{\AA}$  Cr/Au was then carried out to the top and side surfaces of the arrays sub-assemblies. The elements were separated through mechanical scratch-dicing of the top electrode layer and the frame with a 15  $\mu\text{m}$  thickness diamond/nickel hubbed blade. A flexi circuit was bonded to the edges of individual array electrodes. A matching layer of 8.3 MRayl was bonded to the kerfless array with an unloaded epoxy. A lens was also cast on to the conventional arrays using a cylindrical mould. The lens (3.05 MRayl) for the kerfless array was precast and bonded on to prevent lens edge shrinkage and damaging the matching layer. After a flex circuit was attached, the assemblies were encased in a metal/plastic housing for RF shielding and structural support. The kerfless arrays showed comparable results to mechanically diced arrays.

### 2.6.3 *Diced Arrays*

Most of the techniques in array fabrication are directly transferrable from single element transducers. Dicing is done to achieve kerfs between elements. The two common methods found in the literature are laser dicing and using a high precision dicing saw. The blades used usually have diamond grit and can be as small as 10  $\mu\text{m}$

especially for high frequency arrays. However, achieving kerfs of less than 20  $\mu\text{m}$  has seen little success. It is important to get accurate array elements since they affect the overall performance of the transducer. Dicing can create errors in the width and position of the elements which can compromise the transducer performance. The challenges in dicing the transducer stack along with the attached electrical connections has led to some trade-offs so functional transducers are achieved.

Transducers with operational frequencies near 5 MHz were fabricated by (Lee et al. 2004). Even at such low frequency the matching layers were made to be conductive so that a common ground connection is used. The type of transducer used silver epoxy matching layer which is much more attenuating than the conventionally used alumina filled epoxy. The silver epoxy cannot be tailored to have ideal properties for acoustic matching since it has to have a minimum amount of silver particles to be conductive. The active layer was also attached directly on top of a pre-patterned flexi-circuit using conductive silver epoxy. The individual elements were achieved by dicing with a diamond dicing saw (Model 780, Kulicke and Soffa, Willow Grove, PA) with the saw kerf extending into, but not through the 50  $\mu\text{m}$  thick top polyimide layer. The common ground used for these transducer was a 7  $\mu\text{m}$  thick silver foil layer bonded to the elements with a conductive silver epoxy.

With increasing operational frequency, the challenges are increased due to the much smaller dimensions of the transducer. 30 MHz and 35 MHz array transducers by (Cannata et al. 2006) demonstrated the feasibility of having diced arrays at high frequencies. They simplified the fabrication process by using a conductive backing material, E-solder 3022 (Von Roll Isola, Inc., New Haven, CT), for a common ground connection. They also used a rigid frame (machinable glass-mica ceramic, McMaster-Carr Supply Company, Cleveland, OH) to provide structural support to the layers of the transducer once they were diced. It is uncommon to find high frequency transducers which have fully diced elements. This compromise is to protect the delicate elements of the arrays. Cannata et al achieved element separation through dicing the top electrode layer over the composite kerfs and ceramic frame with 50  $\mu\text{m}$  kerf using a 13  $\mu\text{m}$  diamond/nickel hubbed blade (Cannata et al. 2006).

Lukacs et al made a 20 MHz array with 64 elements. They used a UV laser to dice individual elements to separate the elements (Lukacs et al. 2006). An insulating backing was used and laser dicing the kerfs into the stack. The advantage of using laser dicing to separate the elements is that it is easier to position the stack for dicing.

#### 2.6.4 *Piezocomposite fabrication*

The conventional dice and fill method for fabricating piezocomposites has been around for a few decades. This method has been around the longest among all other methods. It involves using a precision wafer dicing saw to cut periodical pillars into a piezoelectric ceramic plate. The kerfs left by the saw are filled with a polymer (Figure 2.13). The limiting factor with this method is the saw blade thickness. With many applications in medical imaging looking for good resolution, the pillars need to be as small as possible. For 50 MHz transducers, the pillars are around 10  $\mu\text{m}$  wide with a spacing of 5  $\mu\text{m}$ . The minimum thickness for commercially available saw blades is 10  $\mu\text{m}$ , which means a minimum kerf of 11  $\mu\text{m}$ . For this reason, this technique cannot be used for transducers operating above 50 MHz.

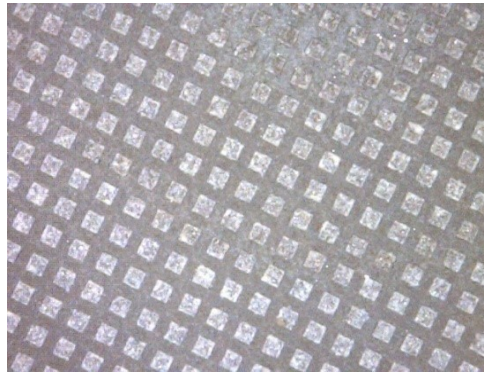


**Figure 2.13: An example of a composite made through the dice and fill method. The piezoelectric pillars are the light squares with the epoxy in the dark shade**

Although the transducer functions best with all the components optimised, the piezoelectric material is taken as the most important part since it is what generates the ultrasound waves. This has therefore led to paying much attention to optimising the fabrication of composites for this active substrate. For high frequency transducers, the challenge is to get a composite with the smallest pitch possible. Fabrication of the composites is conventionally through a dice and fill method (Brown et al. 2007), with other techniques being utilised and investigated. The other methods are laser

micromachining (Farlow et al. 2001), deep reactive ion etching (DRIE) (Jiang et al. 2008), interdigital pair bonding (Cannata et al. 2011), and micro-moulding (Cochran et al. 2004). The composites that are the most frequently used in imaging are in the form of 1-3 such as that shown in Figure 2.13. Tall, narrow pillars of the piezoelectric ceramic are surrounded with epoxy and the combination leads to high sensitivity and lower acoustic impedance as compared to the plain ceramic. The dice and fill method needs to be further improved to adapt it for high frequency array transducers.

### **2.6.5 Fabrication of 1-3 Single Crystals Composites**

Single crystal materials are more desirable since they have better properties compared to polycrystalline ceramic such as PZT. They, are however, very fragile and difficult to work with. As a result, the processes of fabricating transducers with single crystal materials have to be accordingly adjusted. Single crystals do not have grain boundaries and therefore small cracks can easily propagate through the material. Conventional dicing would lead to chipping and cracking of the material. The mechanical stresses from the saw blade can lead to cracks in specific orientations of the material. Spindle vibrations has also been reported to create post breakage as the saw passes through the cut material. The general consensus when dicing single crystals for 1-3 composites includes using a much slower feed rate and spindle speed. Feed rates have of less than 2mm/second have been recommended (Zipparo et al. 1999; Ren et al. 2006; Ritter et al. 2000; Michau et al. 2002; Snook et al. 2006). The spindle speed has been recommended to be below 10000 rpm. The coolant feed rate has also been suggested to have a big effect to the quality of the pillars diced with less than 0.5L/min recommended as suitable (Wallace 2007). New fabrication methods such as laser micromachining, and tape casting extrusion, have enabled the production of materials that operate above 10 MHz (Snook et al. 2006). However, it would be best to make the composites with the conventional dice and fill method since it is cheap and widely used.

## **2.7 Electrical Interconnects**

For high frequency transducers, incorporating electrical interconnects is the most difficult stage of fabrication. The interconnects have to be very small with orientations that allow them to be integrated into compact designs. The first stage in connecting

interconnects is to apply electrodes to the surfaces. This is done in different ways. A common method is where layers of Cr and Au are deposited on the surface using photolithography. Commonly conductive backing is used in high frequency transducers. The ground connection is connected to this backing providing a common ground to the elements (Liu et al. 2008).

For arrays operating at frequencies below 5 MHz, very fine soldering is commonly used to connect a pre-patterned flexi-circuit to the active layer. Wire bonding has also been widely used especially in high frequency arrays (Brown et al. 2007). In this method, fine gold wires are used to connect electrodes on the piezoelectric material to the flexi-circuit. The wire is pressed under high pressure and heat to gold bumps on the material. Ultrasound is used to enable joining of the gold wire and the gold bump together. The limitation of such methods is that they are very time consuming and very challenging to achieve on composite layers since the gold wires do not easily attach to the electrodes on the polymer. Some of the array elements can be as many as 256 for a linear array. The dimensions of the array will limit the minimum size of the bonder. The contact point has to be at least 80  $\mu\text{m}$  for a wire bonder. This limitation has been overcome by creation of fan out in some high frequency transducers (Bernassau et al. 2009). However, the fan out puts a restriction on packing the device into small units such as needles.

Wire bond free interconnection methods for high frequency piezoelectric ultrasound arrays above 30 MHz have also been investigated (Bernassau et al. 2009). This incorporates the use of anisotropic conductive film (ACF) and through silicon via (TSV) technologies which have been previously used as solutions for high density interconnect, low temperature bonding for flat panel displays, and semiconductors packaging applications.

## **2.8 Other Transducer fabrication methods**

There are other methods that have been investigated to make ultrasound transducers. The most common one of these methods is the capacitive micromachined ultrasound transducer (CMUT). CMUTs are based on microfabrication techniques to produce capacitive membranes that can be driven to generate ultrasound waves (Oralkan et al. 2002). CMUTs are fabricated using standard silicon integrated circuit (IC) fabrication

technology, such as photolithography. They have been under investigation for almost two decades as alternatives to the piezoelectric devices but commercial industry is yet to use them as a replacement. They are regarded as a route to overcome some of challenges in fabrication that are associated with either miniaturised piezoelectric devices or where the devices need to be closely integrated with electronics. They do not require matching layers and provide room for complex array designs. They can also be worked at temperatures exceeding 80°C, which is about the limit for their single crystal piezoelectric counterparts (Soh et al. 1996), if materials optimised for tissue imaging are used. The main drawback to these capacitive devices is that they require high voltages of over 100 V/cm to produce electrostatic forces as large as 1kg/cm<sup>2</sup> (Oralkan et al. 2002). They also have very low signal to noise ratio.

## 2.9 Ultrasound Transducers Integrated in Small Packages

For a number of years, different researchers around the world have been interested in integrating ultrasound transducers into needles (Lockwood et al. 1993; Zhou et al. 2007; Paeng et al. 2009). This is to provide a platform to get closer to the region of interest within the body, overcoming the problem of ultrasound energy attenuation. Efforts have been focused on achieving optimised single element transducers, with the micro-scale features of high frequency transducers imposing a challenge on achieving good commercial transducers. VisualSonics develops commercial high frequency ultrasound array transducers that operate up to 70 MHz but these are too big to be incorporated into interventional tools such as biopsy needles (<http://www.visualsonics.com/transducers>). The imaging is done by non-invasive probes for pre-clinical applications. This means that they are most suitable for small animal imaging since the penetration into deeply seated tissue is reduced at high frequencies.

A common area where small ultrasound transducers are used is in vascular imaging. Intravascular ultrasound (IVUS) has employed the ultrasound technology on endoscopic catheters enabling the imaging of blood vessels to identify defects such as plaques and clots (Lockwood et al. 1996). There are a number of commercially available devices such as Boston Scientific's iLab® Ultrasound Imaging System and Volcano's proprietary VH® IVUS technology. These devices are however mainly

based on single element transducers, needing mechanical scanning to generate a radial image. There are some arrays based commercial IVUS systems such as the Siemens' ACUSON AcuNav (Proulx et al. 2005). An early prototype was a 7 MHz, 128 elements 24 Fr size. This rigid device had a diameter of over 8 mm and was introduced into the right atrium through the jugular vein. The promising results obtained by this prototype lead to the subsequent development of smaller devices.

A flexible 7 MHz 64 element array in a 16 Fr catheter preceded the current version which received FDA approval in 1999 and was commercially produced in 2000. The new device was 10 Fr (3.3 mm diameter), while an 8 Fr (2.7 mm diameter) one was later introduced. This single use IVUS is credited with many clinical advances among which are: aiding in the placement of intracardiac devices, monitoring blood flow changes after therapeutic intervention and instant detection of procedure related complications, which enables timely application of reparative measures (Proulx et al. 2005).

Catheter based transducers have been researched as far back as the 60s. In 1968, a 2.5 MHz single element transducer was used to investigate left ventricular diameter in dogs (Carleton and Clark 1968). This transducer in many ways introduced the idea of ultrasound in a needle. A device patented by Eggleton in 1985 presents ultrasound on a needle and is termed an acoustic microscope (Eggleton and Fry 1985). This was designed to use an operational frequency of up to 500 MHz and aimed for examining cellular features of internal tissue or features of tissue architecture and structure at a good enough resolution to determine tissue pathology.

### ***2.9.1 Fabrication of Needle Based Transducers***

Hard needles with integrated ultrasound transducers have mainly focused on single element transducers. These require mechanical scanning for image generation. Work by Lockwood's group has developed several needle based ultrasound transducers. These transducers are high frequency based transducers with operational frequencies of above 30 MHz (Lockwood et al. 1993).

Needle based ultrasound transducers were originally developed to be used as ultrasound biomicroscopes (UBM). These were used to image sub-millimetre features

in eyes, vascular system and small animals. Needle diameters used have been in the range of 1.2 – 2.8 mm. The transducers can be in different orientations to the needle. In their study, Zhou et al illustrated a UBM based in a needle (Zhou et al. 2007). This transducer, as shown in Figure 2.14, illustrates the different layers with specific materials used for the high frequency device. This is a useful reference point for selecting materials for high frequency transducers. A material to note for this thesis is the insulating material, parylene, which is used to electrically isolate the device from the body under examination. The materials of the transducer are however, chosen to simplify the fabrication process. For instance, a conductive silver particle matching layer is used in place of the conventional alumina filled epoxy. This is to enable easy electrical connection to the electrodes of the active piezoelectric substrate. The silver filled epoxy is however more attenuating to the ultrasound energy, and has higher acoustic impedance than an ideal matching layer and therefore would affect the overall performance of the finished prototype.

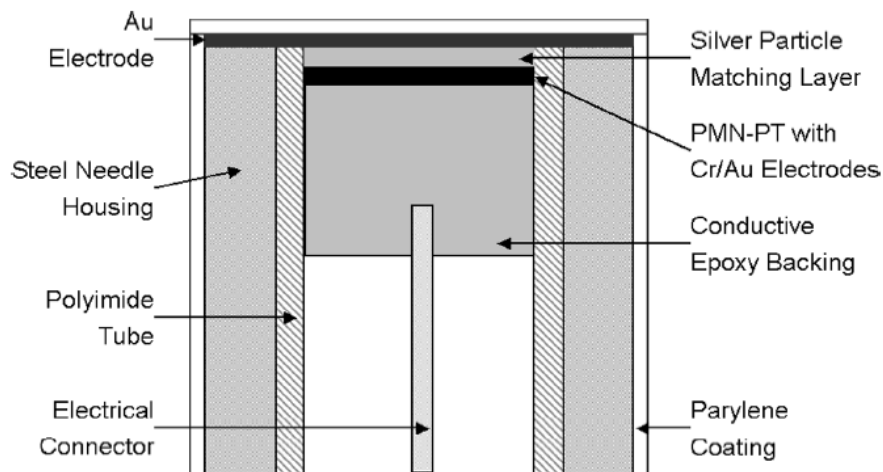


**Figure 2.14: An example of a forward-looking needle transducer used as an ultrasound bio-microscope (Zhou et al. 2007). The active aperture has a diameter 0.44 mm.**

The 44 MHz active substrate was a 50  $\mu\text{m}$  thick PMN-PT single crystal lapped from 700  $\mu\text{m}$  thick. The active aperture was 0.44 mm and a -6 dB fractional bandwidth of 45 % was achieved. Silver filled epoxy was used for matching and backing. The structure was encased in a 0.57 mm inner diameter polyimide tube which provided electrical isolation to a 0.66 mm inner diameter needle, with an outer diameter of 0.99

mm. A sputtered electrode across the matching layer was used for grounding with vapour deposited parylene coating the outside.

## 2.10 Chapter discussion

This chapter has given a comprehensive review of literature that will enable the development of the process for the fabrication of the arrays discussed in the rest of the thesis. The need to use high frequency ultrasound has been discussed, pointing to the use of single crystal materials as the best choice for the active material of the transducers.

Fabrication for composites and arrays has been discussed to form a precursor for the fabrication parameters in this thesis. The literature has informed the design and development of appropriate transducers to be used in interventional tools such as biopsy needles. This literature has demonstrated that fabrication of high frequency array transducers has been previously achieved by various researchers. The limitation is in building these transducers for specific applications. The size of these high frequency transducers mean that they can be incorporated into interventional tools. The information presented in this chapter indicates that techniques are available that will enable the array transducers in the interventional tools. The next chapters will describe the design and development of the transducers based on the literature in this chapter.

## 2.11 References

Acharya, R., Wasserman, R., Stevens, J. and Hinojosa, C. 1995. Biomedical imaging modalities: A tutorial. *Computerized Medical Imaging and Graphics* 19(I), pp. 3–25.

Azhari, H. 2010. *Basics of Biomedical Ultrasound for Engineers*. John Wiley & Sons, Inc.

Bernassau, A.L., Flynn, D., Amalou, F., Desmulliez, M.P.Y. and Cochran, S. 2009. Techniques for wirebond free interconnection of piezoelectric ultrasound arrays operating above 50 MHz. In: *IEEE International Ultrasonics Symposium*. Rome, pp. 1–4.

Bernassau, A.L., McKay, S., Hutson, D., Demoré, C.E.M., Button, T.W. and Mcaney, J.J. 2007. Surface Preparation of 1-3 Piezocomposite Material for Microfabrication of High Frequency Transducer Arrays. *Ultrasonics*, pp. 2007–2010.

Brown, J., Foster, F., Needles, A., Cherin, E. and Lockwood, G. 2007. Fabrication and Performance of a 40-MHz Linear Array Based on a 1-3 Composite with Geometric

- Elevation Focusing. *IEEE Transactions on Ultrasonics, Ferroelectrics and Frequency Control* 54(9), pp. 1888–1894.
- Bushberg, J.T., Seibert, J.A., Leidholdt, E.M.J. and Boone, J.M. 2011. *The Essential Physics of Medical Imaging*. Third Edit. Wolters Kluwers.
- Cannata, J.M., Williams, J. a, Zhou, Q., Ritter, T. a and Shung, K.K. 2006. Development of a 35-MHz piezo-composite ultrasound array for medical imaging. *IEEE transactions on ultrasonics, ferroelectrics, and frequency control* 53(1), pp. 224–36.
- Cannata, J.M., Williams, J.A. and Shung, K.K. 2005. A Kerfless 30 MHz Linear Ultrasonic Array. In: *IEEE International Ultrasonics Symposium*. pp. 109–112.
- Cannata, J.M., Williams, J.A., Zhang, L., Hu, C.-H. and Shung, K.K. 2011. A high-frequency linear ultrasonic array utilizing an interdigitally bonded 2-2 piezo-composite. *IEEE transactions on ultrasonics, ferroelectrics, and frequency control* 58(10), pp. 2202–12.
- Carleton, R.A. and Clark, J.G. 1968. Measurement of Left Ventricular Diameter In the Dog by Cardiac Catheterization: Validation and Physiologic Meaningfulness of an Ultrasonic Technique. *Circulation Research* 22(5), pp. 545–558.
- Clay, A.C., Wooh, S., Azar, L. and Wang, J. 1999. Experimental Study of Phased Array Beam Steering Characteristics. *Journal of Nondestructive Evaluation* 18(2), pp. 59–71.
- Cobbold, R.S.C. 2007. *Foundations of Biomedical Ultrasound*. New York: Oxford University Press.
- Cochran, S., Abrar, A., Kirk, K.J., Button, T.W., Meggs, C. and Porch, N. 2004. Net-shape ceramic processing as a route to ultrafine scale 1-3 connectivity piezoelectric ceramic-polymer composite transducers. In: *IEEE Ultrasonics Symposium, 2004*. IEEE, pp. 1682–1685.
- Curiel, L., Chopra, R. and Hynynen, K. 2007. Progress in Multimodality Imaging: Truly Simultaneous Ultrasound and Magnetic Resonance Imaging. *IEEE Transactions on Medical Imaging* 26(12), pp. 1740–1746.
- Dargaville, T.R., Celina, M.C., Elliott, J.M., Chaplya, P.M., Jones, G.D., Mowery, D.M., Assink, R.A., Clough, R.L. and Martin, J.W. 2005. Characterization , Performance and Optimization of PVDF as a Piezoelectric Film for Advanced Space Mirror Concepts. (November).
- Demore, C.E.M. 2006. Design of Ultrasound Transducer Arrays for Medical Imaging. PhD Thesis, Queen’s University Kingston, Ontario, Canada.

- Draheim, M.R. and Cao, W. 1996. Finite element analysis on impedance matching layer thickness. In: *Applications of Ferroelectrics, 1996. ISAF '96., Proceedings of the Tenth IEEE International Symposium on.* pp. 1015–1018.
- Eggleton, R.C. and Fry, F.J. 1985. Acoustic Microscope.
- Farlow, R., Galbraith, W., Knowles, M. and Hayward, G. 2001. Micromachining of a piezocomposite transducer using a copper vapor laser. *IEEE transactions on ultrasonics, ferroelectrics, and frequency control* 48(3), pp. 639–40.
- Foster, F.S., Pavlin, C.J., Harasiewicz, K.A., Christopher, D.A. and Turnbull, D.H. 2000. Advances in ultrasound biomicroscopy. *Ultrasound in Medicine & Biology* 26(1), pp. 1–27.
- Foster, S.F., Member, S., Harasiewicz, K.A. and Sherar, M.D. 2000. A History of Medical and Biological Imaging with Polyvinylidene Fluoride ( PVDF ) Transducers. *IEEE transactions on ultrasonics, ferroelectrics, and frequency control* 47(6), pp. 1363–1371.
- Fujimoto, J.G., Pitris, C., Boppart, S.A. and Brezinski, M.E. 2000. Optical Coherence Tomography: An Emerging Technology for Biomedical Imaging and Optical Biopsy. *Neoplasia* 2(1-2), pp. 9–25.
- Gabriele, M.L., Wollstein, G., Ishikawa, H., Kagemann, L., Xu, J., Folio, L.S. and Schuman, J.S. 2011. Optical Coherence Tomography : History , Current Status , and Laboratory Work. *Investigative Ophthalmology & Visual Science* 52, pp. 2425–2436.
- Geva, T. 2006. Magnetic Resonance Imaging : Historical Perspective. *Journal of Cardiovascular Magnetic Resonance* 8, pp. 573–580.
- Gururaja, T.R. and Panda, R.K. 1998. Current Status and Future Trends in Ultrasonic Transducers for Medical Imaging Applications. In: *Applications of Ferroelectrics, 1998. ISAF 98. Proceedings of the Eleventh IEEE International Symposium on.* pp. 223–228.
- Hendree, W.R. and Ritenour, E.R. 2002. *Medical imaging physics*. Fourth Edi. New York: Wiley-Liss.
- Hounsfield, G.N. 1973. Computerized transverse axial scanning (tomography): Part I. Description of Systems. *British Journal of Radiology* 46(552), pp. 1016–1022.
- Hunt, J.W., Arditi, M. and Foster, F.S. 1983. Ultrasound transducers for pulse-echo medical imaging. *IEEE transactions on bio-medical engineering* 30(8), pp. 453–81.
- Jiang, X., Snook, K., Cheng, A., Hackenberger, W.S. and Geng, X. 2008. Micromachined PMN-PT single crystal composite transducers -- 15–75 MHz PC-MUT. *2008 IEEE Ultrasonics Symposium*, pp. 164–167.

- Kalender, W. a 2006. X-ray computed tomography. *Physics in medicine and biology* 51(13), pp. R29–43.
- Lee, W., Idriss, S.F., Wolf, P.D. and Smith, S.W. 2004. A miniaturized catheter 2-D array for real-time, 3-D intracardiac echocardiography. *IEEE transactions on ultrasonics, ferroelectrics, and frequency control* 51(10), pp. 1334–46.
- Leiserson, M. 2010. The future of medical imaging. *TUFTSCOPE* 9(II), pp. 17–18.
- Liu, C.G., Wu, D.W., Zhou, Q.F., Djuth, F.T. and Shung, K.K. 2008. High-frequency (50–100MHz) medical ultrasound transducer arrays produced by micromachining bulk PZT materials. In: *2008 IEEE Ultrasonics Symposium*. IEEE, pp. 690–693.
- Liu, R., Harasiewicz, K. a and Foster, F.S. 2001. Interdigital pair bonding for high frequency (20-50 MHz) ultrasonic composite transducers. *IEEE transactions on ultrasonics, ferroelectrics, and frequency control* 48(1), pp. 299–306. Available at: <http://www.ncbi.nlm.nih.gov/pubmed/11367799>.
- Lockwood, G., Ryan, L.K. and Foster, F.S. 1993. A 45 to 55 MHz needle-based ultrasound system for invasive imaging. *Ultrasonic Imaging* 15, pp. 1–13.
- Lockwood, G.R., Turnbull, D.H., Christopher, D. and Foster, F.S. 1996. Beyond 30 MHz, Application of High-Frequency Ultrasound Imaging. *IEEE Engineering in Medicine and Biology*, pp. 60–71.
- Lukacs, M., Yin, J., Pang, G., Garcia, R.C., Cherin, E., Williams, R., Mehi, J. and Foster, F.S. 2006. Performance and characterization of new micromachined high-frequency linear arrays. *IEEE transactions on ultrasonics, ferroelectrics, and frequency control* 53(10), pp. 1719–29.
- Madou, M.J. 1997. *Fundamentals of microfabrication*. Madou, M. ed. London: CRC Press.
- Michau, S., Mauchamp, P. and Dufait, R. 2002. Single Crystal-based Phased Array for Transoesophageal Ultrasound Probe. In: *IEEE Ultrasonics Symposium*. pp. 1269–1272.
- Ming Lu, X. and Proulx, T.L. 2005. Single crystals vs. pzt ceramics for medical ultrasound applications. In: *IEEE Ultrasonics Symposium, 2005*. IEEE, pp. 227–230.
- Mollet, N.R., Cademartiri, F., van Mieghem, C.A.G., Runza, G., McFadden, E.P., Baks, T., Serruys, P.W., Krestin, G.P. and de Feyter, P.J. 2005. High-resolution spiral computed tomography coronary angiography in patients referred for diagnostic conventional coronary angiography. *Circulation* 112(15), pp. 2318–23.
- Neumann, N., Yu, P., Ji, Y., Lee, S.G. and Luo, H. 2011. Application of Single Crystalline PMN-PT and PIN-PMN-PT in High-Performance Pyroelectric Detector. In: *Applications of Ferroelectrics (ISAF/PFM), 2011 International Symposium on and*

2011 *International Symposium on Piezoresponse Force Microscopy and Nanoscale Phenomena in Polar Materials*. pp. 2–5.

Oralkan, Ö., Ergun, A.S., Johnson, J.A., Karaman, M., Demirci, U., Kaviani, K., Lee, T.H. and Khuri-yakub, B.T. 2002. Transducers : Next-Generation Arrays for Acoustic Imaging? *IEEE Transactions on Ultrasonics, Ferroelectrics and Frequency Control* 49(11), pp. 1596–1610.

Paeng, D.-G., Chang, J.H., Chen, R., Humayun, M.S. and Shung, K.K. 2009. Feasibility of rotational scan ultrasound imaging by an angled high frequency transducer for the posterior segment of the eye. *IEEE transactions on ultrasonics, ferroelectrics, and frequency control* 56(3), pp. 676–80.

Paul, Y., Barthez, D., Leveille, R., Peter, V. and Scrivani, D. 1997. Side lobes and grating lobes artifacts in ultrasound imaging. *Veterinary Radiology & Ultrasound* 38(5), pp. 387–393. Available at: <http://doi.wiley.com/10.1111/j.1740-8261.1997.tb02104.x> [Accessed: 29 May 2013].

Price, D., Delakis, I., Renaud, C. and Dickinson, R. 2008. *MRI Scanners : A buyer's guide*.

Proulx, T.L., Tasker, D. and Bartlett-Roberto, J. 2005. Advances in catheter-based ultrasound imaging Intracardiac Echocardiography and the ACUSON AcuNavTM Ultrasound Catheter. In: *IEEE Ultrasonics Symposium, 2005*. IEEE, pp. 669–678.

Qiu, Z., Sadiq, M.R., Démoré, C., Parker, M.F., Marin, P., Mayne, K. and Cochran, S. 2011. Characterization of piezocrystals for practical configurations with temperature- and pressure-dependent electrical impedance spectroscopy. *IEEE transactions on ultrasonics, ferroelectrics, and frequency control* 58(9), pp. 1793–803.

Ren, K., Liu, Y., Geng, X., Hofmann, H.F. and Zhang, Q.M. 2006. Single crystal PMN-PT/epoxy 1-3 composite for energy-harvesting application. *IEEE transactions on ultrasonics, ferroelectrics, and frequency control* 53(3), pp. 631–8.

Ritter, T., Geng, X., Kirk Shung, K., Lopath, P.D., Park, S.E. and Shrout, T.R. 2000. Single crystal PZN/PT-polymer composites for ultrasound transducer applications. *IEEE transactions on ultrasonics, ferroelectrics, and frequency control* 47(4), pp. 792–800.

Roentgen, W.C. 1895. On a New Kind of Rays. *Wuirzburg Physical and Medical Society*.

Rontgen, W.K. 1972. On A New Kind of Rays. *CA: A Cancer Journal for Clinicians* 22(3), pp. 153–157.

Sakas, G. 2002. Trends in medical imaging: from 2D to 3D. *Computers & Graphics* 26(4), pp. 577–587.

- Schmid-Wendtner, M.-H. and Dill-Müller, D. 2008. Ultrasound Technology in Dermatology. *Seminars in cutaneous medicine and surgery* 27(1), pp. 44–51.
- Schmitt, J.M. 1999. Optical coherence tomography (OCT): a review. *IEEE Journal of Selected Topics in Quantum Electronics* 5(4), pp. 1205–1215.
- Shung, K.K., Cannata, J.M. and Zhou, Q.F. 2007. Piezoelectric materials for high frequency medical imaging applications: A review. *Journal of Electroceramics* 19(1), pp. 141–147.
- Shung, K.K. and Zipparo, M. 1996. Ultrasonic Transducers and Arrays. *IEEE Engineering in Medicine and Biology* (December) pp.20-30
- Silva, G.T. and Fatemi, M. 2002. Linear Array Transducer for Vibro - Acoustography. In: *IEEE Ultrasonics symposium*. pp. 629–632.
- Smith, R.S. and Fry, W.R. 2004. Ultrasound instrumentation. *The Surgical clinics of North America* 84(4), pp. 953–71, v.
- Smith, W.A. 1986. Composite Piezoelectric Materials for Medical Ultrasonic Imaging Transducers -- A Review. In: *Sixth IEEE International Symposium on Applications of Ferroelectrics*. IEEE, pp. 249–256.
- Smith, W.A. 1990. The application of 1-3 piezocomposites in acoustic transducers. In: *[Proceedings] 1990 IEEE 7th International Symposium on Applications of Ferroelectrics*. IEEE, pp. 145–152.
- Smits, J.G. 1976. Iterative Method for Accurate Determination of the Real and Imaginary Parts of the Materials Coefficients of Piezoelectric Ceramics. *IEEE Transactions on Sonics and Ultrasonics* 23(6), pp. 393–401.
- Snook, K.A., Jiang, X., Hackenberger, W.S. and Geng, X. 2006. Single Crystals for High Frequency Ultrasound. In: *Ultrasonics*.
- Soh, H.T., Ladabaum, I., Atalar, A., Quate, C.F. and Khuri-Yakub, B.T. 1996. Silicon micromachined ultrasonic immersion transducers. *Applied Physics Letters* 69(December), pp. 3674–3676.
- Szabo, T.L. 2004. Diagnostic Ultrasound Imaging: Inside Out. In: Elsevier Academic Press, pp. 23–26, 269.
- Wallace, M.F. 2007. Single Crystal Acoustic Transducers for High Performance Underwater Sonar Systems. University of West of Scotland.
- Wang, H., Ritter, T., Cao, W. and Shung, K.K. 2001. High frequency properties of passive materials for ultrasonic transducers. *IEEE transactions on ultrasonics, ferroelectrics, and frequency control* 48(1), pp. 78–84.

Zagorchev, L., Oses, P., Zhuang, Z.W., Moodie, K., Mulligan-Kehoe, M.J., Simons, M. and Couffinal, T. 2010. Micro computed tomography for vascular exploration. *Journal of angiogenesis research* 2, p. 7.

Zhou, D., Cheung, K.F., Chen, Y., Lau, S.T., Zhou, Q., Shung, K.K., Luo, H.S., Dai, J. and Chan, H.L.W. 2011. Fabrication and performance of endoscopic ultrasound radial arrays based on PMN-PT single crystal/epoxy 1-3 composite. *IEEE transactions on ultrasonics, ferroelectrics, and frequency control* 58(2), pp. 477–84.

Zhou, Q., Cha, J.H., Huang, Y., Zhang, R., Cao, W. and Shung, K.K. 2009. Alumina/epoxy nanocomposite matching layers for high-frequency ultrasound transducer application. *IEEE transactions on ultrasonics, ferroelectrics, and frequency control* 56(1), pp. 213–9.

Zhou, Q., Xu, X., Gottlieb, E., Sun, L., Cannata, J., Ameri, H., Humayun, M., Han, P. and Shung, K. 2007. PMN-PT single crystal, high-frequency ultrasonic needle transducers for pulsed-wave Doppler application. *IEEE Transactions on Ultrasonics, Ferroelectrics and Frequency Control* 54(3), pp. 668–675.

Zipparo, M., Oakley, C., Hackenberger, W. and Hackenberger, L. 1999. Single crystal composites, transducers, and arrays. *1999 IEEE Ultrasonics Symposium. Proceedings. International Symposium (Cat. No.99CH37027)* 2, pp. 965–968.

# CHAPTER 3

---

## Design Considerations and Evaluation Methods

---

### Chapter Profile

Chapter 3 explains the design approaches that were considered to realise prototypes in this research. A fabrication process was developed to produce high frequency transducers operating up to 15 MHz. The main aim of the work in this thesis is to solve the challenges in packaging of 15 MHz array in a needle, with a view to how that can be translated for a 30 MHz array. The operating frequency for the prototypes in this thesis was chosen to be 15 MHz, because it provides dimensions small enough to fit into the chosen clinical needles to demonstrate proof of principle, without the additional fabrication complexities of the finer-scale arrays and the potential to be driven by commercially available array control systems. Trade-offs are explained to evaluate the feasibility of such transducer with a view to higher frequency, small-scale transducers.

Section 3.7 and onwards of this chapter focus on evaluation methods ranging from characterisation of the active and passive materials used in the transducer to the finished prototype as a whole.

### 3.1 Introduction to Design Considerations

The development of ultrasound transducer arrays in biopsy needles or similar interventional tools requires different design considerations compared to the conventional ultrasound arrays that are used outside the body. The orientation of the transducer in the needle must be such that the ultrasound waves are not obstructed by the outer shell of the needle. The needle should also retain its structural integrity so that it can pierce through the skin and tissue structures. The main areas considered

during the design of the ultrasound transducer integrated in a needle are illustrated in Figure 3.1.

- For application in the clinical environment, the device must meet the clinical need of providing high resolution images. In this regard, high frequency transducers would yield the desired effect.
- The fabrication techniques considered for this research are those that can be used to produce relatively inexpensive high resolution devices and these are further explained in Chapter 5.
- A great deal of attention is paid to the packaging techniques since these enable the fabrication of arrays to fit in small diameter needles. The devices were also designed to be MRI-compatible by choosing the right material for the needle and consideration of electrical shielding.

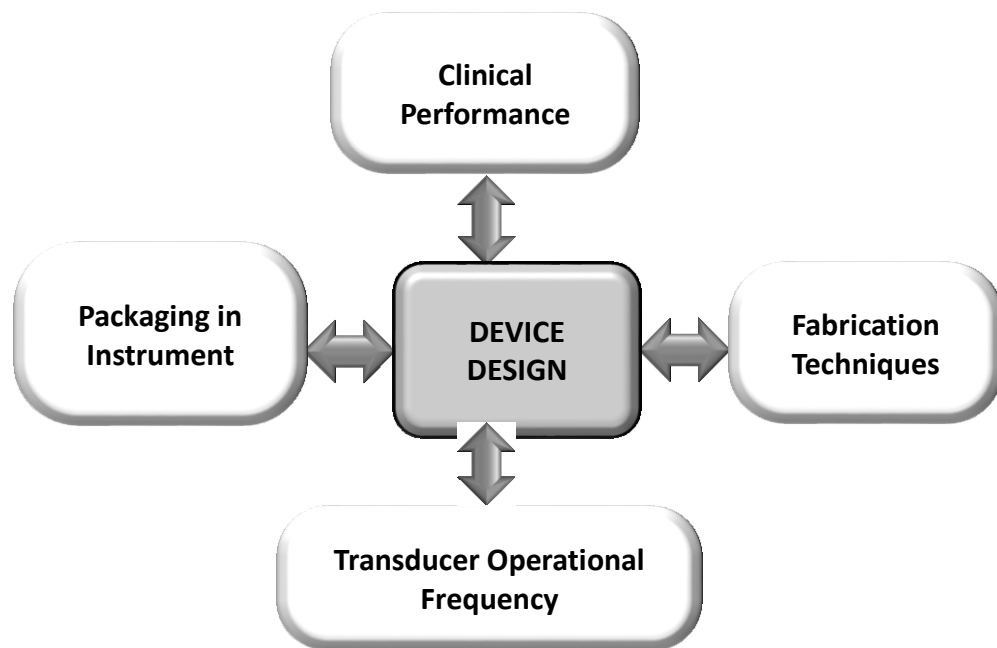


Figure 3. 1: The main areas considered during the device design showing the different aspects that affect the device performance

### 3.2 The Needle Sizes

The first thing to consider is the size of the needles since these will dictate the size of the transducer array package. Needles that penetrate through the skin, called hypodermic needles, have very sharp tips which come in different shapes depending on the application. The lengths of such needles range from 10 to 15 cm. They also have a wide range of outer diameters which are commonly classified using gauge numbers. The larger the gauge number, the smaller the outer diameter. The inner diameter is determined by considering the wall thickness and the gauge number of the needle. (<http://prlabpak.wordpress.com/2012/03/28/needle-gauge-comparison-chart/>).

ISO standards define dimensions for the inner and outer diameters (ID and OD) of the different needles (Ahn et al. 2002; Boutsoukis et al. 2007). The dimensions of transducers and arrays developed in this thesis are designed to fit into ISO standard needles for their prospective application. Biopsy needles typically range from 22 gauge (0.9 mm outer diameter) to 14 gauge (2.15 mm outer diameter) (Ahn et al. 2002). A 14 gauge needle would more easily accommodate an ultrasound transducer due to its size and as such, this was chosen as the main focus for this thesis, to demonstrate feasibility. An empirical design for the biopsy needle was considered by analysing the commercially available needles. These needles have their tips tapered at a bevel angle of approximately  $26^\circ$  in order for them to pierce the skin and tissue structures with ease.

### 3.3 Transducer Operational Frequency

The operational frequency is determined by the thickness and the speed of sound of the piezoelectric material used and this in turn affects many performance aspects of the transducer. These include transducer resolution and the ultrasound energy penetration capability into the tissue. It is important to choose the right operational frequency for a particular application. In order to obtain images of small features, at a good resolution, high frequency transducers are required. Images of cancerous cells that are a few microns thick need transducers operating well over 20 MHz. Arrays at such frequencies do not exist due to the challenges involved in fabrication of the micro-scale devices. Transducers at even higher frequencies would provide improved

resolutions. For example, a transducer operating at 30 MHz yields a better resolution but a reduced penetration depth when compared to a 15 MHz. The operational frequency is used to determine the overall dimensions of the transducer.

For this study, the operating frequency of the transducer was chosen to be 15 MHz, corresponding to an imaging wavelength of 100  $\mu\text{m}$ . This operating frequency was chosen because the transducer would produce acceptable resolution and the dimensions would allow for easier fabrication of prototypes to evaluate feasibility. For clinically oriented characterisation at later stages in development, the array needs to be connected to an array controller and beamformer. Since the few commercially available imaging systems that allow for connection to non-commercial arrays for evaluation operate at 15 MHz maximum, this is an additional motivation for setting the operating frequency at 15 MHz. The dimensions at 15 MHz would be small enough to fit into a biopsy needle or other interventional tools. The theoretical tissue penetration depth at 15 MHz is approximately 40 mm, which is enough to image fine body features at a good distance. It is important to note however that the processes developed in this thesis are designed to also be suitable for the fabrication of transducers above 20 MHz.

### **3.4 Packaging in Instrumentation**

In the current study, only imaging transducers were considered for incorporating into needles. The idea of transducers in a needle can however be extended to therapeutic transducers and other forms of transducers to reach difficult areas such as the prostate. Incorporating high resolution imaging into the core of needles would need to be very close to the tip, which would limit the available space for cables.

A benefit of placing the array at the tip of the needle is the possibility of identifying the position of the needle tip in the tissue, which is another common problem encountered when using conventional ultrasound imaging. Clinicians are unable easily to identify tips of needles such as anaesthetic and biopsy needles, when they are inserted into the body. Knowing where the position of the tip of the needle is essential in acquiring more accurate information from the area of interest.

### 3.4.1 *Array Orientations*

There are different orientations with which an ultrasound array transducer can be fitted into a needle. The easiest one is having a single element transducer in a needle. The dimensions can be selected to fit into many needle sizes, with only one cable for electrical signal needed. The possible transducer geometry and orientations are shown in Figure 3.2. If an annular array or a single element transducer is used, it must be mechanically scanned in order to create a 2D image. For needle or catheter based devices incorporating these types of transducers, a radial 2D scan can be acquired either by rotating an outward-facing transducer or rotating a parabolic mirror in front of a forward facing transducer (van der Steen et al. 2006; Ledworuski et al. 2002). This is what is typically used for IVUS devices. An image can also be created when the device is translated across an area of interest.

Having arrays increases the complexity of fabrication and image acquisition but, because of the increased benefits of improved image quality, it is more useful to use them instead of single element transducers. The ultrasound beam pattern is affected by the size and number of elements, the pitch of elements in arrays and the orientation of the transducer on the needle. At the design stage, it is important to analyse and evaluate different options for an optimised array transducer which can be manufactured at a low cost. Three possible configurations are shown in Figure 3.2: a radial view, a forward view and a side view.

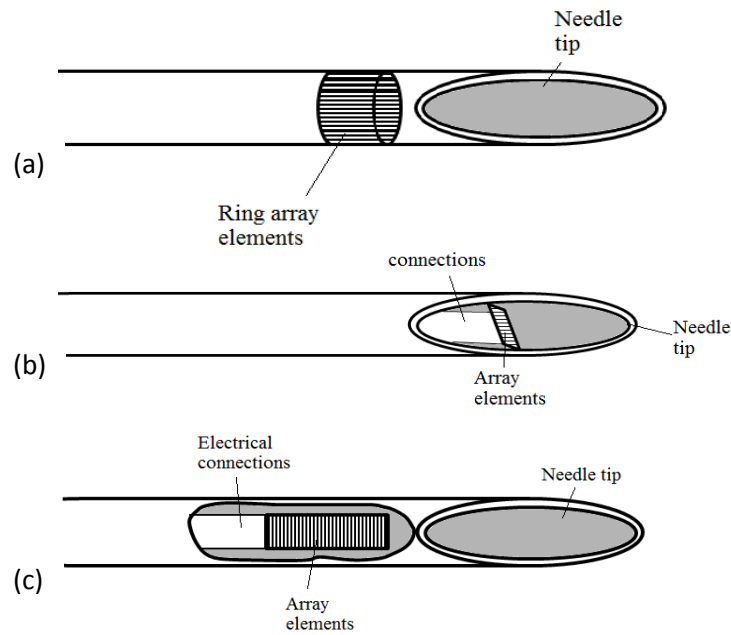


**Figure 3. 2: Possible orientations of an ultrasound transducer on a needle, with direction of the beam indicated; (a) axial cross section, (b) forward viewing, (c) side viewing**

This axial cross section orientation (Figure 3.2 (a)) would mean having the needle broken and the transducer inserted to join the two sections. This would compromise the structural integrity of the needle and might also affect the performance of the transducer. The forward viewing orientation (Figure 3.2(b)) would make it difficult to have a pointed needle. From an application perspective, the side view orientation (Figure 3.2 (c)) is the most viable option. This option means that the piercing end of the needle is free from the transducer. It also provides room for more elements in the array since the diameter is not the limiting factor. More details discussing these orientations are given in Appendix A.

Figure 3.3 shows how the side viewing ultrasound transducer would fit into a needle. This shows more details of the chosen transducer orientation in the needle. The flexi-circuit for the electrical signal transmission has to be either connected from the side of the transducer or by through-via technology. The work in this thesis focused on developing a packaging method with the flexi-circuit connected at the side.

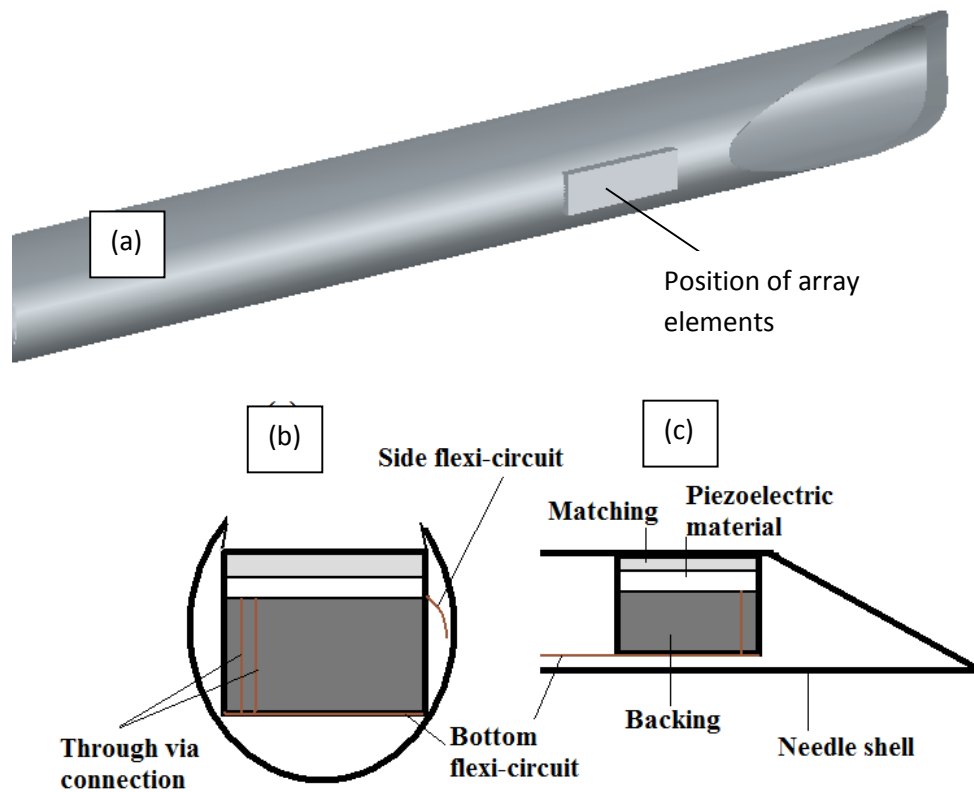


**Figure 3. 3: An illustration of the transducer stack can be fitted into the needle: (a) 3D needle with array elements position indicated, (b) cross section view, (c) side view**

From all the design considerations, a linear array of 15 MHz was chosen for the prototype. The pitch of  $\lambda$  would be ideal to produce a small enough array size to fit in the needle. The elevation width is determined by the inner diameter of the needle it will be fitted in. This has to be between 0.7 and 1 mm for a 1.8 mm inner diameter needle in order to leave enough room for the flexi-circuit. The minimum number of elements was chosen to be 64 and this was based on the way the scanning with the linear array is achieved. More elements would provide an image with a bigger field of view. However, to get prototypes for the feasibility study, 64 elements were enough. Further details of the array design are discussed in Chapter 4.

#### **3.4.2 Flexi Circuit Orientations**

Incorporating the HFUS transducer into the core biopsy needle leaves little space for the cabling. The most straightforward means of connecting to the array is to use coaxial cables to each element, as is typically done in arrays that operate at conventional

frequencies. The smallest commercially available micro coaxial cables have an outer diameter of approximately 0.3 mm (Dickinson and Kitney 2004). Having multiples of these cables to numbers exceeding 64 would not fit in a 2 mm diameter needle. It is of paramount importance to have the array transducer close to the tip of the needle to enable imaging the tissue for biopsy.

A better design for the electrical connections from the transducer to the driving electronics is therefore essential due to the limitation of space within the needle. There are a few ways the connections can be designed to fit into such a limited diameter. The most common of such designs are in the form of multiplexers and multilayer flexible circuits.

Multiplexing is a technique that leads to few cables through the diameter of the needle tube. Switching is used to excite and receive information from the array elements (Dickinson and Kitney 2004; Daviden and Smith 1996; Felix et al. 2005). A multiplexing system is illustrated in Figure 3.4. The advantage of such connection is that it leaves plenty of room within the device. However, it can be more difficult to provide a good real-time image with multiplexers because advanced beamforming algorithms are required.

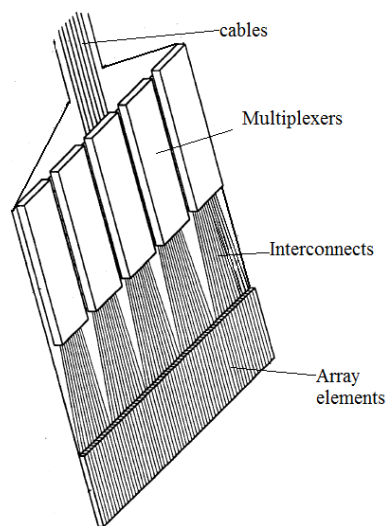


**Figure 3. 4: Example of a multiplexer in arrays edited from (Eberle and Finsterwald 2003)**

Multilayer flexible circuits have layers of flexi circuits one on top of the other where the conductive tracks are connected to the array by either direct bonding or through

micro-vias (Proulx et al. 2005; Stephens et al. 2008; Lee et al. 2004; Smith and Davidsen 1998; Lee et al. 2003). These can be designed to dimensions that fit within confined spaces. As illustrated in Figure 3.5, a flexible circuit can be connected to a number of elements, and through cutting and overlaying layers, the design can be reduced to a much smaller size. This design has a potential for fitting in small tubes, however, it can be very complex and therefore expensive.

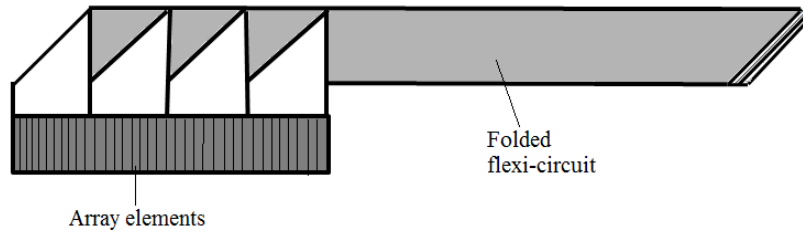


**Figure 3. 5: Multilayer through folding a flexible circuit**

The design for the electrical connection to the array developed in this study takes the form of a flexi circuit rolled into a helix, illustrated in Figure 3.6. By having a helical design, a wide flexible circuit can be fitted into the dimensions of the needle. Advanced designs could incorporate helical multilayers if required. The noticeable problem to overcome with this design is the starting angle for rolling. As will be explained in Chapter 7, a poor angle will lead to bulging of the flexible circuit near the array, making it difficult to fit into the needle. It is also important to have thin flexi circuit as this makes the rolling easy.

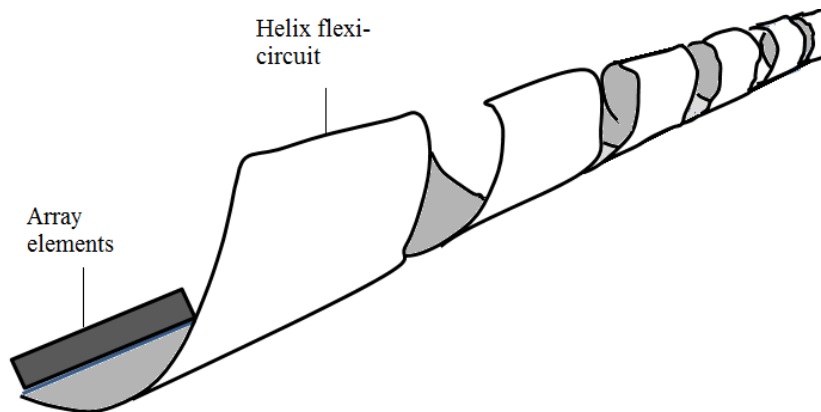


**Figure 3. 6: An example of a helix rolled flexi circuit**

Since multiple conductive tracks can be printed on one surface before rolling, this design is the easiest one to make. Therefore it would provide the cheapest and simplest option for transmitting electrical signals to and from the array. This would in effect reduce the overall cost of the finished device. The fabrication techniques and the interconnect method are discussed in Chapter 5.

### **3.5 Clinical Performance**

The transducers developed as part of this work are intended to meet clinical needs such as *in vivo* imaging of cancerous tissues at early stages. This specific application dictates many aspects of the transducer such as: the operational frequency to achieve the required resolution; the overall dimensions of the transducer; and the type of imaging array to be used. It was important to keep clinical performance at the forefront of the design criteria in order to fabricate high performance prototypes. The required lateral and axial resolutions are important in determining the design of the transducer. The geometry of the transducer, including the number of elements, pitch, total active aperture and elevation dimensions is considered at a design stage to give the desired clinical performance. Ultrasound field simulation is discussed in Chapter 4 as a method to optimise the geometry for clinical performance.

Since the device needs to be MRI compatible, the electrical signal cables are required to have properties that minimise artefacts within the image. Good shielding needs to be used with the cabling to reduce radio frequency (RF) interference (Curiel et al. 2007). Copper sheets are usually used to provide such shielding. The needle also needs to be MRI safe in order to be used around the strong magnets. Materials such as stainless steel 316 alloy have been designed to provide such properties (Holton et al. 2003).

### **3.6 Fabrication techniques**

The piezoelectric materials used in the device dictate restrictions on some of the processes that can be used in the fabrication, but also affect the device performance. Single crystal materials limit the fabrication temperatures to approximately 60°C. The fabrication techniques adapted for the prototypes in this work used low fabrication

temperatures and pressure. The details of the fabrication processes are discussed in Chapter 5.

The fabrication developed was able to yield both single element transducers and arrays.

### **3.7 Performance Characterisation**

#### ***3.7.1 Electrical Characterisation***

The characterisation of the piezoelectric materials was done to determine the basic performance of the material using electrical impedance spectroscopy explained in Section 2.3.2. Impedance magnitude and phase were measured using an impedance analyser, (4395A, Agilent Inc., Edinburgh Park, UK) to establish how the material and the transducer stack operates at each of the different stages of fabrication. The frequency range was chosen to be twice the resonant frequency in order to show if there are any spurious resonances interfering with the main resonance.

The impedance test was important as an initial test to determine whether the material and the prototype as a whole performed as expected. With the typical impedance curve shown in Figure 2. 6, properties such as electromechanical coupling coefficient  $k_t$ , electrical resonance frequency,  $f_e$ , and mechanical resonance frequency,  $f_m$ , were determined

The electrical impedance characterisation can also be used for extracting piezoelectric material properties that can then be used for predicting performance. Software such as Piezoelectric Resonance Analysis Program (PRAP, TASI Technical Software Inc., Ontario, Canada) is used for extracting the full material properties.

#### ***3.7.2 Passive Material Characterisation***

Acoustic characterisation of materials has been established for some time (Selfridge 1985). The pulse-echo method and the through-transmission technique are the two commonly used methods (Selfridge 1985) .

The backing and matching layers, which are the passive layers of the transducer, play an important role in the efficient transfer of ultrasound energy from the transducer to

the tissue and vice-versa. The acoustic properties should therefore be optimised to enable an optimal performance at a given frequency. The backing and matching layers, which are typically polymers filled with either tungsten or alumina, were characterised using single element HFUS transducers (MacLennan 2010). The longitudinal velocity of sound in the passive material was used to determine the thickness of the layer at a given frequency. Longitudinal wave velocities were calculated by measuring the time taken for the sound wave to travel through a material with a given thickness. Two transducers were immersed in water with the material of interest in the middle. The transducers operate in through-transmission mode and the time taken for the pulse to propagate through the material is determined by comparing with the time taken to propagate through the same distance in water. This method, illustrated in Figure 3.7, is what was used in this study. The transmitting and receiving transducers do not need to be in contact with the material being investigated. The distance,  $x$ , between the two transducers and the sample thickness,  $d$ , are known. Where, the transmitting and receiving transducers are in contact with the sample,  $x$  will be equal to  $d$ . The time of propagation between the transducers is measured without and with the sample in the middle.

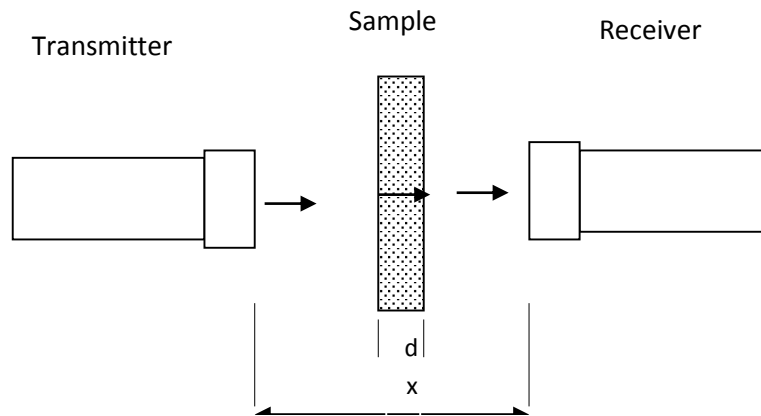


**Figure 3. 7:** Set up for the through transmission measurement. The transmitting transducer emits a signal and the receiving transducer receives the signal.

From this technique, the longitudinal ( $V_l$ ) velocity was determined using Equation 3.1 (Wu 1996) :

$$V_l = \frac{V_w}{1 - \frac{\Delta t \times V_w}{d}} \quad 3.1$$

where  $V_w$  is the velocity sound in water, which is 1490 m/s at room temperature and  $\Delta t$  is the difference in time between the received signal with and without the sample and the transmitted signal.

After measuring the sample density,  $\rho_s$ , the acoustic impedance can be calculated as:

$$Z_l = \rho_s \times V_l \quad 3.2$$

### 3.8 Basic Functional Testing of Prototypes

The functionality of all the fabricated prototypes was tested using pulse-echo measurements. This technique illustrated in Figure 3.8, is used to test whether the element is operational and to determine the axial resolution (pulse-length). This measurement technique requires one transducer for transmitting and receiving; and is what is used by medical imaging transducers to acquire an image.

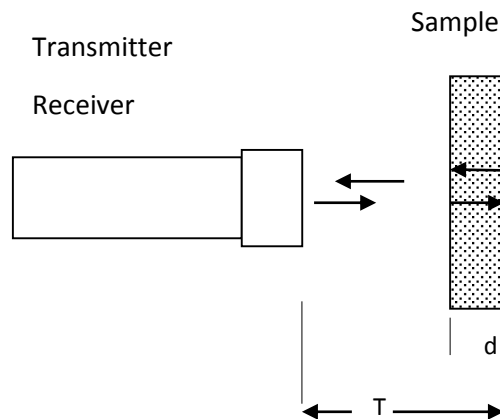


**Figure 3. 8: Set up for the pulse-echo measurement. The same transducer is used for both emitting and receiving the signal.**

To obtain the pulse echo response of both the single element and array transducer prototypes, a stainless steel block was used as a reflector for the ultrasound transmitted by the transducer. Since the transducers were unfocussed, the measurements were taken at a distance beyond the near field boundary (explained in Section 2.4). From

these measurements, axial resolutions,  $R_A$ , were calculated using Equation 2.7. Phantom and tissue scanning was also done using the pulse-echo technique.

The pulse-echo tests of the transducers were done in degassed, de-ionised water at room temperature. The experimental set-up is illustrated in Figure 3.9. A DPR 300 Pulser-Receiver (JSR Ultrasonics, New York, USA) was used to excite the transducers and the echoes were displayed by an oscilloscope. More specific details of the tests are given in Section 3.8.1 and Chapters 6 and 7 for the respective settings of each transducer. Settings were optimised for each individual transducer to obtain the maximum SNR. The frequency spectra of the pulses were analysed and the axial resolution was determined as shown in Equation 2.6. The centre frequency,  $f_c$ , and the fractional bandwidth, BW, at -6 dB were determined by (Li et al. 2011) (Li et al. 2011):

$$f_c = \frac{f_1 + f_2}{2} \quad 3.4$$

$$BW = \frac{f_2 - f_1}{f_c} \times 100\% \quad 3.5$$

where  $f_1$  and  $f_2$  are the lower and upper frequencies at -6 dB of the maximum, that is, the frequencies at which the magnitude in the spectrum is a half of the maximum.

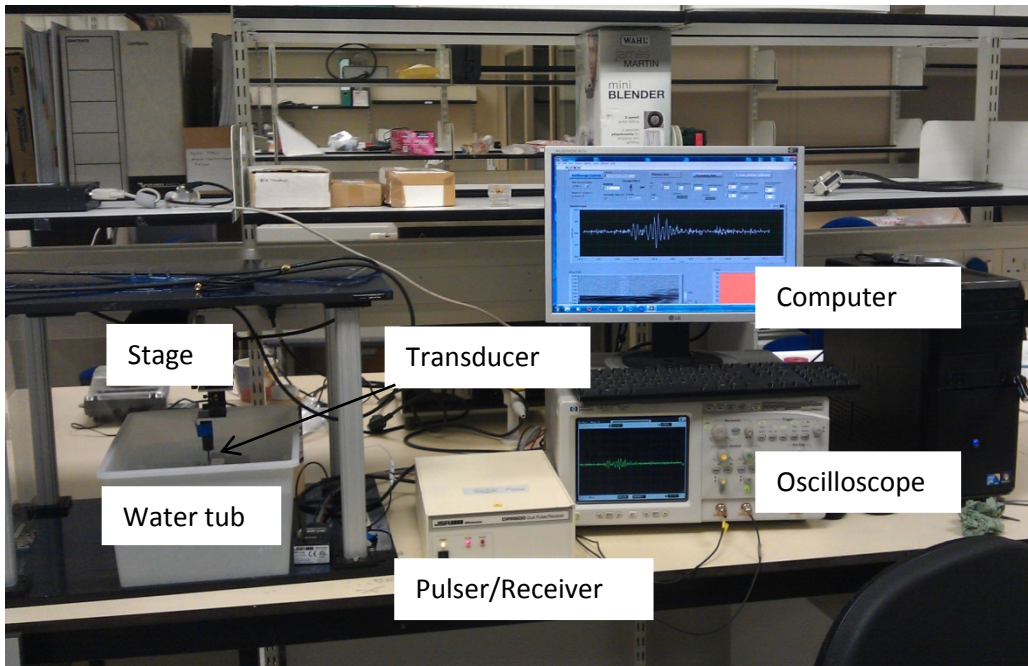
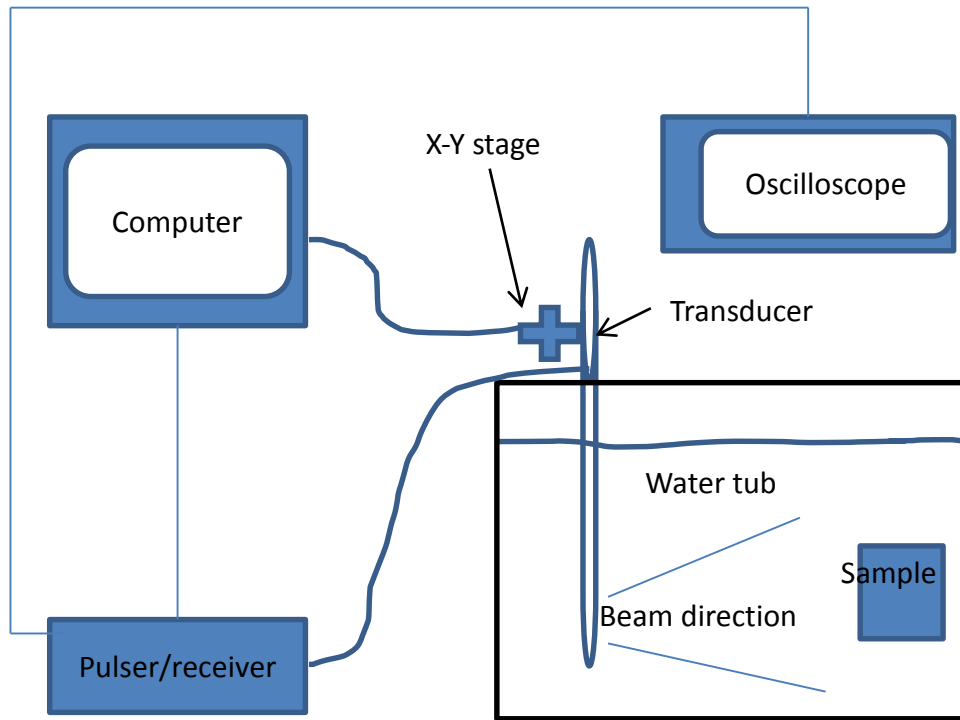


**Figure 3. 9: Apparatus setup of the pulse –echo technique that was used in scanning. The set-up also was used to get signal at one position of a stainless steel block**

### 3.8.1 The scanning system

To obtain a 2D profile image of an object or sample, scanning of the transducer was done using an in-house built scanning system. A block diagram of this system is shown in Figure 3.10 and the different components are discussed below. A LabVIEW (National instruments, Newbury, UK) program with a graphical user interface (GUI) is used to control all the components to produce a scan. The data of the scan is recorded at the end of each scan and MATLAB software (The Mathworks, Cambridge, UK) is used for reconstructing the image.

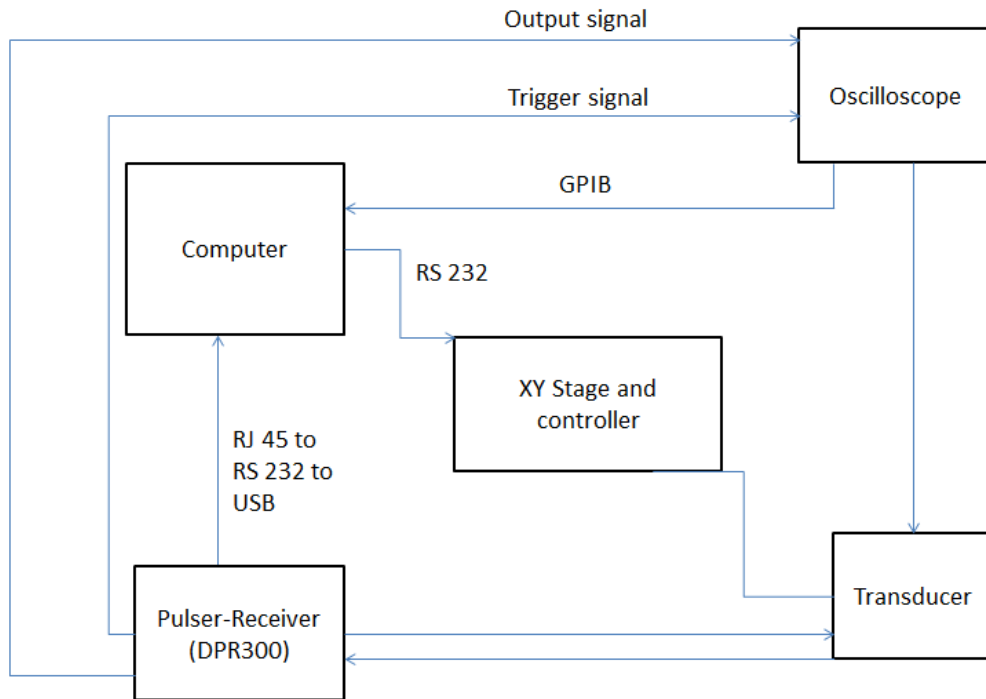


**Figure 3. 10: A block diagram of the in-house built scanning system**

The components of the scanning system are:

- The XY Stage: This is an SG-SP-26-100 XY automatic scanning stage with SHOT-602 stage controller (Sigma Koki, Tokyo, Japan) It has two orthogonal axes (X and Y), moved by stepper motors and connected by an RS232 connection to the computer for control. The minimum resolution of this stage in each direction is 2  $\mu\text{m}$ . The command of this stage is also done by a program written in LabVIEW. The Pulser-Receiver (DPR 300) (JSR Ultrasonics, NY) is connected via USB to the computer. The DPR300 produces a high voltage electrical excitation pulse which is sent to the transducer. The reflections are

detected by the transducer and amplified by the receiver then the output is displayed on the oscilloscope. Control of this pulser-receiver is by the front control panels on the device and the connection to the computer is to interface with the LabVIEW software. Settings such as the receiver gain in dB, pulse energy, and high pass and low pass filter frequency of the pulser-receiver are adjusted on the device. An internal trigger is used and all the other settings can be adjusted to optimise the SNR of the received signal.

- The HP54810A Oscilloscope (Agilent, Edinburgh Park, UK) has two channels with a 500 MHz bandwidth and a sampling frequency 1 GSa/s. It is interfaced with the computer via a GPIB connector. The oscilloscope is also controlled by the LabVIEW software. The sampling frequency and averaging are selected from the software to control the oscilloscope. The range of the time of signal should be selected before a scan is initiated.

MATLAB is used to reconstruct the image from the RF data acquired by the LabVIEW-controlled scanning system. Script files were written to perform signal processing on the data and display B-scan images. The dynamic range of the display image is set by the user. Pulse-echo responses from specific positions were extracted from the data to determine the lateral resolution as explained in Chapter 2.

### 3.8.2 Phantom Imaging

Three different phantoms were used to test the functionality of the single element transducers. These were undertaken using the in-house built scanning system described in Section 3.8.1. The phantoms for testing included wires of different thicknesses attached to a stainless steel block with double sided tape. This was done since it was easy to get a reflection of the sound energy from the stainless steel block (Figure 3.11) which made it less challenging to set up. The wires were 130  $\mu\text{m}$ , 420  $\mu\text{m}$  and 1.16 mm thick; they were spread at arbitrary distances apart.

The wire phantom illustrated in Figure 3.12 is a very common arrangement of test targets for characterising transducers. The phantom tested in this project had two 5  $\mu\text{m}$  diameter tungsten wires at the top and nine 20  $\mu\text{m}$  diameter wires all spaced by 1 mm steps. These were glued to a block as shown in Figure 3.12. The biggest challenge is that it was very easy for these wires, especially the smaller ones, to break. As a

result, some tests were done without the 5  $\mu\text{m}$  wires. The wires also easily displaced from their set positions on the block when immersed in water as the holding glue loosened. From this test, a line spread function was determined for some of the single element transducers discussed in Chapter 6. The transducers were positioned beyond the near field boundary. They were moved laterally to the sample with a scanning step size determined based on the operational frequency and expected lateral resolution of the device. The amplitudes of the responses were plotted against position. The line spread function in this project was used to determine the lateral resolution of the transducers.

Mouse bowel was also scanned using the transducers. The tissue was immersed in Phosphate buffered saline (PBS) (Moser et al. 1993). Tissue does not reflect as highly as stainless steel or tungsten because the acoustic impedance is much lower. Obtaining these images is crucial in establishing that the transducers can image structures similar to that in the human body.

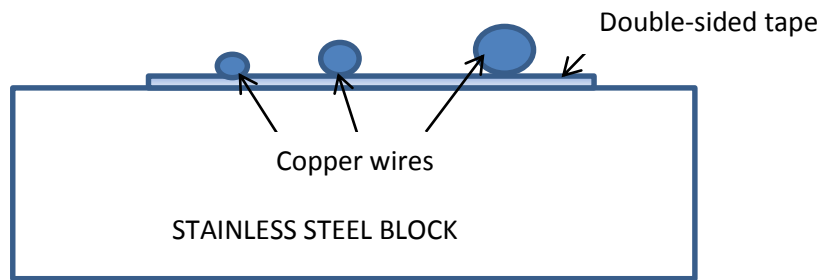


Figure 3. 11: Stainless steel block with wires attached with double sided tape. The wires were 130  $\mu\text{m}$ , 420  $\mu\text{m}$  and 1.16 mm thick; they were spread arbitrary distances apart.

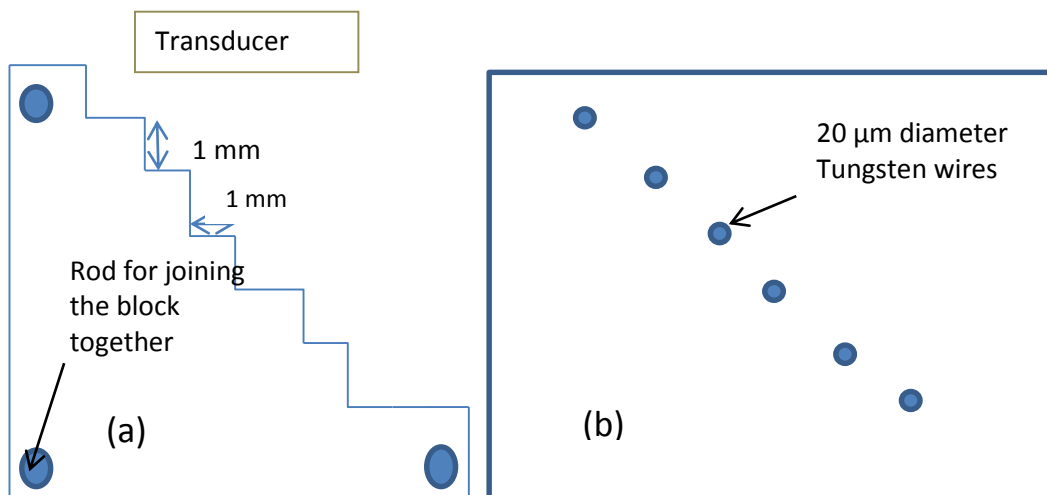


Figure 3. 12: Wire phantom: (a) Block side view configuration, (b) cross-section view with wire positions. The transducer at the top is scanned in a direction lateral to the block. The ultrasound image produced is similar to (b)

### 3.9 Chapter Discussion and Conclusions

This chapter has discussed important aspects to consider when designing transducers for incorporation into needles, such as packaging, clinical performance, and operational frequency which have been detailed to explain needs to account for the confined space packing. The needle sizes have been summarised to give guidance for the design as it is restricted by the commercially available needles. Array orientations have been considered with the side linear array chosen as the best in terms of fabrication and for the application. Helical flexi-circuit orientation has been chosen as the design to be used in this project. Material characterisation and prototype evaluation techniques have been explained in this chapter, providing a foundation for evaluating the devices designed in the subsequent chapters.

The details discussed in this chapter set a good precedent for the design and the fabrication of the prototypes explained in later chapters. It is important to keep in mind what the end product should do and how it will be used. By considering the different topics such as needle sizes and transducer operational frequency, the dimensions of the transducers for the application can easily be determined.

### 3.10 References

- Ahn, W., Bahk, J.-H. and Lim, L.Y.-J. 2002. The “Gauge” System for the Medical Use. *Anesthesia and Analgesia* 95(4), p. 1125.
- Boutsioukis, C., Lambrianidis, T. and Vasiliadis, L. 2007. Clinical relevance of standardization of endodontic irrigation needle dimensions according to the ISO 9,626:1991 and 9,626:1991/Amd 1:2001 specification. *International endodontic journal* 40(9), pp. 700–6.
- Curiel, L., Chopra, R. and Hynynen, K. 2007. Progress in Multimodality Imaging: Truly Simultaneous Ultrasound and Magnetic Resonance Imaging. *IEEE Transactions on Medical Imaging* 26(12), pp. 1740–1746.
- Daviden, R.E. and Smith, S.W. 1996. A Multiplexed Two-Dimensional Array for Real time Volumetric and B-Mode Imaging. In: *IEEE Ultrasonics Symposium* Ultrasonics. pp. 1523–1526.
- Dickinson, R.J. and Kitney, R.I. 2004. Miniature ultrasonic probe construction for minimal access surgery. *Physics in Medicine and Biology* 49(16), pp. 3527–3538.

- Eberle, M.J. and Finsterwald, M.P. 2003. Method for Manufacturing a High Resolution Intravascular Ultrasound Transducer Assembly having a Flexible Substrate.
- Felix, N., Voisin, D., Clade, O. and Dufait, R. 2005. Biplane ultrasound arrays with integrated multiplexing solution for enhanced diagnostic accuracy in endorectal and transvaginal imaging. In: *Ultrasonics Symposium*. pp. 2251–2254.
- Holton, A., Walsh, E., Anayiotos, A., Pohost, G. and Venugopalan, R. 2003. Comparative MRI Compatibility of 316L Stainless Steel Alloy and Nickel-Titanium Alloy Stents. *Journal of Cardiovascular Magnetic Resonance* 4(4), pp. 423–430.
- Ledworuski, R., Lehr, H., Niederfeld, G., Walter, S., Rühl, F. and Tschepe, J. 2002. A new ultrasonic catheter system with LIGA geared micromotor. *Microsystem Technologies* 9(1-2), pp. 133–136.
- Lee, W., Idriss, S.F., Wolf, P.D., Dixon-tulloch, E., Angle, J.F. and Smith, S.W. 2003. Advances in 2-D Array Catheter Transducer for Real-Time Three-Dimensional Intracardiac Echocardiography. In: *IEEE Ultrasonics Symposium*. pp. 672–675.
- Lee, W., Idriss, S.F., Wolf, P.D. and Smith, S.W. 2004. A miniaturized catheter 2-D array for real-time, 3-D intracardiac echocardiography. *IEEE transactions on ultrasonics, ferroelectrics, and frequency control* 51(10), pp. 1334–46.
- Li, X., Wu, W., Chung, Y., Shih, W.Y., Shih, W.-H., Zhou, Q. and Shung, K.K. 2011. 80-MHz intravascular ultrasound transducer using PMN-PT free-standing film. *IEEE transactions on ultrasonics, ferroelectrics, and frequency control* 58(11), pp. 2281–8.
- Maclennan, D. 2010. Fundamental characterisation and early functional testing of micromoulded piezocomposites.
- Moser, A.R., Mattes, E.M., Dove, W.F., Lindstrom, M.J., Haag, J.D. and Gould, M.N. 1993. ApcMin, a mutation in the murine Apc gene, predisposes to mammary carcinomas and focal alveolar hyperplasias. *Proceedings of the National Academy of Sciences of the United States of America* 90(19), pp. 8977–81.
- Proulx, T.L., Tasker, D. and Bartlett-Roberto, J. 2005. Advances in catheter-based ultrasound imaging Intracardiac Echocardiography and the ACUSON AcuNavTM Ultrasound Catheter. In: *IEEE Ultrasonics Symposium, 2005*. IEEE, pp. 669–678.
- Selfridge, A.R. 1985. Approximate Material Properties in Isotropic Materials. *IEEE Transactions on Sonics and Ultrasonics* 32(3), pp. 381–394.
- Smith, S.W. and Davidsen, R.E. 1998. Two-Dimensional Arrays for Medical Ultrasound Using Multilayer Flexible Circuit Interconnection. *IEEE Transactions on Ultrasonics Ferroelectrics and Frequency Control* 45(2), pp. 338–348.

Van der Steen, A.F.W., Baldewsing, R. a, Levent Degertekin, F., Emelianov, S., Frijlink, M.E., Furukawa, Y., Goertz, D., Karaman, M., Khuri-Yakub, P.T., Kim, K., Mastik, F., Moriya, T., Oralkan, O., Saijo, Y., Schaar, J. a, Serruys, P.W., Sethuraman, S., Tanaka, A., Vos, H.J., Witte, R. and O'Donnell, M. 2006. IVUS beyond the horizon. *EuroIntervention : journal of EuroPCR in collaboration with the Working Group on Interventional Cardiology of the European Society of Cardiology* 2(1), pp. 132–42.

Stephens, D.N., Cannata, J., Liu, R., Zhao, J.Z., Shung, K.K., Nguyen, H., Chia, R., Dentinger, A., Wildes, D., Thomenius, K.E., Mahajan, A., Shivkumar, K., Kim, K., O'Donnell, M. and Sahn, D. 2008. The acoustic lens design and in vivo use of a multifunctional catheter combining intracardiac ultrasound imaging and electrophysiology sensing. *IEEE Transactions on Ultrasonics Ferroelectrics and Frequency Control* 55(3), pp. 602–618.

Wu, J. 1996. Determination of velocity and attenuation of shear waves using ultrasonic spectroscopy. 99(August 1995), pp. 2871–2875.

# CHAPTER 4

---

## Array Modelling and Beam Simulation

---

### Chapter Profile

A number of aspects of the configuration and packaging of a transducer in a needle were investigated during the course of this research. This chapter gives the analysis of the imaging performance of the transducer array at a design stage using computational modelling and simulation. One dimensional modelling (ODM) and virtual prototyping with finite element analysis (FEA) were used to determine the characteristics of the transducer stack, and FIELD II, a linear acoustic model, was used to examine the beam pattern produced by different array designs. A resolution integral is evaluated from the simulated beam patterns as a figure of merit to compare the performance of different transducers in terms of resolution over imaging depth of field at a design stage. The beam patterns for both linear and phased arrays were explored, and the effects of dimensional limitations imposed by the requirement to fit the array into a needle are examined by simulation.

Characterisation of the materials used is discussed here as a good tool to enable virtual prototyping which was used as a design tool. Virtual prototyping was done using PZFlex FEA software (Weidlinger Associates, Inc, Mountain View, CA, USA) to investigate the feasibility of modelling devices of single crystal materials. It was also used to study to the effect of different layer thicknesses in a 15 MHz transducer.

A feasibility study was undertaken looking at the design and fabrication of a 30 MHz transducer into a needle and this was used as a precursor to the 15 MHz transducer. A 30 MHz transducer array was considered and the challenges explored with input from a design engineer at Envision Design Limited (Kincardineshire, UK). This is because the 30 MHz array would provide a very good resolution but there was no array control system available to the research group for driving the array at that frequency. The report of the study of the 30 MHz array is detailed in Appendix A. It explores the

challenges in fabrication and explains some of the trade-offs employed in order to get working prototypes.

#### **4.1 Introduction**

It has been explained, in the previous chapters, that the higher the frequency of an ultrasound transducer, the smaller the dimensions. These small features create a great challenge in fabrication and as such it is very expensive and time consuming to fabricate transducer prototypes. Virtual prototyping is a method where prototypes are built and tested in software. This reduces the expense of time, materials and effort that would be invested in building prototypes. Virtual prototyping with FEA can be used to optimise the materials and dimensions of the transducer layers, and determine fabrication tolerances in a cost-effective and time efficient manner. In addition, the impact of design constraints imposed by fabrication processes and packaging requirements for specific applications can be investigated.

To get a good model for virtual prototyping, detailed accurate material properties are essential. Ideally, in-house full material characterisation is recommended (Powell et al. 1997; Abboud et al. 1998) to obtain accurate properties for the specific materials used in the devices. However, for piezoelectric materials, full material characterisation is expensive due to the requirement to have multiple specific sample geometries. The cost in money and time is increased when piezoelectric crystals are used as the active materials. Obtaining accurate piezoelectric properties for most of these materials is difficult and this in turn hugely affects the validity of the simulation evaluation. The characterisation of the PMN-PT single crystal materials that were used in this project was done in a different project (Qiu et al. 2011). However, as it will be explained later on in this chapter, some material properties were modified in the model to get a better match between the experiment and simulation. In this project only the passive materials were characterised for their acoustic performance.

#### **4.2 Transducer Materials**

The choice and characterisation of materials for the prototypes is explained in this section.

#### 4.2.1 *Passive Materials*

Some of the properties of the passive materials that were used for the transducers in this study are summarised in Table 4.1. These properties are important in choosing the right material with the optimum properties for the transducer. The materials were chosen because they are extensively used in the literature (Rhee et al. 2001; Zhou et al. 2009; Wang et al. 2001; Grewe and Gururaja 1989) These materials are epoxies filled with alumina or tungsten, respectively. The epoxy used is Epofix due to its low shrinkage properties during curing (Bernassau et al. 2011). Changing the percentage of the alumina or tungsten particles in the epoxy also changes the acoustic behaviour of the material. Since the matching layer is designed to acoustically match the impedance between the piezoelectric material and the body, the impedance of the matching layer needs to be tailored to the piezoelectric substrate. Standard bulk piezoelectric materials have known acoustic impedances and therefore selection of matching layers can be less challenging. When composites are used as the piezoelectric material of choice, the acoustic impedance of the composite must be measured or calculated. Sometimes multiple matching layers are used and these need to be designed to facilitate efficient transfer of the ultrasonic energy. The passive material properties shown in Table 4.1 are comparable to those found in the literature (Grewe and Gururaja 1989). The matching layer is 15% volume of alumina in epoxy whereas the backing is 30 % volume of tungsten in epoxy. The properties were determined as per methods described in Sections 3.7.2.

**Table 4. 1: Properties of some of the passive materials used in the transducer prototypes**

<b>Material</b>	<b><math>\rho(\text{kg/m}^3)</math></b>	<b><math>V_l(\text{m/s})</math></b>	<b><math>Z(\text{MRayl})</math></b>
<b>Matching</b>	1567	2277	3.6
<b>Epofix epoxy</b>	1152	2497	2.9
<b>Backing</b>	5791	1282	8.2

#### 4.2.2 *Active materials*

Though some prototypes were made from piezoelectric ceramics, the active material of choice for the arrays was single crystal composite due to the enhanced performance as discussed in Chapter 2. Piezocomposites of single crystal piezoelectric materials

have higher coupling coefficients compared to the conventional PZT polycrystalline ceramics. These materials, such as PMN-PT, are relatively new and their properties are still being studied (Qiu et al. 2011; Li et al. 2011). The PMN-PT material used in this study was characterised using PRAP (TASI Software, Kingston, ON, Canada), a piezoelectric material analysis software package, to determine the complete matrix of piezoelectric material properties. The full matrix of material properties is needed for accurate FEA, while only subset of the properties is required for ODM.

### **4.3 Array Modelling and Simulation Methods**

Modelling is a powerful tool in the design phase of ultrasound transducers. Knowledge of the physics of wave propagation, vibrations, electronics and material science is important in analysing the transducer performance. A prediction of behaviour of a transducer can be determined prior to fabrication. This stage eliminates the time consuming process of correcting numerous faults after a device is fabricated. All the components of the transducers including the active substrate, matching backing and cabling can be evaluated through modelling and simulation. ODMs use equivalent circuits to provide first order approximations of the transducer characteristics. FIELD II simulation gives a good approximation of the beam pattern and; FEA facilitates the analysis of both two and three dimensional characteristics, which may include coupling between pillar resonances as well as the kerf filler effects in composites.

### **4.4 One-Dimensional Modelling (ODM)**

This is the easiest and most common method of evaluating the performance of devices, or comparing the effects of materials, layers or layer thicknesses before fabrication. In-house ODM software was used to model the effects of using a composite compared to using a bulk material. This one-dimensional model is based on wave propagation in the device (Cochran et al. 2012). It incorporates the underlying physics which are ultimately based on the constitutive equations of the piezoelectric material discussed in Section 2.3. The model is used to only evaluate the thickness extensional mode behaviour of in ultrasound transducers.

For an array, ODM can be used to define the thickness of the piezoelectric composite, the acoustic impedance of the backing, the acoustic impedance and thickness of matching layers, the effects of bond lines, and the effect of electrical impedance

matching. The acoustic impedance and the thickness of the layers in the stack determine the time domain and the frequency domain response of the transducer (T Ritter 2000). With ODM, the electrical impedance, pulse-echo behaviour and the impulse response of a transducer can also be predicted.

#### 4.4.1 Transducer Stack Model

ODM was used to explore the basic properties of the transducer. It was used to explore the thickness of the transducers for a given frequency before fabrication, including the difference in resonance frequencies between bulk and composite plates. The impedance spectrums of 15 MHz and 30 MHz transducers were calculated to determine the frequency performance of the transducer. The results of the 30 MHz transducer are shown in Appendix A. From Figure 4.1, the transducer structure that was modelled is illustrated. This was used as the basis for the modelling investigating different features about the layers of the transducer. From the model, the expected behaviour of transducer, including the piezoelectric and passive materials, was determined. Properties input into this model include the geometry as well as the material properties of each layer in the transducer.

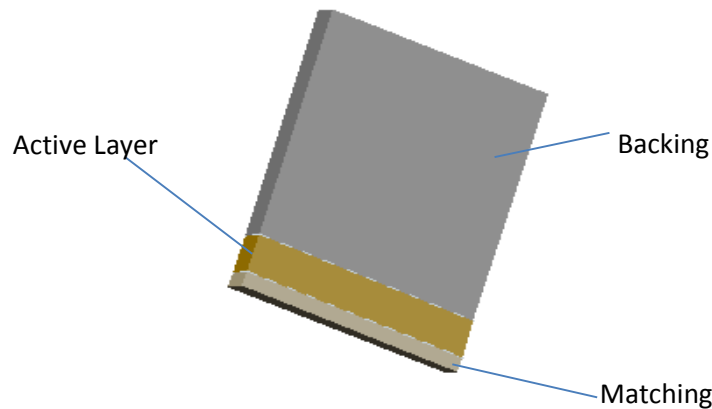


**Figure 4. 1: The transducer stack used for one dimensional modelling, incorporating a matching layer, a piezoelectric material as the active layer and backing layer. Active layer thickness is 80  $\mu\text{m}$ , matching layer thickness is 50  $\mu\text{m}$  and backing thickness is 800  $\mu\text{m}$**

The active layer was chosen to be a composite made from PMN-PT single crystal material and a polymer. PMN-PT provides better properties, such as electromechanical coupling coefficient, than the common piezoelectric ceramics available, making it more sensitive. This material, being very brittle and expensive, meant that modelling

would help to cheaply evaluate many designs. A 1-3 piezocomposite was evaluated with the model, to get the transducer with the best properties. This 1-3 composite provides advantages such improved electromechanical coupling coefficient and reduced acoustic impedance which improves the overall efficiency. It is also important to have an electrical impedance magnitude as close to  $50 \Omega$  as possible since this would reduce the loss of energy as the system is connected to the driving electronics. The driving electronics are designed to have  $50 \Omega$  resistance.

The thickness of the active layer determines the resonance frequency and this can be used to determine the thickness of the matching and the backing layers. The chosen frequency of the transducer was 15 MHz and therefore, an empirical approximation of the thickness was determined. It is important to remember that different piezoelectric materials will have different thicknesses at a given frequency because of the different speeds of sound. The transducer stack was modelled with both a bulk PMN-PT single crystal layer and with a composite PMN-PT/epoxy layer with 36% volume fraction. One element in an array was modelled with the dimensions of  $0.8 \times 0.07 \times 0.12$  mm in terms of length, width and thickness. These dimensions were based on the fact the transducer would fit in a needle of about 1 mm. Inter-elemental pitch of 0.100 mm would mean that the element would be about 0.07 mm and the thickness is determined by the desired frequency.

#### **4.4.2 Transducer stack results**

In Figure 4.2, impedance plots of PMN-PT single crystal and a PMN-PT/epoxy composite are illustrated. There is evidence for the higher thickness-mode coupling coefficient in the composite material. This is seen by the larger separation between the electrical and the mechanical impedance magnitudes. The composite has lower permittivity which leads to higher electrical impedance magnitude at the resonance frequency.

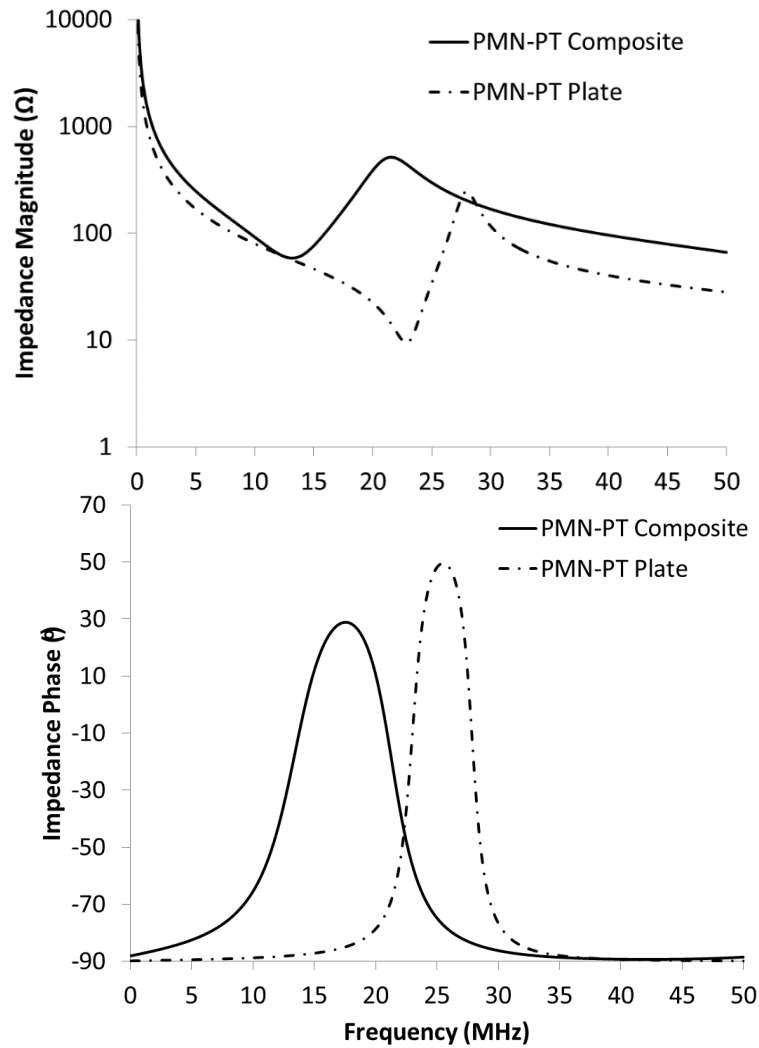


**Figure 4. 2: Electrical impedance magnitude and phase of a 0.082 mm thick element calculated with ODM. The PMN-PT/Epoxy composite element with 0.36 volume fraction; (a) impedance magnitude, (b) impedance phase**

By using a composite instead of a bulk piezoelectric material, a number of important properties are changed. The most important of these properties are the acoustic and electrical impedance, electromechanical coupling coefficient and resonance frequency, and this can be used as a useful guide when designing a composite and building a transducer. Table 4.2 summarises these key differences. The properties of the epoxy filler in Table 4.2 are similar to the Epofix used for the prototypes discussed in this thesis (Bernassau et al. 2011).

Table 4. 2: Comparison of the ODM modelled PMN-PT and PMN-PT/Epoxy composite

Material	PMN-PT	PMN-PT Composite
Epoxy filler	None	CY1301/HY1303 (Marin-Franch et al. 2004) (Bernassau et al. 2011)
Volume fraction	1	0.36
Electromechanical coupling coefficient ( $k_t$ )	0.62	0.83
Impedance Magnitude at resonance frequency	10 $\Omega$	63 $\Omega$
Electrical resonance frequency	22 MHz	12.6 MHz
Acoustic Impedance	37 MRayl	12.78 MRayl

#### 4.5 Virtual Prototyping of Devices

ODM is useful in choosing the piezoelectric, matching and backing materials plus their thicknesses. The inter-elemental pitch can also be studied for its influence on grating lobes. FEA takes this further to enable analysis of two and three dimensional characteristic of the transducer. In effect the entire transducer can be virtual prototyped through FEA.

PZFlex (Weidlinger Associates Inc., Mountain View, CA), a time domain finite element analysis (FEA) software package, was used for virtual prototyping. The electrical impedance of the designed devices at various stages in the fabrication process were predicted using PZFlex. Using realistic 2D and 3D models of the device enables rapid testing of ranges of design parameters. However, for simulated and experimental results to match, accurate material properties are required. An incremental model-build-test approach (Powell, Wojcik et al. 1997) was used to validate the models developed for virtual prototyping (Ssekitoleko et al. 2010). A 5 MHz linear array was modelled at the different fabrication stages. Figure 4.3 shows the models that were evaluated with PZFlex. The dimensions are discussed in the following sections.

Results from the piezoelectric plate and composite models were compared to experimental electrical impedance measurements to verify the input material properties. Once the material properties had been verified, they were used to explore virtual devices at 15 MHz.

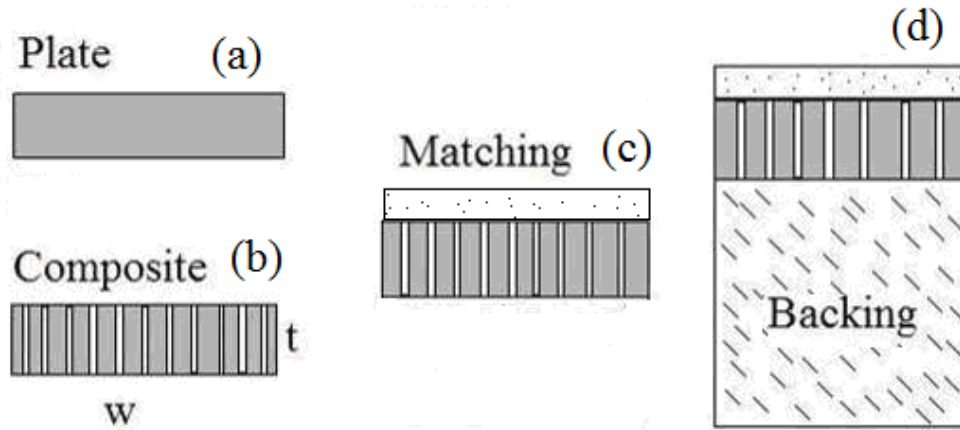


**Figure 4.3: Configurations used in incremental model of linear array. (a) Bulk piezoelectric plate, (b) 1-3 piezocomposite, (c) matched composite transducer, and (d) matched and backed composite transducer. This image gives illustrations of steps taken during simulation.**

#### 4.5.1 Ceramic plate

The models created in PZFlex were initially validated using a 10 mm x 10 mm x 1 mm plate of CTS 3203HD, a material commonly used in medical transducers, with material properties characterised previously (Sherrit et al. 1997). A simple 2D model of the plate in air was used to compare the model to the experimental results. This model was then used to analyse the behaviour of a PMN-PT single crystal plate and obtain the modified material properties required for simulation to match experiment. The results of the CTS 3203HD plate comparing the model to the experiment are shown in Figure 4.4. The accuracy and stability of the material properties of this material means that there was no need for modification of the material properties through the model to obtain a good match. The modelled impedance curve yields a reasonable match to the experimental measurement, both in terms of impedance magnitude and resonant frequencies.

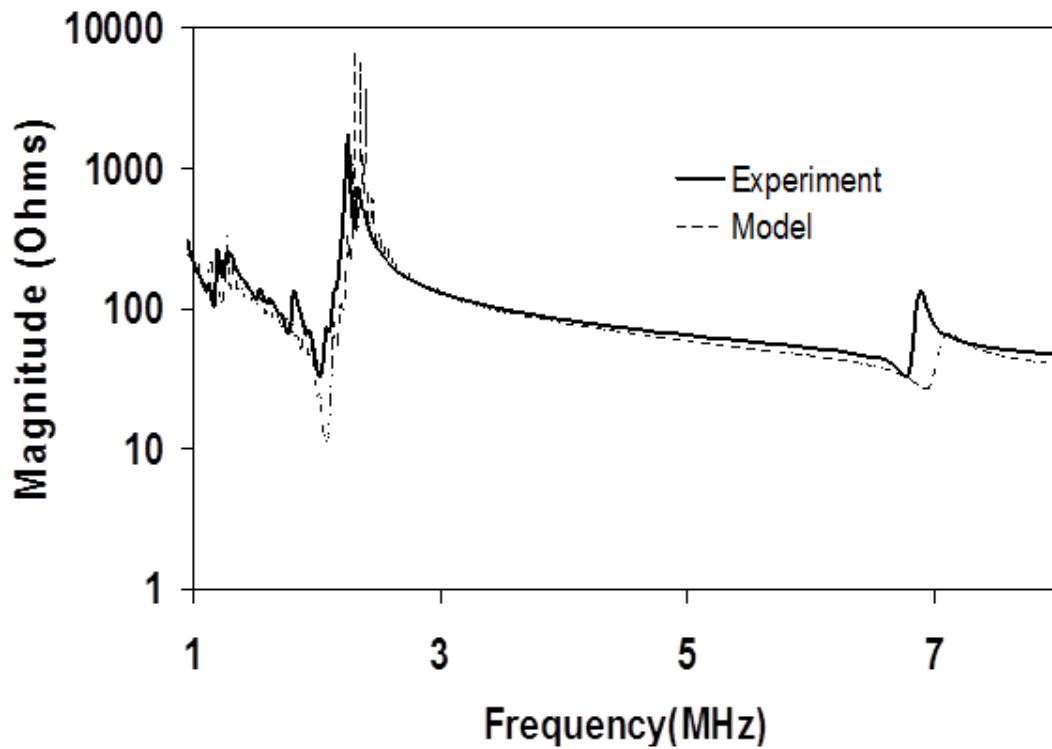


Figure 4.4: Electrical impedance magnitude response for 10 mm square plate with a thickness of 1 mm made of CTS 3203HD material comparing the simulation to the experimental results.

#### 4.5.2 *Single crystal plate*

After validating the 2D plate model with CTS 3203 HD, properties of PMN-PT were loaded into this model and analysed. It can be very challenging to experimentally obtain single crystal properties and therefore the model was used to extract more accurate properties of the PMN-PT as shown in Figure 4.5. The thickness of the sample was 1 mm with a 10 mm width. The impedance magnitude away from the resonance shows a good match to the experiment. This means that the dielectric properties do not have to be modified. However, the mechanical resonance does not agree well with the experiment. This means the piezoelectric constants have to be changed to get a better fit for the simulated impedance results to match the experiment. Model (i) in Figure 4.5 (a) represents the results with the initial properties input into the model. Model (ii) has 20 % larger piezoelectric stress constants, which increases the mechanical resonant frequency. Model (iii), with 50% larger piezoelectric stress constant than the initial values, agrees well with the experimental measurements from both this plate and other

plates from the same supplier, TRS (Figure 4.5 (b)), for which there is only minimal variation in behaviour. The detailed modified properties are shown in Table 4.3.

**Table 4. 3: Material properties of PMN-PT single crystal**

Material Constant	Measured	Modified - Plate	Modified - Composite	% difference	
				Plate	Comp.
$\epsilon_{11}^e$	1220	1220	2196	0	80
$\epsilon_{11}^e$	926	926	1667	0	80
$C_{11}^E (10^{10} \text{N/m}^2)$	10.6	10.6	16.96	0	60
$C_{12}^E (10^{10} \text{N/m}^2)$	9.2	9.2	14.72	0	60
$C_{13}^E (10^{10} \text{N/m}^2)$	10.5	10.5	16.8	0	60
$C_{33}^E (10^{10} \text{N/m}^2)$	11.5	11.5	18.4	0	60
$C_{55}^E (10^{10} \text{N/m}^2)$	6.9	6.9	11.04	0	60
$C_{66}^E (10^{10} \text{N/m}^2)$	2.1	2.1	3.36	0	60
$e_{15} (C/m^2)$	8.8	13.2	11.44	50	30
$e_{31} (C/m^2)$	-5.9	-8.85	-7.67	50	30
$e_{33} (C/m^2)$	21.2	31.8	27.56	50	30
$\rho (kg/m^3)$	8086	8086		0	0

There is a noticeable difference when the same model with PMN-PT properties is compared to other experimental results of PMN-PT from a different supplier, Sinoceramics, as illustrated in Figure 4.5(c).

The resonances seen at approximately 1.5 MHz in Figure 4.5(a) and (b) are a result of minor modes in the materials (Wallace 2007). These resonances are reduced when composites are used. The plates from the second supplier were 0.5 mm thick, and as such the model thickness was adjusted, but the material properties kept the same as in Model (iii). These differences in properties between samples from an individual supplier and the larger variation between suppliers is expected (Qiu et al. 2011), stressing the need for validation of the material properties used in models.

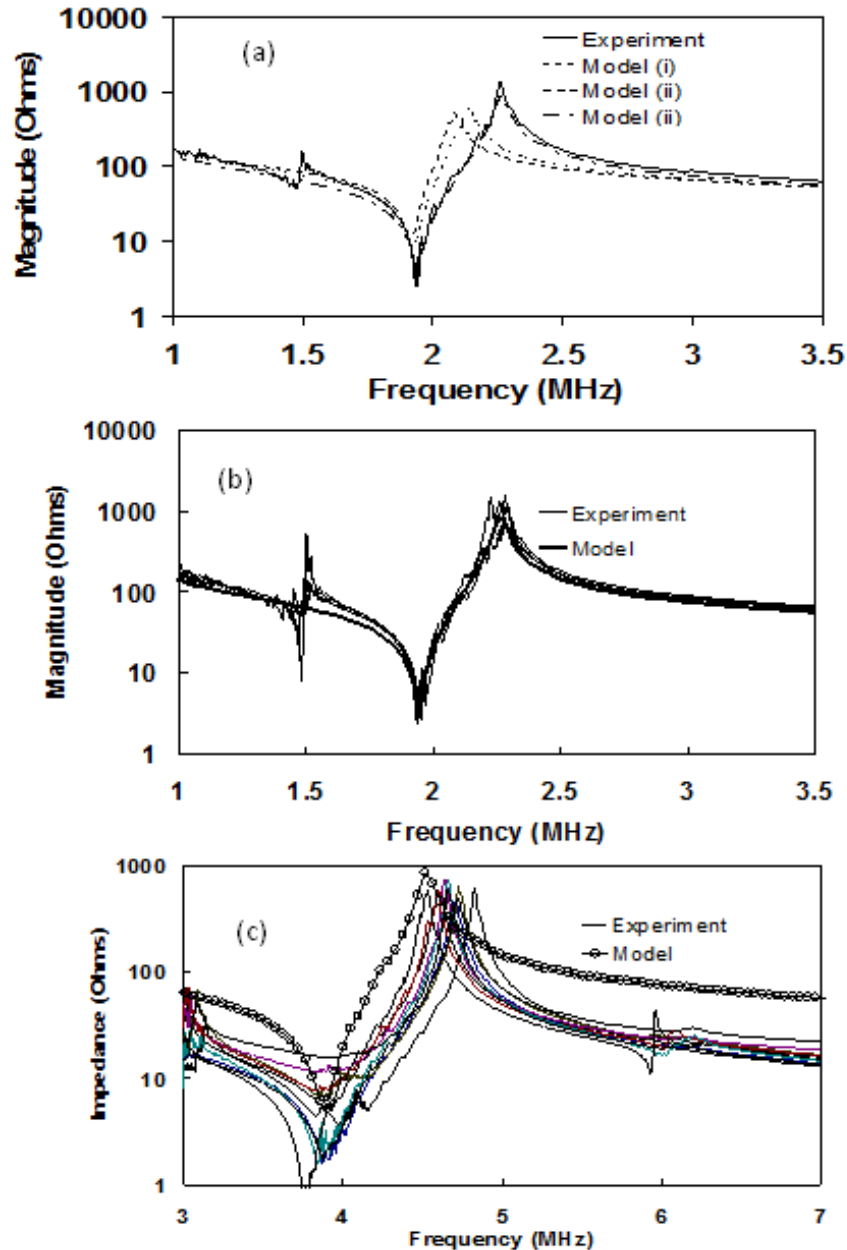


Figure 4. 5: Electrical impedance magnitude response for a PMN-PT single crystal plate. (a) Comparing experimental measurements of 1 mm plate from TRS to simulation results with modified piezoelectric constants. (b) Variation between experimental results for plates from TRS compared to model with modified material properties. (c) Variation between experimental results for 0.5 mm thick plates from Sinoceramics compared to a model with modified material properties.

### 4.5.3 *Single crystal composite*

The simulation model was further extended into 3D to evaluate a unit cell of a 5 MHz, 1-3 piezocomposite with a 0.49 volume fraction of PMN-PT in order to be compared with the experimental results. This volume fraction was used because it lies in the range of 0.3 to 0.5 where the electromechanical coupling coefficient is maximised (Chan and Unsworth 1989; Smith 1986; Zipparo et al. 1999). The experimental plate was 10 mm in length, 5 mm in width with a thickness of 0.5 mm.

The 1-3 piezocomposite model required more detailed change to material properties than the plate model, shown in Table 4.3, and as a result the new properties are significantly different to the initial properties. The reasonable match between the model and the experimental impedance results, shown in Figure 4.6, is a result of these modifications to the properties. In a 1-3 composite, the pillars resonate in a length extensional mode, whereas the initial material properties are influenced more by the thickness extensional mode parameters extracted from a plate. Also, the dice-and-fill fabrication process can affect the poling of the material, particularly at the edge of the pillars. Therefore, to ensure that the piezoelectric material is operating optimally, the fabricated composite plate was re-poled. After re-poling the composite, the anti-resonant frequency increases as expected because the piezoelectric properties improve. However, the changes are small, with the modelled result fitting between the two experimental measurements.

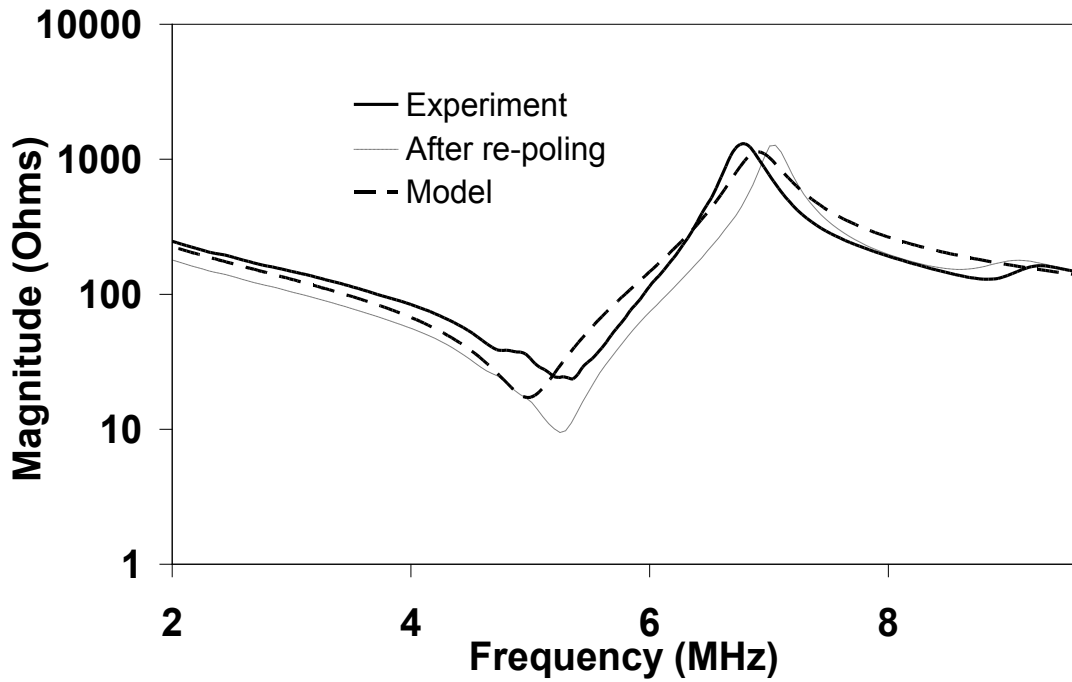


Figure 4.6: Electrical impedance magnitude for a PMN-PT single crystal/epoxy composite, before and after re-poling and compared with simulation using modified material properties.

#### 4.5.4 15 MHz array element stack

A 15 MHz array element was modelled using the composite properties as detailed in Section 4.5.3. Following the validation of the material properties, the acoustic stack of the 15 MHz linear array was modelled to evaluate the effect of matching and backing layers. A single unit cell of the piezocomposite was simulated, with the electrical impedance response scaled to the  $70\mu\text{m} \times 800\mu\text{m}$  element dimensions which are equal to the array element design. The composite with 50  $\mu\text{m}$  and 60  $\mu\text{m}$  thick alumina-filled epoxy matching layers was modelled. Finally, an 800  $\mu\text{m}$  thick tungsten-filled epoxy backing layer was added to the model to evaluate the behaviour of the complete acoustic stack.

Through virtual prototyping, the effect of different thicknesses of matching layers is shown in Figure 4.7. The upward shift in the primary resonant frequency at about 18 MHz and the lower frequency resonance curve at about 10 MHz are due to the matching layer and can be clearly seen. The expected damping of the resonance with the backing layer is also demonstrated. This is shown as an example for investigating different parameters of high frequency arrays. The volume fraction of the backing is 0.3 and that of the matching is 0.15.

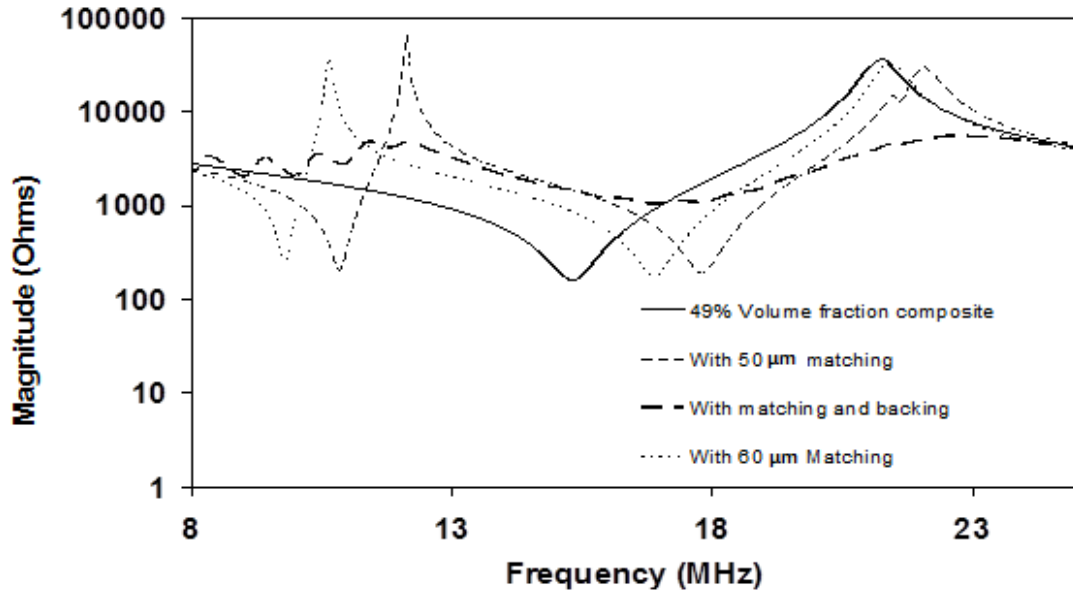


Figure 4. 7: Electrical impedance magnitude response for a modelled high frequency array element with 1-3 piezocomposite of PMN-PT. The thickness of the matching layer for the stack with backing is 50  $\mu\text{m}$ .

The array design for the prototypes was based on a 1-3 piezocomposite substrate, using single crystal PMN-PT for increased sensitivity compared to conventional ceramics like PZT-5H. The initial design is an 80  $\mu\text{m}$  thick, 0.49 volume fraction piezocomposite with 60 $\mu\text{m}$  pillar pitch. The composite fill material is Epofix (Struers, Solihull, UK). The quarter wave matching layer of 15 vol% alumina filled epoxy is 50  $\mu\text{m}$  thick, and the backing layer is 30 vol% tungsten filled epoxy 800  $\mu\text{m}$  thick.

#### 4.6 FIED II Simulation

Field II is a MATLAB based simulation code (Jensen 1991; Jensen and Svendsen 1992) for pressure fields and beam profiles. The software uses the idea of the Rayleigh integral to determine the spatial impulse response of the ultrasound field emitted as a function of the transducer aperture, the position of the point of evaluation in space, and the propagation speed. Through taking a time convolution of the spatial impulse response with the time derivative of the surface vibration velocity, the emitted pressure of a vibrating aperture can be determined. By reciprocating the linear acoustics, the receive response can also be established from the emitted waves from points in the field of propagation. The program uses an integral expression of Huygens principle to calculate the acoustic propagation from the source apertures. Field II can be used to

study such things as beam profiles and to determine if side lobes occur by predicting the azimuth plane beam profile for an array of elements (Timothy Ritter 2000). Side lobes are unwanted regions of the ultrasound beam emitted off axis that are constructive interference and produce image artefacts (Barthez et al. 1996). The main aim of design optimization is to have beam patterns with narrow main lobe width and low amplitude side lobes (Onose et al. 2009).

#### *4.6.1 The beam pattern*

The acoustic beam pattern of an imaging transducer provides important information about the performance of the transducer. It gives the resolution of the transducer as well as indicating any side lobe interference relative to the main lobe. Different design parameters of a transducer will affect the overall beam pattern. By examining the beam pattern at the design stage, geometries can be optimised. The overall results provide a general picture on the trade-offs between system complexity, fundamental electronic characteristics, image quality in relation to ultrasonic fields generated by the physically constrained apertures, and functionality.

Exploring the beam profiles of the transducer before they are made also helps to overcome the laborious process of making the transducers just to see if they work well. FIELD II provides a platform to explore the beam patterns produced by different transducers at a design stage. This software was used to explore parameters such as pitch of the elements, inter-elemental pitch, and the kerf between elements. Appendix A gives details of acoustic beam pattern evaluation of 30 MHz transducers including single element, annular, phased and linear arrays. In this section, 15 MHz phased and linear arrays are studied as they are closer to the work of this thesis. On an empirical scale, the phased arrays have a smaller element pitch and a shorter array length compared to linear arrays, and would therefore fit into smaller spaces. However, they would provide more challenges during fabrication due to the small features.

Two of the key factors in choosing an ultrasound imaging transducer are resolution and penetration depth. Transducers operating at low frequency penetrate deeper into tissue than those at high frequency; however the resolution at these frequencies is low. It is desirable to have good resolution at a large penetration depth. A figure of merit known as the resolution integral was introduced by Pye's group (MacGillivray et al.

2010), as a method to characterise ultrasound images in terms of the ratio of penetration of an ultrasound beam in soft tissue to the ultrasound beam width. The aim of this method is to reduce the level of subjectivity in determining the performance of a transducer. Research has focused on establishing the resolution integral of commercially available transducers on tissue mimicking phantoms. It would be of importance if designers can assess this resolution integral at the design stage using simulations.

The resolution integral (MacGillivray et al. 2010) is a way of evaluating the compromise between image quality and the various design parameters. This is a figure of merit that evaluates the image resolution over the depth of field (Figure 4.8) and can be used to compare two or more transducers. The application of the resolution integral in this thesis is used at a design stage to select the optimal transducer.

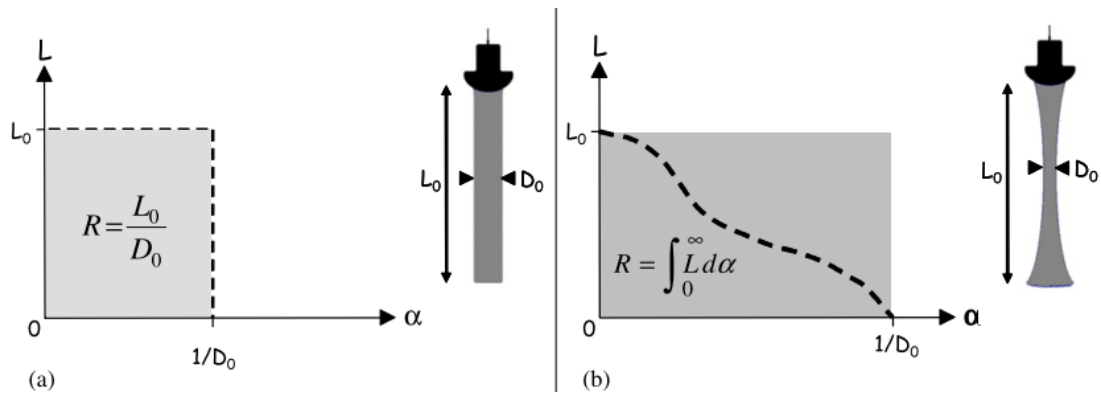


**Figure 4. 8: Plots showing the resolution integral. ‘(a) A graph showing  $L$  against  $\alpha$  for a collimated beam with low contrast penetration  $L_0$  and beam width  $D_0$ .  $\alpha$  is the reciprocal of beam width, and  $L(\alpha)$  corresponds to the depth range in the image over which the beam width is less than  $1/\alpha$ . (b) A plot of  $L$  against  $\alpha$  for a weakly focused ultrasound beam with low contrast penetration  $L_0$  and minimum beam width  $D_0$ . In (a) and (b) the resolution integral  $R$  is equal to the area under the curve’’ (MacGillivray et al. 2010).**

For the simulation the input properties of both the linear array and the linear phased array are shown in Table 4.4. These simulations were particularly important in selecting a good array which is feasible to fabricate. An array with fewer elements would provide less challenge during fabrication, and particularly, arrays with larger element pitch will make the interconnect solution easier.

**Table 4. 4: Input parameters for simulation of the 15 MHz arrays**

Property	Linear Array	Phased Array
Element Thickness (mm)	0.110(1.1 $\lambda$ )	0.110 (1.1 $\lambda$ )
Element length (mm)	0.800(8 $\lambda$ )	0.800(8 $\lambda$ )
Element width (mm)	0.070(0.7 $\lambda$ )	0.035(0.35 $\lambda$ )
Element Pitch (mm)	0.100(1 $\lambda$ )	0.050 (0.5 $\lambda$ )
Scan Geometry	Rectangular	Sector scan

The arrays in the simulations were focused at each depth on both transmit and receive to obtain an optimised response. The two-way response gives the shape of the ultrasound beam produced by the device and this can be measured experimentally by placing a point reflector at each point of interest and measuring the amplitude of the pulse reflected back to the transducer from the point reflector. The beam shape is used to determine the resolution through the depth of the image and the presence of unwanted regions of constructive interference (e.g. side lobes or grating lobes) that can produce artefacts in an image.

The parameters outlined below were evaluated through the simulation. These parameters can be used to quantify the imaging performance of an array (Szabo 2004).

- Minimum lateral resolution of the array: Minimum beam width within imaging depth of field.
- Resolution integral: A measure of image quality accounting for both resolution and depth of field
- Dynamic range of image: Maximum level of secondary lobes in field within imaging depth of field. When a short pulse is transmitted, the echoes from two reflecting surfaces that are close together are easily separated. The envelope of the reflected signals is log compressed so that they give a large dynamic range of signal amplitude. This dynamic range is usually up to 60 dB or a factor of 1000, which can be displayed in the image (Demore 2006).

The results of the simulations of both the linear and phased arrays are shown in Figure 4.9 and 4.10 respectively.

Table 4.5 draws a summary of the parameters obtained from the simulations. A detailed evaluation of the simulation is given after the figures.

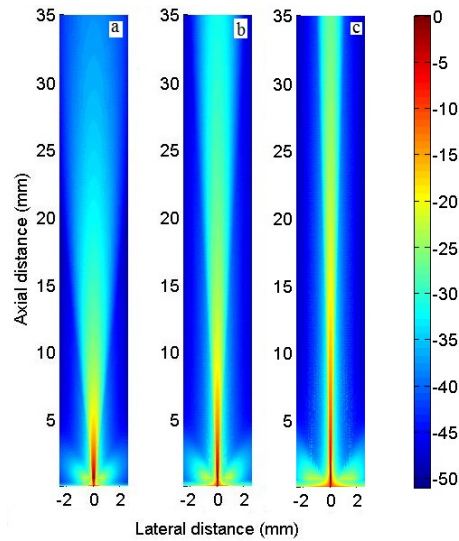


**Figure 4. 9:**Two-way beam plots for linear arrays simulated using Field II, with (a) 8 elements, (b) 16 elements (c) 32 elements in the active aperture. Amplitudes are normalised the peak value. The element pitch is  $\lambda$ .

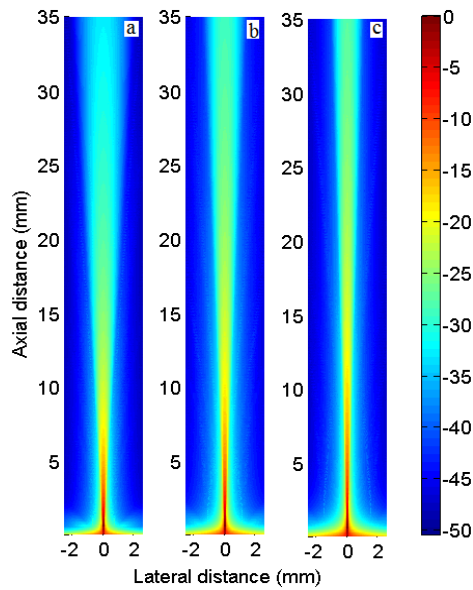


**Figure 4. 10:**Two-way beam plots for phased arrays simulated using Field II, with (a) 32 elements, (b) 48 elements (c) 64 elements in the active aperture. Amplitudes are normalised the peak value. The element pitch is  $\lambda/2$ .

Figures 4.11 and 4.12 illustrate the resolution integral of the linear and phased arrays simulated with their beam plots shown in Figures 4.9 and 4.10.

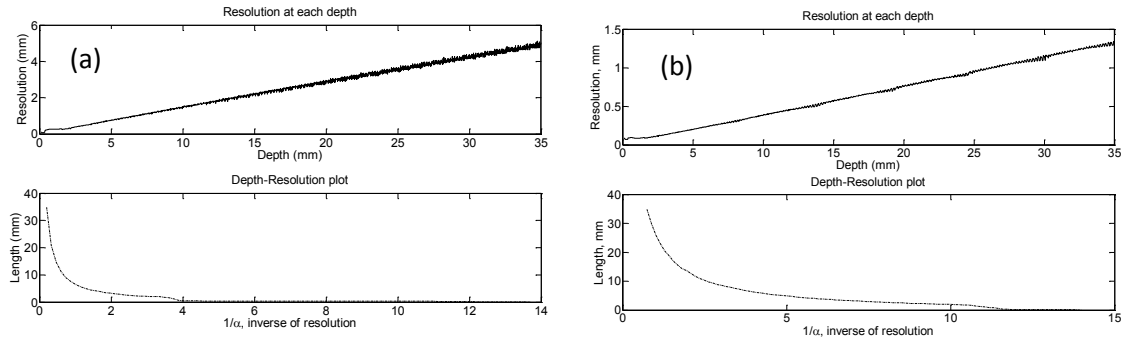


Figure 4.11: Linear arrays plots for obtaining the resolution integral (a) 8 elements, (b) 32 elements

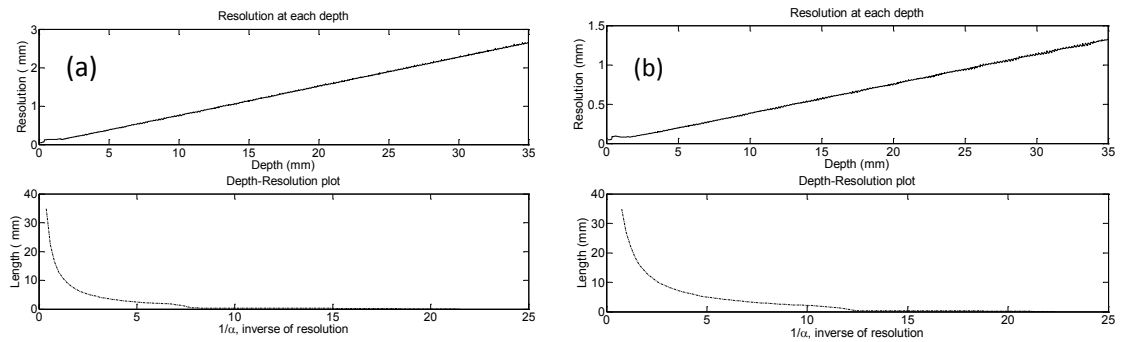


Figure 4.12: Phased arrays plots for obtaining the resolution (a) 32 elements, (b) 64 elements

Table 4.5: Image quality parameters determined from beam simulation of linear and phased arrays

Transducer type	Number of active elements	Minimum resolution (mm)	Resolution integral	Dynamic Range (dB)
Linear	8	0.259	22.58	50
	16	0.136	39.76	50
	32	0.098	67.47	50
Phased	32	0.135	42.03	50
	48	0.106	58.72	50
	64	0.085	71.72	50

#### 4.6.2 Transducer Simulation Evaluation

The sensitivity and dynamic range of the electronics that drives the transducers and acquires the imaging signals affects the maximum imaging depth, as does the sensitivity of the transducer. The imaging depth is limited in high frequency transducers due to attenuation in tissue. In the current study, the maximum imaging depth has been taken to be 35 mm for evaluating the designs. It is thought that the transducers using single crystal materials, and advances in electronics will enable

imaging to this depth. However a more realistic current maximum limit may be 30 mm. It has been explained in the literature that higher ultrasound frequency leads to higher resolution but at a reduced depth of penetration, with probes of 12 MHz and 20 MHz having a maximum depth of penetration of 29 mm and 18 mm respectively (Liu et al. 2006). Other researchers have also reported penetration depths of different transducers such as a 7.5 MHz transducer with a penetration depth of 7–8 cm (Larsen 2002) and a 30 MHz and a 50 MHz transducer with 10mm and 4 mm depth of penetration respectively (Foster et al. 2000). It is for such reasons that 35 mm penetration depth was used for the simulations.

The optimum device design minimises the lateral resolution and maximises the depth of field and field of view, as well as maintaining a dynamic range of 50-60 dB. A dynamic range of 60 dB is what has been found to be useful for clinical imaging. This dynamic range suppresses the secondary lobes to a level which would not cause interference with the main image (Brown et al. 2007). Typically, a linear array would use a 64-element sub-aperture with one wavelength pitch to create each image line. This would create sufficient lateral resolution and be able to suppress the secondary lobes.

The linear array compared with the phased array provides a better resolution integral as is shown with 32 active elements of the linear and the phased array. The linear array provides better resolution, and a bigger aperture with a larger pitch makes it less challenging in fabrication.

The resolution integral for the different array active elements gave a clear demonstration that some transducers are better than others. This is useful in establishing the different trade-offs of different transducers. The active elements in an array are what were simulated but the generation of an image is based on electronically scanning through all elements, which might be as many as 256. The actual size of the array is greater than the active aperture only for the linear array since the scanning is done by exciting small groups of elements. For a phased array, all the elements are excited with time delays to enable steering of the beam.

## 4.7 Chapter discussion and conclusions

This chapter has presented the results of material characterisation of passive materials that were used for the prototypes. These, along with the properties of the PMN-PT single crystal material, were used in a simulation for analysing the effects of layer thickness in 15 MHz virtual prototypes.

The single crystal material properties that were used are similar to those characterised in the same group but by a different researcher (Qiu et al. 2011). The results in this thesis obtained from the validated models demonstrate that PMN-PT single crystal materials vary considerably. State-of-the-art software called PZFlex was used for the simulation to allow for the optimisation of the array design before fabrication, therefore reducing the overall cost of the process spent in making multiple prototypes. Since the simulation accuracy depends on how accurate the material properties are, a model-build-test approach was applied to modify the material properties to match the results in the simulation.

The elements of an ideal device would have  $50 \Omega$  electrical impedance magnitude for optimal matching to standard  $50 \Omega$  circuitry. In addition, the number of elements in the device should be minimised to limit the complexity of the electronics in the system and the size of the array. A compromise was made between these design specifications to get a prototype. The composite (in Figure 4.2) gave electrical impedance close to the  $50 \Omega$  needed for matching to the electronics. For this reason, it would be easy to do impedance matching. Since the model explained in Figure 4.2 is only for the active layer, other added layers like the matching and backing will change the minima and maxima impedance. This is demonstrated in Figure 4.7 where the active layer combined with the matching and backing gave an impedance of about  $400 \Omega$ .

Re-poling for the single crystal material may be needed after it has been worked upon. This would improve properties such as the electromechanical coupling coefficient ( $k_t$ ). However, looking at Figure 4.6, it seen that the changes are not so big. Focus should therefore be paid to the fabrication process to see that the single crystal keeps its properties after it has been worked upon. This would eliminate the challenge of re-poling a finished transducer prototype.

An important note is that modelling of single crystal materials is a challenge. This is because, the properties vary a lot between the same materials but from different manufacturers. In-house characterisation is almost inevitably required to obtain accurate properties for the simulation.

The beam patterns demonstrated the differences between the linear and phased arrays. Linear arrays are characterised with side lobes which are mainly due to the large pitch whereas the phased arrays do not have side lobes and would allow imaging closer to the elements as well as beam steering. However, the resolution integral demonstrated that for the same number of active elements, a linear array has a higher resolution integral compared to a phased array. The linear array is also less challenging to manufacture for the same operating frequency.

The linear array with 64 elements was chosen as for demonstrating the feasibility of fitting an ultrasound array in a needle. This is because it would provide a good resolution over a large depth of field and it has a bigger pitch than a phased array at the same frequency which would make fabrication slightly less challenging. The active aperture for this array would be 16 elements. This gives a resolution of  $0.136 \mu\text{m}$  and would allow for less complicated driving electronics. Also, the fewer active elements allow for imaging close to the elements. The 64 elements of the 15 MHz array at wavelength pitch would give an image width of 6.4 mm. It should be noted however that to get a good resolution below  $100 \mu\text{m}$  the 64 elements would be used as the sub-aperture in a bigger array of about 256 elements.

## 4.8 References

Abboud, N.N., Wojcik, G.L., Vaughan, D.K., Mould, J., Powell, D.J. and Nikodym, L. 1998. Finite Element Modeling for Ultrasonic Transducers. In: *Ultrasound Transducer Conference*.

Barthez, P.Y., Léveillé, R. and Scrivani, P. V 1996. Side lobes and grating lobes artifacts in ultrasound imaging. *Veterinary radiology & ultrasound: the official journal of the American College of Veterinary Radiology and the International Veterinary Radiology Association* 38(5), pp. 387–93.

Bernassau, A.L., Hutson, D., Démoré, C.E.M. and Cochran, S. 2011. Characterisation of an Epoxy Filler for Piezocomposite Material Compatible with Microfabrication

- Processes. *IEEE transactions on ultrasonics, ferroelectrics, and frequency control* 58(12), pp. 2473–2478.
- Brown, J., Foster, F., Needles, A., Cherin, E. and Lockwood, G. 2007. Fabrication and Performance of a 40-MHz Linear Array Based on a 1-3 Composite with Geometric Elevation Focusing. *IEEE Transactions on Ultrasonics, Ferroelectrics and Frequency Control* 54(9), pp. 1888–1894.
- Chan, H.W. and Unsworth, J. 1989. Simple model for piezoelectric ceramic/polymer 1-3 composites used in ultrasonic transducer applications. *IEEE transactions on ultrasonics, ferroelectrics, and frequency control* 36(4), pp. 434–41.
- Cochran, S., Courtney, C.R.P. and Démoré, C.E.M. 2012. Modelling ultrasonic transducer performance: one-dimensional models. In: *Ultrasonic Transducers: Materials, Design and Applications*. pp. 187–219.
- Demore, C.E.M. 2006. Design of Ultrasound Transducer Arrays for Medical Imaging. PhD Thesis, Queen's University Kingston, Ontario, Canada.
- Foster, F.S., Pavlin, C.J., Harasiewicz, K.A., Christopher, D.A. and Turnbull, D.H. 2000. Advances in ultrasound biomicroscopy. *Ultrasound in Medicine & Biology* 26(1), pp. 1–27.
- Grewe, M.G. and Gururaja, T.R. 1989. Acoustic Properties of Particle/Polymer Composites for Transducer Backing Applications. In: *Ultrasonics Symposium*. pp. 713–716.
- Jensen, J.A. 1991. A Model for the Propagation and Scattering of Ultrasound in Tissue. *Journal of Acoustical Society of America* 89, pp. 182–190.
- Jensen, J.A. and Svendsen, N.B. 1992. Calculation of Pressure Fields from Arbitrarily Shaped, Apodized, and Excited Ultrasound. *IEEE Transactions on Ultrasonics, Ferroelectrics and Frequency Control* 39(2), pp. 262–267.
- Larsen, S.S. 2002. Endoscopic ultrasound guided biopsy of mediastinal lesions has a major impact on patient management. *Thorax* 57(2), pp. 98–103.
- Li, F., Zhang, S., Lin, D., Luo, J., Xu, Z., Wei, X. and Shrout, T.R. 2011. Electromechanical properties of  $\text{Pb}(\text{In}(1/2)\text{Nb}(1/2))\text{O}(3)\text{-Pb}(\text{Mg}(1/3)\text{Nb}(2/3))\text{O}(3)\text{-PbTiO}(3)$  single crystals. *Journal of applied physics* 109(1), p. 14108.
- Liu, J., Carpenter, S., Chuttani, R., Croffie, J., Disario, J., Mergener, K., Mishkin, D.S., Shah, R., Somogyi, L., Tierney, W. and Petersen, B.T. 2006. Endoscopic ultrasound probes. *Gastrointestinal endoscopy* 63(6), pp. 751–4.
- MacGillivray, T.J., Ellis, W. and Pye, S.D. 2010. The resolution integral: visual and computational approaches to characterizing ultrasound images. *Physics in medicine and biology* 55(17), pp. 5067–88.

- Marin-Franch, P., Cochran, S. and Kirk, K. 2004. Progress towards ultrasound applications of new single crystal materials. *Journal of Materials Science: Materials in Electronics* 15(11), pp. 715–720.
- Onose, L., Moraru, L. and Nicolae, M.C. 2009. Simulation of Acoustic Fields from Medical Ultrasound Transducer. *Romanian Journal of Biophysics* 19(4), pp. 277–283.
- Powell, D.J., Wojcik, G.L., Desilets, C.S., Gururaja, T.R., Guggenberger, K., Sherrit, S., Mukherjee, B.K., Associates, W., Altos, L., Corporation, U. and Packard, H. 1997. Incremental “Model-Build-Test” Validation Exercise for 1-D Biomedical Ultrasonic Imaging Array. In: *IEEE International Ultrasonics Symposium*. pp. 1–6.
- Qiu, Z., Sadiq, M.R., Démoré, C., Parker, M.F., Marin, P., Mayne, K. and Cochran, S. 2011. Characterization of piezocrystals for practical configurations with temperature- and pressure-dependent electrical impedance spectroscopy. *IEEE transactions on ultrasonics, ferroelectrics, and frequency control* 58(9), pp. 1793–803.
- Rhee, S., Ritter, T. a., Shung, K.K., Wang, H. and Cao, W. 2001. Materials for acoustic matching in ultrasound transducers. *2001 IEEE Ultrasonics Symposium. Proceedings. An International Symposium (Cat. No.01CH37263)* 2, pp. 1051–1055.
- Ritter, T. 2000. Design, Fabrication and Testing of High Frequency (>20 MHz) Composite Ultrasound Imaging Arrays. The Pennsylvania State University.
- Ritter, T. 2000. Design, Fabrication and Testing of High Frequency (>20 MHz) Composite Ultrasound Imaging Arrays. The Pennsylvania State University.
- Sherrit, S., Wiederick, H.D. and Mukherjee, B.K. 1997. Complete characterization of the piezoelectric, dielectric, and elastic properties of Motorola PZT 3203 HD, including losses and dispersion. In: Hoffman, E. A., Hanson, K. M., Horii, S. C., Shung, K. K., Kim, Y., Van Metter, R. L., Kundel, H. L., Beutel, J., and Blaine, G. J. eds. *Proceedings of the SPIE Medical Imaging*. pp. 158–169.
- Smith, W.A. 1986. Composite Piezoelectric Materials for Medical Ultrasonic Imaging Transducers -- A Review. In: *Sixth IEEE International Symposium on Applications of Ferroelectrics*. IEEE, pp. 249–256.
- Szabo, T.L. 2004. Diagnostic Ultrasound Imaging: Inside Out. In: Elsevier Academic Press, pp. 23–26, 269.
- Wallace, M.F. 2007. Single Crystal Acoustic Transducers for High Performance Underwater Sonar Systems. University of West of Scotland.
- Wang, H., Ritter, T., Cao, W. and Shung, K.K. 2001. High frequency properties of passive materials for ultrasonic transducers. *IEEE transactions on ultrasonics, ferroelectrics, and frequency control* 48(1), pp. 78–84.

Zhou, Q., Cha, J.H., Huang, Y., Zhang, R., Cao, W. and Shung, K.K. 2009. Alumina/epoxy nanocomposite matching layers for high-frequency ultrasound transducer application. *IEEE transactions on ultrasonics, ferroelectrics, and frequency control* 56(1), pp. 213–9.

Zipparo, M., Oakley, C., Hackenberger, W. and Hackenberger, L. 1999. Single crystal composites, transducers, and arrays. *1999 IEEE Ultrasonics Symposium. Proceedings. International Symposium (Cat. No.99CH37027)* 2, pp. 965–968.

# CHAPTER 5

---

## Fabrication Process Development

---

### Chapter Profile

As explained in the previous chapters, there are many challenges to overcome when fabricating a high frequency transducer array integrated in a needle. A well-defined fabrication process is crucial in achieving operational prototypes. A wafer-scale fabrication process was developed for the fabrication of the prototypes devices in this thesis. This is to enable fabrication of multiple units at a time which would reduce costs. It is also done to minimise or eliminate any manual fabrication steps.

The aim of this chapter is to explain in detail the development of fabrication processes for integrating a high frequency ultrasound transducer into a needle. The micro-fabrication methods employed are explained. Techniques of characterising the active and passive materials as well as the finished prototypes are described in Chapter 3. The process for making high frequency piezocomposites from PMN-PT single crystals is explained.

The different fabrication steps that were investigated to develop a feasible device are also discussed in this chapter. The chapter starts with an overview of the general fabrication and packaging process steps required for high frequency arrays integrated into a needle. These processes form the basis for the experimental work discussed in Chapters 6 and 7.

The electrical interconnect between the piezoelectric material and the signal cabling is a crucial part of the solution to create a working and feasible device. A good strong and electrically conductive bond was required for the micro-scale features of the high frequency arrays. Magnetically aligned UV curable anisotropic conductive adhesive

(ACA) and ultrasonic bonding were investigated as bonding techniques. Stencil printing was investigated to print some of the layers such as matching and ground connection. Dicing was also studied as a way of making fine tracks on polyimide when copper was diced.

## 5.1 Process Development

The development of a fabrication process suitable for manufacturing miniaturised arrays integrated into biopsy needles formed the main focus of this research. Multiple processes for critical fabrication steps were evaluated before the final process steps were chosen. The different possibilities investigated for the fabrication steps and processes are summarised in Table 5.1 and more details are given in Appendix B. The basic aims of the fabrication are to achieve a fully functional high frequency transducer by:

- Making a composite from the piezoelectric material
- Applying electrodes to the piezoelectric layer
- Connecting electrical signal cabling to electrodes with an interconnect system
- Adding matching layer
- Adding backing layer
- Defining the array elements

The process does not necessarily have to follow this order defined above but all the steps are required to get a functional transducer. The order varies depending on the different fabrication methods that are used.

**Table 5. 1: Summary of the different fabrication processes considered**

Process name and number	Key points
<b>Silicon micro-vias</b> PD01/RTS/010610	<ul style="list-style-type: none"> <li>• Micro-vias through the backing layer used for electrical interconnects</li> <li>• Easy for wafer-scale fabrication since the flexi-circuit is attached at the end of the process</li> <li>• Multiple micro-vias present a big challenge in the confined space</li> </ul>
<b>Conductive Matching</b> PD02/RTS/031210	<ul style="list-style-type: none"> <li>• Matching layer is used as a common ground</li> <li>• Ground is at the front face of the transducer, providing electrical shielding, which improves safety</li> <li>• Ultrasound energy attenuation is increased through the conductive matching due to the heavy metal particles</li> </ul>
<b>Conductive backing</b> PD03/RTS/010211	<ul style="list-style-type: none"> <li>• Backing layer is used as a common ground</li> <li>• The active surface is at the front face of the transducer</li> <li>• Needs extra ground on the front of the transducer for shielding and safety</li> <li>• Difficult to optimise the backing due to the metal particles in the epoxy for conductivity</li> </ul>
<b>Flexi-circuit matching</b> PD04/RTS/080711	<ul style="list-style-type: none"> <li>• Matching layer is replaced by a flexi circuit with the array electrode pattern</li> <li>• Number of material layers is reduced</li> <li>• Good design is needed to minimise attenuation at the front face of the transducer</li> <li>• Alignment and electrical connection between electrodes on piezoelectric substrate and flex circuit can be challenging</li> </ul>
<b>Wafer scale</b> PD05/RTS/010811	<ul style="list-style-type: none"> <li>• Multiple devices are defined on a single large plate of composite</li> <li>• Strips of epoxy are cast between regions of active composite and make space for the interconnects</li> <li>• Connections are away from the path of the ultrasound wave</li> <li>• Uses the conventional materials for all the layers</li> </ul>

The earlier versions (described in detail in Appendix B) of the fabrication processes were not taken forward to make prototypes due to the different limitations they possessed.

The process with the silicon micro-vias had the advantage of using optimised materials for both the matching and the backing. Micro-vias through the backing layer would

create the link to the ground electrode at the back of the active layer. This process would be the most ideal for wafer scale fabrication since different layer electrical connections would be among the last steps of the process. The limitation for this was to get the multiple micro-vias of about 100  $\mu\text{m}$  through the backing layer with an aspect ratio of 8. This would mean making the vias through the backing and then attaching the backing to the active layer with conductive epoxy. The possible options for making the micro-vias included sand blasting and laser drilling.

The conductive matching process meant that the acoustic attenuation at the front end of the transducer would be too high. To get a good conductive layer, high volume fractions of silver or gold particles would have to be added to epoxy. For this reason, it would be impossible to have a good acoustic matching with good conductivity.

The conductive backing process presented the opportunity of have the highly acoustically attenuative material at the back of the transducer. The main reason for this is to reduce the number of layers and the fabrication steps. The limitation with this process is that the active electrical connection is at the front of the transducer making it close to the body being examined. This would mean that extra shielding would be needed to increase safety. It is also difficult to optimise the backing material.

The flexi-circuit matching process served as a way to reduce the number of layer and to ease the fabrication due to the reduced steps. Layers of the optimised matching need to be investigated as well as the bonding layers and techniques so that layers did not create many hard boundaries. This process presents great potential and it is something to investigate as the next stage of development following on from the feasibility study presented in this thesis.

It is important to develop a process that makes fabrication simple to reduce the cost and also to enable simultaneous fabrication of multiple transducers. The process termed “wafer scale” (PD05/RTS/010811) from Table 5.1 was chosen for the array development mainly because it maintains the use of conventional materials for all layers of the transducer and it simplifies the interconnect method. This process is further explained in Figure 5.1. It focuses on two areas:

1. It introduces potential for wafer scale fabrication of arrays and single element transducers, and
2. Packaging of these transducers into small tubes which represent needles.

The fabrication of a single element transducer presents fewer challenges when compared to an array, which has multiple elements, each with its own independent electrical signal connection. Figure 5.1 illustrates the final process steps developed for fabricating the transducers in this thesis. The wafer scale fabrication process highlights the steps in making an ultrasound transducer. Since the dimensions are small, the transducers are made from large section and only cut down to individual transducers or arrays at a late stage.

The active substrates of the different prototypes fabricated in this thesis were either made of CTS 3203HD (a PZT-5H type material), or one of the two single crystal materials: lead magnesium niobate-lead titanate (PMN-29PT) (a binary single crystal material) and manganese-doped lead indium niobate-lead magnesium niobate-lead titanate (Mn:PIN-PMN-PT) (a ternary single crystal material). The single element transducers were made from 1-3 composites of the single crystal materials to demonstrate feasibility of fabrication with these materials at low temperatures. The results of these single element prototypes are discussed in Chapter 6. The results in Chapter 7 demonstrate the arrays that were made using the process described in Figure 5.1. These were mainly to demonstrate the feasibility of the electrical interconnect and element definition process steps. CTS 3203HD was used for these arrays, and even though these can withstand higher temperatures and pressure than the PMN-PT piezocrystals, the process followed that of the single crystal materials prototypes.

The maximum working temperature PMN-PT materials in medical imaging transducers is approximately 60 °C (Qiu et al. 2011). It is therefore important that the fabrication processes for devices incorporating these materials must be kept below this limit. The maximum working temperature in the process developed was 50 °C.

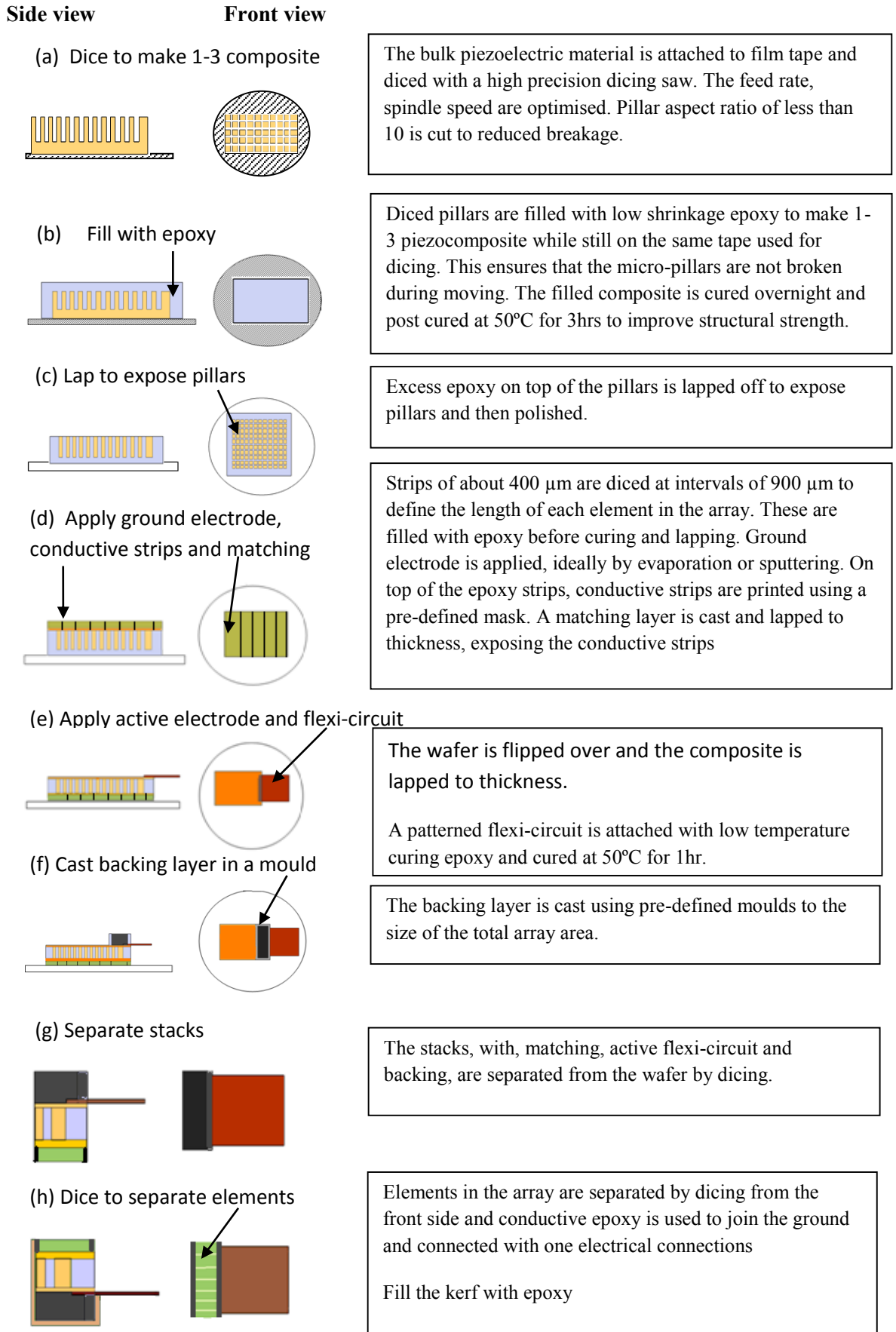


Figure 5. 1: The process flow diagram for fabricating an ultrasound array that can be integrated into a biopsy needle

## 5.2 Transducer Fabrication Process

### 5.2.1 The Transducer Stack

The fabrication steps illustrated in Figure 5.1 are explained in more detail in this section. These fabrication steps, explained in detail in the following sequence, have been developed to be suitable for small wafer-scale manufacturing, and compatible with processing PMN-PT single crystal materials. The process steps presented here can also be adapted to higher frequency devices with thinner piezoelectric layers because the array is always handled on a substrate until fully encapsulated.

1. To make the active transducer substrate, a piezocrystal plate is placed on a tape substrate, and diced in two orthogonal directions using a high precision dicing saw (MicroAce, Loadpoint, Swindon, UK) (Figure 5.1(a) and Figure 5.2). By using a blade spindle speed as low as 10000 rpm and material feed rate of 0.25 mm/s, sets of cuts in two orthogonal directions were made in one process step. Piezocrystal composites with a pitch as small as 50  $\mu\text{m}$  were fabricated with a 15  $\mu\text{m}$  thick blade, suitable for transducers operating at up to 25 MHz. This is to achieve an aspect ratio (height to width) of 1.67 which is the maximum acceptable for a 1-3 composite (Liu et al. 2001).

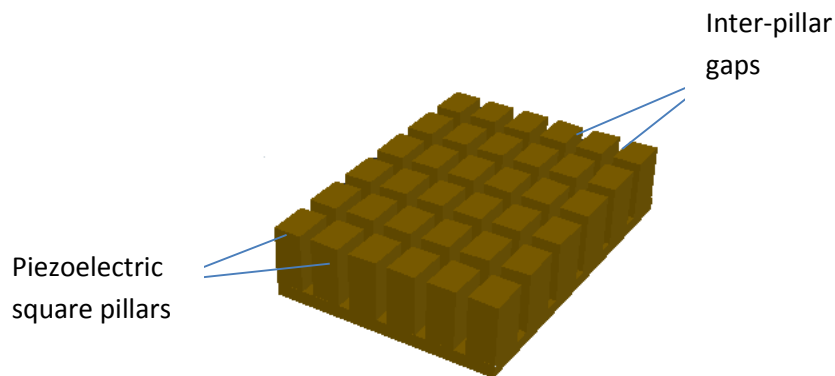


**Figure 5. 2: Diced piezoelectric material before filling with epoxy**

2. The diced pillars are then filled with low shrinkage epoxy as shown in Figure 5.3, to make 1-3 piezocomposite. After filling the diced plate with a low shrinkage epoxy (EPOFIX, Struers, UK), the substrate is left to cure at room temperature before post-curing at 50°C for 3 hours (Figure 5.1(b)). The post

cure is used to increase the glass transition temperature of the epoxy, which makes the wafer more temperature resistant (Bernassau et al. 2011). The epoxy is filled to at least 2 mm above the pillars to allow for the curvature formed when curing. If this curvature touches the pillars, it is possible to get some areas of the pillars that are not filled with epoxy.

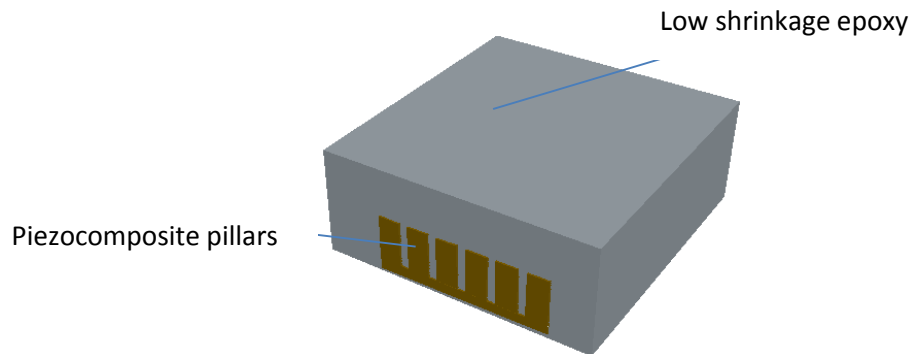


**Figure 5. 3: Piezocomposite pillars filled with epoxy before lapping**

3. For wafer-scale fabrication,  $400\ \mu\text{m}$  wide channels with  $900\ \mu\text{m}$  pitch are diced through the piezocomposite wafer, defining the location of multiple arrays on a single substrate. The channels are filled with epoxy. At later fabrication stages, the epoxy channels beside the active piezocomposite are underneath the electrical interconnect. This is so that the connections are away from the active area of the device to prevent interference to passage of the ultrasound wave.
4. The composites are then removed from the tape and attached with a thin layer of wax to a glass substrate. The composites are thinned using a lapping and polishing machine (Logitech Ltd, Old Kilpartrick, Scotland, UK) to expose the pillars on one face of the piezocomposite (Figure 5.1(c)) and Figure 5. 4.

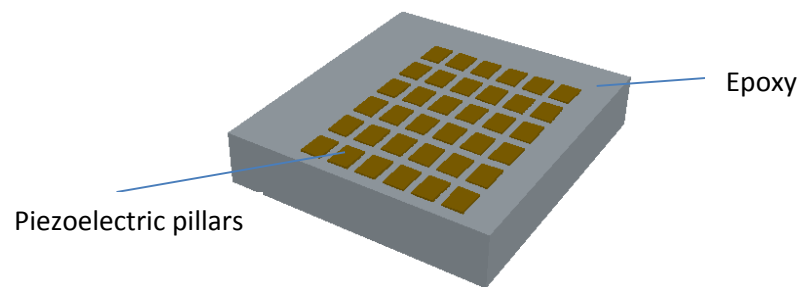


**Figure 5. 4: Lapped composites showing the pillars and epoxy**

5. A silver paint electrode (Electrodag 1415M) is applied to the surface of the piezocomposite shown in Figure 5.5, forming the ground electrode on the front face of the array elements. In manufacturing, the electrode would either be sputtered or evaporated since these methods would give controllability to the thickness of the electrode, and improved conductivity. Some composite plates in this thesis had evaporated electrodes of Cr-Au as discussed under the electrode definition later in this section.

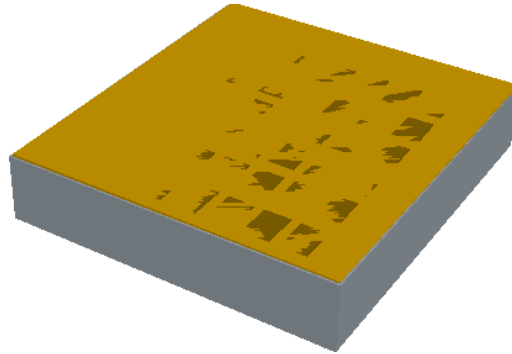


**Figure 5. 5: Illustration of a conductive electrode on top a piezoelectric composite**

6. Strips of silver isotropic conductive adhesive (ICA) epoxy (Agar Scientific Limited, UK) as shown in Figure 5. 6 are cast, using a mylar mask, above the 400  $\mu\text{m}$  wide passive epoxy channels. This step would ideally be achieved through stencil printing for commercial manufacturing of the devices. The silver epoxy layer is used as the access for the ground connection.

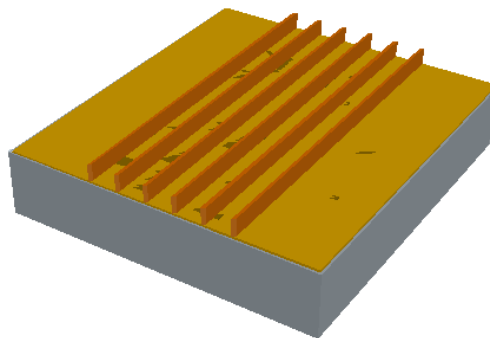


**Figure 5. 6: Printed conductive strips on top of the conductive layer**

7. The matching layer is cast on the front face of the piezocomposite to avoid the bond-lines (Figure 5.7). The matching layer is Epofix epoxy loaded with 15 % alumina by volume, using 3  $\mu\text{m}$  alumina powder. This content of alumina is adjusted according to the acoustic impedance of the active substrate. The

matching layer is then lapped down to  $\frac{1}{4}$  wavelength thickness at the specified operating frequency. Since the matching for the 15 MHz prototypes was thinner than 60  $\mu\text{m}$ , it is important to cast a thin layer of the material to reduce the time required for the lapping step. The overall cast matching layer before lapping should not exceed 500  $\mu\text{m}$  thick. Due to its low viscosity, early tests of patterning the matching layer in this study showed that it could not be easily stencil printed. After lapping, the front surfaces of the conductive epoxy strips are exposed and give access to the ground electrode (Figure 5.1(d)) and Figure 5.7.

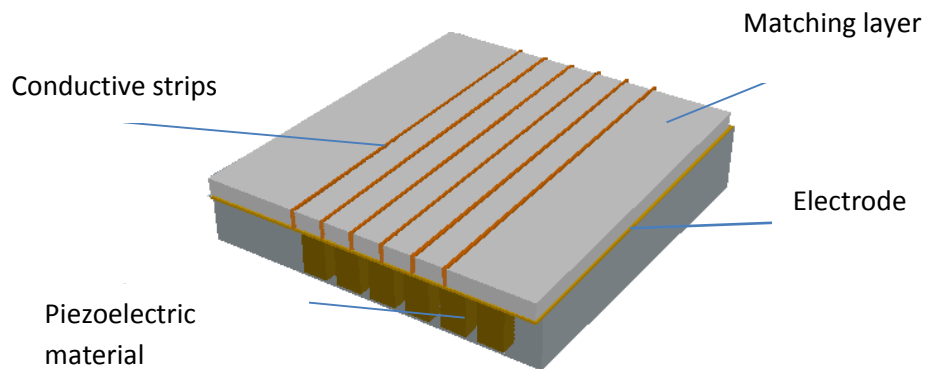


**Figure 5. 7: Illustration of matching layer on top of the piezoelectric material with an electrode in the middle**

8. The wafer is inverted on the glass substrate, and lapped to expose the back surface of the piezocomposite (Figure 5.8).

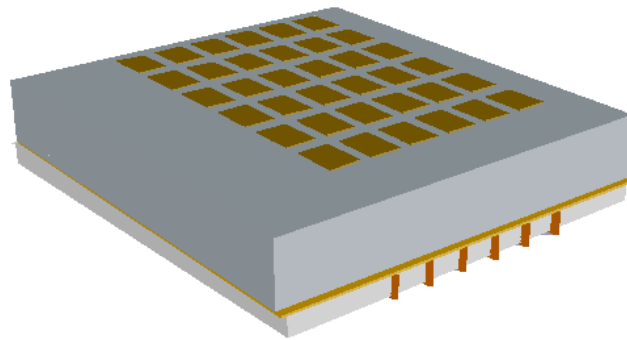


**Figure 5. 8: Stack after lapping the back face to apply the back electrode**

9. Silver paint electrodes are applied to the back face of the piezocomposite, forming the signal electrodes (Figure 5.9). It is important to note that sputtered or evaporated electrodes would be better but the silver paint was used to

quickly get prototypes. The wafer is diced so that a passive epoxy channel, over which the array interconnects can be positioned, is at the edge of the wafer.

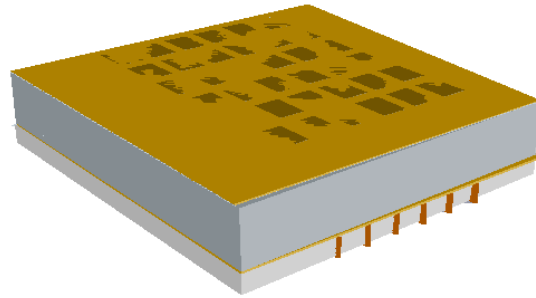


**Figure 5. 9: Back face electrode on top of the other layers**

10. A patterned flex-circuit is bonded to the electrode above the passive epoxy channels using a low temperature curing conductive epoxy described in Step 5, and cured at 50°C for 40 minutes to achieve good conductivity (Figure 5.1(e) and Figure 5.10). The ICA used for bonding the flexi-circuit to the substrate was thin coated at the edge of the substrate using a mylar sheet as a guide mask. More details about the flexi-circuit fabrication are discussed in Section 5.7.

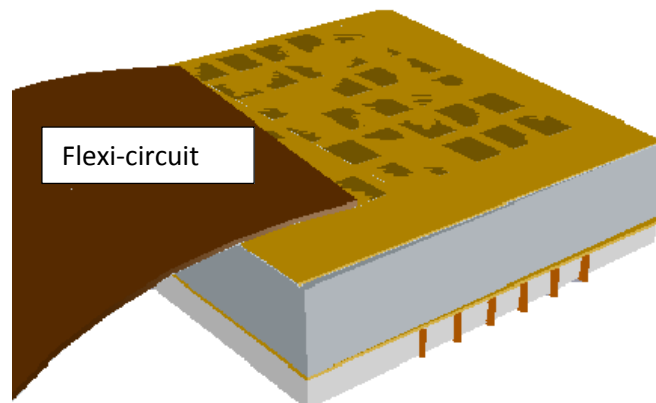


**Figure 5. 10: Flexi circuit bonded on to the back electrode**

11. An absorbing backing layer is cast into a mould placed onto the back surface of the array and the edge of the flex circuit that covers the 400  $\mu\text{m}$  wide passive epoxy channel in the piezocomposite (Figure 5.1(f) and Figure 5.11). The backing layer consists of epoxy loaded with 30% tungsten by volume, using 5  $\mu\text{m}$  powdered tungsten. The volume of the tungsten in the epoxy can be adjusted to get the best trade-off between good bandwidth and sensitivity. Since the overall dimensions of the transducer stack are limited by the size of the biopsy needle into which they will be placed, the backing is limited to about

1 mm thick. If this thickness is not enough to attenuate ultrasound pulses for a given operating frequency, the back face can be curved by machining to prevent coherent reflections.

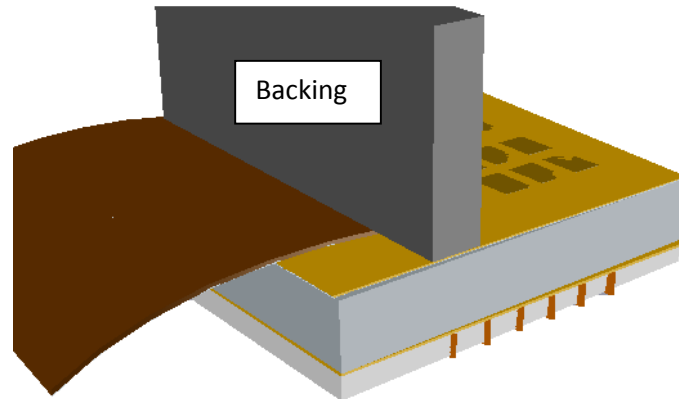


**Figure 5. 11: Backing layer cast on top of the other layers**

12. After all layers have been cast in place, the wafer is diced to separate the completed acoustic stack from the rest of the array (Figure 5.1(g)).
13. The array elements are then diced. This is done by re-mounting the single device after separating from the main wafer. The arrays are then diced using a high-precision dicing saw. The array elements were diced to separate them mechanically and electrically, defining the array in the final step (Figure 5.1(h)). The array is diced from the front face through the composite layer, to the edge of the flex circuit, and part way into the backing layer to inhibit mechanical crosstalk between elements. The alignment for dicing the array elements is taken from the patterned tracks on the flex circuit, which are facing toward the front face of the array and easily visible when dicing. Careful sanding of the backing layer was done to achieve a flat base which is needed for the dicing to separate the elements. A flat holder for the array might provide a better alternative for holding the array on the tape film during dicing. The array elements were found to be very robust when a blade of less than 30% of the overall pitch was used.
14. For electrical insulation and improved structural integrity, electrical insulating varnish (commonly used to insulate printed circuit boards (PCB)) was used to carefully fill the kerfs of the arrays using a small paint brush.

15. The ground electrode was then painted to connect all the array elements and to the back of the flexi-circuit. This ground electrode was used to join all the elements at the front end of the transducer at the side where there was ICA, explained in Step 5. This formed a common electrical contact that was used for the ground connection.
16. After the array is completed and removed from the dicing tape, the novel polyimide flexi-circuit is twisted into a spiral shape to fit within the core of the biopsy needle. This geometry permits large numbers of electrode tracks, and consequently elements, because the width of the flex circuit is not limited by the width of the needle. Since the fabrication steps involving critical transducer thicknesses (active substrate, matching, interconnects and backing) are completed on the wafer, the process is compatible with small wafer scale manufacturing. The flex-circuit interconnect and cast backing layer can be completed for a row of arrays on the wafer to parallelize the later stages of fabrication.

### 5.2.2 *Electrode Definition*

Silver paint was used to get quick prototypes to test the fabrication process. Thin electrodes were obtained this way for the prototypes. Cr-Au electrodes would provide a better connection to the silver paint and therefore it was investigated how it can fit it with the process. The thin film coating on the both sides of the active element was important for the electrical linkage to the driving electronics. Earlier prototypes in this project had silver paint or silver ink applied by hand to allow for yielding prototypes quickly and to test the process. Electron-beam (E-beam) evaporation as shown in Figure 5.12 was then used as the preferred method for coating the active layers with thin (0.5  $\mu\text{m}$ ) layer of gold with chromium as an adhesion layer. With this method, it was easy to distinguish between the piezoelectric material and the epoxy surrounding it. The excess epoxy was used to provide extra space for bonding the flexible circuit interconnects.

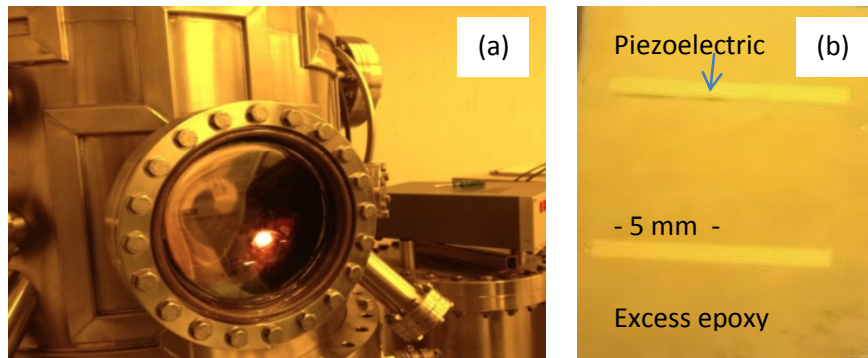


Figure 5. 12: (a) E-beam evaporation chamber and (b) sample with evaporated thin film electrode. Two regions of piezoelectric material from which arrays can be made are shown surrounded by epoxy.

### 5.3 Single Element Transducer Fabrication

#### 5.3.1 The Transducer Stack

Single element transducers operating up to 22 MHz were fabricated using the steps described in Figure. 5.1(a-g) to test the feasibility of the process steps for a miniature, high frequency transducer. The single element prototypes discussed in this thesis were made from 1-3 composites of CTS 3203HD, PMN-29PT (binary material) and Mn:PIN-PMN-PT (doped ternary material). The specific details of these transducers are discussed in Chapter 6. As an example, the PMN-PT composite single element transducer fabrication is given below.

- A 1-3 piezocomposite with 36% volume fraction PMN-29%PT was fabricated, and a matching layer of 15%vol alumina-loaded epoxy was cast on the front face for the matching layer.
- The matching layer was lapped to 40  $\mu\text{m}$  and the piezocomposite lapped to 86  $\mu\text{m}$ .
- Multiple single element transducers with dimension (length x width x thickness) 1.5 mm x 1 mm x 1 mm were cut from a 4 mm x 4 mm x 1 mm transducer stack.
- Each single element transducer had a short section of flex circuit connected to the signal (back) electrode with conductive epoxy using the same process developed for the array, illustrated in Figure 5.1(e). A micro-coaxial cable was attached to the flex circuit to connect to driving circuitry. The cable was trimmed to  $\frac{1}{4}$  wavelength at the driving frequency to match the electrical

impedance of the transducer to  $50 \Omega$  (Ritter 2000; Ritter et al. 2002). The completed transducer stack was placed into a slot cut into a 2.13 mm diameter tungsten tube, and fixed with epoxy.

#### 5.4 Piezoelectric Composite Fabrication

The 1-3 piezocomposite was made from CTS 3203HD and two single crystal materials (binary PMN-PT single crystal and doped ternary Mn:PIN-PMN-PT), which are fragile materials (Zipparo et al. 1999). The specific details of the fabricated composites are discussed in Chapter 6. Conventionally, such composites are made using a dice and fill method (Smith 1989), and this was adapted for the fine-scale composite fabrication in this thesis. Figure 5.13 illustrates the dicing saw (MicroAce 66, Loadpoint, Swindon, UK) that was used for dicing to make micro-pillars. By using carefully controlled parameters such as dicing spindle speed, feed rate and coolant feed rate, the breakage of the pillars was minimised during dicing.

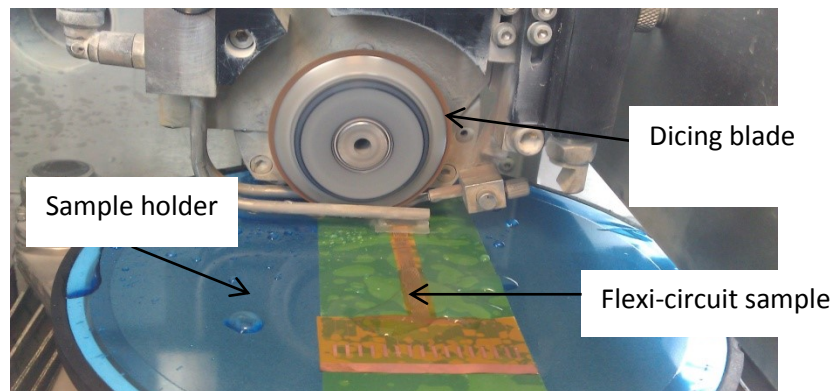


**Figure 5. 13: An illustration of the MicroAce dicing saw interior and the array with the flexi-circuit during dicing**

Multiple piezocomposites were fabricated; the main driving factor for the pillar size and volume fraction was the desired frequency for the transducer. Since the height to width pillar aspect ratio in a composite has to be  $> 1.6$ , the pillars were diced with an aspect ratio of 8. It was found from experience that it was important to dice an aspect ratio of  $< 10$  to minimise pillar breakage. The coolant feed rate was set to 0.9 L/min as this was enough to wash away any dust and cool the sample as well as being gentle to the fragile pillars (Wallace 2007).

The sample feed rate through the blade determines how long dicing the entire sample would take. Feed rates below 0.25 mm/s yielded good pillars as long as the blade spindle speed was at 10000 rpm. This rpm was chosen based on the literature discussed in Section 2.6.5. This rpm was initially kept as the standard for dicing. Higher feed rate and spindle speed increased the likelihood of pillar breakage. Examples of single crystal materials diced are shown in Figure 5.14. The composite in (b) was diced with a higher feed rate than that in (a). Both composites were achieved by dicing two orthogonal directions before filling with epoxy.

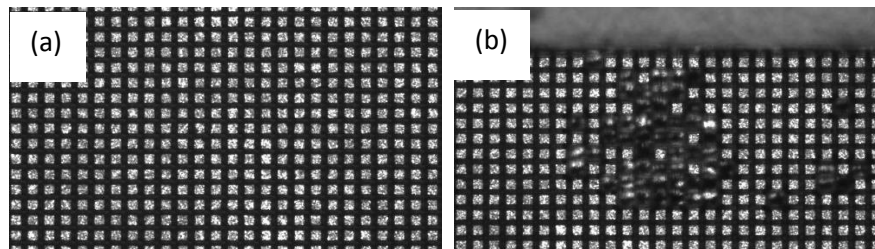


**Figure 5. 14: Single crystal material after dicing but before filling to make a composite; (a) shows good pillars, (b) shows pillars which have been broken during dicing.**

It has been suggested that for high frequency composites, it would be preferable to dice one direction, fill with epoxy and then lap before doing the same to the perpendicular direction, with some researchers dicing rectangular pillars instead of square ones (Michau et al. 2002; Ren et al. 2006). This is to cause as few pillar breakages as possible. This way of making composites is rather time consuming for a process that is slow anyway. An example of the dicing in this thesis is of the binary single crystal material used for the prototype discussed in Chapter 6 with a snapshot given below:

- By using different feed rates and cut depths for the different sides of the crystal, good 1-3 pillars were achieved in one dicing step.
- A feed rate of 0.25 mm/s was used for the first cut and then reduced to 0.2 mm/s for the second cut.
- The cut depth of 260  $\mu\text{m}$  for the first pass and 230  $\mu\text{m}$  for the second was used for pillars aimed to work at 15 MHz.
- Both orthogonal cuts were made before filling with epoxy

- The composite samples were lapped after filling with epoxy to achieve the desired thickness for the operational frequency

## 5.5 Material Thinning

The thickness of the active layer of an ultrasound device determines the resonance frequency. For this reason, the material is thinned down to get the desired frequency. The matching layer is thinned down to achieve optimised acoustic matching between the transducer and the body to be investigated. This fabrication step is therefore very important for optimising the layers for the desired performance of the device.

The passive and active layers of the transducer were thinned down using a lapping and polishing machine (PMS, Logitech, Old Kilpatrick, Scotland, UK) shown in Figure 5.15. An abrasive slurry with 20  $\mu\text{m}$  alumina powder was used first to reduce the thickness of the material to approximately 300  $\mu\text{m}$ . A smaller alumina particle size of 9  $\mu\text{m}$  was then used in the abrasive slurry to thin the material further before a 3  $\mu\text{m}$  particle size was used to thin down to the final thickness (Bernassau et al. 2007). This was done to ensure that the right thickness is obtained and the roughness of the surface is minimised. The sample thickness was measured with a lapping jig during lapping and polishing and it was confirmed on a granite master flat (Logitech Ltd, Old Kilpatrick, UK) after the sample was de-bonded from the lapping substrate.

Polishing suspension type SF1 (Logitech, Old Kilpatrick, Scotland, UK) was thereafter used for polishing the surface before conductive electrodes were applied. The lapping plate flatness was monitored using a flatness monitor.

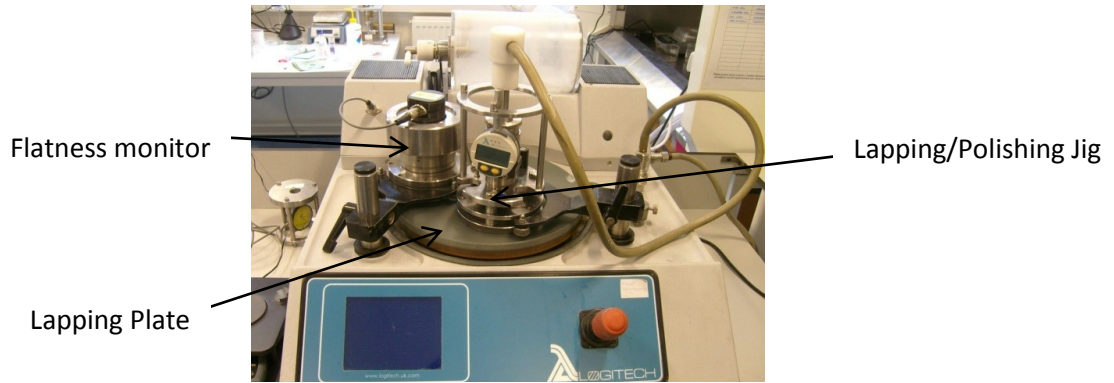


**Figure 5. 15: An illustration of a lapping and polishing machine used for thinning down active and passive layers**

During lapping, it is important to have the lapping plates properly maintained as this greatly affects the flatness of the finished surface. A flatness gauge was used to determine whether the plate was flat, and a flatness monitor used to enable the flatness to be maintained through a feedback system.

#### **5.4.1 Surface Profile**

The piezocomposite surface needs to be prepared to a standard that would facilitate easy application of subsequent layers. After lapping, the 1-3 piezocomposite has height differences between the pillars and the epoxy filler making it difficult to get a smooth and planar surface (Bernassau et al. 2011). Without planar surfaces, it is difficult to deposit and pattern continuous electrodes with techniques such as photolithography. Lapping and polishing was done on the composites to achieve a smooth surface. Surface analysis of the composite was performed using a Zygo NewView 5200 white light interferometer (Zygo Corporation, CT, USA) to check the difference in height between the pillars and the epoxy. An example is shown in Figure 5.16. The composite tested in this figure shows a maximum height difference of  $0.75\ \mu\text{m}$  which was obtained after lapping with  $3\ \mu\text{m}$  alumina slurry and polishing for 30 minutes. More polishing would create a smoother surface and therefore such testing can be used to optimise the surface smoothness for a particular processing technique. While some roughness on a surface is needed to promote adhesion of thin film deposited electrodes, patterning of electrodes with photolithography requires a very flat surface with minimal difference in height between materials. It should also be noted that although

photolithography was not used in the work in this thesis, it is likely to be incorporated in future development.

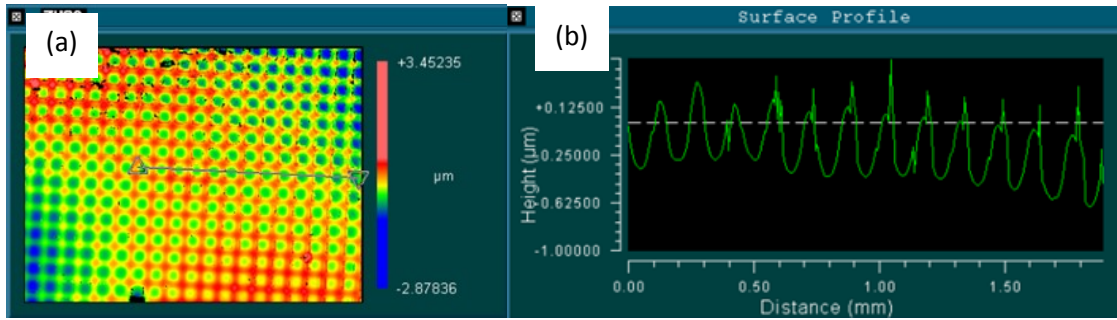


Figure 5.16: An example of a surface profile of a lapped and polished composite with Zygo white light interferometry: (a) is the surface view of the composite with the red colour highlight areas with raised surfaces, (b) is the surface profile across the line in (a).

## 5.6 Flexi-Circuit Design and Fabrication

The flexi-circuit design is highly depended on how it to be fitted into the needle after it is attached to the array. The connection of the flexi-circuit to the array is shown in Figure 5.17. An example of a commercially available biopsy needle is also illustrated. With the inner diameter of 1.5 mm the array width would have to be less than 1.2 mm.

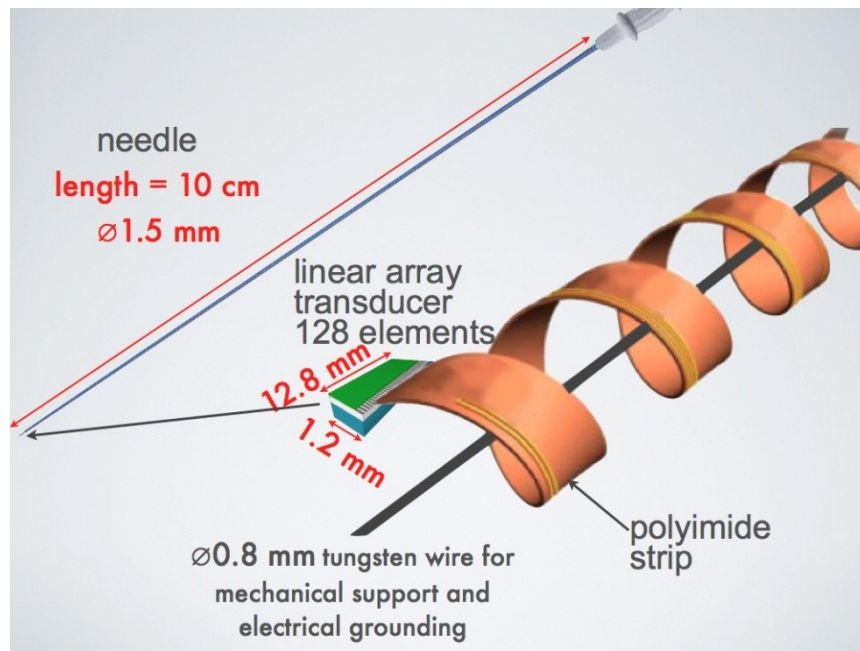
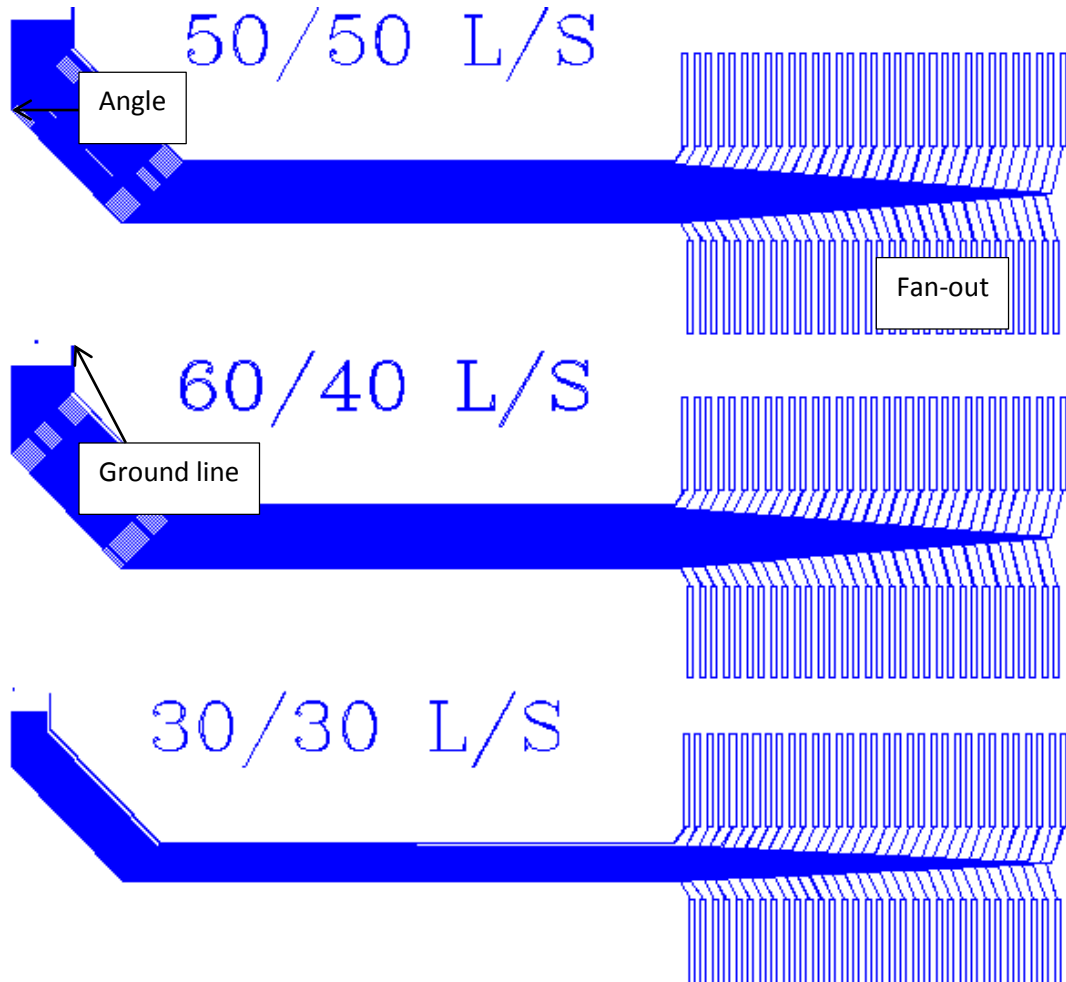


Figure 5.17: A schematic illustration of a spirally rolled flexi-circuit attached to the side of an ultrasound array. A commercial needle is also shown; it has a length of 10 cm and an inner diameter of 1.5 mm (Ng et al. 2011).

The flexi-circuit was designed using AutoCAD (Autodesk, CA, USA) design software. The aim was to get a flexi-circuit with a pitch of 100  $\mu\text{m}$  at the tip where it was to be

connected to the array. Figure 5.18 shows the flexi-circuit mask that was designed. For the 100  $\mu\text{m}$  pitch, the conductive lines (L) of 50  $\mu\text{m}$  and separation (S) of 50  $\mu\text{m}$  were designed alongside that of 60/40 (L/S). A smaller pitch of 60  $\mu\text{m}$  was also added to test the limit of the fabrication process.



**Figure 5. 18: The flexi-circuit designed to meet the challenges of fitting into a needle. The tip is straight to allow for dicing and the angle allows for rolling.**

The angle of 45° allows rolling of the flexi-circuit so that it does not cover the front side of the active array. The tip of the flexi-circuit is straight so that it is easily connected to the array and diced to separate the elements. Such design can be slightly changed where dicing to separate the elements is not required. Rolling of this flexi-circuit might need half folding at the tip so that the array is cleared. The dimensions of the flexi-circuit are shown in Figure 5.19 below.

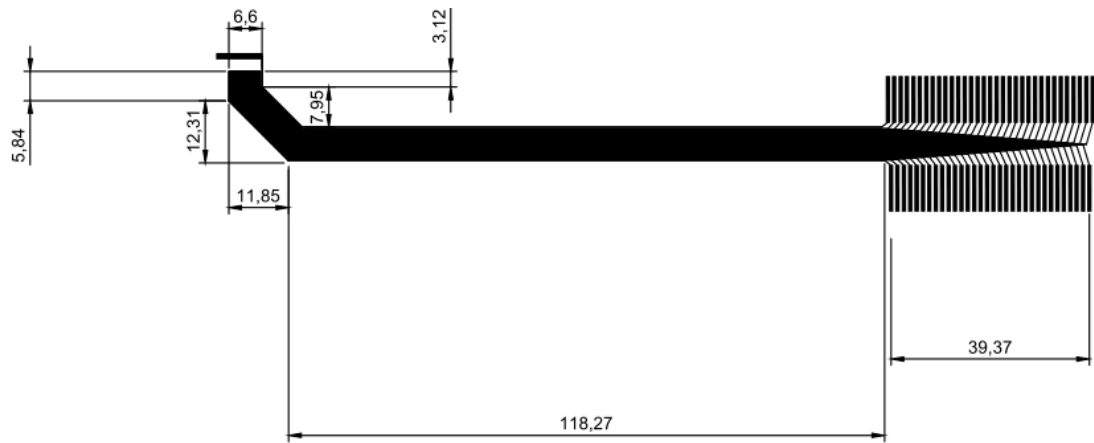


**Figure 5.19:** The designed flexi-circuit with all the dimensions. The dark part is where the pitch is too small to be shown.

The flexi-circuit shown in Figure 5.20 has some adjustments to that shown in Figure 5.19 to enable testing of different properties. The pitches of below  $60\ \mu\text{m}$  were designed on the short tracks with fan-outs on both ends. This was to enable testing for continuity and shorting between tracks. The fan-out for the flexi-circuit was designed to enable easy soldering of micro-coaxial wires. The fan-out in this design did not follow the  $45^\circ$  angle discussed above. This is because it was less time consuming to design it this way. This was done to enable prototypes to be achieved.

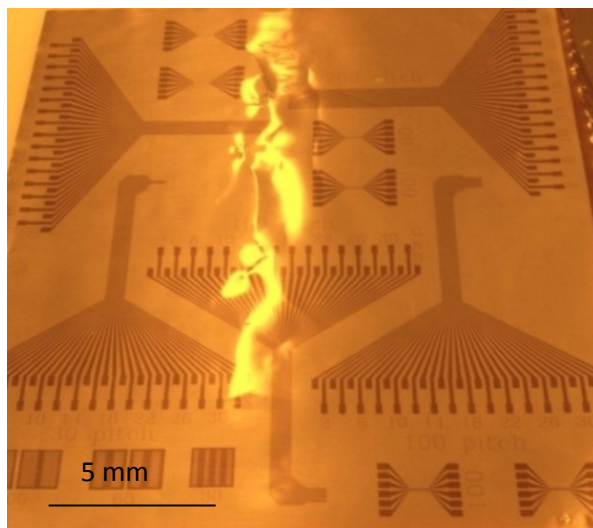


**Figure 5.20:** The second design of flexi-circuit that was used to get more prototypes

### 5.6.1 Dicing to Pattern the Flexi-Circuit

Achieving a very fine-pitch flexi-circuit presents many challenges. Dicing to remove strips of copper from polyimide was looked at as a way to make micro-pitched conductive tracks. The rationale behind this is that the thinnest dicing blades on the

market are 10  $\mu\text{m}$ . This can theoretically be used to make flexi-circuit with 30  $\mu\text{m}$  pitch tracks. The prototype shown in Figure 5.21 was of a large pitch of 300  $\mu\text{m}$  and finer pitches were beyond the scope of this study as a different method (explained in Section 5.6.2) for getting the desired flexi-circuit for the 15 MHz prototypes was developed.

The limitation to the diced flexi-circuits is that they still need a fan-out for the cable connections. A added component needs to be made using a different method and connected to the flexi-circuit which can later be diced to separate the tracks. Photolithography on silicon can achieve very fine features and could be used to get a good connection to the flexi-circuit.

Another challenge with this method is that the scratch diced flexi-circuit is a lot more rigid than a photolithography patterned one. This would make it more difficult to roll into the design chosen for the prototypes in this thesis.

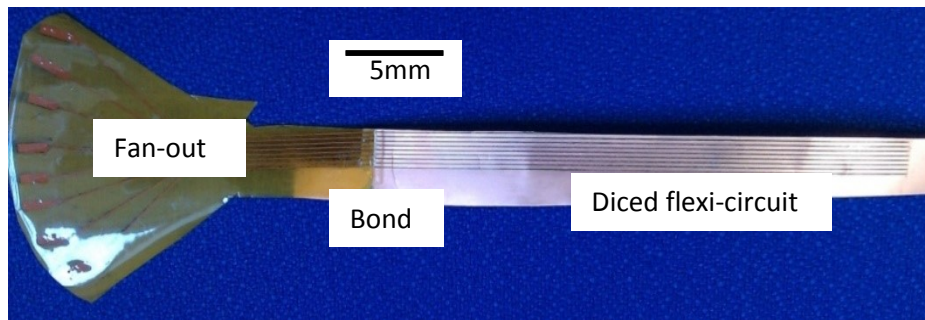


Figure 5. 21: Diced flexi-circuit with and etched fan-out. A photolithography patterned end was attached to a diced flexi-circuit.

### 5.6.2 Chemical copper etching of the flexi- circuit

One of the biggest challenges in high frequency transducers lies in electrical connections and how they are bonded to the active layers (Liu et al. 2008). For efficient performance, the electrical connections should be attached away from the path of the ultrasound energy as explained in Section 5.2.

A flex circuit connected to the piezoelectric material was patterned with 100  $\mu\text{m}$  pitch conductive tracks to define array elements suitable for a 15 MHz linear array. The polyimide flexible printed circuit, with fine pitch traces, was twisted into a helical

structure in order fit within the core of the biopsy needle and permit large numbers of elements and electrode traces.

A custom in-house photolithography method to fabricate the flex-circuit was developed by the Micro Systems Engineering Centre (MISEC) group at Heriot-Watt University as part of the Integrated Silicon Piezoelectric Ultrasound Devices (ISPUD) project. This photolithography method was used to pattern a standard copper/polyimide flexible circuit that is commonly used in electronics. The measured thickness of the copper is 18  $\mu\text{m}$  with a combined thickness with the polyimide of 63  $\mu\text{m}$ . This thickness means the polyimide is strong enough to allow the rolling to make a spiral flexi-circuit.

The flexi-circuit fabrication was achieved using the steps below;

1. Dry-film photoresist (Ordyl Alpha 940, Elga Europe, Italy) was laminated on to the copper/polyimide sheet.
2. A photomask was placed on top of this laminate before exposing under UV (Model 152R, Tamarack Scientific) light for 3 seconds at energy level of 35  $\text{mJ}/\text{cm}^2$  to produce a result such as that shown in Figure 5.20. The laminating step eliminated the need for a dedicated copper/polyimide sheet tensioner that would be needed for tensioning the polyimide sheet in case the standard spin-on photoresist was used.
3. The exposure is left to sit for 30 minutes so that the polymer cures. Too long will lead to over curing.
4. Development and etching was carried out to leave the desired conductive tracks on the polyimide. This was achieved through application of acoustic streaming using a 1 MHz ultrasound transducer (Costello et al. 2011; Kaufmann et al. 2008). Figure 5.22 is an illustration of the experimental set-up of the acoustic streaming method. The ultrasound transducer is placed at a distance away from the developing solution or copper etching bath, and the acoustic radiation force from the transducer induces streaming in the fluid.

In the etching process, the acoustic streaming enhances the fluid flow around the flexible circuit substrate (Costello et al. 2011), and enables the formation of streaming

micro air bubbles that improves the efficiency of the wet chemistry processes for developing and copper etching on the bumpy flexible substrate. The air bubbles are mainly created in the cupric chloride etching solution and significantly improves the copper oxidation uniformity which would otherwise be challenging due to the fact the flexible substrate is un-tensioned. The tiny air bubbles through cavitation also allow more oxygen to reach inside the narrow gaps for more efficient etching through the air regenerative cupric chloride etching bath (Ng, Ssekitoleko, Flynn, Kay, Demore, et al. 2011).

The method explained above is a low cost alternative to applying the large scale fabrication equipment to flatten the large flexible copper/polyimide sheet so a liquid photoresist can be used. The application and patterning photoresist usually requires a very flat surface so that the photoresist can be spun on to a very accurate and consistent thickness.

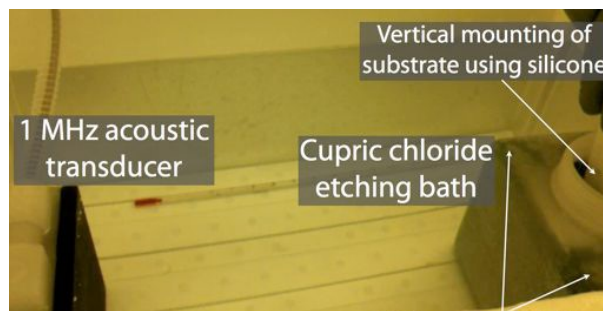


**Figure 5. 22: The set up for the water tank used for acoustic streaming for enhancing etching efficiency for flexible substrates (Ng et al., 2011)**

Tracks with a pitch of 100  $\mu\text{m}$  (35  $\mu\text{m}$  line, 65  $\mu\text{m}$  gap) copper tracks as illustrated in Figure 5.23, were fabricated with this method for the 15 MHz transducers. These results were good enough to produce continuous conductive tracks. Reducing the etching time and optimising the acoustic streaming would help to produce tracks with increased width. The smallest pitch achieved with this method was 60  $\mu\text{m}$ . Further investigations of employing a specialty grade high resolution dry film photoresist and further optimising the acoustic streaming for definition of tracks below 40  $\mu\text{m}$  pitch would be needed.

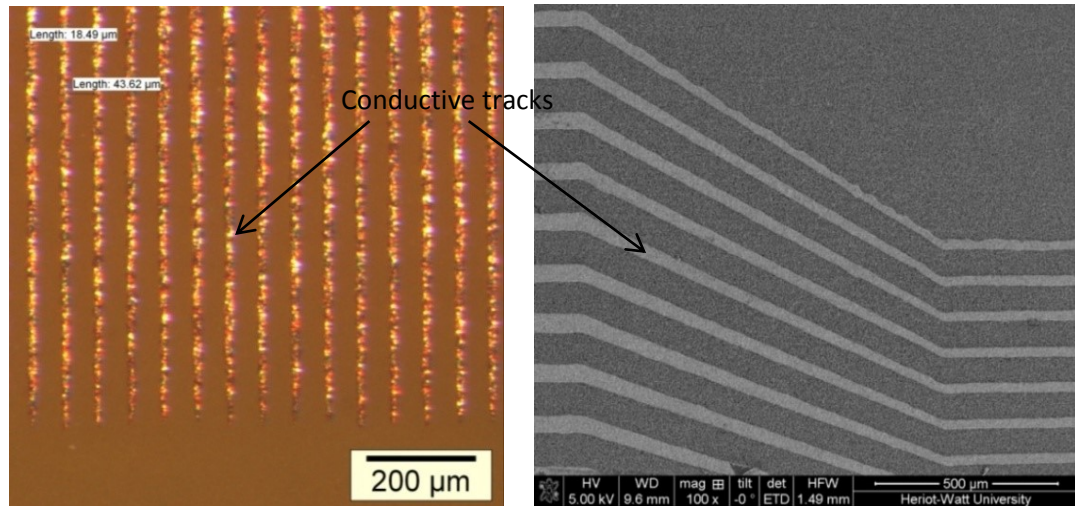


**Figure 5.23:** Microscope image of copper micro-tracks on polyimide. The copper tracks at the tip are  $18.49\ \mu\text{m}$  with a gap of  $43.62\ \mu\text{m}$  giving a pitch of  $62.11\ \mu\text{m}$ . The gray-scale image shows that the tracks widen as well as the gap when they are away from the tip-end of the flexi-circuit.

## 5.7 Novel Conductive Bonding and Interconnect Methods

The dimensional constraints for the interconnects have been discussed in Section 5.2. The elements for the 15 MHz array would leave a space of about  $70\ \mu\text{m}$  by  $200\ \mu\text{m}$  and therefore the bonding method should allow bonding to such contact pad. However, it should be remembered that dicing to separate the elements is carried out a few steps after bonding. This would leave a stronger bond since all the other layers are added before dicing. Also, in case of kerfless arrays, dicing is not needed and therefore the contact pad area is increased.

Bonding proved to be one of the bottle necks for packaging of the ultrasound arrays into a biopsy needle. The use of fine pitch flexi-circuit for electrical connections meant that it had to have a good electrical bond to the other layers in the transducer. Room temperature curable isotropic conductive adhesive (ICA) (silver-loaded conductive epoxy) was used in all the prototypes demonstrated in this thesis. The thickness and width of the ICA could be improved by knife coating using a mask or through stencil printing.

However, other bonding methods, including UV curable anisotropic conductive adhesive (ACA) and ultrasonic bonding, were investigated (Ng, Ssekitoleko, Flynn,

Kay, Demore, et al. 2011). This work was done in parallel with the development of the prototypes, so was not used in fabrication of the prototypes.

The main challenges that the work in this thesis was aiming to solve are relating to bonding of interconnects to the transducer arrays include;

- Bonding to small contact pads since there is no room for fan-out
- Using low temperature methods due to the single crystal material used as the active substrate
- Alignment of the flexi-circuit to the substrate

### 5.7.1 *UV Curable Anisotropic Conductive Adhesive*

If a kerfless array is required, ACAs provide an alternative to isotropic conductive adhesive that can be used when the array elements are mechanically separated after being connected to the flexible circuit. These adhesives only conduct electricity in one direction and they therefore cannot cause shorting between elements when used in an array. Kerfless arrays can be achieved by either scratch dicing or photolithography to define the electrodes of active elements. The disadvantage of such arrays is the increased crosstalk that would be introduced as a result of the absence of air gaps to separate the elements. The crosstalk can however be minimised by appropriate composite and array design (Demore 2006).

Bonding of the flexi-circuit to the patterned active elements would need to use ACA. ICA would not provide the electrical isolation for each element which is needed for exciting elements for beam focusing and steering, hence the need for anisotropic adhesive. Thermally curable ACA is widely available and used in industry but the minimum curing temperature is over 150°C (Bernassau et al. 2009). This is very high for the PMN-PT single crystal which has a phase transition at 80°C. UV curable ACA provides a route where the sample is not exposed to high temperatures.

This ACA (UV ZTACH™ 830NS, SunRay Scientific) consists of conductive particles with paramagnetic cores and UV curable epoxy. A magnetic field is used for alignment of the particles into columns which allows for the small contact pad area thereby conducting in only one direction (z-axis). The particle size is 3 µm and this allows for

it to be used with small pad area on both the element and the flexi-circuit. It is a two-part adhesive with a mixing weight ratio of 96:4, epoxy to catalyst. A schematic of the ACA and the experimental set-up for its curing are shown in Figure 5.24.

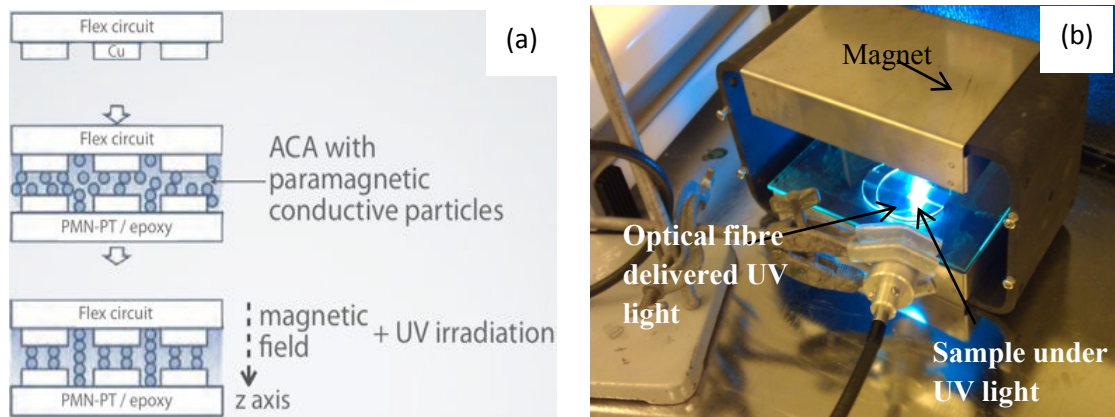


**Figure 5. 24: (a) A schematic of the of room-temperature ACA bonding using paramagnetic conductive particles and UV curable epoxy, (b) experimental set-up.**

A bonding method similar to the flip-chip bonding for anisotropic conductive film (ACF) would be required to align the fine pitch connection of the flexi-circuit and the defined active electrodes. ACF is commonly used in the electronics industry but it needs high pressure and temperature for a good bond and therefore is not suitable for the PMN-PT single crystal composites. The recommended UV intensity for curing the ACA is  $800 - 1700 \text{ mW/cm}^2$  for 2-5 minutes with a magnetic field of at least 400 Gauss. The depositing thickness of 75 to 150  $\mu\text{m}$  is also recommended for good curing. UV light is used to irradiate the ACA, curing the epoxy and therefore providing a good bond between the flexi-circuit and the array elements. The minimum bond area recommended for this ACA is 40  $\mu\text{m}$  by 40  $\mu\text{m}$  which means that this bonding mechanism has a potential of being used for arrays of up to 30 MHz with a pitch of 50  $\mu\text{m}$  and a separation of 10  $\mu\text{m}$ . Since this ACA is 3  $\mu\text{m}$  particles, it would be ideal for the application.

Preliminary experiments to test how well the UV curable ACA would perform, demonstrated that for opaque substrates where the UV light had to be irradiated from the side, the adhesive that was between the substrates did not cure even with a very large UV dose. Different dimensions of the epoxy were tested with different thickness. As shown in Figure 5.25, thin stencil printed bumps of 290  $\mu\text{m}$  diameter cured well whereas lines did not cure well. The thinnest line was closest to the UV light and cured

where others did not cure. After testing with transparent conductive materials it was seen that curing occurred and a good mechanical and electrical bond was achieved (Ng et al. 2011). Therefore, subsequent experiments were done where the flexi-circuit had a laser cut-through through the polyimide layers, leaving the copper tracks, as shown in Figure 5.26, to allow UV light to reach the epoxy. The wavelength of UV light (LiNOS Photonics LQ UV 1000) used was 320-340 nm and the maximum UV intensity used was  $160 \text{ mW/cm}^2$  for 25 minutes.

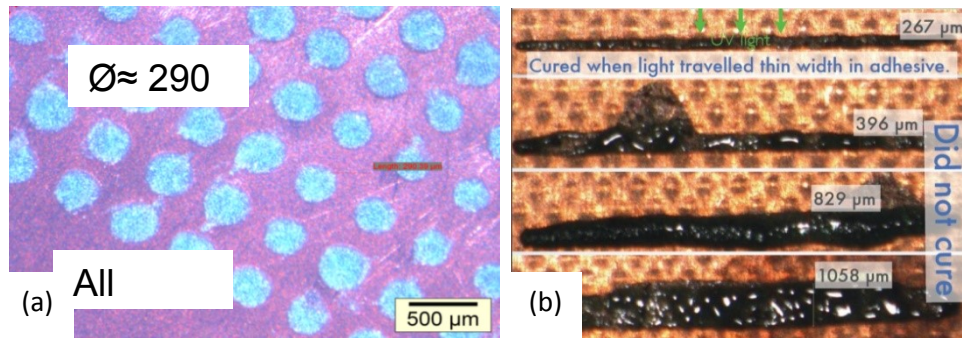


**Figure 5. 25: (a) All the bumps of the epoxy cured under UV light, (b) Thick lines above  $267 \mu\text{m}$  did not cure under UV light**

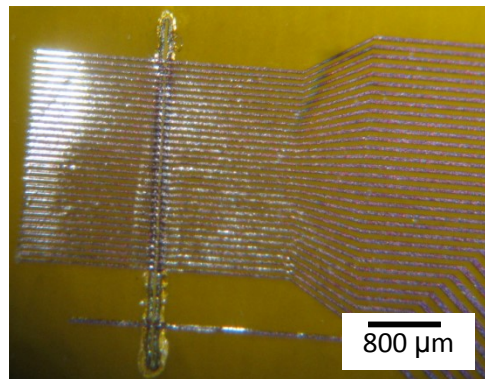


**Figure 5. 26: A flexi-circuit with a laser cut-through to allow UV light to reach the epoxy for curing**

A kerfless array was made to test the functionality of the flexi-circuit bonded to the elements using the UV curable ACA. To make the kerfless array, scratch dicing was done on a PMN-PT plate to separate the electrodes into individual elements as shown in Figure 5.27. The pitch of the scratch dicing was  $300 \mu\text{m}$  with  $80 \mu\text{m}$  separation.

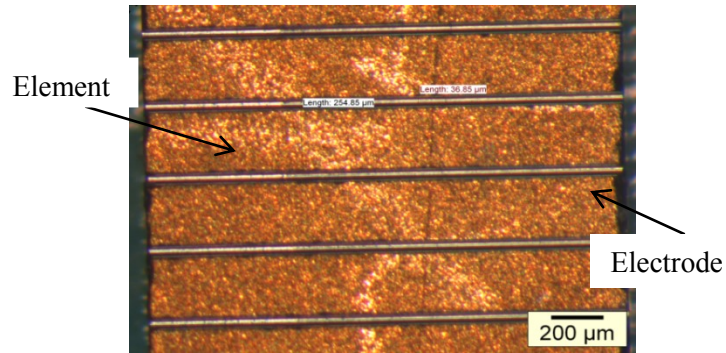


**Figure 5. 27: Scratch diced PMN-PT single crystal plate for kerfless arrays**

A flexi-circuit with the same pitch was attached to the scratch diced piezoelectric material (Figure 5.28(a)). The flexi-circuit with the laser cut-through enabled epoxy curing with the UV light. The impedance results (Figure 5.28(b)) showed that a good connection was achieved on four out of 18 elements in this first prototype. This prototype demonstrates that the UV curable epoxy works. Further optimisation to how the flexi-circuit is held onto the elements during curing would improve the results. There was no shorting of any elements when tested with a multi-meter. The multiple resonances seen on the graph are due to the dimensions of the active element and due to the fact the material is not a composite. The bonds were however not very strong and needed the use of an under-fill to improve the mechanical integrity.

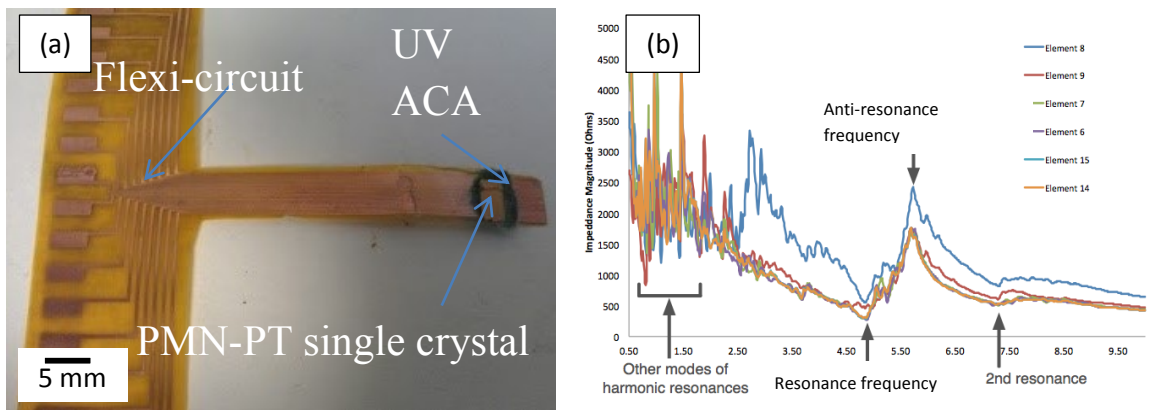


**Figure 5.28: (a) Scratch diced array of PMN-PT single crystal material attached to a flexi-circuit by UV ACA, (b) Electrical impedance magnitude plots of the working elements on the array.**

### 5.7.2 *Ultrasonic Bonding*

Under ultrasonic bonding, ultrasound vibration is used to provide energy for bonding two surfaces. The two surfaces, each with a good electrode are joined together with the aid of ultrasound excitation.

Early test results to determine how good the bonds were showed that ultrasonic bonding might be a way to bond without introducing foreign bonding materials such as epoxy. The flexi-circuit was bonded directly to the piezoelectric sample and subsequent dicing was used to separate the elements in the array. It was noticed that the surface roughness of the sample played an important role in getting a good bond. Successful bonding was only achieved when the samples were lapped with 20  $\mu\text{m}$  or 9  $\mu\text{m}$  alumina abrasive. The 3  $\mu\text{m}$  lapped surface did not yield a successful bond. The copper surface on the flexi-circuit also needed to be rough for a good bond. Figure 5.29 shows the results of the surface analysis with a Zygo white light interferometer that were done for ultrasonic bonding. The sample lapped with 3  $\mu\text{m}$  alumina abrasive shows a smoother surface than that lapped with the 9  $\mu\text{m}$ . The average roughness (Ra) was measured as 0.384  $\mu\text{m}$  for the 3  $\mu\text{m}$  lapped and 0.751  $\mu\text{m}$  for the 9  $\mu\text{m}$  lapped samples.

The dimensions of the sample were also restricted by the placement tool and therefore bonding to a large substrate was not possible. The bond was very weak and fragile and needed mechanical support such as an under-fill.

This method needs further investigation and the empirical results obtained in this study do not provide enough information to conclude on the effectiveness of application of this technique. It would be worth exploring it further.

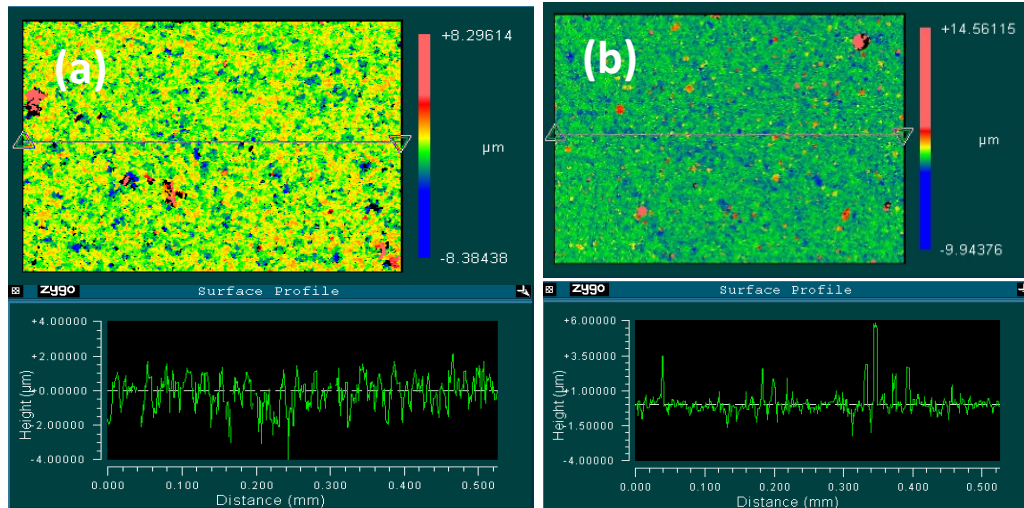


**Figure 5.29:** Zygo white light interferometry images of lapped samples: (a) lapped with a 9  $\mu\text{m}$  alumina abrasive, (b) lapped with 3  $\mu\text{m}$  alumina abrasive

## 5.8 Chapter Discussion and Conclusions

The manufacturing process steps developed in this chapter form the basis for the fabrication of the prototypes demonstrated in the following chapters. The fabrication process steps required for creating a working prototype have been discussed, and options for key process steps have been investigated. The fabrication of flexi-circuit was detailed as a method to achieve fine-scale pitch flexi-circuit for high frequency arrays. Special attention was paid to the bonding method since no suitable bonding mechanism and adhesive was already established for the low temperature and pressure requirements of this application. Ultrasonic bonding was at an early stage of investigation at the time of writing this thesis. Magnetically aligned UV light curable ACA showed promising results since it met the requirement of low temperature and pressure for bonding. However, this method is not well researched and further studies would need to be undertaken to establish its effectiveness.

The fabrication process was used to get prototypes which are discussed in Chapters 6 and 7. The process was successful but left some areas for improvement. Such areas included the bonding of the flexi-circuit to the substrate. Better alignment techniques need to be developed to get the flexi-circuit to the small bond area. Sanding of the

backing layer would also prove time consuming for wafer-scale fabrication. Other details of improvement to the process are discussed in Chapters 7 and 8.

## 5.9 References

- Bernassau, A.L., Flynn, D., Amalou, F., Desmulliez, M.P.Y. and Cochran, S. 2009. Techniques for wirebond free interconnection of piezoelectric ultrasound arrays operating above 50 MHz. In: *IEEE International Ultrasonics Symposium*. Rome, pp. 1–4.
- Bernassau, A.L., Hutson, D., Démore, C.E.M. and Cochran, S. 2011. Characterisation of an Epoxy Filler for Piezocomposite Material Compatible with Microfabrication Processes. *IEEE transactions on ultrasonics, ferroelectrics, and frequency control* 58(12), pp. 2473–2478.
- Bernassau, A.L., McKay, S., Hutson, D., Demore, C.E.M., Button, T.W. and Mcaney, J.J. 2007. Surface Preparation of 1-3 Piezocomposite Material for Microfabrication of High Frequency Transducer Arrays. *Ultrasonics*, pp. 2007–2010.
- Costello, S., Strusevich, N., Patel, M., Bailey, C., Flynn, D., Kay, R., Price, D., Bennet, M., Ones, A.C., Habeshaw, R., Demore, C., Cochran, S. and Desmulliez, M.P.Y. 2011. Characterisation of ion transportation during electroplating of high aspect ratio microvias using megasonic agitation. In: *18th European Microelectronics and Packaging Conference (EMPC)*. pp. pp.1–7.
- Demore, C.E.M. 2006. Design of Ultrasound Transducer Arrays for Medical Imaging. PhD Thesis, Queen’s University Kingston, Ontario, Canada.
- Kaufmann, J., Desmulliez, M.P.Y., Price, D., Hughes, M., Strusevich, N. and Bailey, C. 2008. Influence of megasonic agitation on the electrodeposition of high aspect ratio blind vias. In: *2008 2nd Electronics Systemintegration Technology Conference*. IEEE, pp. 1235–1240.
- Liu, C.G., Wu, D.W., Zhou, Q.F., Djuth, F.T. and Shung, K.K. 2008. High-frequency (50–100MHz) medical ultrasound transducer arrays produced by micromachining bulk PZT materials. In: *2008 IEEE Ultrasonics Symposium*. IEEE, pp. 690–693.
- Liu, R., Harasiewicz, K. a and Foster, F.S. 2001. Interdigital pair bonding for high frequency (20-50 MHz) ultrasonic composite transducers. *IEEE transactions on ultrasonics, ferroelectrics, and frequency control* 48(1), pp. 299–306. Available at: <http://www.ncbi.nlm.nih.gov/pubmed/11367799>.
- Michau, S., Mauchamp, P. and Dufait, R. 2002. Single Crystal-based Phased Array for Transoesophageal Ultrasound Probe. In: *IEEE Ultrasonics Symposium*. pp. 1269–1272.

Ng, J.H., Ssekitoleko, R.T., Flynn, D., Kay, R.W., Cochran, S. and Desmulliez, M.P.Y. 2011. Innovative manufacturing and 3-dimensional packaging methods of micro ultrasonic transducers for medical applications. In: *18th European Microelectronics and Packaging Conference (EMPC)*. pp. 1–5, 12–15 Sept. 2011.

Ng, J.H., Ssekitoleko, R.T., Flynn, D., Kay, R.W., Demore, C.E.M., Cochran, S. and Desmulliez, M.P.Y. 2011. Design, manufacturing and packaging of high frequency micro ultrasonic transducers for medical applications. In: *IEEE 13th Electronics Packaging Technology Conference*. IEEE, pp. 93–98.

Qiu, Z., Sadiq, M.R., Démoré, C., Parker, M.F., Marin, P., Mayne, K. and Cochran, S. 2011. Characterization of piezocrystals for practical configurations with temperature- and pressure-dependent electrical impedance spectroscopy. *IEEE transactions on ultrasonics, ferroelectrics, and frequency control* 58(9), pp. 1793–803.

Ren, K., Liu, Y., Geng, X., Hofmann, H.F. and Zhang, Q.M. 2006. Single crystal PMN-PT/epoxy 1-3 composite for energy-harvesting application. *IEEE transactions on ultrasonics, ferroelectrics, and frequency control* 53(3), pp. 631–8.

Ritter, T. 2000. DESIGN, FABRICATION AND TESTING OF HIGH FREQUENCY(>20 MHz) COMPOSITE ULTRASOUND IMAGING ARRAYS. The Pennsylvania State University.

Ritter, T. a, Shrout, T.R., Tutwiler, R. and Shung, K.K. 2002. A 30-MHz piezo-composite ultrasound array for medical imaging applications. *IEEE transactions on ultrasonics, ferroelectrics, and frequency control* 49(2), pp. 217–30.

Smith, W. a. 1989. The role of piezocomposites in ultrasonic transducers. *Proceedings., IEEE Ultrasonics Symposium*, pp. 755–766.

Wallace, M.F. 2007. Single Crystal Acoustic Transducers for High Performance Underwater Sonar Systems. University of West of Scotland.

Zipparo, M., Oakley, C., Hackenberger, W. and Hackenberger, L. 1999. Single crystal composites, transducers, and arrays. *1999 IEEE Ultrasonics Symposium. Proceedings. International Symposium (Cat. No.99CH37027)* 2, pp. 965–968.

# CHAPTER 6

---

## Single Element Transducers Results: Fabrication and Performance

---

### Chapter Profile

This chapter presents the results from the fabrication of single element ultrasound transducers using the fabrication process described in Chapter 5. The chapter's main aim is to address two key points:

- to validate the fabrication process developed for arrays with single element transducers;
- to give results of transducers made from fine scale single crystal composites.

These results are obtained by employing precision micromachining and other micro-fabrication processes to overcome the technical challenges encountered in fabrication of miniature transducers. Low temperature methods were used to make fine-scale composites from PZT-5H, and two piezocrystal materials, a binary and a doped ternary material. Micro-coaxial cables were used for electrical impedance matching of the devices. Acoustic matching and backing was achieved with cast layers of loaded epoxies on different sides of the piezocomposite active substrate. Preliminary results obtained with prototype single element devices were used as validation of the fabrication process and to demonstrate functionality. Pulse-echo results highlight the resolution, operational frequency and bandwidth of these devices.

It is important to note that the single element transducers developed were intended to validate the process for the arrays and therefore are not designed to operate as ideal single element transducers. They, however, provide good pulse-echo results, especially the two made from the single crystal materials.

### 6.1 Introduction

The fabrication of the single element transducers follows the process described in Chapter 5, which is aimed at obtaining high frequency arrays integrated into medical

interventional tools. The process has three key differences when compared to the array fabrication:

- The single element transducers separated at the end of the process in Figure 5.1 were much larger than the individual elements in an array.
- The flexi-circuit was un-patterned since one element was used for each device.
- The individual element was connected to a micro-coaxial cable near the transducer for electrical impedance matching. This would be difficult to achieve with arrays since multiple cables could not fit in the small diameter tube.

Fine scale composites were made and the other layers, matching and backing, cast as detailed in Figure 5.1 (a-c). The prototypes of the single element transducers in this thesis were fabricated from a fine grained ceramic, a binary single crystal material and a doped ternary single crystal material. The results of devices fabricated with these materials are discussed in the following sections of this chapter.

The following points must be considered when determining the design of a composite, and deciding on a compromise between maximising the performance of a device and minimising the fabrication challenges.

- The frequency of the transducer is important in determining the resolution with higher frequency meaning better resolution.
- The thickness determines the frequency of the transducer.
- The volume fraction of a composite determines whether the composite is good for pulse-echo (transmission-reception) testing. The composite volume fraction determines the electromechanical coupling coefficient.
- The pillar width is important in obtaining a good composite for imaging. The smallest pillar width would give good thin-tall pillars which are useful for reducing lateral modes in the composite with improves the image. The thickness of the commercially available blades limits the minimum achievable kerf and dicing depth, which consequently limits the minimum achievable pillar width.
- The aspect ratio is defined as the ratio of the pillar width to the height. The height of the pillar is the thickness of the composite substrate. The smaller the

aspect ratio, the better the composite. This is because the lateral resonances are reduced when the pillars are thin and tall. Also, the length extensional mode is much stronger than all the other modes. This is important for imaging transducers since all the ultrasound energy is directed to the desired vibration mode. In Table 6.1 the ternary material has the best aspect ratio. It is important to note that this is also mainly due to the dicing pitch used in the composite.

- The electromechanical coupling coefficient is improved when a material is made into a 1-3 composite. This is because the pillars resonate in thickness extensional mode. This in turn improves the energy transfer between mechanical and electrical energy which improves the SNR.

## 6.2 High Frequency Piezocomposite Fabrication

The 1-3 piezocomposites were fabricated using the widely established dice-and fill method. High frequency piezocomposites are difficult to achieve and the difficulty increases when they are made from the fragile, temperature sensitive single crystal materials. In this report, three different types of composites from different materials are reported in this thesis: a fine grain ceramic CTS 3203HD (PZT-5H), and two piezocrystal materials; PMN-29PT (binary material) (Sinoceramics, Inc., Shanghai, China) and Mn:PIN-PMN-PT (doped ternary material) (TRS Technologies, State College, PA, USA). They are more fragile when dicing and have a lower Curie temperature when compared to PZT-5H. Plates of these materials were made into high frequency composites to be used in the single element transducers. Some parameters such as the thicknesses of the active substrate and the matching layer were investigated using simulation and modelling explained in Chapter 4.

The dicing parameters, such as feed rate, spindle speed and coolant feed rate, for making the composites were determined by studying literature detailed in Chapter 2. These were then adjusted with practice according to the material being diced and the size of the blade used. These are discussed in the respective section outlining the composites. The CTS 3203HD/Epofix composite was made with a wider blade as a starting point for setting the parameters used in dicing the more delicate single crystal

materials. Figure 6.1 is an illustration of one of the piezocomposites fabricated. The successful composite is shown in Figure 6.1 (a) and (b) without any pillar breakage.

For the earlier single crystal composites made in this study, pillar breakage was very common during dicing. This problem is common in literature as it was discussed in Section 2.6.5 of Chapter 2. In Figure 6.1(c), strips of the material were undesirably removed. Such an incident depends on a number of factors including the inter-elemental pitch, spindle speed, material feed rate, coolant rate, depth of cut and the type of the material being diced. It was important to ‘fine tune’ a number of these factors to be able to cut two orthogonal sides of the material before filling with epoxy, which is crucial in reducing the overall fabrication time. Generally, by using a slower feed rate, slower spindle rotation rate, lower coolant feed rate and a large inter-pillar pitch, the composite yield is improved. Another common problem in the earlier composites was bubble formation at pillars (Figure 6.1(d)) after filling with epoxy due to the small spaces between the pillars. These were minimised by careful casting of epoxy as well de-gassing in a vacuum chamber for over five minutes.

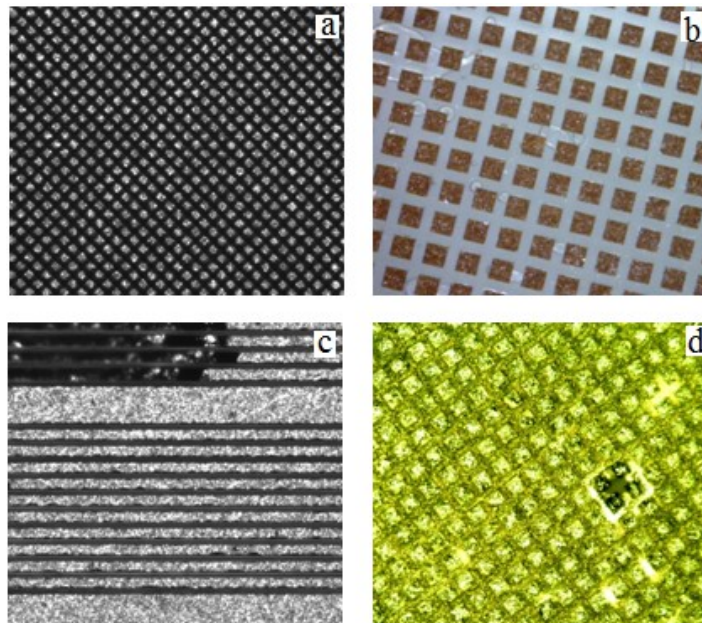


**Figure 6. 1: Examples of 1-3 piezocomposite : (a) After dicing both directions before filling with epoxy; (b) After filling with epoxy and lapping; (c) an example of strips of piezoelectric material removed by dicing in the first direction; (d) an example of air bubble after filling with epoxy**

The properties of the composites made are summarised in Table 6.1 and discussed in the following sections. These are compared to a bulk PMN-PT material whose properties were measured in-house. The electromechanical coupling coefficient was calculated using Equation 2.6. The diagram to compare the dimensions of each composite made into a transducer as shown in Figure 6.2 and in Table 6.2.

**Table 6.1: Comparison of properties of fabricated piezoelectric composites and a bulk single crystal material**

Material	Frequency (MHz)	Thickness ( $\mu\text{m}$ )	Volume fraction	Pillar width ( $\mu\text{m}$ )	Pillar Aspect ratio	Electromechanical coupling coefficient ( $k_t$ )
PMN-PT (Bulk)	1.9	400	1	—	—	0.50
CTS 3203HD/Epofix (PZT-5H)	14.6	118	0.40	60	0.508	0.59
Binary	21.8	86	0.36	30	0.349	0.71
Doped Ternary	15.4	99.6	0.36	30	0.301	0.68

The results in Table 6.1 show that the electromechanical coupling coefficients for the single crystal composites are higher than that for the ceramic composite. This is expected as demonstrated in literature (Michau et al. 2002).

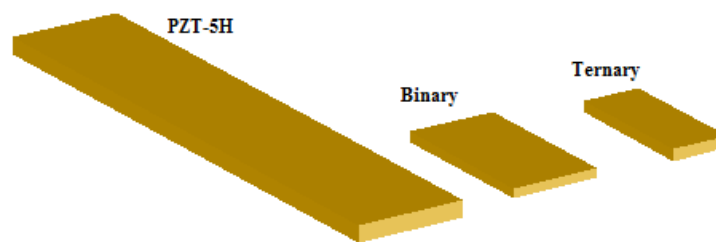


**Figure 6. 2: A diagram comparing the dimensions of the three transducer active elements fabricated**

**Table 6. 2: A table comparing the dimensions of the composites made into transducers**

	<b>PZT-5H</b>	<b>Binary</b>	<b>Ternary</b>
<b>Length (mm)</b>	5	1.5	1.3
<b>Width (mm)</b>	1	0.8	0.52
<b>Thickness (mm)</b>	0.14	0.086	0.099
<b>Frequency (MHz)</b>	15	22	17

### 6.3 Device Fabrication

#### 6.3.1 CTS 3203HD Composite Transducer

The CTS 3203HD material is a type of PZT-5H which is commonly used in commercial ultrasound imaging transducers. A composite was made from this material to set the preliminary parameters for dicing which were later adjusted to make composites from the fragile PMN-PT single crystal materials. Composites have been widely made from this material and therefore there were plenty of references in the literature (Yuan et al. 2006; PhamThi et al. 2009). Parameters such as spindle speed, feed rate and water coolant rate were faster than those used in the making composites from the single crystals as will be explained below.

The 1-3 piezocomposite that was used for the active substrate was made of 40% volume fraction of the CTS 3203HD in epoxy. The piezoelectric materials were obtained in bulk form. They were diced to make composites and then filled with low shrinkage epoxy (EPOFIX, Struers, UK) (Bernassau et al. 2011). Dicing to make composites was done using a high precision dicing saw (MicroAce66, Loadpoint, Cricklade, UK). The pillars in this composite had a pitch of 95  $\mu\text{m}$  fabricated with 30  $\mu\text{m}$  thick blade. The dicing blade spindle speed of 30,000 rpm and material feed rate of 1.15 mm/s with a coolant feed rate of 1.1 L/min were used to cut a depth of 375  $\mu\text{m}$  into the 1 mm material. The two sets of cuts in orthogonal directions were made before filling with epoxy.

The composite was lapped to a thickness of 118  $\mu\text{m}$  to give an operational frequency of 14.6 MHz. Silver paint electrodes were applied to both sides of the composite. A 15% volume fraction alumina filled epoxy was cast on the composite as a matching layer. It was then lapped to a thickness of 50  $\mu\text{m}$ . An un-patterned flexi-circuit was

attached to the back using silver epoxy. A 30% volume fraction tungsten filled epoxy was then cast at the back of the composite as matching. This was sanded down to give an overall stack thickness of 1 mm.

### 6.3.2 *Binary composite Transducer*

The transducer active substrate of the 1-3 piezocomposite from the PMN-29PT single crystal had a volume fraction of 36% in epoxy. Similar to the PZT-5H composite, the bulk single crystal materials were diced to make composites and then filled with low shrinkage Epofix epoxy (Struers, UK). The pillars in the composite had a pitch as small as 50  $\mu\text{m}$  fabricated with 15  $\mu\text{m}$  thick Disco hubbed blade. By using blade spindle speed as low as 10,000 rpm and material feed rate below 0.25 mm/s, sets of cuts in two orthogonal directions were made before filling with epoxy. The composite was lapped to a thickness of 82  $\mu\text{m}$  which gave an operational frequency of 21.83 MHz shown in Figure 6.7. The acoustic impedance of the composite was calculated to be 12 MRayl.

The 50  $\mu\text{m}$  thick matching layer for this transducer was 15% volume fraction alumina in epoxy. A 15% alumina filled epoxy has an acoustic impedance of 4.1 MRayl with an attenuation of 15.5 dB/mm. The backing of 1 mm thickness was 20% volume fraction of tungsten in epoxy. This has an acoustic impedance of 8 MRayl with an attenuation of 27.5 dB/mm. Single element transducers were made from PMN-PT composite with a frequency of approximately 22 MHz. The transducers with the active element, matching and backing were 0.8 by 1.5 by 2 mm<sup>3</sup>.

### 6.3.3 *Ternary Composite Transducer*

The parameters used in making this composite are the same as those used to make one from PMN-29PT. The composite pitch was 50  $\mu\text{m}$  with a 15  $\mu\text{m}$  thick Disco hubbed blade. The average kerf width was 20  $\mu\text{m}$  which gave a volume fraction of the 1-3 piezocomposite of 36% volume fraction of Mn:PIN-PMN-PT/Epoxy. The different sides were cut to different depths to prevent pillar breakage. The first pass of kerfs were diced to 210  $\mu\text{m}$  deep, and the orthogonal pass of cuts were diced to 190  $\mu\text{m}$  deep. The composite was cut into two separate sections which were lapped to a thickness of 99.6  $\mu\text{m}$  and 111.4  $\mu\text{m}$ . These yielded operational frequencies of 17 MHz

and 15 MHz respectively. An illustration of the impedance plot of the 15 MHz composite transducer is discussed in Section 6.5.4.

The matching layer for this transducer was 15% volume fraction alumina particles in epoxy and the backing of 1 mm thickness was 30% volume fraction of tungsten particles in epoxy.

The transducer active element dimensions were  $1.34 \times 0.52 \times 0.099 \text{ mm}^3$  and this was combined with a  $50 \text{ }\mu\text{m}$  thick matching and a 1 mm thick backing.

#### **6.4 The Imaging Transducer**

An example of a complete single element transducer with the matching, composite and backing is illustrated in Figures 6.3 and 6. 4. The CTS 3203HD transducer was attached to components such as the rod in Figure 6.3 to facilitate testing. The image in Figure 6.3 is of a single element transducer in a tungsten tube. The absence of extra bond layers is evident where the matching and backing are directly attached to the active substrate. The active substrate, shown in cross-section in Figure 6.3, is a 1-3 composite with the CTS 3203HD pillars and the clear polymer filler. The tube with the transducer is attached to a rod which is held in a characterisation tank for testing. A micro-coaxial cable of  $300 \text{ }\mu\text{m}$  in diameter was used for transmitting signals. The details were the same for the other fabricated single elements.

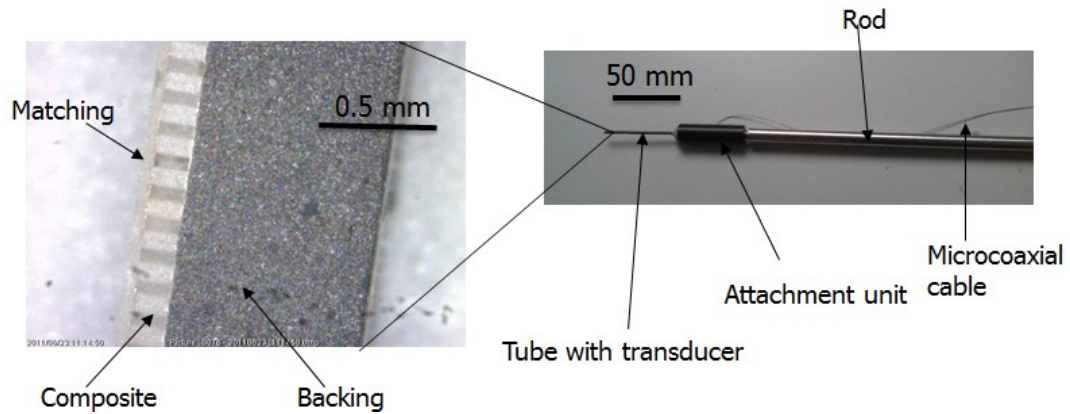


**Figure 6. 3:** An illustration of a single element transducer in a metal tube attached to a rod for easy testing. The active area is magnified to show the layers of matching with alumina filled epoxy, composite and the backing with tungsten filled epoxy

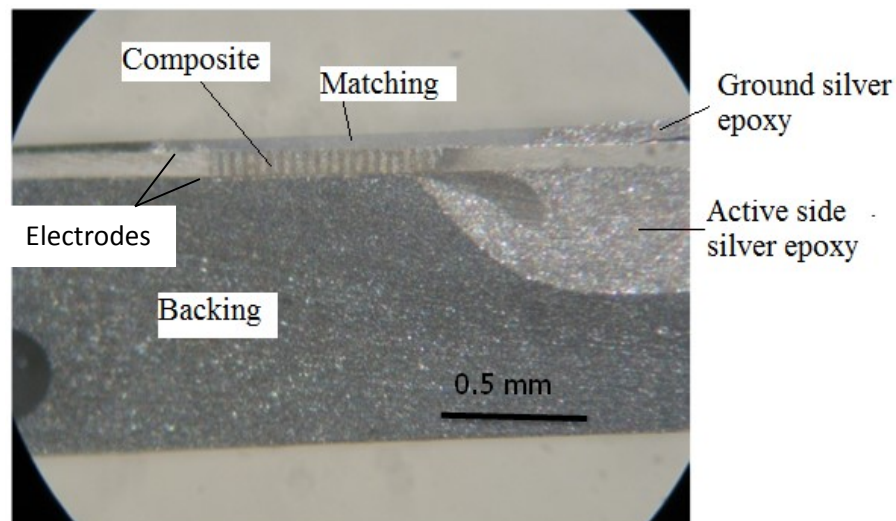


**Figure 6. 4:** A transducer showing matching layer, backing layer, active composite, conductive epoxy for electrical connection to the cabling. This Figure is for the same element as that shown in Figure 6.2.

## 6.5 Electrical Characterisation

The impedance response of each transducer was determined by attaching a coaxial cable of 10 cm length, with diameter of 2 mm to the micro-coax. This coaxial cable had an SMA connector at one end. This was needed to connect to the pulser-receiver for exciting the transducer during testing. Only the micro-coaxial cable was used to match the impedance of the transducer and therefore any extra coaxial cable for connection had to be as short as possible.

### 6.5.1 *Electrical Impedance Matching*

Each single element transducer had a micro-coaxial cable attached with conductive silver epoxy for transmission of power and signal. The electrical impedance of the transducer was tested at different stages of fabrication using an impedance analyser (4395A, Agilent Ltd, West Lothian, UK). It is important to measure the impedance of the transducer before the coaxial cable is attached since the coaxial cable was used to match the electrical impedance to the driving electronic equipment, which was matched to 50  $\Omega$ .

To match the impedance of the single element transducer to the 50  $\Omega$  the high impedance coaxial cable, by the transmission line theory was used as a quarter wavelength long transformer between the transducer stack with impedance  $Z_e$  and the system with impedance  $Z_s$ . The required impedance of the coaxial cable  $Z_0$  can be determined by (Ritter, Shrout et al. 2002):

$$Z_0 = \sqrt{Z_e \times Z_s} \quad 6.1$$

An impedance plot of 1 m micro-coaxial cable is illustrated in Figure 6.5. This was measured using an impedance analyser (4395A, Agilent Ltd, West Lothian, UK) and for the 1 m coaxial cable the impedance magnitude at about 15 MHz is 221  $\Omega$ , 143  $\Omega$  at 22 MHz and 189  $\Omega$  at 17 MHz which are the frequencies of all the three transducers reported in this chapter.

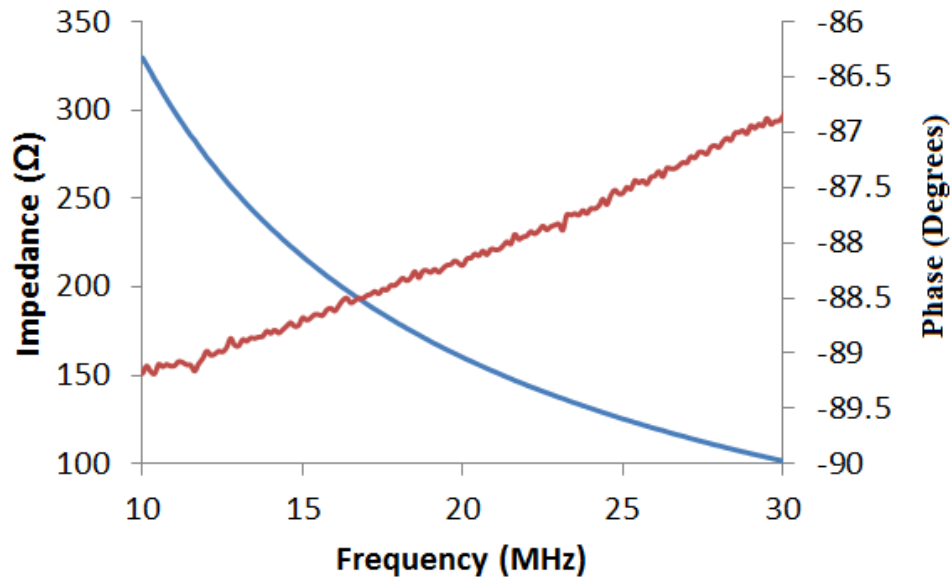


**Figure 6. 5: Impedance magnitude and phase plot of a 1 m coaxial cable. The impedance magnitude at 15 MHz is about 221  $\Omega$ , at 22 MHz is about 143  $\Omega$  and at 17 MHz is about 189  $\Omega$**

The matching with a micro-coaxial cable also increases the bandwidth of the system and filters out reactive components. Where the element has impedance lower than 50  $\Omega$  as is the case in most single element transducers, a low impedance coaxial or coaxial cables in parallel may be utilised.

After the impedance of the active stack with the coaxial cable was measured, it was fitted into a tungsten tube and glued with epoxy before the impedance of the finished prototype was measured.

### 6.5.2 CTS 3203HD Composite Transducer

The results shown in Figure 6.6 were obtained with a single element transducer of 1 x 5 x 0.140 mm<sup>3</sup> active element. The far field transition based on the azimuth plane is 60 mm as approximated by Equation 2.10.

Figure 6.6 shows the impedance of the transducer before and after matching with a micro-coaxial cable. The impedance magnitude at about 14.8 MHz is shown to have been reduced from over 1500  $\Omega$  to less than 110  $\Omega$ , with a 1.5 m micro-coaxial cable.

The 110  $\Omega$  is much closer to 50  $\Omega$  which is the standard impedance of the driving electronics. The electrical impedance from Figure 6.6(a) is smoothed when a micro-coaxial cable is attached as shown in Figure 6.6(b) and the resonances are also very damped. This increases the overall bandwidth of the transducer. The blip at about 15 MHz in the graph (Figure 6.6(b)) is likely to be due to the matching layer.

The coaxial cable to perfectly match the impedance would have an impedance magnitude of about 273  $\Omega$  as calculated using equation 6.1 with the system impedance being 50  $\Omega$ .

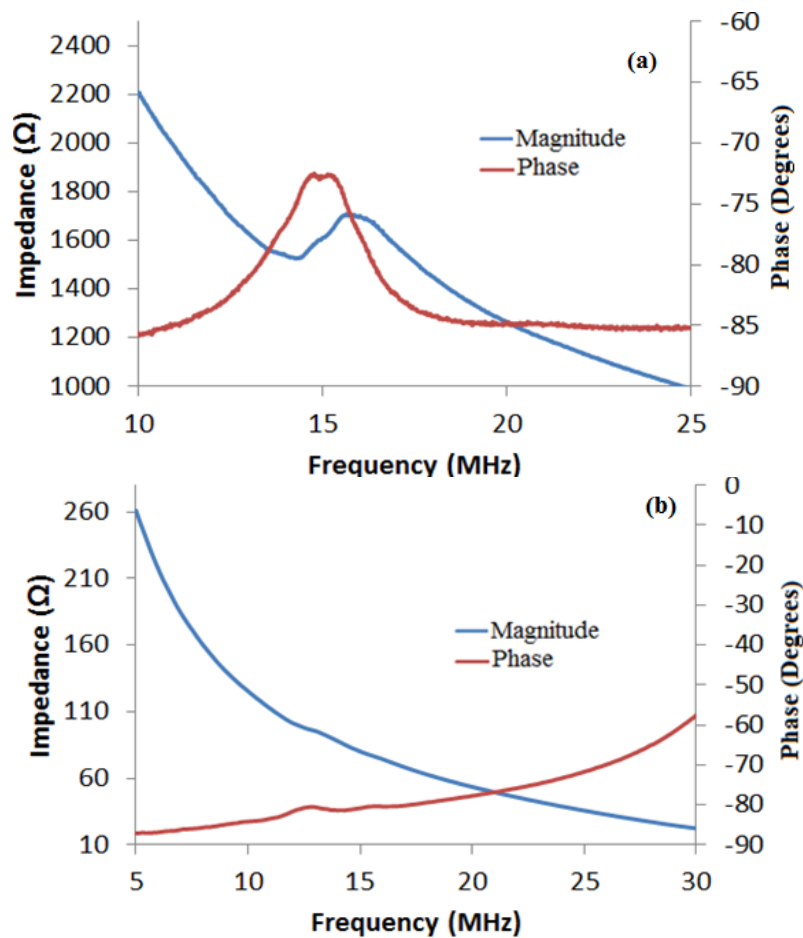


Figure 6. 6: Impedance magnitude and phase of CTS 3203HD/Epofix composite transducer with acoustic matching and backing at 15 MHz; (a) before electrical impedance matching, (b) after electrical impedance matching with coaxial cable

### 6.5.3 Binary Single Crystal Composite Transducer

The results shown in Figure 6.7 were obtained with a single element transducer of 0.8 mm x 1.5 mm x 0.086 mm active element. The far field transition based on the azimuth plane is 8 mm as approximated by Equation 2.10.

Figure 6.7 illustrates the electrical impedance of the binary composite transducer that was tested. The electrical resonance frequency was at 21.83 MHz. In the figure there is a lateral resonance artefact at about 13 MHz which is caused by the matching layer. This resonance is at a low enough frequency not to cause interference with the main resonances.

Electrical impedance matching was achieved by using a 1.2 m micro-coaxial cable. Figure 6.7 shows the impedance of the transducer before and after matching with a micro-coaxial cable. The impedance magnitude in Figure 6.7 is shown to have been reduced from 290  $\Omega$  to 70  $\Omega$ , with a 1.2 m micro-coaxial cable. The coaxial cable to perfectly match the impedance would have an impedance magnitude of about 120  $\Omega$  as calculated using Equation 6.1 for the system impedance of 50  $\Omega$ .

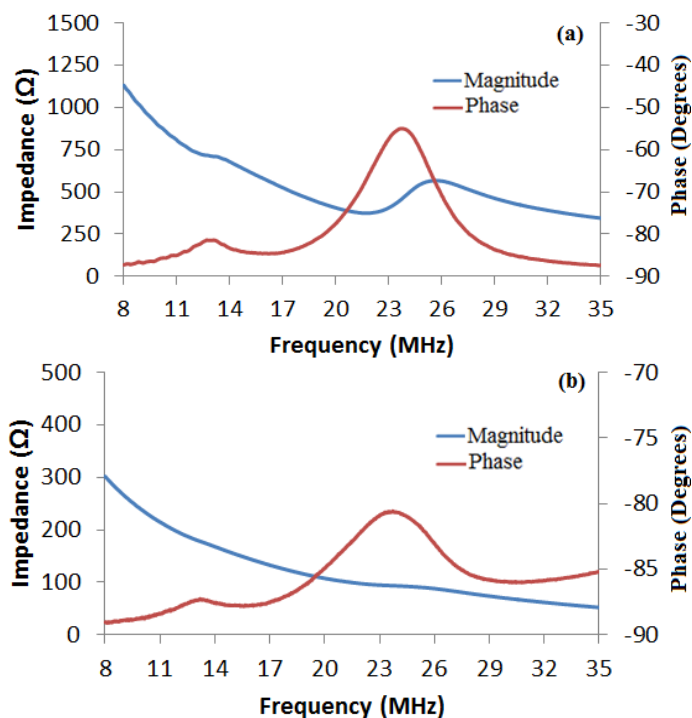


**Figure 6. 7: Impedance magnitude and phase of PMN-PT composite transducer at 21.83 MHz; (a) before electrical impedance matching which was measured at the end of the flex circuit, (b) after impedance matching with coaxial cable**

### 6.5.4 Ternary Composite Transducer

The results shown in Figure 6.8 were obtained with a single element transducer of 1.3 mm x 0.52 mm x 0.099 mm. The far field transition based on the azimuth plane is 4.96 mm as approximated by Equation 2.10 in Chapter 2

Figure 6.8 illustrates the electrical impedance of the ternary composite transducer that was tested. The electrical resonance frequency was at 17 MHz. This transducer does not have lateral resonance effects and therefore would perform very well in the thickness-extensional mode. The damping by the micro-coaxial matching is illustrated and the impedance magnitude is reduced to about 90  $\Omega$ . The coaxial cable to perfectly match the impedance would have an impedance magnitude of about 120  $\Omega$  as calculated using Equation 6.1 the system impedance being 50  $\Omega$ .

The transducer stack produced an electrical impedance of approximately 400  $\Omega$  which would be too high for the driving electronics. After matching with a 1.4 m micro-coaxial cable, this was reduced to about 90  $\Omega$  which is closer to the 50  $\Omega$  of the driving electronics

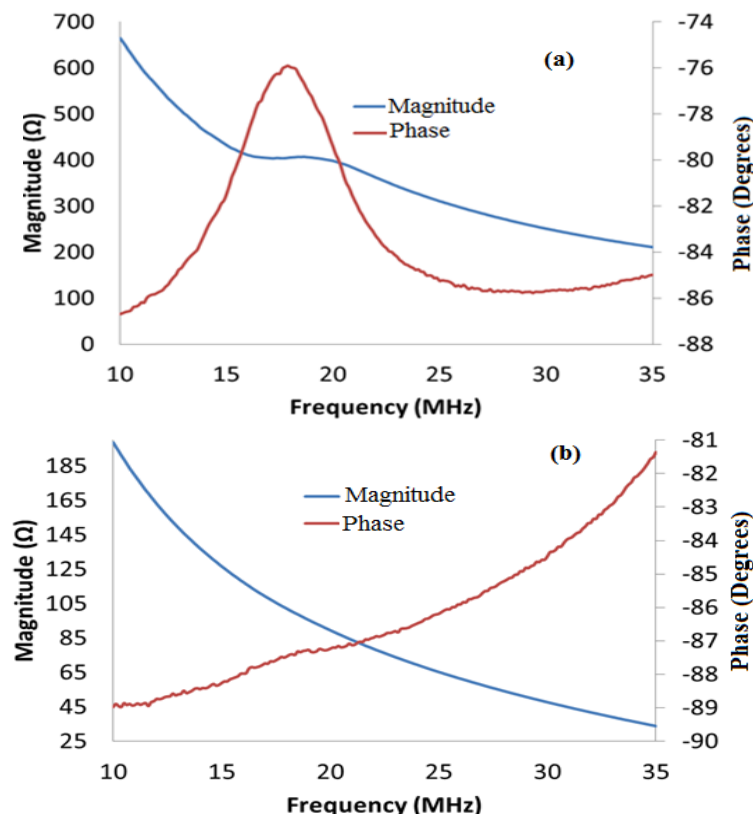


Figure 6. 8: Impedance magnitude and phase of Mn-PIN-PMN-PT composite transducer at 17 MHz; (a) before electrical impedance matching, (b) after impedance matching with coaxial cable For all these elements, is the electrical impedance as expected for the dimensions and VF of the composite

## 6.6 Acoustic Characterisation

The scanning of all the transducers was along the elevation (width) of the element. Mouse bowel was also scanned using the transducers. Ex vivo Bowel tissues resected from two different mice, Mouse A and Mouse B, were imaged with the transducer. The tissue was immersed in Phosphate buffered saline (PBS) (Moser et al. 1993) which is a solution used to mimic physiological fluids. Tissue does not reflect as highly as stainless steel or tungsten because the acoustic impedance is much lower. Obtaining these images is crucial in establishing that the transducers can image structures similar to that in the human body.

It should be noted however that the images produced by the transducers are expected to be of poor lateral resolution because the single element transducers were unfocussed.

### 6.6.1 CTS 3203HD Composite Transducer

The stainless steel block from the test in Figure 3.11 was used to obtain the pulse waveform response, shown in Figure 6.9, of the transducer. A summary of the results from this figure are in Table 6.3. A broadband excitation signal was applied to the transducer by a DPR 300 pulser-receiver (JSR Ultrasound, Pittsford, NY, USA). The settings of the pulser-receiver were adjusted to obtain maximum signal amplitude which was detected using a digital oscilloscope. The receiver gain was 40 dB, the high pass filter was set to 5 MHz and the low pass filter set to 22.5 MHz, the damping was 12 and pulse energy set to the maximum. The centre frequency of the transducer is 14.6 MHz and this yielded a bandwidth of 77 %. The pulse length is 0.45  $\mu$ s corresponding to 346.5  $\mu$ m.

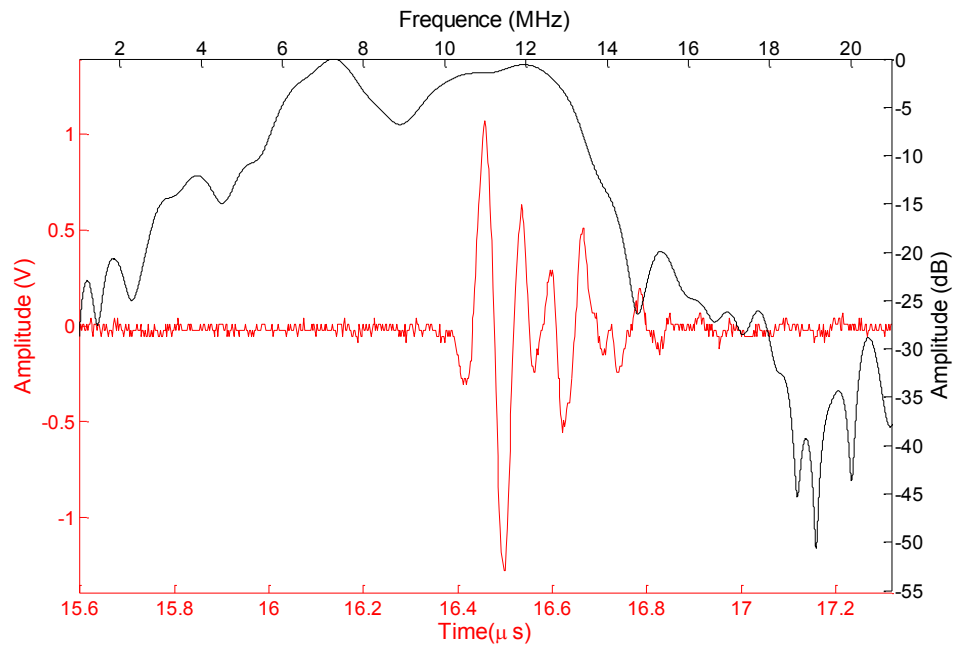


**Figure 6. 9:** The measured pulse-echo waveform reflected from a steel block showing the pulse length and the frequency spectrum of the CTS 3203HD/Epofix composite transducer

The image in Figure 6.10 is of the wires attached to a stainless steel block shown in Figure 3.11. The image reconstructed in MATLAB was set to a dynamic range of -40 dB. The image quality is good enough to show the different wires illustrated by numbers 1 to 3 in the image. The bright artefact shown in the image from about 11.5 mm to 14.5 mm in the lateral distance was due to interference in the signal which reduced the SNR during scanning.

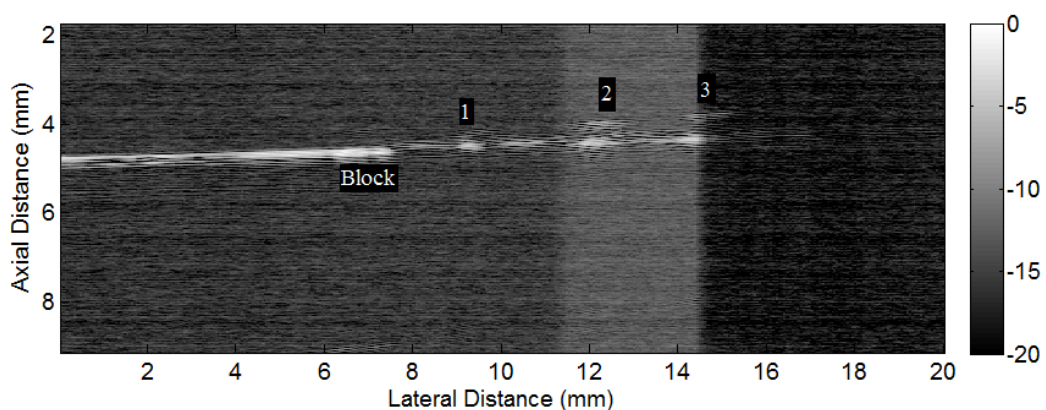


**Figure 6. 10:** Image of the three wires on a stainless steel block obtained with the CTS 3203HD/Epofix composite transducer

### 6.6.2 Binary Single Crystal Composite Transducer

The reflection from the stainless steel block was used to obtain the pulse waveform response, shown in Figure 6.11, of the transducer. A summary of the results from this figure are in Table 6.3. The centre frequency is 21.83 MHz with a bandwidth of 72%.

The pulse ring down time (-6 dB), corresponds to an axial resolution distance. The pulse length of the binary single element transducer was found to be 254.1  $\mu\text{m}$ . The pulse is longer than what is desired and this is caused by the insufficient damping from the backing. More damping would reduce the pulse length and increase the bandwidth. The pulse is reasonably short and the some of the ringing may still be due to alignment with the flat reflector especially when the beam is not fully in the far field.

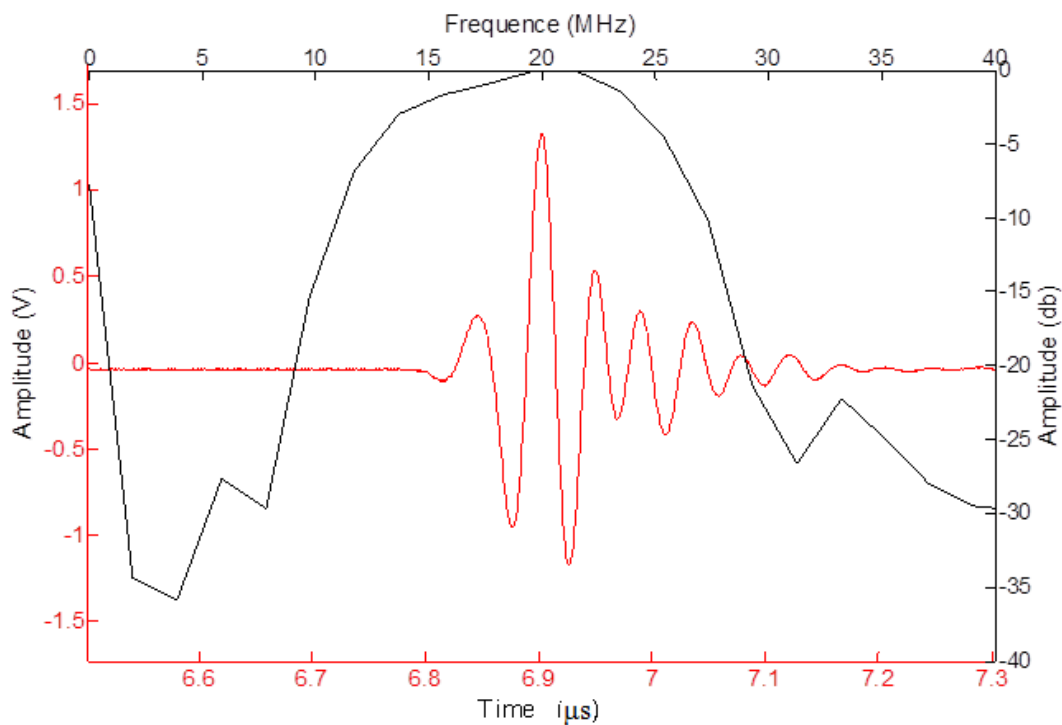


**Figure 6. 11: The measured pulse-echo waveform reflected from a steel block showing the pulse length and the frequency spectrum of the PMN-PT/Epofix composite transducer**

The wires attached on the stainless steel block are shown in Figure 6.12 (a). More details of the wires are shown when this transducer is used compared to using the CTS 3203HD/Epofix composite transducer. The main reason is that the binary composite has

a higher frequency and therefore better resolution. The single crystal material also provides better sensitivity.

The wire phantom image shown in Figure 6.12 (b) shows the line spread function of the different wires positioned at approximately 1 mm away from each other in width and depth. The first position on the top left of the figure is a reflection from a 5  $\mu\text{m}$  wire. The spread of the wires in the lateral dimensions is about as expected for this unfocussed transducer.

Figure 6.12(c) was obtained from Figure 6.12(b) and it illustrates a lateral resolution of 0.45 mm. The plot is from a wire positioned at 5.5 mm in the lateral position and at a depth of 5 mm in the image. All the other plots at different positions in the image gave a similar lateral resolution. This resolution could be improved by using a lens to focus the transducer in the lateral direction, if a single element transducer is required for the application.

This PMN-PT single crystal transducer was also used to image details of mouse bowel tissue pinned to a 3% volume agar substrate in water. Images of tissues from two different mice are shown in Figure 6.13 (a) and (b). In tissue from Mouse A, the basic outline of the tissue can be visualised. For Mouse B, the muscle layer can be distinguished by the bright line indicating stronger reflections about a millimetre below the top surface of the tissue. The strong reflections from pins used to hold the tissue on the agar substrate, can be seen below the tissue.

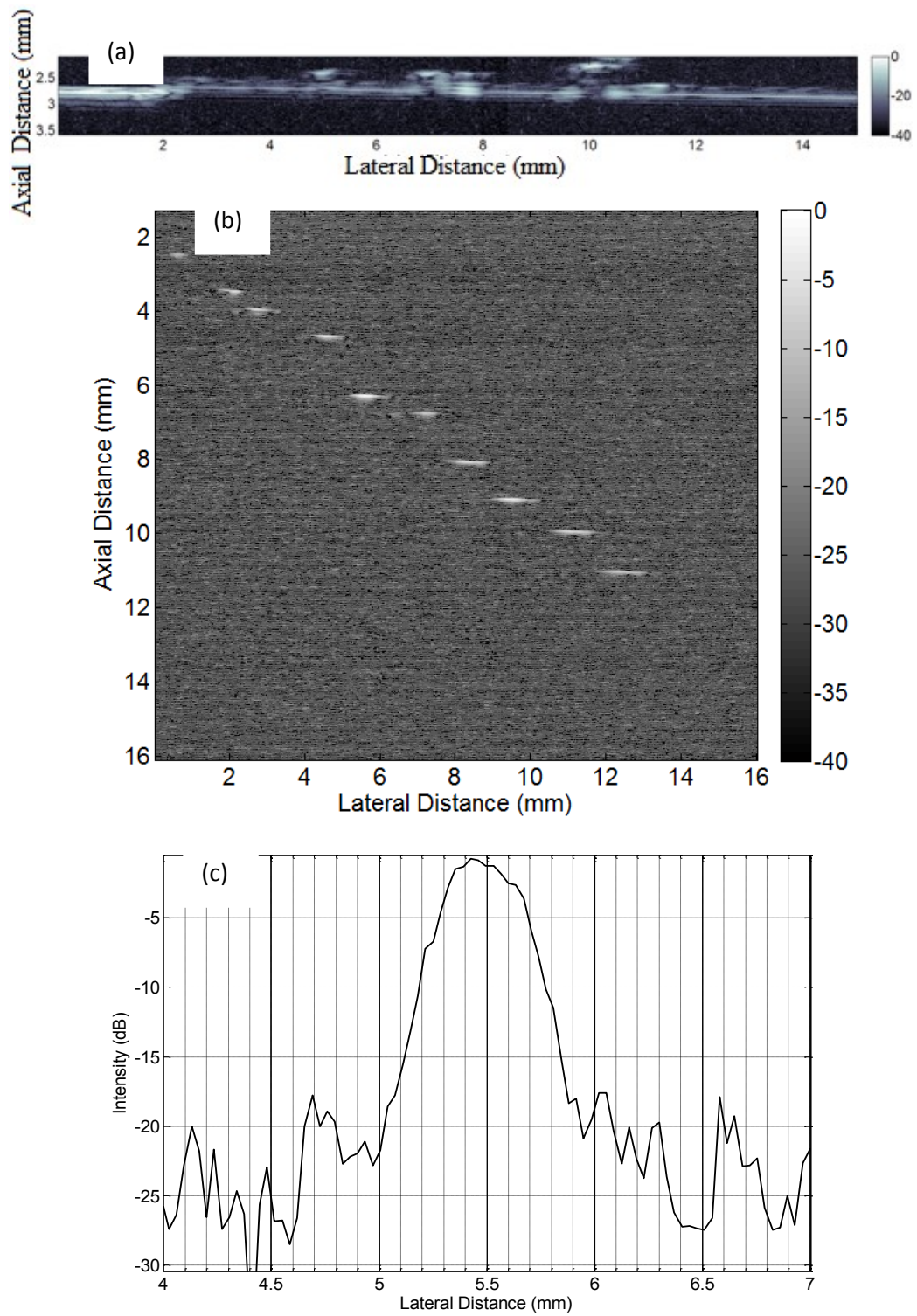


**Figure 6.12: Images with the PMN-PT composite transducer: (a) Steel block with three wires on double sided tape produced good results; (b) Wire phantom with nine 20 μm tungsten wires; (c) Lateral envelop of echo signals from the wires located at 5.5 mm from the PMN-PT/Epofix composite transducer**

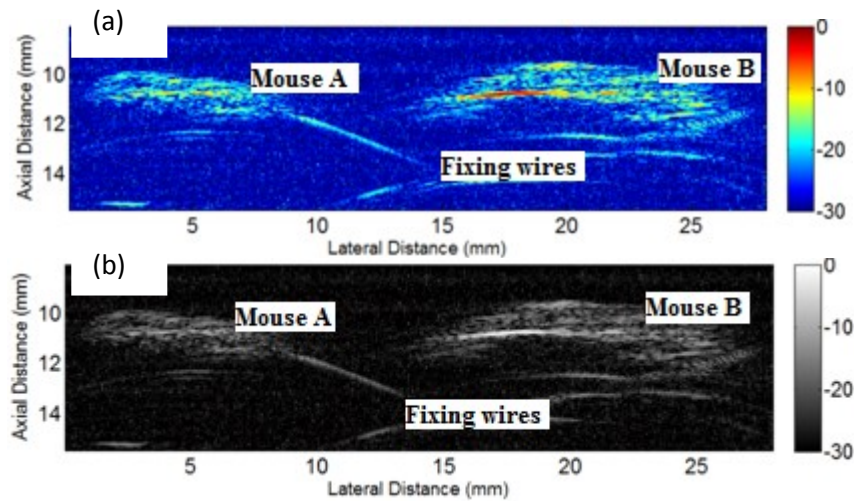


Figure 6. 13: Image of ex-vivo bowel tissue resected from two mice with ultrasound image represented in (a) false colour and (b) greyscale

### 6.6.3 Ternary Composite Transducer

The pulse waveform obtained from the stainless steel in this test is shown in Figure 6.14, with the results summarised in Table 6.3. The centre frequency is 17 MHz with a bandwidth of 98 %. This is a good bandwidth which is a result of the short pulse length caused by good backing and acoustic matching. The micro-coaxial cable for electrical matching also increases the bandwidth.

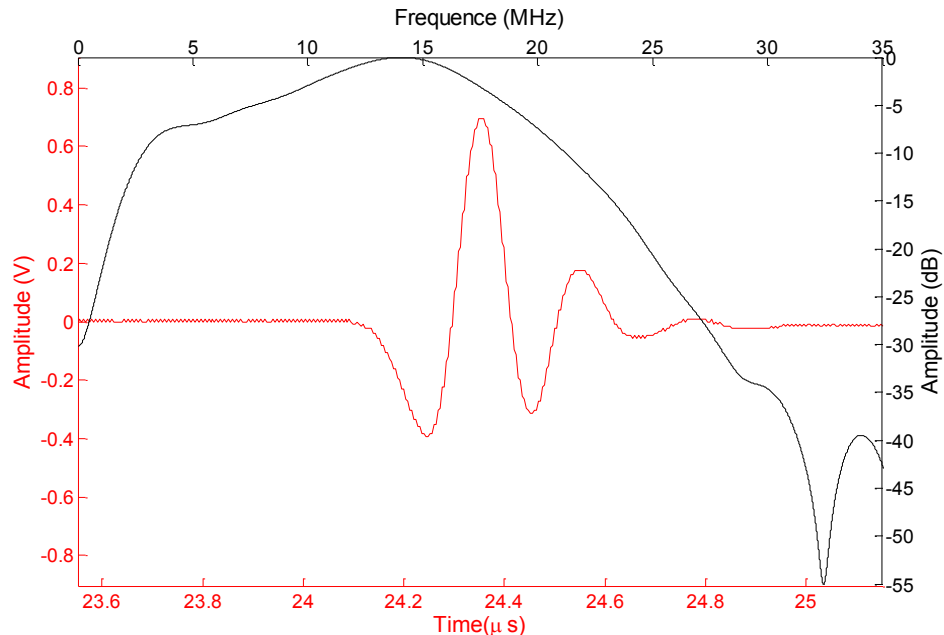
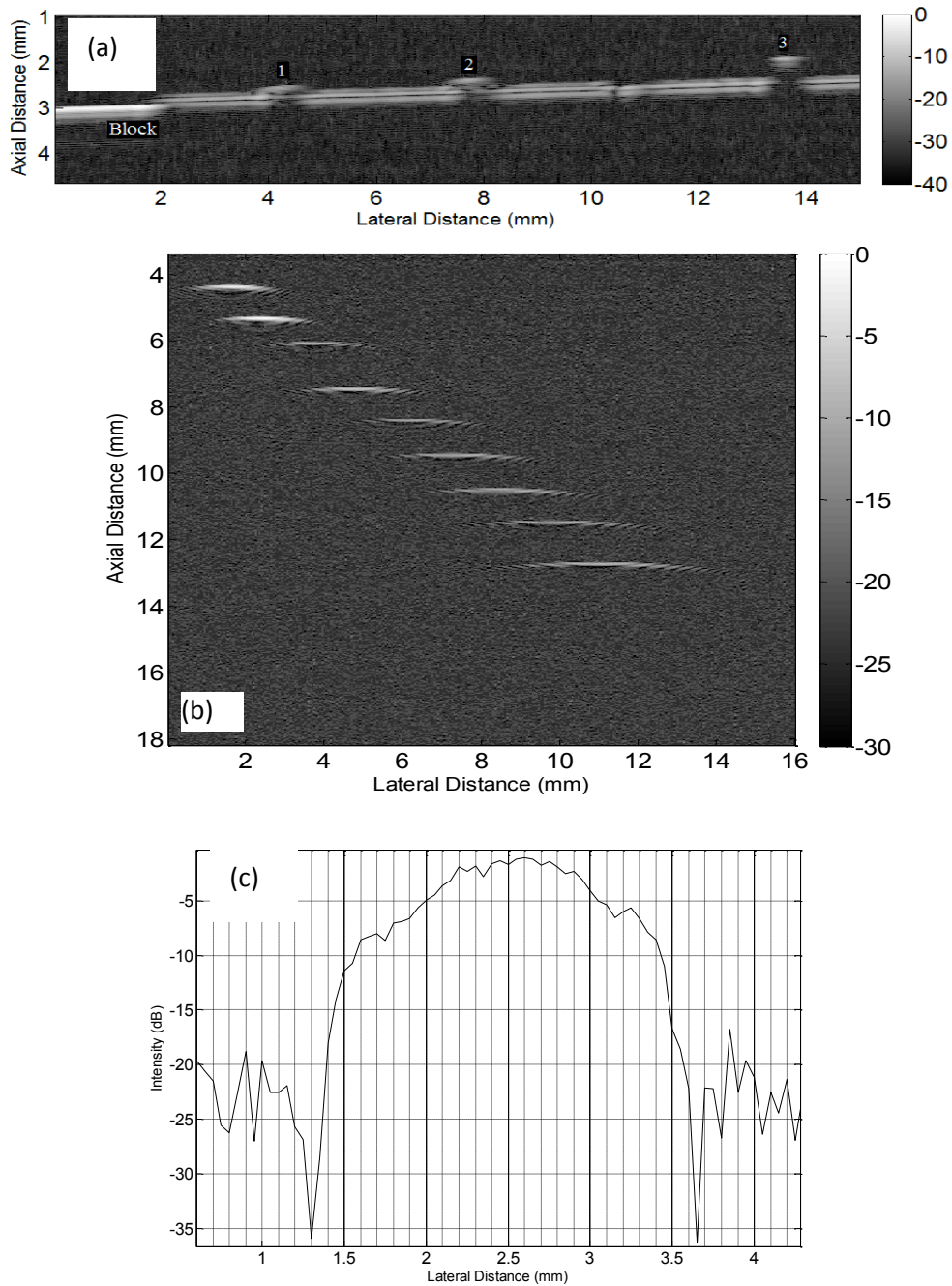


Figure 6. 14: The measured pulse-echo waveform reflected from a steel block showing the pulse length and the frequency spectrum of the Mn:PIN-PMN-PT/Epofix composite transducer

The wires attached on the stainless steel block are shown in Figure 6.15 (a). The details are clearly shown with shadows under each wire. These shadows are as a result of the most of the ultrasound energy being reflected by the wires. At 10 mm there is detail of the tape where one wire was attached but then moved to a different position.

The wire phantom image shown in Figure 6.15 (b) illustrates the line spread function of the different wires positioned at approximately 1 mm away from each other. The spread of the wires in the lateral dimensions for this unfocussed transducer was determined to give a -6dB resolution of 1.15 mm as shown in Figure 6.16(c). This figure was obtained from Figure 6.15(b) at a position of 2.5 mm in the lateral position. The other lateral positions also gave a similar resolution. This lateral resolution at 17 MHz is very big but can be reduced by using a lens to focus in the lateral dimensions. This would be important if the transducer is used as a single element transducer. If it is made into an array the focusing in the azimuth direction is done by electronic focusing.

The transducer was used to image details of mouse bowel tissue. The images of bowel tissue shown in Figure 6.16 demonstrate the ability to show contrast between types of tissue, particularly for Mouse B where the muscle layer tissue can be visualised.



**Figure 6. 15: Images with the Mn-PIN-PMN-PT composite transducer: (a) Steel block with three wires on a double sided tape produced good results; (b) Wire phantom with nine 20  $\mu$ m tungsten wires; (c) Lateral envelop of echo signals from the wires located at 5.5 mm from the Mn:PIN-PMN-PT/Epofix composite transduce**

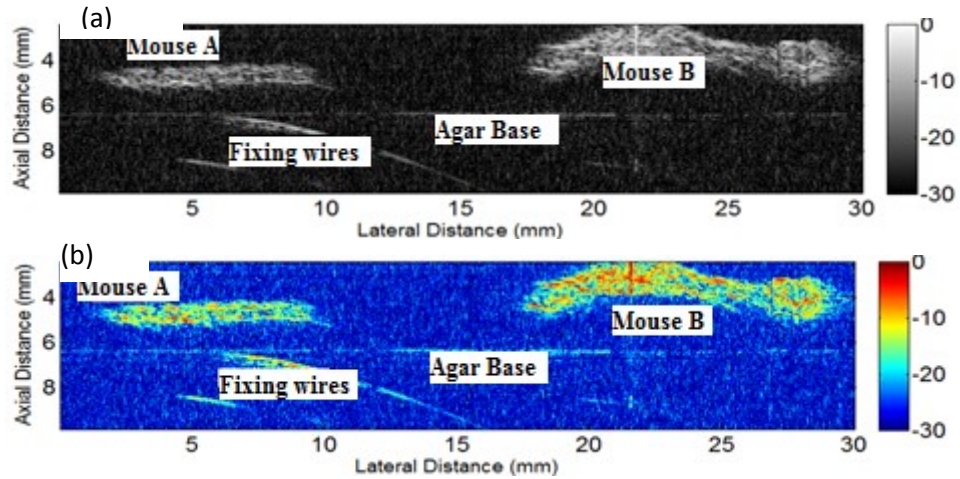


Figure 6. 16: Image of ex-vivo bowel tissue resected from two mice with ultrasound image represented in (a) false colour and (b) greyscale

## 6.7 Chapter discussion and conclusions

The single element transducers developed in this project were instrumental in answering many questions about integrating an ultrasound transducer into a needle. The process explained in Chapter 5 was validated and challenges identified with such transducers. The aim of fabricating such transducers was not to get optimised single element transducers but to confirm the feasibility of the process developed for the array fabrication. The main focus was to fabricate high frequency transducers from PMN-PT and Mn:PIN-PMN-PT single crystal composites using the widely accepted dice and fill method. These composites were fabricated to the limit of the mechanical dicing saw capability, which is restricted by the size of the thinnest blade. Also, the fabrication processes were kept to a maximum 50°C to minimise or prevent de-poling of the single crystal materials.

Some of the properties of the composites are summarised in Table 6.1. The electromechanical coefficients in this table indicate that composites from the single crystal materials have superior  $k_t$  values when compared to the bulk material and to

the PZT-5H composite. This is in line with literature where it is established that single crystal materials yield superior results when compared to the polycrystalline materials (Chan and Unsworth 1989; Zhen et al. 2007; Yuan et al. 2006; MacLennan et al. 2007) Composites further improve these material properties with  $k_t$  as an example in this case. The improved  $k_t$  means that more electrical energy is converted to mechanical energy and vice-versa. This means there will be better SNR, therefore improving the image quality. Since the performance parameters are close to those expected from the literature (Michau et al. 2002), it can be concluded that the fabrication processes are suitable for working with the binary and doped-ternary single crystal materials.

Different functional properties were obtained from impedance and pulse-echo tests of the different transducers. Some of those obtained are summarised in Table 6.3. Among the most important of these properties are the beam width and the bandwidth of the transducer. A broadband transducer is desired since it is more sensitive to a range of frequencies and produces a shorter ultrasound pulse corresponding to better axial resolution. An ideal electrically matched transducer has a higher bandwidth compared to one with poor electrical matching (Ritter et al. 2002).

**Table 6. 3: Summary of the properties of the single element transducers developed**

Transducer	Frequency (MHz)	Pulse length ( $\mu$ s)	Axial resolution ( $\mu$ m)	Bandwidth (%)
CTS 3203HD/Epofix	14.6	0.45	346.5 (3.4 $\lambda$ )	77
PMN-29PT/Epofix	21.8	0.33	254.1(3.7 $\lambda$ )	72
Mn:PIN-PMN-PT/Epofix	15.4	0.48	369.6 (3.8 $\lambda$ )	98

The axial response of the 14.6 MHz, CTS 3203HD/Epofix transducer was 346.5  $\mu$ m; that of the 21.8 MHz, PMN-29PT/Epofix transducer was 254.1  $\mu$ m, and that of the 15.4 MHz Mn:PIN-PMN-PT/Epofix transducer was 369.6  $\mu$ m. These are within the reasonable range of the transducers at these given operational frequencies (Li et al. 2011). The ultrasound beam profile for single element transducers depends on the diameter of the transducer and the wavelength of the beam (Gururaja and Panda 1998; Lockwood et al. 1996).

The axial resolution of a transducer depends on how well the transducer is damped as well as the operational frequency. Using backing and matching layers improve the damping and henceforth bandwidth of the transducer. The single element transducer with the best bandwidth and  $k_t$  was the Mn:PIN-PMN-PT/Epofix transducer. The pulse-echo response of the single element transducer shown in Figure 6.14 has a reasonably short two way pulse, at about 3 cycles long, with a 98% fractional bandwidth. The pulse shape and spectrum can be also improved with further optimization of the piezocomposite layer in the transducer (Brown et al. 2009).

The main ways to improve bandwidth are using a well fabricated composite with a good pillar aspect ratio, suitable acoustic backing and matching as well as electrical matching which was through the coaxial cables for the single element transducers in this thesis. Any acoustic or electrical mismatch will result in some signals being reflected and therefore affect the overall bandwidth of the transducer.

One of the main benefits of the Mn-doped ternary single crystal is the higher Curie temperature, which reduces the restrictions on the process temperature. The composites made from this material have comparative  $k_t$  values to the binary single crystal materials as is shown in Table 6.1. The doped-ternary material can also be used to produce transducers with good bandwidths as it is illustrated in Figure 6.14. The relaxed temperature restriction for these materials would mean that they should replace the binary PMN-PT single crystal materials to make imaging transducers. The only downside is that these materials are not yet readily commercially available.

The two single crystal transducers demonstrated clear results of the mouse bowel tissue. These results were important since the tissue has similar properties to that of human where the array transducers would be used. Features of the tissue structures, such as the muscle layer of the resected bowl tissue for Mouse B in Figure 6.16, can be seen even with the relatively poor lateral resolution from the single element transducers. These images would be much better with focusing using an array. Picking out such features *in-vivo*, and any changes relative to normal tissue structures, with the transducers on biopsy needles would be very important for establishing early diagnosis

of cancerous tissues, with the possibility of reducing or eliminating the need for central laboratory analysis of samples.

These single element transducers fabricated set a prerequisite for the fabrication of arrays. The same process was used as that which was used for the fabrication of the arrays which are detailed in Chapter 7. Some of the main challenges encountered in fabrication of the single element transducers included:

- Lapping the thin composite. Application of acetone on the thinned down composite softened the material and the pillars dropped out. This was mainly because a low temperature of 50°C was used for post curing of the epoxy. Typically, the epoxy would be post-cured at 100 °C (Bernassau et al. 2011). This problem would be eliminated when the Mn doped ternary single crystal materials replace the currently used binary single crystal materials. This is because these new materials can withstand higher temperatures, up to 100°C.
- Attaching of the coaxial cable to the transducer stack. The dimensions of the stack were very small and attaching a micro-coaxial cable with conductive epoxy by hand was difficult. This is avoided with the array by using an array interconnect solution.
- Inserting the transducer into the metal tube. It was important to have the correct size of transducer on all the sides. This became a challenge when the backing had to be sanded down to the right size. It was also difficult to get the right size of the conductive epoxy for holding the coaxial cable firmly on to the stack. This is a manufacturing challenge that will need to be investigated with continued development of ultrasound devices integrated into needles.

## 6.8 References

Bernassau, A.L., Hutson, D., Démoré, C.E.M. and Cochran, S. 2011. Characterisation of an Epoxy Filler for Piezocomposite Material Compatible with Microfabrication Processes. *IEEE transactions on ultrasonics, ferroelectrics, and frequency control* 58(12), pp. 2473–2478.

Brown, J.A., Chérin, E., Yin, J. and Foster, F.S. 2009. Fabrication and performance of high-frequency composite transducers with triangular-pillar geometry. *IEEE transactions on ultrasonics, ferroelectrics, and frequency control* 56(4), pp. 827–36.

- Chan, H.W. and Unsworth, J. 1989. Simple model for piezoelectric ceramic/polymer 1-3 composites used in ultrasonic transducer applications. *IEEE transactions on ultrasonics, ferroelectrics, and frequency control* 36(4), pp. 434–41.
- Gururaja, T.R. and Panda, R.K. 1998. Current Status and Future Trends in Ultrasonic Transducers for Medical Imaging Applications. In: *Applications of Ferroelectrics, 1998. ISAF 98. Proceedings of the Eleventh IEEE International Symposium on*. pp. 223–228.
- Li, X., Wu, W., Chung, Y., Shih, W.Y., Shih, W.-H., Zhou, Q. and Shung, K.K. 2011. 80-MHz intravascular ultrasound transducer using PMN-PT free-standing film. *IEEE transactions on ultrasonics, ferroelectrics, and frequency control* 58(11), pp. 2281–8.
- Lockwood, G.R., Turnbull, D.H., Christopher, D. and Foster, F.S. 1996. Beyond 30 MHz, Application of High-Frequency Ultrasound Imaging. *IEEE Engineering in Medicine and Biology*, pp. 60–71.
- MacLennan, D., Elgoyhen, J., Button, T.W., Démoré, C.E.M., Hughes, H., Meggs, C. and Cochran, S. 2007. Properties and Application-oriented Performance of High Frequency Piezocomposite Ultrasonic Transducers. *IEEE Ultrasonics Symposium*, pp. 100–103.
- Michau, S., Mauchamp, P. and Dufait, R. 2002. Single Crystal-based Phased Array for Transoesophageal Ultrasound Probe. In: *IEEE Ultrasonics Symposium*. pp. 1269–1272.
- Moser, A.R., Mattes, E.M., Dove, W.F., Lindstrom, M.J., Haag, J.D. and Gould, M.N. 1993. ApcMin, a mutation in the murine Apc gene, predisposes to mammary carcinomas and focal alveolar hyperplasias. *Proceedings of the National Academy of Sciences of the United States of America* 90(19), pp. 8977–81.
- PhamThi, M., Le Khanh, H., Ekeom, D., Hladky-Hennion, A.-C., Tran-Huu-Hue, L.-P., Lethiecq, M. and Levassort, F. 2009. Fabrication and characterization of large area 1–3 piezo-composites based on PMN-PT single crystals for transducer applications. *2009 IEEE International Ultrasonics Symposium*, pp. 1745–1748.
- Ritter, T. a, Shrout, T.R., Tutwiler, R. and Shung, K.K. 2002. A 30-MHz piezo-composite ultrasound array for medical imaging applications. *IEEE transactions on ultrasonics, ferroelectrics, and frequency control* 49(2), pp. 217–30.
- Yuan, J.R., Jiang, X., Cao, P., Sadaka, A., Bautista, R., Snook, K. and Rehrig, P.W. 2006. High Frequency Piezo Composites Microfabricated Ultrasound Transducers for Intravascular Imaging. *IEEE Ultrasonics Symposium*, pp. 264–268.
- Zhen, Y., Li, J.-F. and Zhang, H. 2007. Electrical and elastic properties of 1–3 PZT/epoxy piezoelectric composites. *Journal of Electroceramics* 21(1-4), pp. 410–413.

# CHAPTER 7

---

## Array Transducers Results: Fabrication and Performance

---

### Chapter Profile

The previous chapters in this thesis highlight many points to consider for designing and fabricating ultrasound transducer arrays to be fitted into interventional tools such as biopsy needles. Here, in this chapter, details of the arrays fabricated are presented, underlining the key results at different stages. Arrays operating at 5 MHz were fabricated before the 15 MHz arrays, using the same process. This is because the 5 MHz features are bigger and therefore can enable easier fabrication of prototypes to further evaluate the feasibility of the process developed. The results presented also demonstrate the success of the steps of the wafer-scale fabrication process, emphasising some of the challenges and how they were overcome. Flexi-circuit design and fabrication is detailed, in this chapter, as a key step for achieving multiple electrical connections to the array elements in the confined needle space. Results of electrical impedance spectra, and pulse echo tests of the arrays are also presented. The 5 MHz array was fitted into a needle, and electrical impedance and pulse-echo tests showed functionality. The 15 MHz arrays also had dimensions which were small enough to fit in a needle. The arrays in this chapter were fabricated from PZT-5H (CTS 3203HD) but the low temperature methods were used similar to the single element transducers in Chapter 6.

### 7.1 Array fabrication

The combined results from previous chapters set established a strong foundation for the fabrication of array transducers. The key design parameters of the desired 15 MHz linear array transducer are outlined in Table 7.1. This table gives the parameters of the

ideal finished prototype, with this chapter giving details of how much has been achieved through this project. The wavelength element pitch is 100  $\mu\text{m}$ , requiring high precision fabrication techniques to achieve accurate dimensions. At 64 elements, the array is suitable for clinical imaging, and the field of view will be on the order of the array length, 6.4 mm. The element length, which is also the array width, of 0.8 mm, is constrained by fitting the width of array within the core of a <2 mm diameter biopsy needle. The array substrate is fabricated from PZT-5H (CTS 3203HD) but low temperature fabrication methods applicable to PMN-PT were used.

**Table 7. 1: Design parameters for miniature array on needle**

Frequency	15 MHz
Array elements	64
Element pitch	100 $\mu\text{m}$ (wavelength spacing)
Element length	0.8 mm
Element width	0.070 mm
Piezoelectric layer	1-3 composite of PMN-29%PT
Matching layer	$\frac{1}{4}$ Wavelength, 15% Alumina loaded epoxy
Backing layer	30% Tungsten loaded epoxy
Cabling	Patterned flex-circuit, spirally-wound
Housing	2 mm biopsy needle

The fabrication of the arrays mainly focused on using low temperature and pressure processes due to the fragile nature of the single crystal PMN-29%PT material that was chosen as the ideal active material. This material is limited to about 60°C due to the Curie temperature or phase transition temperature being as low as 80°C. The prototypes presented here were fabricated from PZT-5H (CTS 3203HD) but using the same process as that explained for the fragile single crystal materials; the prototype single element transducers presented in Chapter 6 showed that the process is suitable for the single crystal materials. Matching and backing layers of loaded epoxies were cast on the electroded front and back surfaces of the piezocomposite. A flexible printed circuit was connected to back surface electrodes using low temperature bonding methods. After bonding all the layers together, the elements were diced for mechanical and electrical separation.

The following sections present details of the arrays prototypes at different stages of fabrication with the 5 MHz arrays shown as a precursor to the 15 MHz. Separate details will be explained for the 5 MHz array and for the 15 MHz array. The main focus in this chapter is the packing of fine-scale arrays into biopsy needles.

## 7.2 The 5 MHz Arrays

### 7.2.1 Array Fabrication

The 5 MHz array transducer prototypes were fabricated as an easier option to the higher frequency arrays. These were developed using the process explained in Chapter 5 and they were made small enough to fit in 2 mm diameter biopsy needles. Figure 7.1 shows some of these arrays at selected stages of fabrication.

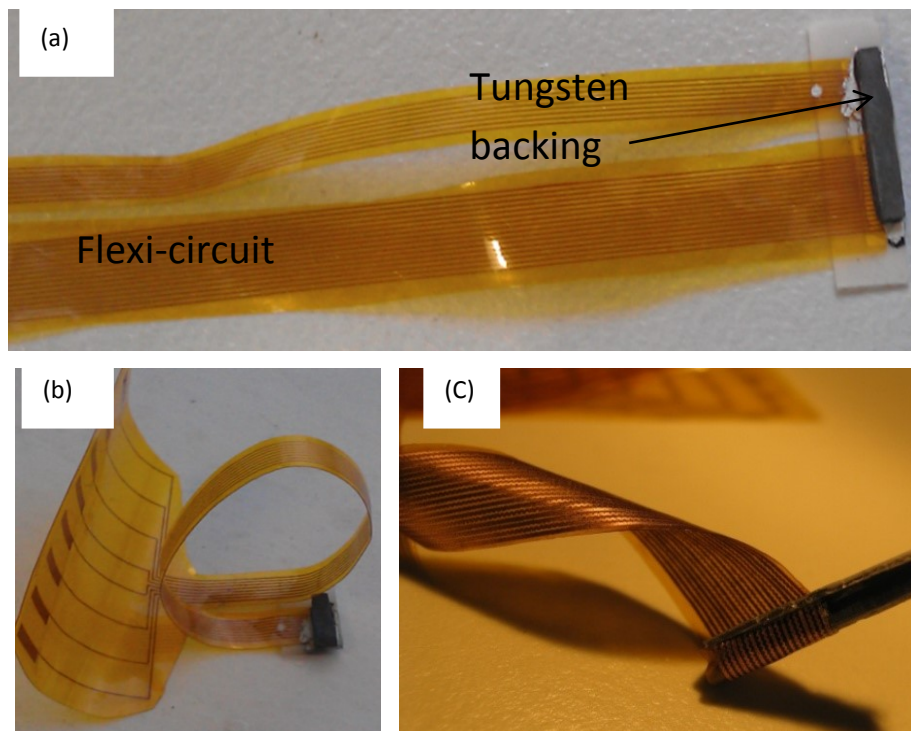


**Figure 7. 1: Some of the stages of array fabrication: (a) two flexi-circuits are connected to a piezoelectric stack to get different sets of arrays at the same frequency; (b) an 8-element 5 MHz array with the flexi-circuit fan-out for cable connection; (c) the initial rolling of the flexi-circuit for the array to fit into a tube**

These arrays were diced with an 80  $\mu\text{m}$  blade at a pitch of 300  $\mu\text{m}$ . An example is shown in Figure 7.2 where the active area is 0.5 by 2.4 by 1.8  $\text{mm}^2$  with the conductive epoxy for the ground connection being 0.7 mm wide. The close-up images in Figure

7.3 show clear dicing through the flexi-circuit indicating that the elements were separated. A multi-meter was used to test neighbouring elements for electrical isolation after dicing. This confirmed that the dicing yielded electrically isolated elements.

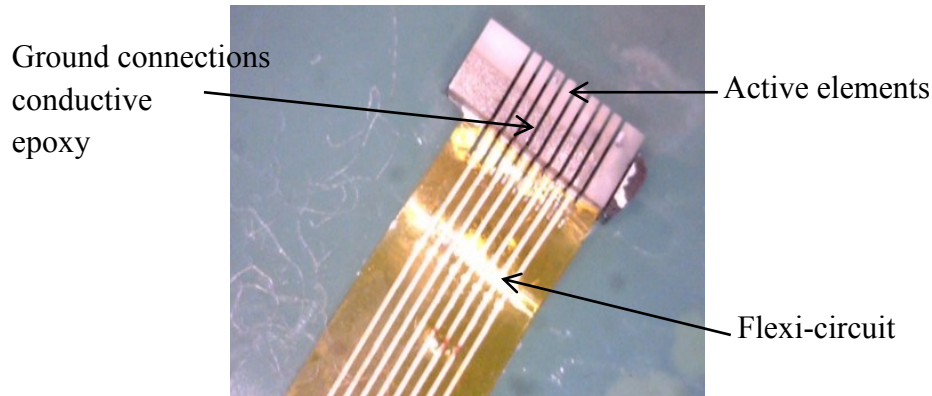


**Figure 7. 2: An example of a diced 5 MHz array. The inter-elemental pitch is 300  $\mu\text{m}$  and the elevation length is 1.8 mm**

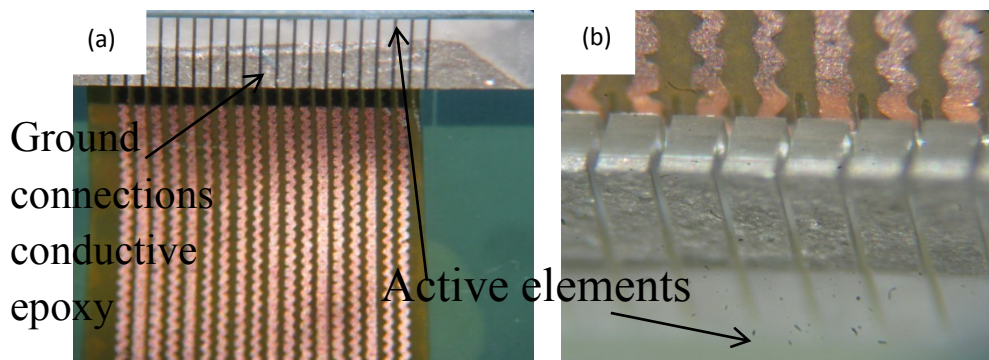


**Figure 7. 3: Close-up images of an 18-element 5 MHz array after dicing: (a) Top view; (b) perspective view. The inter-elemental pitch is 300  $\mu\text{m}$  and the elevation length is 1.2 mm**

For the earlier prototypes, the ground connection was made through a wire attached by conductive epoxy as illustrated in Figure 7.4. The wire also acted as a guide for rolling the flexi-circuit and for pulling the device through the intended metal tube casing. A very obvious problem is that this increases the size and therefore becomes difficult to fit into small spaces.

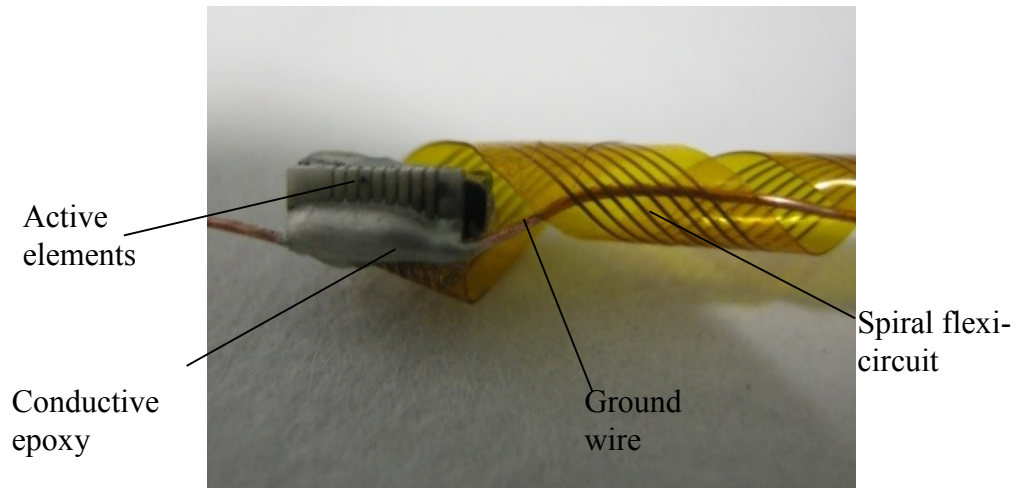


**Figure 7. 4: A finished 5 MHz prototype before it is inserted into a metal tube. The inter-elemental pitch is 300  $\mu\text{m}$  and the elevation length is 1.8 mm**

After dicing, electrical insulating varnish, commonly used in printed circuit boards (PCB) was used as an under-fill to serve various purposes. It partially filled the diced kerfs separating the arrays to increase the mechanical integrity. It was also used to ensure electrical insulation since these arrays would be used in water. Some active parts of the flexi-circuit tracks were exposed and therefore good insulation was a necessity. The varnish was also used as a coating layer on the flexi-circuit to provide electrical insulation. Eventually, this could be replaced with a more flexible material such as parylene that can be deposited more accurately.

The final stages of the prototypes are shown in Figure 7.5. These show arrays being inserted into tubes and micro-coaxial cables attached for testing.

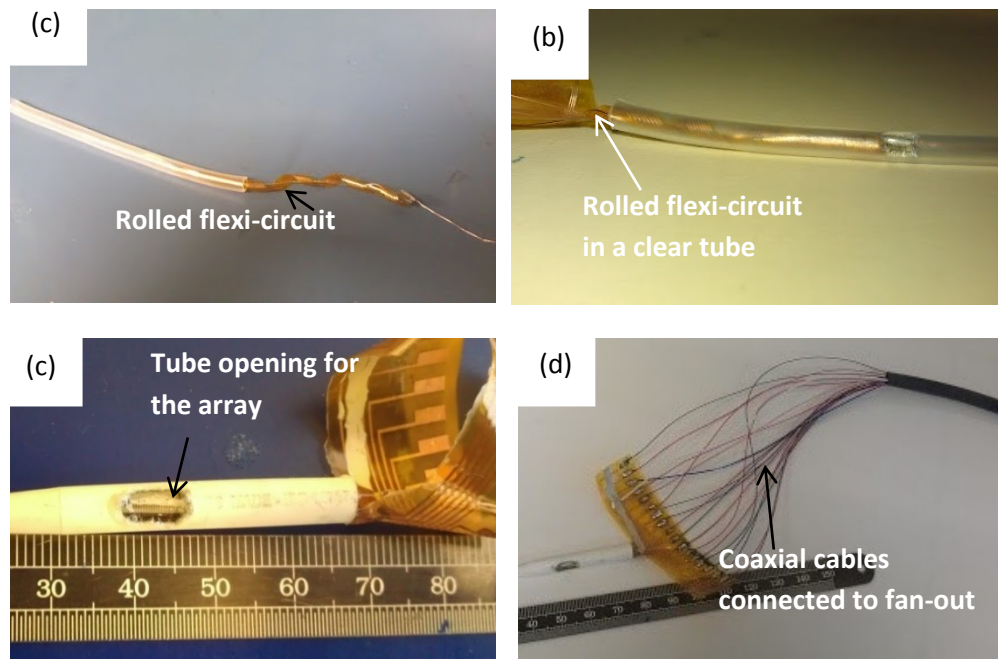


**Figure 7. 5: Arrays inserted into tubes of approximately 3 mm inner diameter for pulse-echo testing: (a) rolled flexi-circuit before insertion into tube; (b) rolled flexi-circuit after insertion into tube; (c) flexi-circuit in a tube with opening for the array; (d) micro-coaxial cables attached to a flexi-circuit fan-out**

### 7.2.2 *Electrical Impedance testing*

Testing for the impedance magnitude and phase is a simple way of determining that the device works at different stages of fabrication. A piezoelectric plate was measured on its own before it was made into a transducer, then at each stage in the fabrication process where there was access to the front and back electrodes to check that the device is functional. After the device was fabricated and the array elements defined, the electrical impedance magnitude and phase of each array element were measured using an impedance analyser (4395A, Agilent Ltd, Edinburgh Park, UK). In one of the prototypes (Figure 7.6), 12 of 18 elements showed response. It is important to note that this does not necessarily mean that the other elements are not working. The impedance phase for the same array transducer shows 13 out of 18 elements working. With high damping, some of the elements cannot yield a good visible impedance magnitude or phase response. A pulse-echo test can also be done to test all the elements.

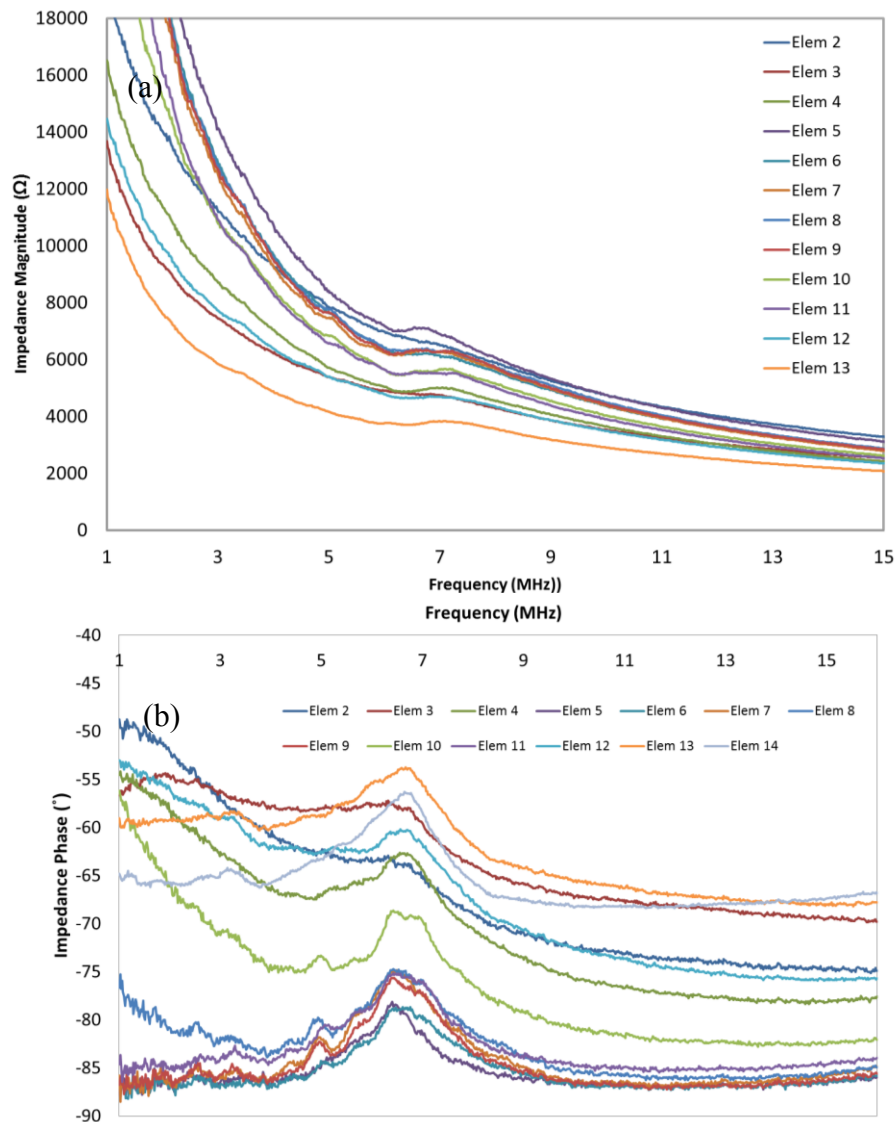


**Figure 7.6: Impedance magnitude (a) and phase (b) plots of a 5 MHz transducer array showing elements with a measurable impedance response. Twelve elements (#2-13) have a magnitude response and thirteen elements (#2-14) have a phase response, out of 18 elements in the array.**

The impedance magnitude for these 5 MHz elements was very high; over 5 kΩ which can be attributed to the small lateral dimensions of the elements. At this relatively low frequency, the small elements are expected to yield a high impedance magnitude.

### 7.2.3 Pulse-echo testing

Pulse echo tests were done as described in Section 3.8 in Chapter 3. The pulse from the transducer is reflected off a stainless steel block at a distance of approximately 4 mm from the transducer. The pulse-echo tests with 5 MHz arrays indicated that more elements were working that were not picked up with the impedance analyser. Figure 7.7 shows that all the 18 elements worked well for an array which had shown only 13 working during the impedance magnitude and phase test. Elements 1, 17 and 18 show much lower signals than the other elements. This is likely to be from detaching of the electrodes from the active elements.

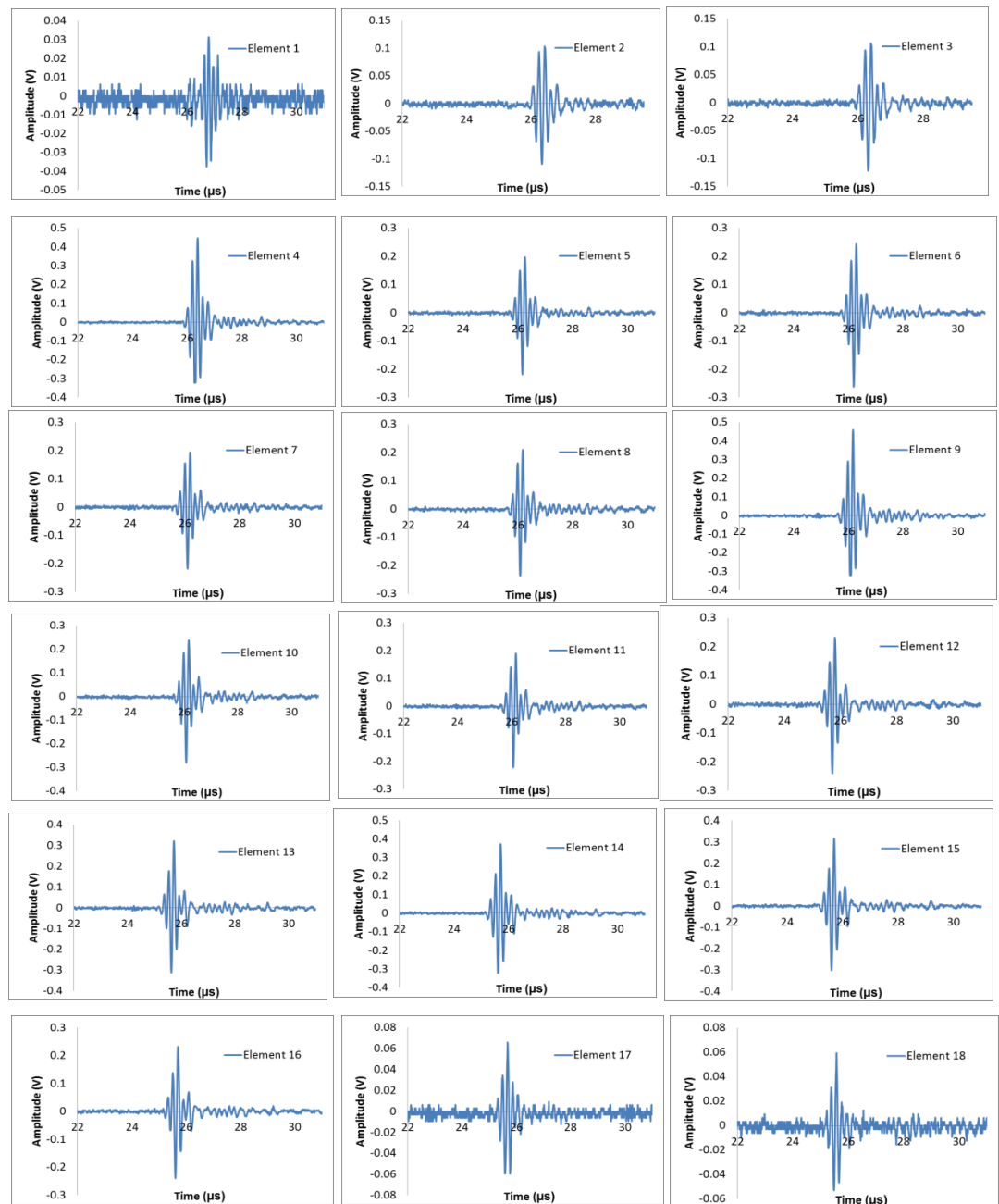
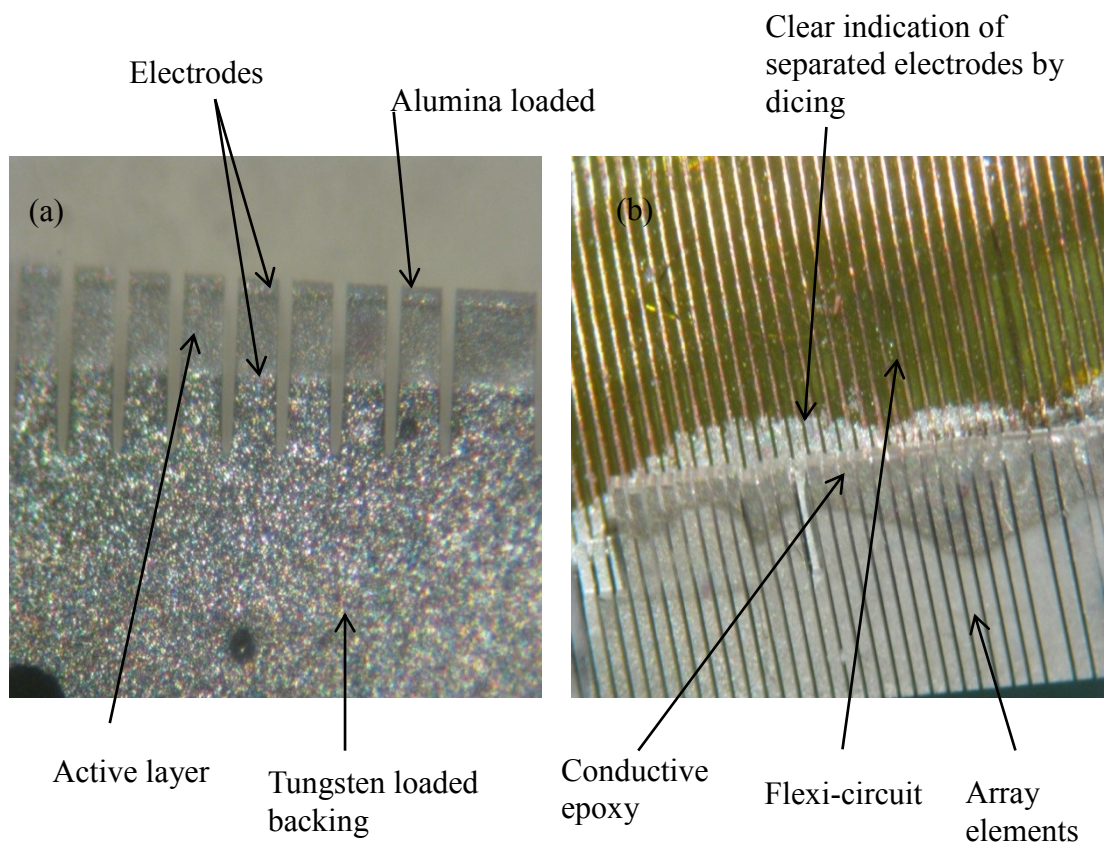


Figure 7. 7: Pulse echo responses of all the 18 elements of the 5 MHz array transducer array.

### 7.3 The 15 MHz Arrays

#### 7.3.1 Array Fabrication

The 15 MHz arrays were fabricated following the success of the 5 MHz arrays. One set of arrays had 64 elements and another 32. The pitch of 100  $\mu\text{m}$  was initially diced with a 30  $\mu\text{m}$  blade and element breakage and de-bonding was noticed. This led to the later prototypes to be diced with a 20  $\mu\text{m}$  blade. The flexi-circuit with 65  $\mu\text{m}$  tracks and separation of 35  $\mu\text{m}$  was bonded with room temperature curable conductive epoxy which was cured at 50°C. The de-bonding might have been due to poor adhesion of the epoxy. Some of the process images for the 15 MHz arrays are given in Figure 7.8.



**Figure 7. 8: Diced elements for the 15 MHz arrays: a) clear indication of the cast layers and dicing through the backing; b) separation of elements and some breakage. The inter-elemental pitch is 100  $\mu\text{m}$  with the active layer thickness of 120  $\mu\text{m}$  and matching layer thickness of 51  $\mu\text{m}$ .**

The 100  $\mu\text{m}$  pitch of the flexi circuit was only at the tip where the flexi-circuit was bonded to the active substrate. The tracks were widened after this short distance of about 2 mm to minimise the risk of breakage. Two designs of the flexi-circuit attached

to the elements are shown in Figure 7.9. Figure 7.9 (b) shows a commercially available biopsy needle for neurosurgery with 1.80 mm outer diameter and 1.43 mm inner diameter. The fabricated array is small enough to fit in the opening in the biopsy needle.

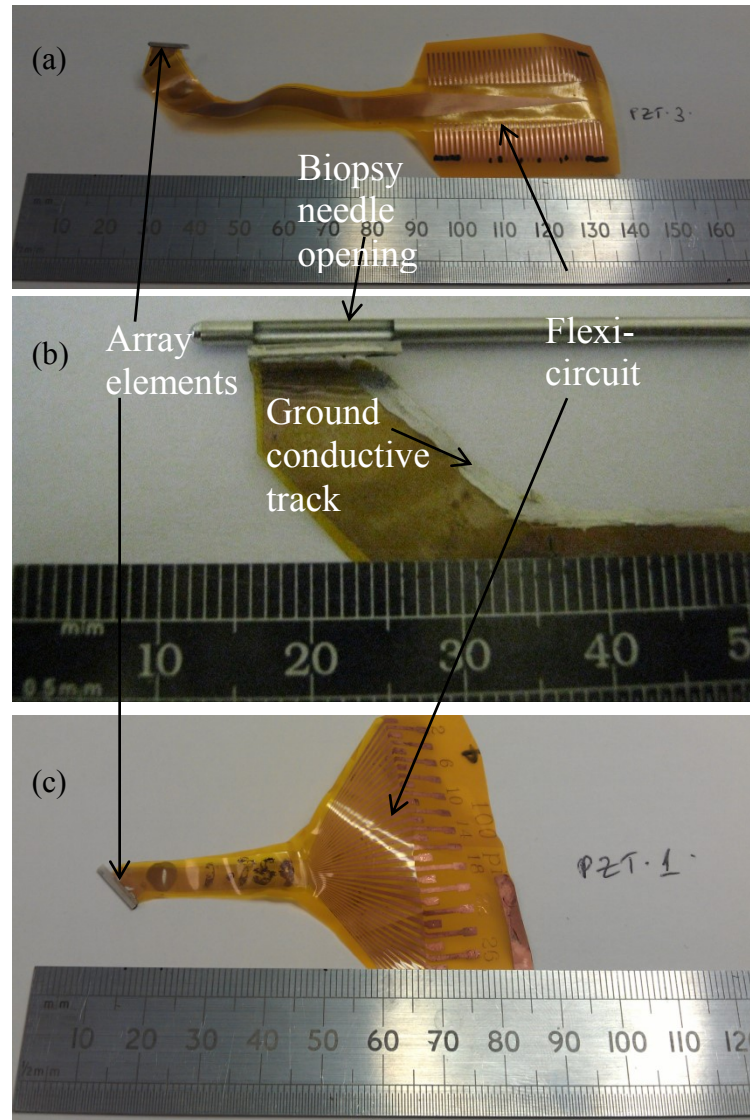


**Figure 7.9:** Example of diced 15 MHz array elements with flexi-circuit: (a) is a flexi-circuit with a 64 element array connected at the tip; (b) the 64 element array next to a commercial neurosurgery biopsy needle; (c) is another 32 element array set with a different type of flexi-circuit;

### 7.3.2 Electrical Impedance testing

The impedance results of one of the 15 MHz arrays fabricated is shown in Figure 7.10. The impedance magnitude showed no response while the impedance phase gives a response at about 15 MHz for 14 out of 32 elements.

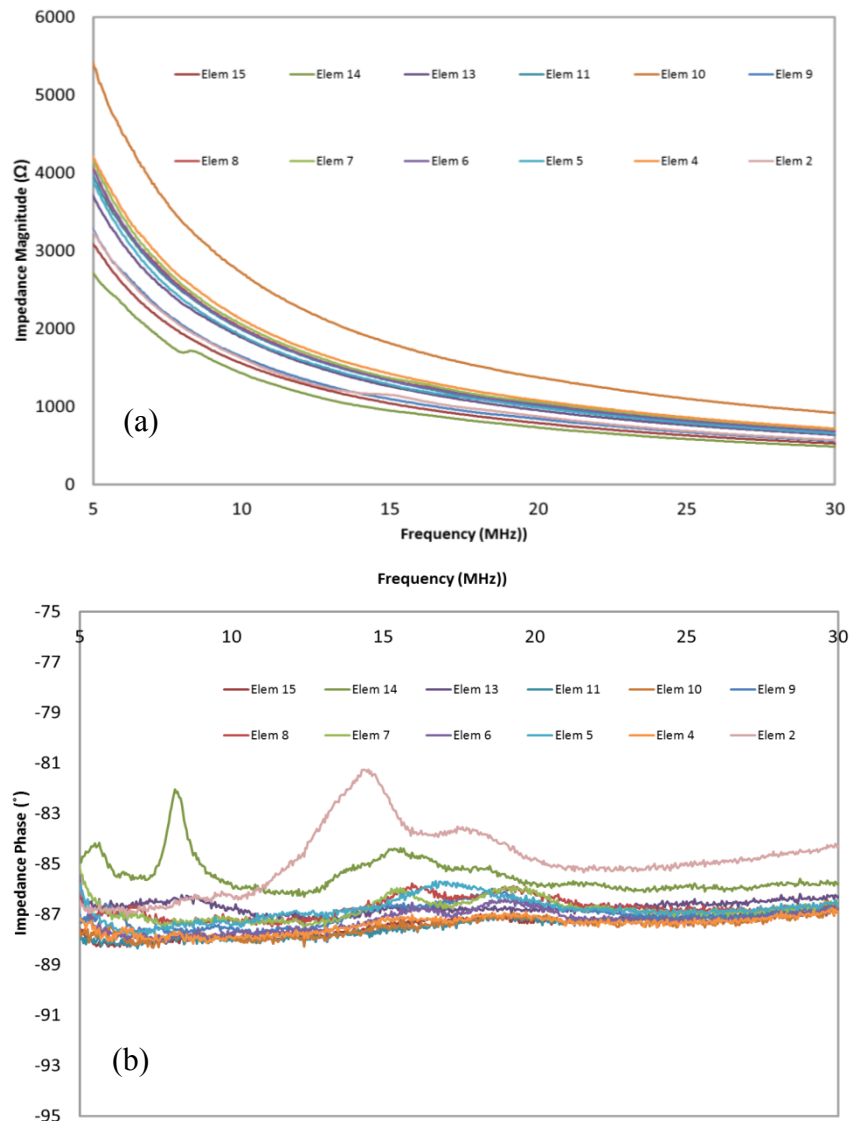


Figure 7. 10: Impedance magnitude (a) and phase of elements in a 15 MHz array

The impedance plots in Figure 7.10 agree with the simulation in Figure 4.7 in Chapter 4. The impedance magnitude in Figure 7.10 is more damped than that in Figure 4.7 mainly because of the coaxial cable used for the electrical connection. Also, a composite single crystal was used in the simulation whereas a bulk ceramic material

was used for the experiment. The impedance magnitude of the experimental results is higher than that in the simulation and this might be due to the fact that a bulk material was used for the experiment.

### 7.3.3 Pulse-echo testing

Pulse-echo responses of two elements from the 15 MHz array are shown in Figure 7.11. These are used as an indication that the array elements can be used for imaging. The elements chosen were those that provided good responses during the pulse-echo testing.

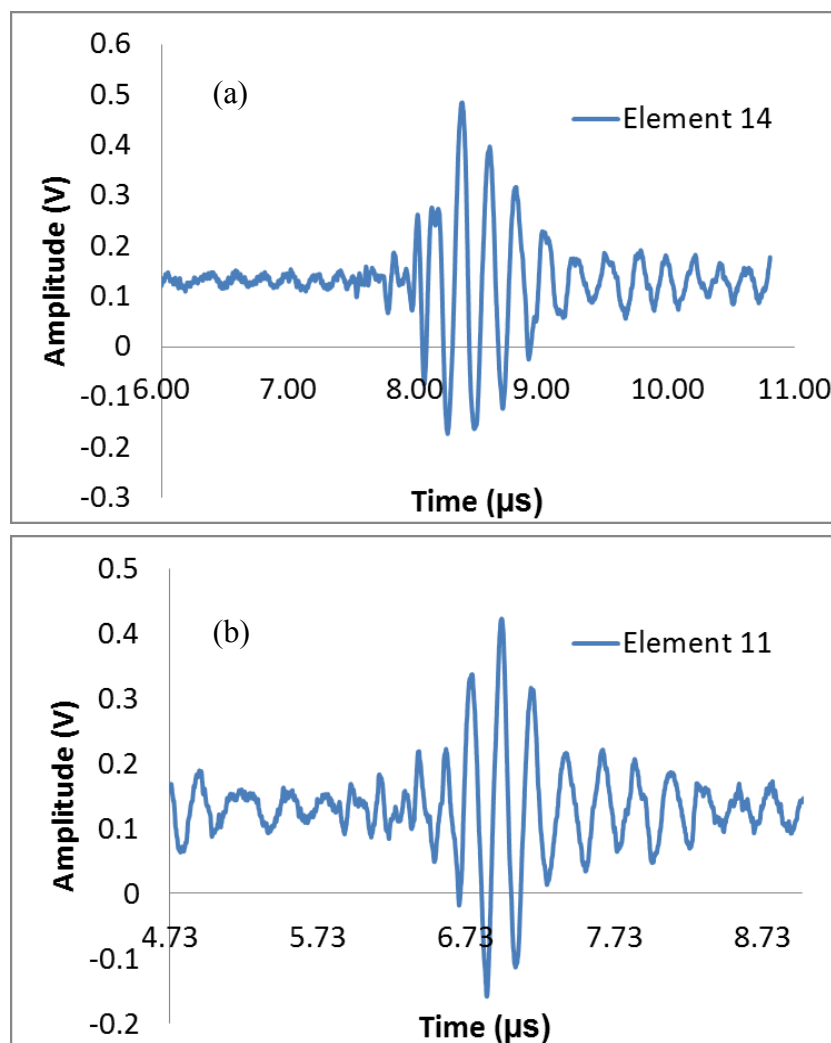


Figure 7. 11: Example pulse-echo responses of two elements of the 15 MHz array

## 7.4 Chapter discussion and conclusions

This chapter presented results of the array prototypes fabricated using the process explained in Chapter 5. This is a new approach for manufacturing and packaging on miniaturised linear array transducers for use in biopsy needles or other interventional tools. This wafer-scale fabrication permits production of multiple transducers in each process.

Flexi-circuits with micro-pitch tracks have been fabricated. The circuits shown in this chapter had 100  $\mu\text{m}$  pitch, and could be made routinely with continuous tracks. Continuing work on the flexible circuits show there is the potential of reducing the pitch to as low as 40  $\mu\text{m}$ .

The arrays were made from a bulk ceramic which meant that the results produced can be improved by using a composite single crystal material. The prototypes made from single crystal composite are discussed in Chapter 6. The results here however, demonstrated the feasibility of the dimensions of these arrays to fit in a needle.

5 MHz array transducers were developed to test the feasibility of the array fabrication and electrical interconnect process before fabricating the 15 MHz arrays.

The process for the array fabrication was reasonably successful, producing functional arrays that are small enough to fit within a biopsy needle including cabling. Further improvement of the steps will be discussed in Chapter 8. Some of the areas include alignment of the flexi-circuit to the active area. This is because the active area is small and alignment would improve the connection to this area.

One set of arrays had 64 elements and another 32. The pitch of 100  $\mu\text{m}$  was initially diced with a 30  $\mu\text{m}$  blade and element breakage and de-bonding was noticed. This led to the later prototypes to be diced with a 20  $\mu\text{m}$  blade. This pitch was slightly bigger than that for making composites described in Chapter 6 where blades of 10 and 15  $\mu\text{m}$  were used.

# CHAPTER 8

---

## Discussion, Conclusions and Future Work

---

### Chapter profile

This chapter reviews findings in the preceding chapters of this thesis. The results presented throughout the previous sections are important in setting the groundwork for fabrication of high frequency, high resolution array transducers in interventional tools such as biopsy needles. The possible future directions leading from the research presented in this thesis are highlighted in this chapter.

### 8.1 Summary of results

The main focus of the work presented in this thesis was on developing and evaluating the feasibility of fabrication processes for integrating micro-scale high resolution transducers into biopsy needles. A comprehensive review of literature highlighted the research undertaken all over the world on high frequency array transducers. There is a general consensus that high frequency arrays present many challenges in fabrication due to the micro-scale features of the different layers in the transducer elements. The higher the operational frequency, the smaller the array elements. Different researchers have focussed on some aspects of these arrays and not the complete integration for application-based devices with miniaturised packaging. As a result, there are no commercially available high frequency array transducers and imaging systems that are suitable for clinical needs. This absence of application based transducer arrays brought about the necessity for the research in this thesis. The work was set out to establish a process that would enable the development of needle based high frequency arrays.

#### *8.1.1 Fabrication process development*

A detailed process was developed for fabrication of high frequency linear arrays integrated into needles. These needles, such as biopsy needles, would be used in imaging areas where high resolution is needed but there is a limitation due to the penetration capability of the ultrasound energy from such arrays. Different processes

were evaluated and one was chosen due to its various advantages. Wafer-scale fabrication was adopted to reduce the overall cost of fabrication and a spiral-helical multiple conductive track flexi-circuit design was used to fit into a small diameter needle. The process developed was aimed at fabrication of arrays into needles but single element transducers were also fabricated using the same method. These single element transducers were used to validate the process before further validation by fabricating 5 MHz arrays and 15 MHz arrays.

### ***8.1.2 Simulation and modelling***

At the design stage, software including ODM, FIELD II simulation and PZFlex were used to evaluate the expected performance of the designed transducers. This was important as it was a means of saving time spent in fabrication. Different properties of the transducer, including operational frequency, impedance magnitude and beam pattern, were examined. The resolution integral was adapted from Pye's group (MacGillivray et al. 2010) to be used as a figure of merit to determine how well the transducers would perform from simulations. This combines both the image resolution and the depth of field. A transducer with a higher resolution integral would have a narrow beam width at -6 dB over a long distance. Linear arrays were chosen for fabrication over phased arrays since, among other advantages, they would present fewer fabrication challenges at a given frequency due to the larger element pitch. The process however, can also be applied to phased arrays. The chosen frequency for the arrays was 15 MHz mainly to enable connection to commercially available systems with further development of the imaging system.

While there are some commercially available imaging systems with arrays that operate in the 20-50 MHz range, most commercial array controllers operate only up to 15 MHz. It is possible to connect these controllers, given the correct pin-out for connecting to the electronics. Therefore 15 MHz was chosen as the maximum operating frequency to enable connection to commercially available systems in on-going work, and because the resolution is sufficient for the target imaging applications.

### ***8.1.3 Fabricated transducers***

Transducers from single crystal 1-3 piezocomposites were fabricated with specially adapted low temperature fabrication processes. PMN-PT single crystal was chosen as

the core piezoelectric material for the devices because it is a high performance material and is now widely used in high-end commercial clinical imaging systems at conventional frequencies. However, it is much more fragile than the conventional piezoelectric ceramics, and sensitive to high temperatures ( $>80^{\circ}\text{C}$ ). The dicing to make composites with this material involved using relatively low spindle speed, feed rate, coolant rate and a low aspect ratio to prevent breakage of composite pillars. The maximum working temperature was chosen to be  $50^{\circ}\text{C}$  to prevent depoling of the single crystal material. This was used for both post-curing of the passive epoxy in the composite, matching and backing layers, and the bonding of the flexible circuit to the array for the electrical interconnect. The passive composite filler and matching layer epoxy cured at a temperature higher than  $50^{\circ}\text{C}$  became bowl shaped. This was especially the case when the layers were very thin. It was therefore important to cure at room temperature and only post cure at the moderate elevated temperature.

Single element transducers were fabricated to validate the process. Much emphasis was paid to the composite development from PMN-PT and Mn:PIN-PMN-PT. Blades as small as  $15\ \mu\text{m}$  were used to make composites with a pitch as small as  $50\ \mu\text{m}$ . Electrical impedance matching with a micro-coaxial cable was demonstrated. Images of fine tungsten wires and *ex-vivo* mouse bowel were obtained with these transducers. Arrays at 5 MHz and 15 MHz were fabricated with a connected flexible circuit that could be rolled so the whole array and cabling could be fitted into tubes. A novel connection to the arrays was explained. This involved connecting on the side of the array, away from the active area of the transducer. The arrays were inserted into needles and some pulse-echo results were obtained.

The fabrication process detailed in this thesis also explains how the different parts of the transducer are made. A big challenge was the connection of the flexible circuit to the array. Due to the nature of the PMN-PT single crystal material, low temperature bonding methods were studied. These included: room temperature curing conductive epoxy, ultrasonic bonding, and magnetically aligned anisotropic UV-cured epoxy. The flexible circuit itself was patterned using a novel technique employing dry-film photoresist and Megasonic agitation to produce very fine pitch conductive tracks array on a polyimide polymer. This is a very cost efficient method of making flexi-circuits.

Tracks with a pitch of 60  $\mu\text{m}$  have been achieved. Wire bonding to connect the flexi-circuit to the active elements was avoided as it is very time consuming and not usable on polymers. It also has a limit of 60 – 100  $\mu\text{m}$  as a minimum pitch which would make it difficult for high frequency transducers.

The challenges encountered during the fabrication of the arrays in this thesis have been explained through the chapters. Some of the solutions to these were not fully developed in the duration of this project but have established a good starting point to accomplish fully functional transducers in a needle.

The key challenges include;

- Bonding of the flexi-circuit to the array: This was mainly done using room temperature cured conductive epoxy which presented problems such as not getting good strength bond to the flexi-circuit. The solution to this problem would be to use other low temperature techniques, including ultrasonic bonding and UV curable epoxy, which were also investigated in this research but not used in a complete fabricated device.
- Having a good ground connection to the electrode: The ground connection was done through casting room temperature curable conductive epoxy to the ground electrode. The epoxy used for the prototypes was cured at 50°C. However, this presented a problem of not getting a very good electrical and mechanical connection especially when this layer was lapped down. A possible solution here would be to use stencil printing to get a good ground connection.
- Rolling of the flexi-circuit to fit well in the small tube: The polyimide thickness of 25  $\mu\text{m}$  meant that it presented a thick layer especially after coating with electrical insulating varnish. The thick layer introduced a challenge of rolling the flexi circuit at a position near the array elements. A possible solution would be to use a thinner polyimide and, probably more importantly, to use a thinner electrical insulator coating such as deposited parylene film, after connecting to the array.
- Sealing the arrays after dicing into individual elements: The arrays in this project were electrically and mechanically insulated using parylene or electrical insulating varnish, which is common in PCBs, as an under-fill.

However, this limits the mechanical strength of array elements, and a kerf filler may be needed for a manufactured device.

- Positioning of flexi-circuit: Positioning of the flexi circuit at the side of the active layer proved to be much of a challenge since the surface where it was attached was only about 200 - 300  $\mu\text{m}$  wide. A pick-and-place mechanism needs to be developed to ensure accurate alignment.

## 8.2 Suggestions for future work

The extensive research that has gone into high frequency transducers, especially arrays, has opened many exciting areas for their applications. The literature is full of examples of where researchers are trying to achieve higher frequencies for transducers, reducing the complexities in fabrication of small pitch arrays and integration of electronics. These areas have provided a platform for the next stage where these transducers are developed based on specific biomedical applications. This section describes how the application based array transducers in interventional tools such as biopsy needle can be further developed using the work in this thesis as a foundation. The improvements given here are based on the process developed in this thesis which was explained in Chapter 5.

### 8.2.1 *Composite fabrication*

Much of work presented in this thesis is based on fabrication of high frequency composites from the delicate temperature sensitive PMN-PT single crystal material. The process used for making these composites is the conventional, widely accepted dice and fill method. Whereas this method is cheap and extensively used, it can only produce composites that work up to approximately 30 MHz operational frequencies due to the limitation of the thickness of dicing blades. Another promising method has been concurrently studied at the University of Birmingham, to produce high frequency composites. This, with the illustration in Figure 8.1, is based on micro-moulded randomised piezocomposites and the method is capable of achieving composites operating at frequencies of 100 MHz, which will open up a window for making ultra-high frequency arrays.

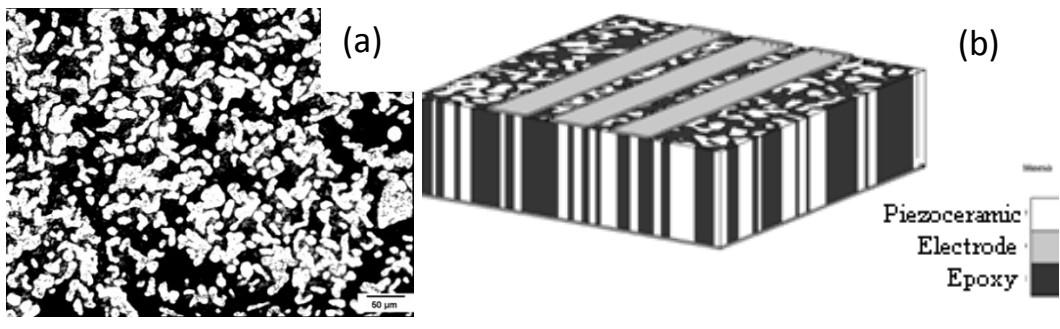


Figure 8. 1: An example of random micromoulded composites. (a) Optical images of a typical random composite (Jiang et al. 2012); (b) kerfless array sections with micro-moulded piezocomposite (Démoré et al. 2009)

### 8.2.2 Array element definition

Dicing to separate elements in an array is useful in overcoming mechanical cross-talk; however, this method is also limited to transducers up to about 30 MHz, where the element pitch in a linear array is 50 μm. Mechanical separation also introduces spaces which reduce the overall mechanical strength of the array. Patterning arrays with techniques such as photolithography, as shown in Figure 8.1(b), would enable easier fabrication of high frequency transducer arrays (Bernassau et al. 2007). These patterns, also shown in Figure 8.2, would define the electrodes on the active elements. For a linear or phased linear array, a scratch diced pattern would achieve a desired effect but a photolithography pattern would achieve the same but at much smaller scale, which allow for higher frequencies.

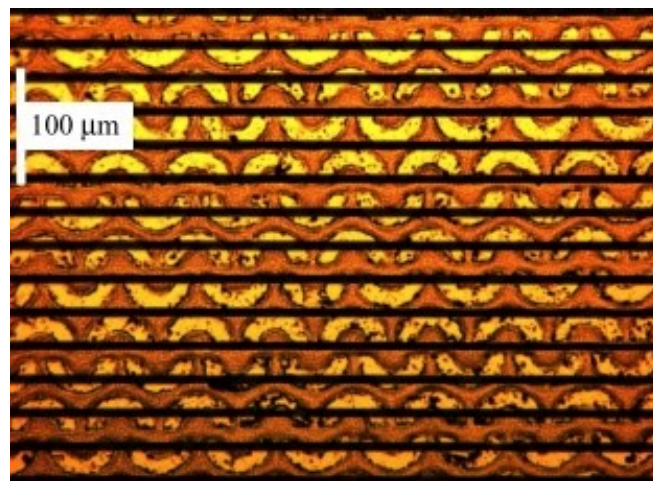


Figure 8. 2: A photolithography electrode pattern on top of a diced and filled composite (Bernassau et al. 2009)

With patterned electrodes on the arrays, ACAs can be used to connect pre-patterned flexi-circuits to the active area. Such approach has been attempted in previous work (Bernassau et al. 2009). Anisotropic conductive film (ACF) was investigated for bonding a silicon wafer to an array. The limitation was that the pressure and temperature needed were too high for the delicate composites. In this study, the aim was to connect to a flexi-circuit. UV curable and ultrasonic curable anisotropic conductive adhesives (ACA) were studied and their use would help to overcome the problem of excessive pressure and temperature on the composites and on the flexible circuits. Using ACA bonding methods also overcomes the need to use room-temperature curable conductive epoxy for bonding. These types of epoxies have weak bonding strength and electrical conductivity. The high temperature of about 100°C used in baking in photolithography would be a problem for the PMN-PT single crystal materials. Alternative materials such as PZT may be used to overcome this problem, but at the cost of reduced piezoelectric performance. More research is also going into improving the temperature resistance of single crystal materials based on PMN-PT (Neumann et al. 2011; Li et al. 2011). In the future the single crystal materials will be able to be used in devices developed using photolithography methods.

### ***8.2.3 Silicon integration***

There is also a need to explore integrating silicon and using integrated circuits into the device near the array. When microchips are incorporated in the silicon, it would be a way to overcome the need to use the wide and long flexi-circuit. It might also be a way of reducing the number of the highly expensive micro-coaxial cable if microprocessors are incorporated into imaging arrays. Such ideas are about to be investigated through follow-on projects such as the ultrasound capsule through the SonoPill project (EPSRC Reference EP/K034537/1). The silicon would provide room to use some of the semiconductor fabrication techniques already established.

### ***8.2.4 Stencil printing of layers***

Using masks for casting and printing matching, backing and conductive layers was explored in this thesis and further work should pay close attention to extending this technique. This will become even more necessary when the arrays go over 30 MHz.

Features that are below 200 $\mu\text{m}$  are best achieved using a well-designed mask and appropriate patterning techniques.

Stencil printing (Kay and Desmulliez 2012) of materials was investigated as a means to add different layers. The ground conductive connection at the side of the matching layer was chosen as the most suitable for the stencil printing. Through using this wafer-scale fabrication process, multiple samples would be done at the same time. A good stencil printed layer depends on a number of related factors determined by the viscosity of the materials. Among these factors are: print speed, applied pressure on the squeegee, the stencil thickness, and roughness of the substrate. These factors will affect the print quality such as slumping of edges, porosity, and discontinuity.

Matching layers were also studied for stencil printing but the 10-15% alumina-loaded epoxy demonstrated very low viscosity for stencil printing. Printing the ground connect would provide a more accurately controlled thin line which is required for the connection in the confined space. Further studies need to be carried out to develop this process into a standard procedure.

Other areas to study include complete needle design, connection to commercial imaging systems, exploring biocompatibility issues, and increasing the number of elements in the array to increase the imaging field of view.

### **8.3 Further Grants Awarded**

The work in this thesis has led to further grants being awarded. One of the grants was awarded to develop an array in a needle for neurosurgical applications, USINN (Ultrasound in a Needle for Neurosurgery) (EPSRC Reference EP/K02025/1). This involves three Universities: IMSaT at the University of Dundee, Heriot-Watt University and University of Birmingham.

The other grant was awarded for the miniaturisation of devices, specifically aimed to develop an ultrasonic capsule, SonoPill (EPSRC Reference EP/K034537/1). The collaborating institutions are University of Dundee, Heriot-Watt University and the University of Glasgow.

## 8.4 References

- Bernassau, A.L., Flynn, D., Amalou, F., Desmulliez, M.P.Y. and Cochran, S. 2009. Techniques for wirebond free interconnection of piezoelectric ultrasound arrays operating above 50 MHz. In: *IEEE International Ultrasonics Symposium*. Rome, pp. 1–4.
- Bernassau, A.L., McKay, S., Hutson, D., Demoré, C.E.M., Button, T.W. and Mcaney, J.J. 2007. Surface Preparation of 1-3 Piezocomposite Material for Microfabrication of High Frequency Transducer Arrays. *Ultrasonics*, pp. 2007–2010.
- Démoré, C.E.M., Cochran, S., Garcia-Gancedo, L., Dauchy, F., Button, T.W. and Bamber, J.C. 2009. 1-3 Piezocomposite Design Optimised for High Frequency Kerfless Transducer Arrays. In: *IEEE International Ultrasonics Symposium*. Rome.
- Jiang, Y., Démoré, C.E., Meggs, C., Cochran, S. and Button, T.. 2012. Micro-moulded Randomised Piezocomposites for High Frequency Ultrasound Imaging. In: *IEEE International Ultrasonics Symposium*. Berlin.
- Kay, R. and Desmulliez, M. 2012. A review of stencil printing for microelectronic packaging. *Soldering & Surface Mount Technology* 24(1), pp. 38–50. Available at: <http://www.emeraldinsight.com/10.1108/09540911211198540> [Accessed: 6 August 2013].
- Li, F., Zhang, S., Lin, D., Luo, J., Xu, Z., Wei, X. and Shrout, T.R. 2011. Electromechanical properties of  $\text{Pb}(\text{In}(1/2)\text{Nb}(1/2))\text{O}(3)$ - $\text{Pb}(\text{Mg}(1/3)\text{Nb}(2/3))\text{O}(3)$ - $\text{PbTiO}(3)$  single crystals. *Journal of applied physics* 109(1), p. 14108.
- MacGillivray, T.J., Ellis, W. and Pye, S.D. 2010. The resolution integral: visual and computational approaches to characterizing ultrasound images. *Physics in medicine and biology* 55(17), pp. 5067–88.
- Neumann, N., Yu, P., Ji, Y., Lee, S.G. and Luo, H. 2011. Application of Single Crystalline PMN-PT and PIN-PMN-PT in High-Performance Pyroelectric Detector. In: *Applications of Ferroelectrics (ISAF/PFM), 2011 International Symposium on and 2011 International Symposium on Piezoresponse Force Microscopy and Nanoscale Phenomena in Polar Materials*. pp. 2–5.

## APPENDIX A

---

# **Needle-Based Ultrasound Imaging Device**

## **SUPA Start KT Project and Feasibility Study**

Final Report, Part 2

28 February 2011

Jonathan Marsh, Envision Design Limited

Christine Demore, University of Dundee

Robert Ssekitoleko, University of Strathclyde

and University of Dundee

Srikanta Sharma, University of Dundee

## I. BACKGROUND

Ultrasound scanning is now an essential tool for medical imaging of soft tissues, central to the diagnosis and monitoring of many conditions. Real-time, high resolution ultrasound, which can achieve image resolution of 0.1 mm or less, is an active topic of research, with significant potential benefits for accurate and timely characterisation of lymph nodes, leading to in vivo pathology. For example, with gastrointestinal cancers, patient quality of life and treatment efficiency would be improved if the clinician could determine during a procedure whether the cancer has spread to the lymphatic system. With accurate diagnosis, clinicians could confidently remove only the diseased tissues with a minimal surrounding margin. However, ultrasound probes incorporated into needles and surgical tools are required to obtain high resolution images at close proximity to tissues of interest. The physical constraints of miniaturisation directly affect the acoustic field and it is essential to determine and optimise the device configuration taking this into account. The aims of the project are two-fold:

- To investigate the feasibility of miniature ultrasound probes incorporated into biopsy needles, in terms of:
  - The acoustic fields they produce
  - Manufacturability
- To explore the benefits of integrating industrial design with physics research

In this study, a needle suitable for incorporating an ultrasound device will be designed, taking into account the electrical cabling required for operation, and, in the case of a single element transducer or an annular array, mechanical scanning to create a 2-D image. The viability in terms of acoustic fields, and manufacturability will be considered at all stages. The use of new single-crystal materials will also be considered to enhance device performance.

## II. DEVICE CONFIGURATIONS

Four different types of transducers are investigated for use in needle-based ultrasound probe: a single element transducer, an annular array and a side viewing linear array and a forward viewing linear phased array. The trade-offs between system complexity, fundamental electronic characteristics, image quality in relation to ultrasonic fields generated by the physically constrained apertures, and functionality associated with these devices have been evaluated using simulation techniques and prototype transducers.

The geometry and orientation of the image planes for each device configurations are shown in Figure.1 Both the annular array and the single element transducer must be mechanically scanned in order to form a 2D image. For needle or catheter based devices, a radial 2D scan can be acquired either by rotating an outward-facing transducer or rotating a parabolic mirror in front of a forward facing transducer.



**Figure 1.** Diagrams of transducer configurations for (a) a side viewing linear array, (b) forward viewing linear phased array and (c) axial cross section with single element transducers or annular arrays.

For linear arrays and linear phased arrays, the 2D image is created by electronically scanning the ultrasound beam. A linear array or linear phased array placed along the length of a needle will be side-viewing, with the image plane positioned by rotating the needle. A linear phased array placed at the needle tip will produce a forward viewing image plane, enabling visualisation of structures along the path of the needle. The angle of the image plane can be oriented by rotation of the needle.

### III. NEEDLE SPECIFICATION

The transducers are to fit within the dimensions of a standard soft tissue biopsy needle, which range in size from 22 gauge (0.9 mm diameter) to 14 gauge (2.11 mm diameter). For the current feasibility study and transducer design, the 14 gauge needle will be used. In the current study we have considered designs of needles for imaging only. Combining core tissue biopsy with the high resolution imaging would require location of the biopsy channel in very close proximity to the array to be able to image the location of the tissue biopsy. This would reduce the space available for cabling. However, this can be revisited as the miniature ultrasound imaging technology is further developed.

A basic needle design was determined from examination of commercially available needles. The needle tip is tapered to produce a sharp point for insertion and to separate tissue as it is pushed into the tissue. The tip taper angle for the needles provided by clinicians has been measured to be approximately  $26^\circ$ . The transducer or array needs to be located as close to the tip as reasonably possible so that the clinician knows position of the tip, and so the tip does not penetrate further than needed into the tissue.

### IV. TRANSDUCER STACK

#### A. Design for operating frequency

The transducer operating frequency has been set at 30 MHz, corresponding to an imaging wavelength of  $50 \mu\text{m}$ . At this operating frequency, an ultrasound system is capable of resolving very fine details of potentially diseased soft tissues and therefore likely suitable for in vivo pathology. The maximum imaging depth at 30 MHz, due to attenuation of the ultrasound pulse in tissue, is approximately 20 mm.

Transducers designed with piezoelectric composites are used to evaluate feasibility of devices, particularly the basic electrical properties of a given design. Piezoelectric composites improve the overall performance of a transducer because of a reduction in acoustic impedance and an increase in sensitivity compared to bulk piezoelectric materials. For pulse-echo ultrasound imaging, piezoelectric/epoxy composites with 1-3 connectivity, with pillars of the piezoelectric material embedded in a polymer, are used to take advantage of the increased electromechanical coupling coefficient associated with tall, thin pillars of piezoelectric material.

In order to obtain the best performance from the transducers, new single crystal piezoelectric materials will be used. These new materials, such as Lead Magnesium Niobate – Lead Titanate (PMN-PT), have, among other benefits, higher electromechanical coupling efficiency when used in a composite than the standard piezoelectric ceramics commonly used in commercial transducers, leading to improved sensitivity for the devices and improved image quality.

The thicknesses of the transducer layers, shown in Figure 2 and detailed in Table 1, are determined by the required operating frequency and speed of sound in the materials. The matching layer improves transmission of the ultrasound pulse to the tissue, while both the matching and backing layers improve the bandwidth of the transmitted pulse, and consequently the axial resolution. The transducer stack parameters are determined via standard transducer design methods, using a  $\frac{1}{2}$  wavelength thickness piezoelectric layer and  $\frac{1}{4}$  wavelength thickness matching layer. The electrical impedance of the designed transducer stack, simulated with in-house design software, is shown in Figure 3. The shapes of the curves are as expected for a well matched and backed transducer. The electrical impedance for a given device will have the same shape and, but the impedance magnitude scales inversely with the transducer element area.

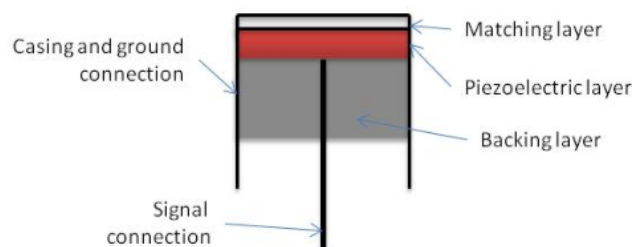


**Figure 2.** Diagram of transducer stack in a single element configuration

Table I. Transducer Plate Parameters

Transducer operating frequency	30 MHz
Piezoelectric layer material	50 % volume fraction 1-3 composite with PMN-PT single crystal piezoelectric material embedded in Epofix epoxy
Piezoelectric layer thickness	35 $\mu\text{m}$
Matching layer material	Alumina loaded Epofix epoxy
Matching layer thickness	15 $\mu\text{m}$
Backing layer material	Tungsten loaded Epofix epoxy
Backing layer thickness	1 mm

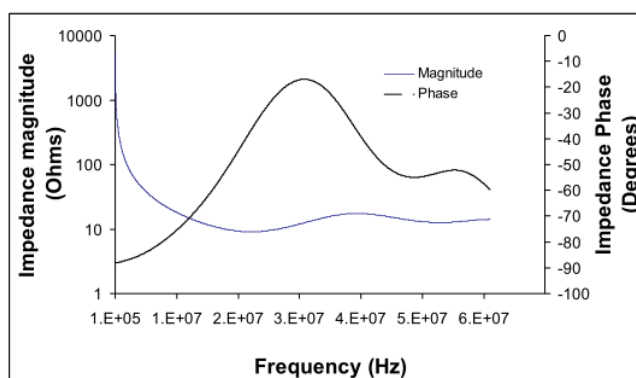


**Figure 3.** Electrical impedance magnitude and phase for 1 mm x 1 mm piezoelectric composite plate with matching and backing layer.



**Figure 4.** An example of a piezocomposite made by dice and fill method. The brown pillars are surrounded by transparent epoxy

### B. Manufacturability of Composite

Piezoelectric composites are used widely in transducers for imaging, where they are typically fabricated by dicing cuts, called kerfs, into a plate of piezoelectric material, then filling the kerfs with epoxy and lapping to the desired thickness. The top surface of a 1-3 piezocomposite made using this dice-and-fill method is shown in Figure 4.

As the transducer operating frequency increases, the thickness of the piezoelectric layer decreases, and consequently the lateral dimensions of the pillars must decrease to maintain the same pillar aspect ratio. For 30 MHz transducers, the pillars should be 20  $\mu\text{m}$  wide or less. At these scales two possible manufacturing methods are suggested for fabricating the

piezoelectric composite layer from piezoelectric single crystal: high precision dicing and deep reactive ion etching (DRIE).

High precision dicing can be used to either create 1-3 composite materials, on which array elements can be defined with photolithography, or to create long and narrow bars in the single crystal substrate, defining the individual elements. Dicing has been used to successfully make 1-3 composites with triangular pillars piezoelectric ceramic materials that operate up to 40 MHz [1], and this should also be feasible with single crystal materials. Using the smallest available dicing blades, 10  $\mu\text{m}$ , it will be feasible to dice pillars or bars with 25  $\mu\text{m}$  pitch; the remaining piezoelectric material is narrow enough to prevent lateral modes the pillars or bars coupling into the thickness mode vibrations.

DRIE can be used to pattern single crystal substrates to create bars or pillars for composites [2]. Combining techniques discussed in [3] with DRIE techniques, randomised patterns that disrupt any lateral modes so that the composite resonates only in its thickness will also be feasible, and even higher operating frequencies can be achieved.

## V. TRANSDUCER DESIGN EVALUATION

Design parameters for each of the four transducer configurations have been investigated to determine the optimised geometry. The electrical characteristics, the acoustic field pattern and scan geometry were evaluated for each variation in configuration. The electrical impedance magnitudes for the elements, which determines how well the elements are matched to electrical circuitry and consequently affects the sensitivity of the devices, has been calculated with in-house one dimensional modelling software.

The acoustic field produced by the linear and phased arrays has been simulated with Field II [4], while the acoustic field produced by the focused single elements and the annular arrays has been simulated with in-house numerical models [5]. For both types of simulation, impulse response techniques are used to calculate the two-way (transmit and receive) response over a region of interest for given device configuration. The two-way response gives the shape of the ultrasound beam produced by the device; this can be measured experimentally by placing a point reflector at the each point of interest and measuring the amplitude of the pulse reflected back to the transducer from the point reflector. The beam shape is used to determine the resolution through the depth of the image and the presence of unwanted regions of constructive interference (e.g. side lobes or grating lobes) that can produce artefacts in an image. For each of the arrays the beam is dynamically focused, i.e. focused at each depth in the region of interest, indicating the expected response after implementing beamforming techniques for imaging.

When using high frequency ultrasound transducers the imaging depth is limited by attenuation in tissue. The sensitivity and dynamic range of the electronics that drives the transducers and acquires the imaging signals affects the maximum imaging depth, as does the sensitivity of the transducer. In the current study, the maximum imaging depth has been taken to be 20 mm for evaluating the designs in anticipation that transducers using single crystal materials, and advances in electronics will enable imaging to this depth, however a more realistic current maximum limit may be 15 mm.

The following parameters relating to image quality are evaluated from the simulated two-way ultrasound beam:

- Best lateral resolution      Minimum beam width within imaging depth of field
- Imaging depth of field      Depth over which beam is focussed and secondary lobes suppressed to at least -40 dB of peak amplitude
- Resolution integral          A measure of image quality accounting for both resolution and depth of field
- Dynamic range of image      Maximum level of secondary lobes in field within imaging depth of field
- Scan line step                Angular or linear step size between lines in image; scan line sampling step should be  $\frac{1}{2}$  minimum resolution
- Scan format                  Geometry, image size, and number of image lines

The preferred device design minimises the lateral resolution and maximises the depth of field and field of view, preferably while maintaining a dynamic range of 50-60 dB. A dynamic range of 60 dB is what has been found to be useful for clinical imaging. The elements of an ideal device would have 50 Ohm electrical impedance magnitude for optimal matching to standard 50 Ohm circuitry. In addition, the number of elements in the device should be minimised to limit the complexity of the electronics in the system. A compromise must be made between these design specifications.

One means of evaluating the compromise between image quality and the various design parameters is to determine the resolution integral [6], a metric combining both the image resolution and the depth of field.

The resolution integral is the area under a curve relating inverse of resolution and depth, so that larger values for the resolution integral indicate better (i.e. narrower) resolution over a larger depth of field.

#### A. Mechanically scanned single element transducer

Array aperture: 1.5 mm, geometrically focussed  
 Scan method: Rotated element or mirror  
 Scan geometry: Axial cross section



**Figure 5.** Drawing of single element transducer in needle.

A single element transducer incorporated into a needle is shown in Figure 5. A single element transducer is the simplest of ultrasound transducer devices. However, there is a direct trade-off between the resolution and the depth of field, as illustrated in Figure 6 and summarized in Table II. The resolution is dictated by the focal power of the transducer, the ratio of the focal distance to the aperture diameter. An aperture of 1.5 mm is chosen so that the transducer can fit within the interior of the needle, with room for cabling and for motorization

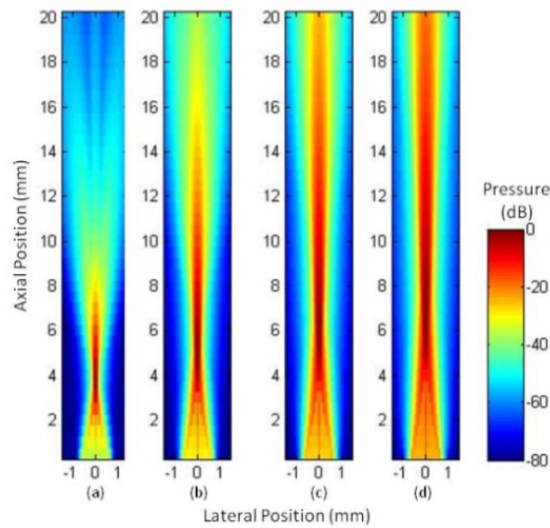


**Figure 6.** Simulated two-way radiation patterns for 1.5 mm diameter single element transducers focused at (a) 4 mm, (b) 6 mm (c) 8 mm and (d) 10 mm, normalised to the peak amplitude for each case.

As expected, with the constant element aperture, increasing the geometric focal distance increases both the resolution and the depth of field. Although the resolution integral is larger for the elements focused at 8 and 10 mm, one cannot image objects closer than 3.5 mm or 4 mm with either of these transducers. Therefore, if a single element transducer is used, a 6 mm focus, with a minimum imaging distance of 3 mm, is recommended. The diameter of the transducer determines the electrical impedance; the 20 Ω impedance is suitable for driving with standard systems, but could benefit from electrical impedance matching on the element to improve transferred power.

Although fabrication of a single element transducer is relatively straight forward, they cannot be used for Doppler imaging of flow in vessels because of the mechanical scanning. Doppler imaging, or colour flow imaging, is potentially highly useful for imaging the vasculature of small tumours, thereby providing more information about the stage and morphology of a tumour.

Table II. Summary of Single Element Transducer Image Parameters

Geometric focus (mm)	Electrical Impedance (Ohms)	Minimum Resolution (μm)	Depth of field (mm)	Resolution Integral	Dynamic Range (dB)	No. Scan Lines
4	20	120	5.5	28	40	314
6	20	160	9	35	40	314
8	20	180	14.5	42	45	349
10	20	210	16	43	50	300

## B. Mechanically scanned annular array

Array aperture: 1.5 mm, planar

Focus: dynamically focussed on both transmit and receive

Scan method: Rotated element or mirror

Scan geometry: Radial cross section



**Figure 7.** Drawing of a side-viewing annular array positioned in a needle

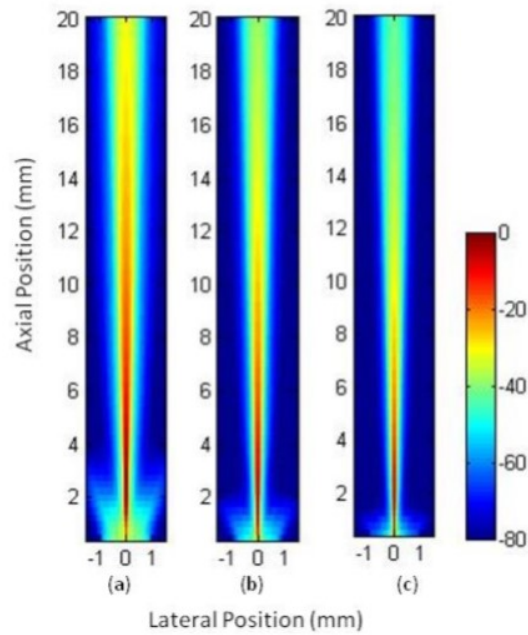
An annular array overcomes the trade-off between depth of field and resolution found with single element transducer, and with a small number channels for beamforming. The beam patterns, shown in Figure 8 and summarised in Table III, illustrate the effect of adding elements to an annular array. For the three arrays, the minimum imaging point was taken to be 3 mm, where the f-number, the ratio of the focal distance to aperture is 2. In order to image closer, a minimum f-number of 2 would be used, and the outer elements would not be used.

Table III. Summary of Annular Array Imaging Parameters

Number of elements	Electrical impedance (Ohms)	Minimum Resolution ( $\mu\text{m}$ )	Depth of field (mm)	Resolution Integral	Dynamic Range (dB)	No. Scan Lines
5	103	110	18.5	55	60	343
7	144	110	18.5	55	60	343
9	200	110	18.5	55	60	343

Annular arrays lead to a significant improvement in resolution over a wide field of view compared to focused single element transducers, even with as few as 5 elements. Increasing the number of elements in the array does not significantly change the resolution that can be achieved, but does reduce the amplitude of secondary lobes close to the array. The beam from the 9-element array has a higher peak amplitude close to the array, owing to improved focusing at short distances, and therefore has a larger dynamic range over the full beam plot. Since there is no significant improvement in the resolution over the depth of the image, a 5-element annular array will minimise system complexity by limiting channels. A 5-element annular array also maintains an electrical impedance close to the desired 50  $\Omega$ .

As with single element transducers, annular arrays also cannot be used for imaging flow because of the mechanical scanning.



**Figure 8.** Two-way radiation patterns for annular arrays with (a) 5 elements, (b) 7 elements and (c) 9 elements, normalised to the peak amplitude for each case.

**C. Side-viewing linear array**

- Element pitch: 0.05 mm
- Element width: 0.04 mm
- Elevation aperture: 1.5 mm
- Focus: dynamically focused on both transmit and receive
- Scan Geometry: rectangular

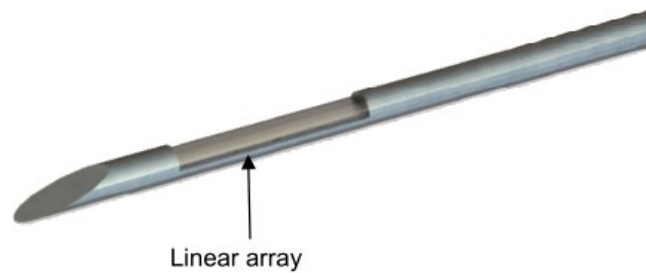


**Figure 9.** Drawing of side-viewing linear array.

The primary advantage of linear arrays and linear phased arrays over single element and annular arrays is the absence of mechanical scanning. Scanning is carried out electronically by exciting a group of elements at a time. The beam produced by the active subset of elements is switched along the length of the array to build up a 2D scan. The electrical scanning means that imaging flow is feasible with a linear array and linear phased array, providing more functionality compared to the mechanically scanned transducers.

Linear arrays are designed with approximately wavelength element pitch to prevent grating lobes. The image quality, particularly the resolution, for a linear array largely depends on the number of elements in the active subset – the active aperture, as shown in Figure 10. The image size is determined by the total length of the array. Therefore, increasing the number of elements in the active aperture and the total aperture improves the image quality and increases the image size. The effect of increasing the active and total aperture are summarised in Table IV.

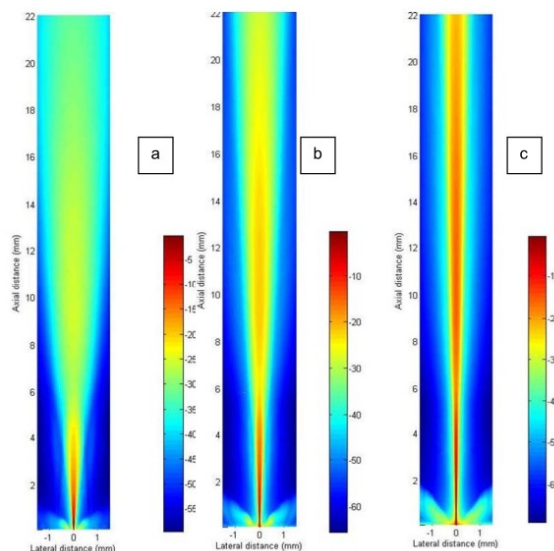


**Figure 10.** Two-way beam plots for linear arrays simulated using Field II, with (a) 8 elements, (b) 16 elements (c) 32 elements in the active aperture. Amplitudes are normalised the peak value.

**Table IV.** Linear Array Imaging Parameters

Number of elements	Number of Active elements	Electrical Impedance (Ohms)	Minimum Resolution ( $\mu\text{m}$ )	Depth of field (mm)	Resolution Integral	Dynamic Range (dB)	No. Scan Lines	Image size (mm)
32	8	350	72	5.2	17	45	25	1.25
64	8	350	72	5.2	17	45	57	2.85
64	16	350	56	14.4	37	45	49	2.45
128	16	350	56	14.4	37	45	113	5.65
128	32	350	50	16.8	62	55	97	4.85
256	32	350	50	16.8	62	55	225	11.85

As expected, there is an inverse relationship between resolution and the number of elements in the active aperture. In addition, there is an approximately linear increase in the resolution integral, indicating the significant improvement in the depth of field with more elements. The beam plots show that an array with 32 elements in the active aperture gives the most collimated beam over the largest depth, and therefore the best imaging.

The depth of field listed in Table IV reflects the minimum and maximum imaging depths. The minimum depth increases with number of active elements, and is limited by the appearance of secondary lobes in the beam plot. As for the annular array, for imaging close to the array, a smaller active aperture is used, with a minimum f-number of 2, so that the secondary lobes will be suppressed.

Increasing the total number of elements in the array increases the image window. A 128 element array will provide a 5 mm wide image, which may not be large enough for some clinical applications. Therefore, a 256 element array, with almost a 12 mm field of view, is

preferable to provide the maximum field of view for the clinician. Commercial linear arrays operating at conventional imaging frequencies can have as many as 512 elements, this would become prohibitively long on a needle.

For a linear array, the 350  $\Omega$  electrical impedance magnitude for an individual element in the array means that it may be necessary to use an impedance matching circuit to match the 50  $\Omega$  driving electronics. This would add to the difficulty in fabrication where capacitor and inductors are introduced to the system for each element. However, it may be possible to reduce the impedance by increasing the element dimensions without significantly degrading the image quality; this can be investigated in optimisation of the device.

#### D. Forward viewing linear phased array

##### Design specifications:

Element pitch:	0.025 mm
Element width:	0.015 mm
Elevation aperture:	0.8 mm
Focus:	dynamically focussed on both transmit and receive
Scan geometry:	sector scan.

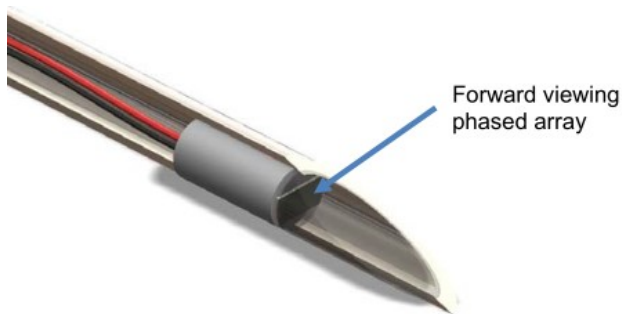


**Figure 11.** Drawing of forward viewing linear phased array placed in the tip of a needle.

The fundamental difference in imaging with a phased array as opposed to a linear array is that all the elements in the array are excited with electronically triggered time delays for focusing and steering, and all elements are driven for each image line. This means that fewer elements need to be connected to driving circuitry than a linear array, but the driving and beamforming system is more complex.

A linear phased array is designed with  $\frac{1}{2}$  wavelength element pitch to avoid grating lobes and enable steering as well as focusing of the beam. A 2D sector scan is built up by scanning the beam over a 90 degree field of view. The effect of increasing the number of elements on the beam shape is shown in Figure 12, and summarised in Table V.

Increasing the numbers of elements improves both the resolution and the depth of field. The minimum resolution was again taken at f-number = 2 for each aperture; fewer elements would be used for imaging closer, maintaining constant f-number. Any grating lobes have been suppressed. In order to optimise the image quality for a linear phased array, 64 elements are recommended; this gives the same aperture as the recommended linear array active aperture.

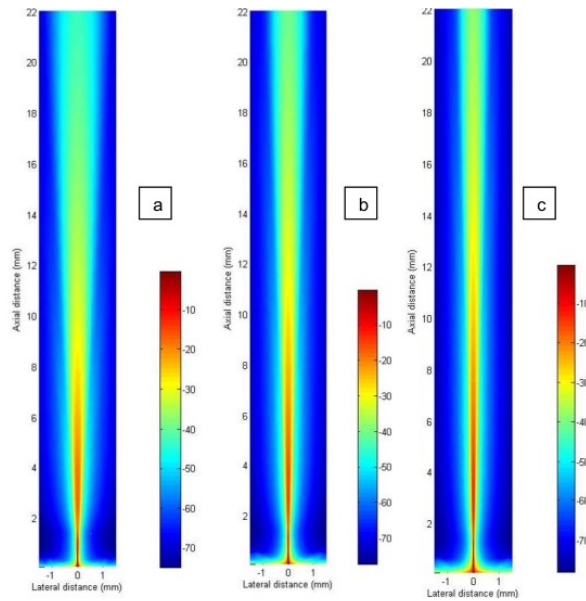


**Figure 12.** Two-way beam plots of a 30 MHz linear phased array simulated using FIELD II with (a) 32 elements, (b) 48 elements (c) 64 elements in the aperture. Amplitudes normalized to the peak value in each field.

**Table V.** Summary of Linear Phased Array Imaging Parameters

Number of elements	Electrical Impedance (Ohms)	Minimum Resolution ( $\mu\text{m}$ )	Depth of field (mm)	Resolution Integral	Dynamic Range (dB)	No. Scan Lines	Image size (Degrees)
32	1050	130	10.4	33	55	50	90
48	1050	130	13.6	46	60	70	90
64	1050	130	16.8	63	75	110	90

The electrical impedance of the linear phased array elements is approximately  $1000 \Omega$ , significantly higher than the standard system impedance of  $50 \Omega$ . In order for these elements to be used efficiently for pulse-echo imaging, a matching circuit will be required, preferably as close to the array elements as possible.

A forward viewing linear phased array should be positioned at the front edge of the needle and oriented, as illustrated in Figure 13. The needle bevel is open and therefore must be filled after assembly of the array with the needle with an acoustically transparent material. The array is oriented such that the scan plane bisects the slope of needle bevel. For a needle with a 30 degree tip angle, the sector scan angle will be reduced to 60 degrees to avoid the edges of the bevelled needle tip. While this reduces the field of view, it is still large enough to provide clinically relevant images.

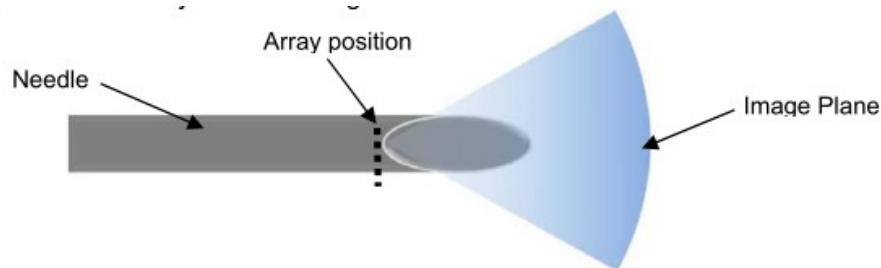


**Figure 13.** Top view of forward facing linear phased array in needle, showing sector image plane

## **VI. CABLING AND MANUFACTURABILITY**

### **A. Cabling for mechanically scanned single element transducer**

The smallest commercially available micro coaxial cable has an outer diameter of 0.25 mm (PicoCoax<sup>®</sup>, Axon Cable, Dunfermline, UK). This means the cable would fit easily into the needle, and with only one element to contact, bonding to the active substrate will be straight forward with standard fabrication techniques, such as wirebonding, or soldering.

Mechanical scanning with single element transducers is widely established and currently it has a valuable application in intravascular imaging. In many forms the transducer part is attached to a motor whereas in other applications the transducer is fixed and a rotating mirror is used to reflect and receive the ultrasound energy. The real-time image quality of these transducers will depend on the frame rate, which would be determined by the rotational speed of the motor.

In the first option, the transducer would face outwards, as shown in Figure 5, and a micro-motor attached to the transducer, possibly using the electrical cable as the drive shaft. Micro-motors including electromagnetic and ultrasonic types are currently available with diameters as small as 1 mm, making them suitable for the ultrasound imaging needle. In the second option, the transducer would be fixed and face forwards. A parabolic acoustic mirror attached to a micromotor would be positioned in front of the transducer to reflect the ultrasound beam radially outwards from the centre of the needle.

### **B. Cabling for mechanically scanned single element transducer**

With the small micro-coaxial cables available, it is possible to fit over 100 cables into a 2.11 mm diameter tube, plenty for an annular array. The increase in fabrication complexity compared to a single element transducer comes from connecting to each of the elements. However, various solutions including wirebonding to an interposer, or connection via radial electrode tracks on the surface of the array have been developed by other research groups [7, 8].

Similar to single element transducers, annular arrays need mechanical scanning for 2D imaging. A motorized parabolic mirror is needed to scan the beam while a forward-facing array remains fixed to allow direct connection to the array elements. The mechanical scanning of the beam from the annular array will not add significant fabrication complexity compared to a single element transducer, and the needle core will still have enough room for the cables, micromotor and parabolic mirror.

### **C. Acoustic window for single element transducer or annular array**

The ultrasound beams from the single element and annular array devices must be rotated about the needle axis to create a 2D image. Therefore, an acoustically transparent window is required about the full circumference of the device. The acoustic window could be a material such as polyurethane, which can be cast to the shape required. There will be a trade-off between the attenuation of the signal through the acoustic window and the acoustic matching to water or tissue, so as thin a layer as possible would be required. This is particularly important because attenuation increases with frequency.

The acoustic window, being made of a polymer rather than metal, will reduce the strength of the needle, possibly making it challenging to maintain the desired path when inserting a

needle into tissue. Stronger materials that transmit ultrasound with minimal attenuation will distort the ultrasound beam, thereby degrading the image capability.

The acoustic window area must also be fluid filled since either the transducer or a mirror must rotate while maintaining acoustic coupling. This makes for complex assembly between the transducer section and the metal tip and shaft sections. Mechanically scanned devices such as this work well in catheters for intravascular imaging where whole casing of the device can be a polymer, but are unlikely to be suitable for needle-based devices needing strength along the axis and a sharp tip.

#### D. Cabling for linear array and linear phased array

Although over 100 micro-coaxial cables could fit within the needle core, even for a 64-element linear array or linear phased array, a flexible printed circuit is preferable as a cabling solution. It will not be possible with the element dimensions required for the 30 MHz arrays to connect micro-coaxial cables to each individual element. A flex-circuit is a thin printed circuit that can be bent or shaped to fit in small areas, or where flexibility in the device is required; they are currently used for connecting to elements conventional ultrasound imaging arrays.

In this case, a flex-circuit with electrode tracks for each element channel can be wound in a spiral on the inside of the needle. An example of this is shown in Figure 14, with a flex circuit shaped into a helix tight enough to fit in the core of a 2 mm needle. The helical design allows for flex-circuit wider than the needle core width to be used. In the example shown in Figure 14, the 4.5 mm wide flex-circuit has 64 electrode tracks with 70  $\mu\text{m}$  pitch; this is a commercially available flex-circuit from WL Gore and Associates (UK) Ltd. With a larger helical pitch, more elements with the same electrode pitch can be used and still fit within the needle core. However, the development of a flex-circuit with smaller pitch electrode tracks is being investigated by collaborators in another project. The design of the new flex circuit cable will enable up to 128 tracks to be wound in into a helix and still fit in the needle core.



**Figure 14.** An example of a helical circuit next to a 2 mm diameter tungsten tube.

A flex-circuit can be attached to the array elements with a conductive polymer adhesive. The elements can then be separated by dicing, or by using an anisotropic conductive film (ACF). This approach has been shown to be promising for connection to miniature arrays [9], and the feasibility is being further investigated in a separate project on microfabrication techniques involving the University of Dundee and Heriot-Watt University.

For the linear phased array, because of the much narrower pitch (25  $\mu\text{m}$  at 30 MHz), the method of making connections at the array elements will need to be further tested. A fan-out from the connections at the elements to the 70  $\mu\text{m}$  pitch flex-circuit tracks could be used.

A second method would have alternate elements connected on opposing sides of the array, which would have the same 50  $\mu\text{m}$  pitch as the linear array.

#### **E. Manufacturability of linear array**

At operating frequencies above 30 MHz, the most viable fabrication method for defining arrays is with photolithography. Array electrodes can be patterned directly on a piezoelectric composite substrate, and an anisotropic conductive film used to make connections cabling. At 30 MHz or below, precision dicing to define elements and separate between electrode tracks on a flex-circuit is still feasible.

To incorporate a linear array in the metal casing of a needle, a slot can be cut near the tip of the needle, as illustrated in Figure 15. A linear array can be fabricated with the cabling connected and wound into a helix. The cabling can be passed into the slot and fed through the core of the needle until the array sits in the slot. With the cabling integrated with all the layers of the array, with the connections encased in the backing epoxy, the array will be robust enough for this manufacturing step.

The slot in the needle will be at deepest half the needle thickness, to maintain the strength of the tube for penetration into tissue. With the linear array design, the rigidity of the needle will also be reinforced by the solid backing epoxy layer.

The primary challenge in the fabrication of a side-viewing linear array, other than making reliable connection to the array elements as mentioned above, is in minimizing attenuation through the acoustic window. An acoustically transparent layer is needed to fill the space at the top of the array to make the outer surface of the needle cylindrical. However, as previously noted, materials acoustically matched to water or tissue at the desired operating frequencies are typically attenuating, while less attenuating materials can distort the beam. One solution is to test the feasibility of a flattened needle surface for penetrating into the tissue while maintaining acoustic contact with the tissue. For the initial prototype testing, an acoustic window of cast urethane is recommended; any refraction due to acoustic mis-match will be symmetrical on the array elements and can be accounted for. To minimize attenuation, the surface of the array should be positioned as close to the outer edge of the needle as possible.

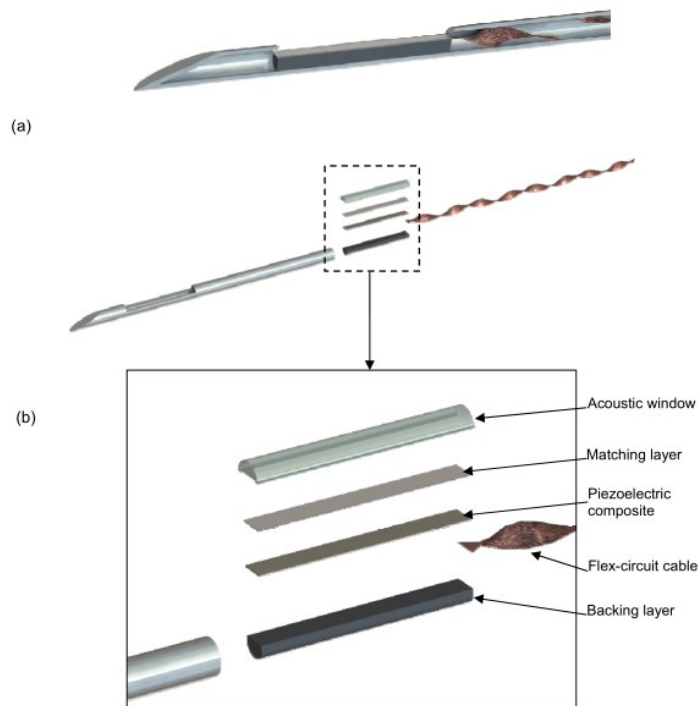


**Figure 15.** Drawing of (a) linear array integrated into needle and (b) exploded view of array layers and components

#### F. Forward viewing linear phased array

Because a phased array operating at the same frequency as a linear array has a significantly smaller total aperture, it can fit in a much more confined space. Therefore a linear phased array could fit within the core of a needle to face forwards. Fabrication challenges arise again from connection to cabling and the form of the acoustic window. Using photolithography to define the array elements, and the ACF mentioned above to connect the flex-circuit cable, manufacture of the array is expected to be feasible following further optimization of the microfabrication processes. As with the linear array, the helically wound flex-circuit cable can be fed through an opening in the beveled front of the needle.

However, with the array will facing forwards, a solid material must be cast to fill the bevel so that the needle can penetrate into tissue. Without a solid acoustic window, there would be unnecessary tissue damage due to cutting a core of tissue with the bevel tip, and forcing the needle into the tissue would be difficult. With the bevel filled with a solid acoustically transparent material, the needle surface will behave as usual. However, as has been noted previously, materials acoustically matched to water are attenuating at the frequencies required for high resolution imaging. Less attenuating materials will not be as well matched to the tissue, causing the acoustic beam to be refracted at the angled surface of the acoustic window, and therefore the image plane will no longer be directly in front of the needle.

## VII. EARLY PROTOTYPE TRANSDUCER

A prototype single element transducer in a needle has been built to investigate some of the design and fabrication issues that have been highlighted in this study. A planar single element transducer was placed in a slot cut in a 2 mm diameter hollow tungsten tube as substitute for a needle. The resonance frequency of this element was 15 MHz for initial testing. A single micro-coaxial cable, which was used for electrical connection to the element, was connected to the transducer element. The cable was fed through the slot into the tube then attached to a connector. In the case of an array, a flex-circuit would be more suitable to fit into the confined space in the tube. Later prototypes will have a cap of acoustically transparent material cast on top of the transducer to seal the needle and make a smooth surface. This demonstrates one potential method for assembly of an ultrasound transducer within a needle.

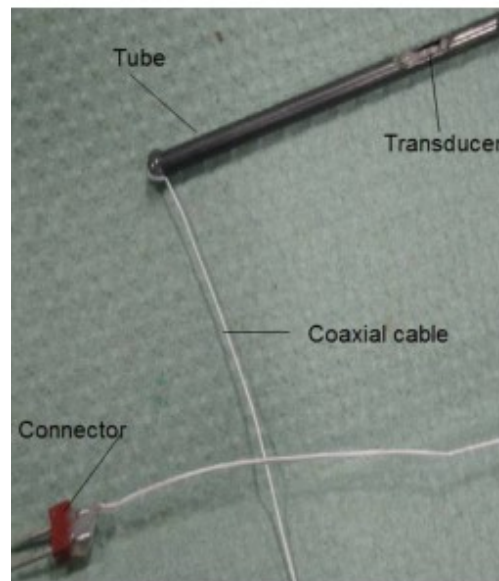


**Figure 15:** The assembled single element transducer

## VIII. SUMMARY AND RECOMMENDATIONS

### A. Design recommendations

The feasibility of incorporating ultrasound transducers into a biopsy needle for high resolution imaging towards *in vivo* pathology has been investigated. Four transducer configurations have been investigated: mechanically scanned single element transducers and annular arrays, side-viewing linear arrays and forward viewing linear phased arrays.

The mechanically scanned single element transducers and annular arrays produce axial cross-section scans usually used in intravascular imaging. While these transducers provide good image quality with minimal system complexity, two limitations prevent them from being recommended for needle-based imaging applications. First, it is expected that Doppler imaging of blood flow will be highly beneficial for diagnostic imaging small tumours. The mechanically scanned arrays cannot provide this information due to the motion of the transducer or parabolic mirror used to scan the beam. Secondly the circumferential acoustic

window in the needle will reduce the rigidity of the needle, or significantly distort or attenuate the ultrasound signal.

With the current materials available, the single element transducers and annular arrays are not recommended for needle based high resolution imaging. However, for applications where an axial cross section image plane is useful, a polymer housing is feasible, and device rigidity is not required, an annular array with a parabolic mirror is recommended.

Linear phased arrays operating at conventional medical imaging frequencies are used in situations where a wide field of view is required, but a limited space is available for positioning the array, such as in cardiac imaging. A forward viewing linear phased array placed at the tip of a needle also conforms to this situation. Using microfabrication technology currently in development for miniature ultrasound arrays, it is expected to be feasible to build a forward-viewing linear phased array.

However, the image quality will be severely affected by the material used to fill the needle taper. At lower operating frequencies there are materials that are truly acoustically transparent, in that they are acoustically match to water or tissue, and have minimal attenuation, new materials would be required to obtain the same performance at 30 MHz or above. Only if and when acoustically transparent materials are developed for high frequency applications will forward facing linear phased arrays integrated into needles be feasible. For other applications not requiring a tapered needle tip, the forward viewing linear phased array with 64 elements should be pursued, but challenges associated with electrical impedance matching must be taken into account.

While a side viewing linear phased array could be developed, the moderate improvement in image quality does not justify the increased system complexity and the challenges in fabrication and electrical impedance matching due to the smaller element dimensions. In addition, linear phased arrays have very narrow field of view close to the transducer, while linear arrays have the same field of view through the depth of the image. The wide field of view close to the transducer will benefit the clinician wanting to image as large region of tissue as possible.

Side-viewing linear arrays are therefore the recommended configuration for needle-based imaging. Various microfabrication methods for connecting cabling to the array elements are being investigated in other projects, with promising preliminary results. Cabling solutions using flex-circuits wrapped into helices that can fit within the core of a needle will enable up to 128 elements to be connected will be used. The preferred linear array configuration is 256 elements in the total aperture with 32 elements in the active aperture. It is not expected that the helical flex cable can be designed to have that many channels and still fit within the needle core, so electronics will need to be integrated at the tip of the needle to switch between the elements. Therefore, the current recommended specification is a 128 element linear array with 32 active elements to demonstrate the capability of needle-based high resolution imaging, increasing to 256 with advances in available switching electronics.

As electronic components become smaller, it will be feasible to place more and more electronics at the site of the array, including pulsing and receiving chips. This will reduce the space required for cabling, enabling integration of a side-viewing linear array in a needle with a biopsy channel.

## B. Impact of industrial design on device development

Incorporating manufacturability considerations concurrent with physics research into device design through involvement of industrial design at the earliest stages of device development has reduced the time required to determine a recommended design for a specific application. Explicit discussion of the manufacturability of components, such as the needle tip design and cabling, has lead quickly to decisions regarding the feasibility of the configurations for the current application.

For example, discussions of expected manufacturability and strength of the needle structure lead to the mechanically scanned transducers being discounted early as not suitable for the integration in a needle. The annular arrays would have otherwise been further developed as potentially feasible devices because of the high image quality with minimal system complexity. Similarly, evaluation of the needle design incorporating a forward viewing array lead to this configuration being discounted for this application.

## C. Continuing development

The development of a side-facing linear array will continue to be developed. In the short term, a PhD student and an MSc student will evaluate early prototypes of side-viewing devices based on single element transducers and simple arrays operating at lower frequencies. Further funding for fabrication of a prototype high frequency device will be sought on the basis of this study. The incorporation of electronic components will also be investigated with further funding. Industrial design will continue to be incorporated into the design and development process for this device to continue evaluation of feasibility and manufacturability. For other transducers for ultrasonic applications investigated by this research group, funding for incorporating industrial design early in the research and design process will be sought to improve the efficiency of developing new technologies based on physics research.

## REFERENCES

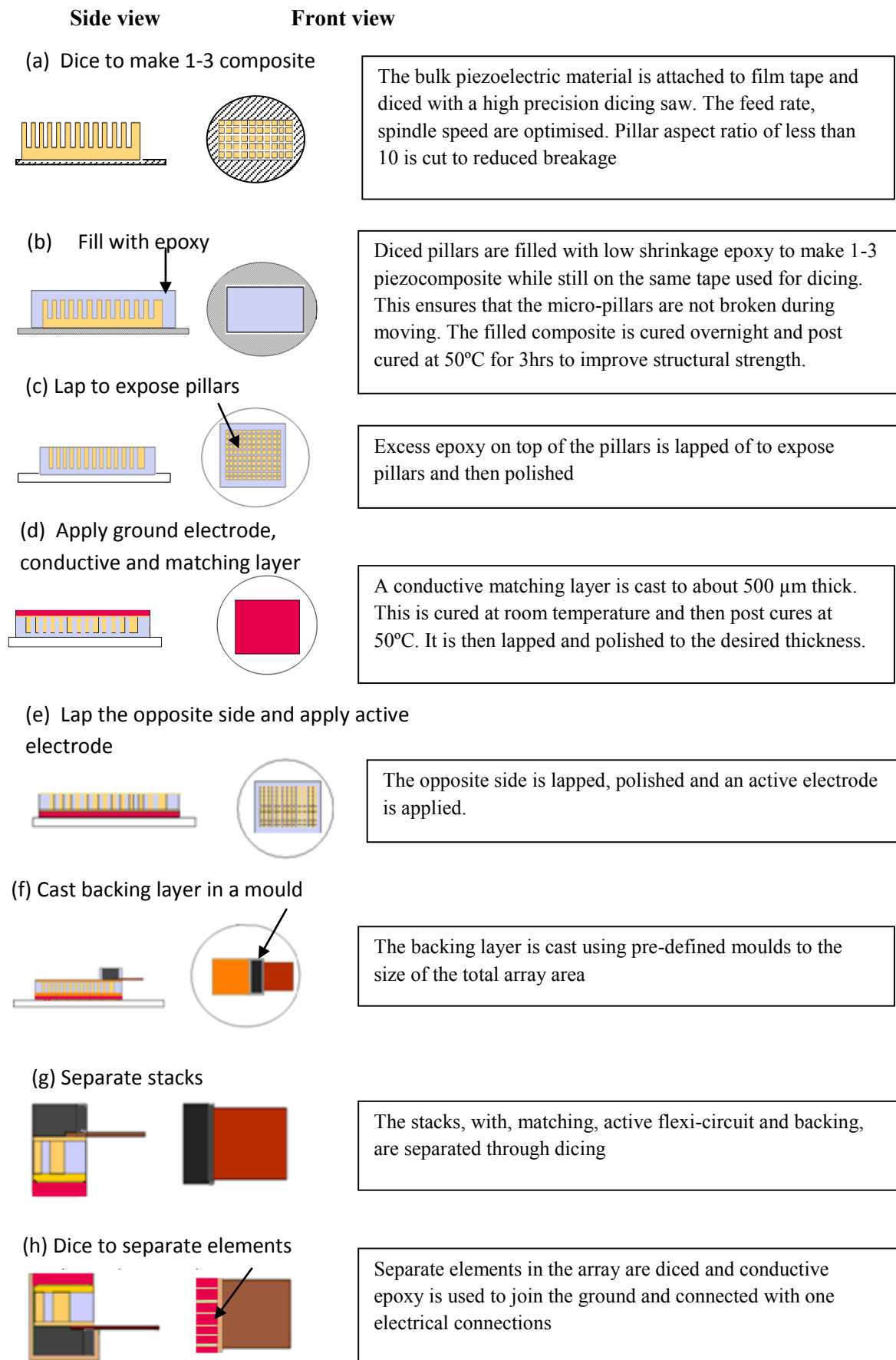
1. Brown, J.A., et al. Fabrication and Performance of a High-Frequency Geometrically Focussed Composite Transducer with Triangular Pillar Geometry. in *Ultrasonics Symposium*, 2007. IEEE. 2007.
2. Yuan, J.R., et al. High Frequency Piezo Composites Microfabricated Ultrasound Transducers for Intravascular Imaging (Invited). in *Proceedings of the 2006 IEEE Ultrasonics Symposium*. 2006.
3. Demore, C.E.M., et al. 1-3 piezocomposite design optimised for high frequency kerfless transducer arrays. in *Ultrasonics Symposium (IUS), 2009 IEEE International*. 2009.
4. Jensen, J.A., *Field: A Program for Simulating Ultrasound Systems*. Medical & Biological Engineering & Computing, 1996. 34(Supplement 1, Part 1): p. 351-353.
5. Demore, C.E.M., J.A. Brown, and G.R. Lockwood, Investigation of cross talk in kerfless annular arrays for high-frequency imaging. *IEEE Transactions on Ultrasonics, Ferroelectrics and Frequency Control*, 2006. 53(5): p. 1046-1056.
6. Pye, S.D. and et al., Medical ultrasound: a new metric of performance for grey-scale imaging. *Journal of Physics: Conference Series*, 2004. 1(1): p. 187.
7. Brown, J.A., C.E. Morton, and G.R. Lockwood. Fabrication and performance of 40-60 MHz annular arrays. in *Proceedings 2003 IEEE Ultrasonics Symposium*. 2003. Honolulu, USA.
8. Ketterling, J.A., et al., Design and fabrication of a 40-MHz annular array transducer. *IEEE Transactions on Ultrasonics, Ferroelectrics and Frequency Control*, 2005. 52(4): p. 672-681.
9. Bernassau, A.L., et al. Techniques for wirebond free interconnection of piezoelectric ultrasound arrays operating above 50 MHz. in *2009 IEEE International Ultrasonics Symposium (IUS), 2009*

## APPENDIX B

The different fabrication processes that were thought of during this study are detailed below. These are summarised in Table B.1 which is the same as Table 5.1.

**Table B. 1: Summary of the different fabrication processes considered**

Process name and number	Key points
<b>Silicon micro-vias</b> PD01/RTS/010610	<ul style="list-style-type: none"> <li>• Micro-vias through the backing layer used for electrical interconnects</li> <li>• Easy for wafer-scale fabrication since the flexi-circuit is attached at the end of the process</li> <li>• Multiple micro-vias present a big challenge in the confined space</li> </ul>
<b>Conductive Matching</b> PD02/RTS/031210	<ul style="list-style-type: none"> <li>• Matching layer is used as a common ground</li> <li>• Ground is at the front face of the transducer, providing electrical shielding, which improves safety</li> <li>• Ultrasound energy attenuation is increased through the conductive matching due to the heavy metal particles</li> </ul>
<b>Conductive backing</b> PD03/RTS/010211	<ul style="list-style-type: none"> <li>• Backing layer is used as a common ground</li> <li>• The active surface is at the front face of the transducer</li> <li>• Needs extra ground on the front of the transducer for shielding and safety</li> <li>• Difficult to optimise the backing due to the metal particles in the epoxy for conductivity</li> </ul>
<b>Flexi-circuit matching</b> PD04/RTS/080711	<ul style="list-style-type: none"> <li>• Matching layer is replaced by a flexi circuit with the array electrode pattern</li> <li>• Number of material layers is reduced</li> <li>• Good design is needed to minimise attenuation at the front face of the transducer</li> <li>• Alignment and electrical connection between electrodes on piezoelectric substrate and flex circuit can be challenging</li> </ul>
<b>Wafer scale</b> PD05/RTS/010811	<ul style="list-style-type: none"> <li>• Multiple devices are defined on a single large plate of composite</li> <li>• Strips of epoxy are cast between regions of active composite and make space for the interconnects</li> <li>• Connections are away from the path of the ultrasound wave</li> <li>• Uses the conventional materials for all the layers</li> </ul>



PD02/RTS/031210

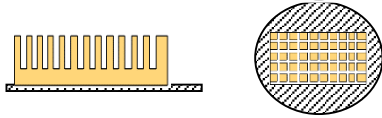
Conductive Matching

Figure B. 1: Fabrication process plan incorporating a conductive matching layer

**Side view**

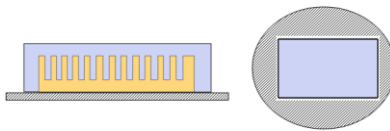
**Front view**

(a) Dice to make 1-3 composite



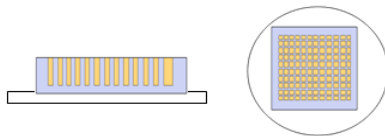
The bulk piezoelectric material is attached to film tape and diced with a high precision dicing saw. The feed rate, spindle speed are optimised. Pillar aspect ratio of less than 10 is cut to reduced breakage

(b) Fill with epoxy



Diced pillars are filled with low shrinkage epoxy to make 1-3 piezocomposite while still on the same tape used for dicing. This ensures that the micro-pillars are not broken during moving. The filled composite is cured overnight and post cured at 50°C for 3hrs to improve structural strength.

(c) Lap to expose pillars



Excess epoxy on top of the pillars is lapped of to expose pillars and then polished

(d) Apply ground electrode



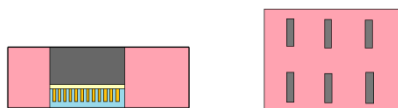
A ground electrode is applied through e-beam evaporation

(e) Cut and put into a mould



The composite is cut into the size of the array and put into a mould of machineable ceramic. The unlapped side faces the outside of the mould.

(f) Cast backing layer in a mould



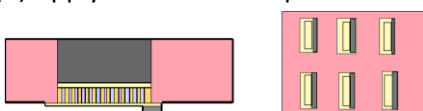
The backing layer is cast using pre-defined moulds to the size of the total array area

(g) Lap the bottom and apply active electrode



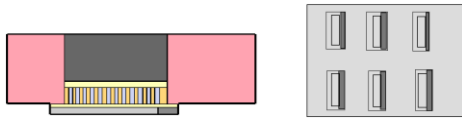
The active side is lapped and an electrode applied.

(h) Apply conductive strips



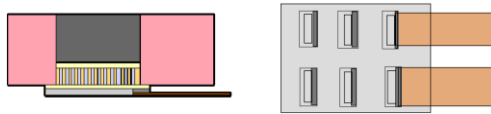
Conductive strips are applied on the side of the active layer

(h) Cast matching layer



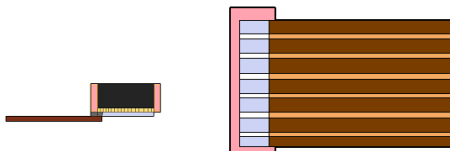
A matching layer is cast to about 500  $\mu\text{m}$  and cured at room temperature for 5 hours before post curing at 50°C. It is then lapped to the desired thickness

(h) Attach flexi circuit



Flexi-circuits are attached to the conductive strips on the side of the matching

(h) Dice to separate elements



Separate elements in the array are diced and conductive epoxy is used to join the ground and connected with one electrical connections

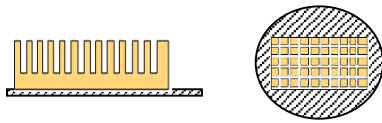
PD03/RTS/010211

Conductive backing

Figure B. 2: Fabrication process plan incorporating a conductive layer

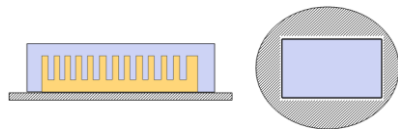
**Side view**                      **Front view**

(a) Dice to make 1-3 composite



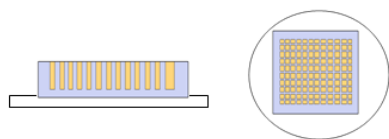
The bulk piezoelectric material is attached to film tape and diced with a high precision dicing saw. The feed rate, spindle speed are optimised. Pillar aspect ratio of less than 10 is cut to reduced breakage

(b) Fill with epoxy



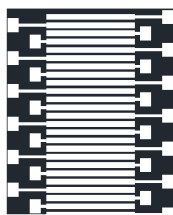
Diced pillars are filled with low shrinkage epoxy to make 1-3 piezocomposite while still on the same tape used for dicing. This ensures that the micro-pillars are not broken during moving. The filled composite is cured overnight and post cured at 50°C for 3hrs to improve structural strength.

(c) Lap to expose pillars



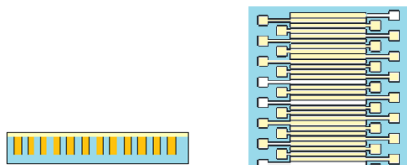
Excess epoxy on top of the pillars is lapped of to expose pillars and then polished

(d) Pattern silicon wafer



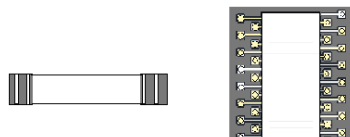
Silicon wafer is patterned with conductive tracks to make small fan-outs able to fit in the dimensions of a needle. The pads are 200µm squares. The middle area is where the composite will fit.

(e) Pattern the composite



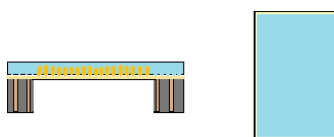
Composite is patterned with conductive tracks to allow to the arrays. This will be bonded to the silicone with matching tracks. The pads are on the excess epoxy on the side of the composite

(f) Make holes through the silicon



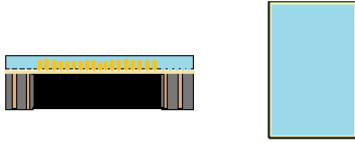
A middle hole is careful made through either sandblasting or laser drilling. Micro-vias are also made through the pads by the sides of the middle hole

(g) Bond composite to silicon



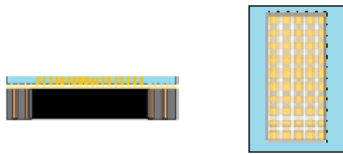
The composite is carefully bonded to silicon so that the pads on the composite match the micro-vias on the silicon having filled them with conductive filling

(h) Fill with backing



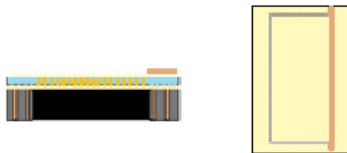
The silicon middle hole is filled with backing and then lapped.

(i) Lap front end



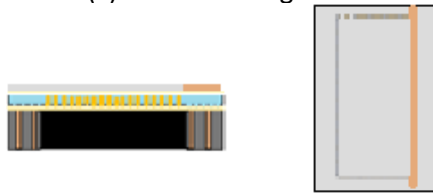
The front end is lapped to leave a thickness corresponding to the desired frequency

(J) Add conductive strip



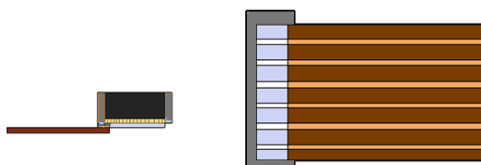
A conductive strip is printed on the edge of the front layer. This strip can be up to 300µm wide.

(k) Cast matching



A matching layer is cast and lapped to leave a thickness for the desired frequency. The conductive strip is also exposed

(l) Attach flexi-circuit



A pre-patterned flex-circuit is attached to the front for the ground connection.

PD01/RTS/010610

Silicon micro-vias

Figure B. 3: Fabrication process plan incorporating silicon micro-vias

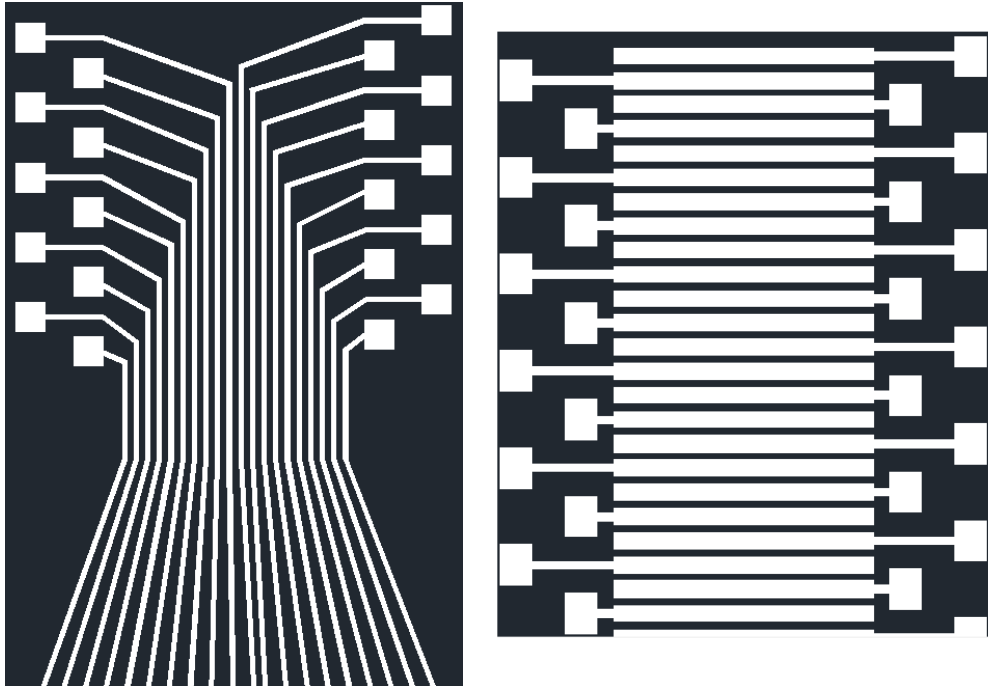
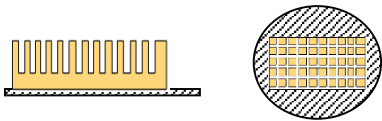


**Figure B. 4: Example of flexi-circuit bond pads to be bonded at the back end of the silicon holding the transducer stack**

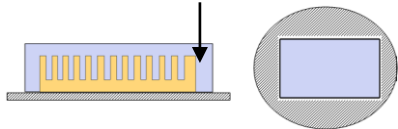
**Side view**                      **Front view**

(a) Dice to make 1-3 composite



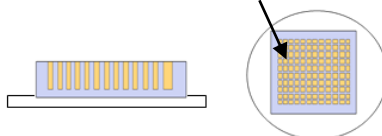
The bulk piezoelectric material is attached to film tape and diced with a high precision dicing saw. The feed rate, spindle speed are optimised. Pillar aspect ratio of less than 10 is cut to reduced breakage

(b) Fill with epoxy



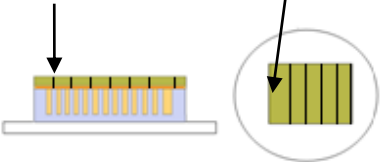
Diced pillars are filled with low shrinkage epoxy to make 1-3 piezocomposite while still on the same tape used for dicing. This ensures that the micro-pillars are not broken during moving. The filled composite is cured overnight and post cured at 50°C for 3hrs to improve structural strength.

(c) Lap to expose pillars



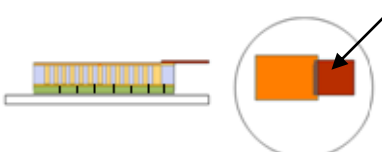
Excess epoxy on top of the pillars is lapped of to expose pillars and then polished

(d) Apply ground electrode, conductive strips and matching



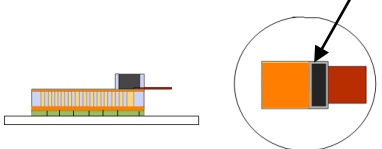
Strips of about 200 μm are diced at intervals of 800 μm to determine the length of each element in the array. These are filled with epoxy before curing and lapping. Ground electrode is applied, ideally through evaporation or sputtering. On top of the strips, conductive strips are printed using a pre-defined mask. A matching layer is cast and lapped to thickness exposing the conductive strips

(e) Apply active electrode and flexi-circuit



A patterned flexi-circuit is attached with room temperature curing epoxy and cured at 50°C for 1hr.

(f) Cast backing layer in a mould



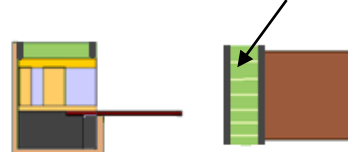
The backing layer is cast using pre-defined moulds to the size of the total array area

(g) Separate stacks



The stacks, with, matching, active flexi-circuit and backing, are separated through dicing

(h) Dice to separate elements



Separate elements in the array are diced and conductive epoxy is used to join the ground and connected with one electrical connections

PD05/RTS/010811

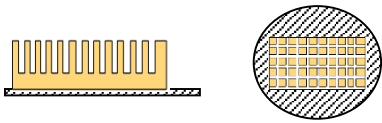
Wafer scale

Figure B. 5: Fabrication process plan incorporating wafer scale

Side view

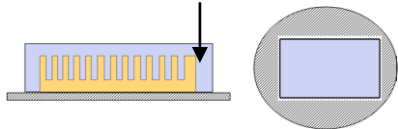
Front view

(a) Dice to make 1-3 composite



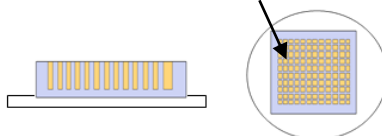
The bulk piezoelectric material is attached to film tape and diced with a high precision dicing saw. The feed rate, spindle speed are optimised. Pillar aspect ratio of less than 10 is cut to reduced breakage

(b) Fill with epoxy



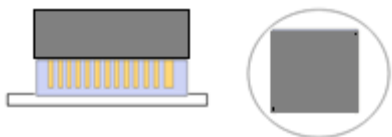
Diced pillars are filled with low shrinkage epoxy to make 1-3 piezocomposite while still on the same tape used for dicing. This ensures that the micro-pillars are not broken during moving. The filled composite is cured overnight and post cured at 50°C for 3hrs to improve structural strength.

(c) Lap to expose pillars



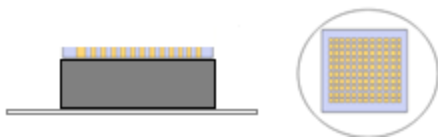
Excess epoxy on top of the pillars is lapped off to expose pillars and then polished

(d) Cast a conductive backing layer



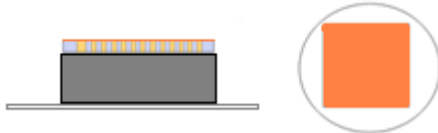
A conductive backing layer is cast on top of an electrode at the active layer.

(e) Lap active layer to desired frequency



The active layer is lapped to correspond to the desired thickness

(f) Apply top electrode



An electrode is applied to the front end of the active layer

(h) Attach flexi-circuit and dice to separate elements



A patterned flexi-circuit is attached and elements are diced. The flexi-circuit is used as a matching layer

PD04/RTS/080711

Flexi-circuit matching

Figure B. 6: Fabrication process plan incorporating flexi-circuit matching

## APPENDIX C

---

### Publications

#### Conference presentations

**Robert Ssekitoleko**, Christine Demore, Jack Hoyd-Gigg Ng, Marc Desmulliez, Sandy Cochran. Development of Miniaturised Linear Arrays for Integration with Interventional Tools; *IUS*; July 21-25, 2013, Prague, Czech Republic

Christine E.M. Demore , **Robert T. Ssekitoleko** , Jack Hoyd-Gigg Ng, Yun Jiang , Srikanta Sharma , Tim W. Button , Jeffrey C. Bamber , Marc P.Y. Desmulliez, and Sandy Cochran. Miniaturised transducer arrays for high resolution clinical imaging; *Ultrasonic Transducer Engineering Conference*; 17-19 April 2013, Los Angeles, CA

**R.T. Ssekitoleko**, J.H.G. Ng, S. Sharma, C. Démoré, D. Flynn, G. A. Corner, M.P.Y. Desmulliez, S. Cochran. *Development and testing of high resolution ultrasound transducers for interventional medical applications*. Scottish Ultrasound Meeting, February 10th 2012, Glasgow, Scotland, UK

C. E. M. Demore, Z. Qiu, M. R. Sadiq, **R. T. Ssekitoleko**, and S. Cochran. *Single crystal 1-3 piezocomposites for high performance transducers*. International Symposium on Piezocomposite Applications, Dresden, Germany, 22-23 September, 2011

**R T Ssekitoleko**, S Sharma CEM Demore, S Cochran. *Prediction of ultrasound imaging transducers performance through simulated resolution integral*. IPEM EMPEC2011 – 1st – 3rd September 2011, Dublin, UK

**R.T. Ssekitoleko**, J.H.G. Ng, C. Démoré, D. Flynn, G. A. Corner, M.P.Y. Desmulliez, S. Cochran. *Towards in vivo Pathology: Integrating High Frequency Ultrasound with Interventional Tools*. BMUS2011 – 15th – 17th October 2011, Brighton, UK

C.E.M. Demore, **R. Ssekitoleko**, T.W. Button, S. Cochran. *Progress in high resolution ultrasound towards in vivo pathology*. 22<sup>nd</sup> International Conference of the Society for Medical Innovation and Technology, Trondheim, Norway, 2<sup>nd</sup> - 4<sup>th</sup> September 2010 (Oral).

**R.T. Ssekitoleko**, C.E.M. Démoré, T.W. Button, S. Cochran, *Progress in high resolution ultrasound towards in-vivo pathology*. Sinapse Annual Scientific Meeting 16<sup>th</sup> June 2010 (Poster), Edinburgh, Scotland, UK

## Conference papers

Jack Hoyd-Gigg Ng, **Robert T Ssekitoleko**, David Flynn, Robert W Kay, Christine Demore, Sandy Cochran, Marc P Y Desmulliez. *Innovative manufacturing and 3-dimensional packaging methods of micro ultrasonic transducers for medical applications*. 18th European Microelectronics Packaging Conference (2011) (EMPC2011) 12th -15th September 2011, Brighton, UK Publisher: IEEE, Pages: 1-5 ISBN: 9781467306942

Jack Hoyd-Gigg Ng, **Robert T. Ssekitoleko**, David Flynn, Robert W. Kay, Christine E. M. Démoré, Sandy Cochran and Marc P. Y. Desmulliez. *Design, Manufacturing and Packaging of High Frequency Micro Ultrasonic Transducers for Medical Applications*. 2011 13<sup>th</sup> Electronics Packaging Technology Conference 07 Dec - 09 Dec 2011, Singapore, Electronics Packaging Technology proceeding- in press 2011

**Robert Ssekitoleko**, Jack Hoyd-Gigg Ng, Christine Demore, David Flynn, Marc Desmulliez, Sandy Cochran. *Design and Fabrication of High frequency Ultrasound Imaging Arrays Integrated into Medical Interventional Tools*. IUS2011- 18th – 21st October 2011- Orlando, U, IEEE International Ultrasonics Symposium Proceedings, Orlando, FL, in press, 2011

Jack Hoyd-Gigg Ng, David Flynn, Yves Lacrotte, Marc P.Y. Desmulliez, **Robert Ssekitoleko**, Christine Démoré and Sandy Cochran. *Progress towards the development of novel fabrication and assembly methods for the next generation of ultrasonic transducers*. ESTC 2010 Electronic System-Integration Technology Conference (ESTC), 2010 3<sup>rd</sup> 13-16 Sept. 2010 Page(s): 1-6 Berlin, in press

**R.T. Ssekitoleko**, C.E.M. Démoré, G. Harvey, Z Qiu, M. R. Sadiq, S Cochran. *Virtual Prototyping for the Design of High Frequency Ultrasound Transducer Arrays*. Proceedings of the Ultrasonics Industry Association Symposium 2011, Glasgow, UK, in press 2011.

J.H.G. Ng, **R.T. Ssekitoleko**, D. Flynn, M.P.Y. Desmulliez, C.E.M. Démoré and S. Cochran. *Design, manufacturing and packaging of a micro ultrasonic transducer for medical applications*. Proceedings of the 22nd Micromechanics and Micro systems Europe Workshop, Toensberg, Norway, pp. 298-301, 2011.